รายงานวิจัยฉบับสมบูรณ์

โครงการ
การศึกษากลไกทางจลนศาสตร์ของเอนไซม์ glycerol 3-phosphate oxidase จากเชื้อ *Mycoplasma pneumoniae*
(Kinetic studies of glycerol 3-phosphate oxidase from *Mycoplasma pneumoniae*)

โดย
นายสมชาติ แม่นปืน

25 กุมภาพันธ์ 2558

สัญญาเลขที่ MRG5580066

รายงานวิจัยฉบับสมบูรณ์

โครงการ
การศึกษากลไกทางจลนศาสตร์ของเอนไซม์ glycerol 3-phosphate oxidase จากเชื้อ *Mycoplasma pneumoniae*
(Kinetic studies of glycerol 3-phosphate oxidase from *Mycoplasma pneumoniae*)

นายสมชาติ แม่นปืน
ภาควิชาชีวเคมี คณะวิทยาศาสตร์
มหาวิทยาลัยบูรพา

สนับสนุนโดยสำนักงานกองทุนสนับสนุนการวิจัย

Abstract/บทคัดย่อ

Project Code : MRG5580066

Project Title : การศึกษากลไกทางจลนศาสตร์ของเอนไซม์ glycerol 3-phosphate oxidase จากเชื้อ *Mycoplasma pneumoniae*
(Kinetic studies of glycerol 3-phosphate oxidase from *Mycoplasma pneumoniae*)

Investigator : นายสมชาติ แม่นปืน

E-mail Address : somchart@buu.ac.th

Project Period : 2 ก.ค. 2555 - 2 ก.ค. 2557

Abstract

L-α-glycerophosphate oxidase is an FAD-dependent enzyme that catalyzes the oxidation of L-α-glycerophosphate (Glp) by molecular oxygen to generate dihydroxyacetone phosphate (DHAP) and hydrogen peroxide (H_2O_2). The catalytic properties of the recombinant His_6-GlpO from *Mycoplasma pneumoniae* (His_6-*Mp*GlpO) were investigated with transient and steady-state kinetics and ligand binding. The results indicate that the reaction mechanism of His_6-*Mp*GlpO follows a ping-pong model. Double-mixing stopped-flow experiments show that after flavin-mediated substrate oxidation, DHAP leaves rapidly prior to the oxygen reaction. The values of the individual rate constants and k_{cat} (4.2 s^{-1} at 4 ^{o}C) determined, in addition to the finding that H_2O_2 can bind to the oxidized enzyme suggest that H_2O_2 release is the rate-limiting step for the overall reaction. Results indicate that His_6-*Mp*GlpO contains mixed populations of fast and slow reacting species. Only the fast reacting species predominantly participates in turnovers. Different from other GlpO enzymes previously reported, His_6-*Mp*GlpO can catalyze the reverse reaction of reduced enzyme and DHAP. This result can be explained by the standard reduction potential value of His_6-*Mp*GlpO (-167 $\pm$ 1 mV), which is lower than those of GlpO from other species. We found that DL-glyceraldehyde 3-phosphate (GAP) can be used as a substrate in the His_6-*Mp*GlpO reaction, although it exhibited a~100-fold lower k_{cat} value in comparison to the reaction of Glp. These results also imply the involvement of GlpO in glycolysis, as well as in lipid and glycerol metabolism. The kinetic models and distinctive properties of His_6-*Mp*GlpO reported here should be useful for future studies of drug development against *Mycoplasma pneumoniae* infection.

บทคัดย่อ

เอนไซม์กลีเซอโรฟอสเฟตออกซิเดสเป็นเอนไซม์ที่มีโคแฟคเตอร์เป็น FAD ที่ทำหน้าที่เร่งปฏิกิริยาการเกิดออกซิเดชันของกลีเซอโรฟอสเฟตโดยออกซิเจนเพื่อสร้างเป็นไดไฮดรอกซีอะซีโตนฟอสเฟตและไฮโดรเจนเปอร์ออกไซด์ ในรายงานฉบับนี้เป็นการศึกษาคุณสมบัติการเร่งปฏิกิริยาของเอนไซม์รีคอมบิแนนท์ของกลีเซอโรฟอสเฟตออกซิเดสจากเชื้อ *Mycoplasma pneumoniae* ซึ่งก่อให้เกิดโรคปอดอักเสบ โดยใช้เทคนิคต่างๆ ได้แก่ จลนศาสตร์ที่สภาวะก่อนคงตัว และที่สภาวะคงตัว รวมทั้งการจับกันของเอนไซม์กับสารที่เป็นลิแกนด์ ซึ่งผลจากการศึกษาทำให้ทราบว่ากลไกการเร่งปฏิกิริยาของเอนไซม์นี้มีรูปแบบเป็น ping-pong mechanism โดยยืนยันผลการทดลองที่ได้นี้ด้วยเทคนิค double-mixing stopped-flow spectrophotometry ซึ่งทำให้พบว่าสารผลิตภัณฑ์ไดไฮดรอกซีอะซีโตนฟอสเฟตที่เกิดขึ้นหลังจากการเกิดปฏิกิริยาออกซิเดชันของสารตั้งต้นกลีเซอโรฟอสเฟตนั้นจะหลุดออกมาจากบริเวณเร่งของเอนไซม์ก่อนที่เอนไซม์ที่อยู่ในรูปรีดิวซ์จะทำปฏิกิริยากับออกซิเจน ผลการศึกษายังทำให้ค้นพบว่า ขั้นกำหนดอัตราเร็วของปฏิกิริยานั้นเป็นขั้นตอนการปล่อยไฮโดรเจนเปอร์ออกไซด์ซึ่งมีค่าคงที่อัตราของการเร่งปฏิกิริยาเท่ากับ 4.2 ต่อวินาทีที่อุณหภูมิ 4 องศาเซลเซียส นอกจากนั้นผลการศึกษาเชิงลึกยังทำให้ทราบว่าเอนไซม์นี้มีอยู่ด้วยกัน 2 กลุ่มที่ผสมกันอยู่โดยกลุ่มหนึ่งนั้นทำปฏิกิริยากับสารตั้งต้นได้เร็วในขณะที่อีกกลุ่มหนึ่งทำปฏิกิริยาได้ช้ากว่า และเป็นกลุ่มที่ทำปฏิกิริยาได้เร็วเท่านั้นที่เกี่ยวข้องกับการเร่งปฏิกิริยาของเอนไซม์ ที่น่าสนใจยิ่งกว่านั้นก็คือเอนไซม์ที่อยู่ในรูปรีดิวซ์นี้สามารถทำปฏิกิริยาย้อนกลับกับสารผลิตภัณฑ์ไดไฮดรอกซีอะซีโตนฟอสเฟตภายใต้สภาวะที่ไม่มีออกซิเจน ได้เป็นกลีเซอโรฟอสเฟตและเอนไซม์ที่อยู่ในรูปออกซิไดซ์ได้ นั่นแสดงให้เห็นถึงคุณสมบัติอุณหพลศาสตร์ของเอนไซม์ โดยพบว่าเอนไซม์นี้มีศักย์ไฟฟ้าของครึ่งปฏิกิริยารีดักชันเท่ากับ -167 $\pm$ 1 มิลลิโวลต์ ซึ่งต่ำกว่าค่าที่ได้จากเอนไซม์นี้จากสิ่งมีชีวิตชนิดอื่น การศึกษาค้นคว้ายังทำให้พบอีกว่าเอนไซม์นี้สามารถเร่งปฏิกิริยาโดยใช้กลีเซอรอลดีไฮด์ฟอสเฟตเป็นสารตั้งต้นได้อีกด้วยถึงแม้ว่าปฏิกิริยาจะเกิดขึ้นได้ช้ากว่าการใช้กลีเซอโรฟอสเฟตเป็นสารตั้งต้น ซึ่งจากผลการทดลองนี้เองที่ทำให้เห็นความเชื่อมโยงของเอนไซม์กลีเซอโรฟอสเฟตออกซิเดสกับกระบวนการไกลโคไลซิสรวมทั้งเมทาบอลิซึมของลิพิดและกลีเซอรอล ซึ่งจากผลการทดลองทั้งหมดที่ได้นี้น่าจะเป็นประโยชน์สำหรับการศึกษาในอนาคตเพื่อการพัฒนาตัวยาสำหรับการต้านเชื้อโรคปอดอักเสบที่เกิดจากการติดเชื้อ *Mycoplasma pneumoniae*

Keywords : L-α-glycerophosphateoxidase; flavoproteinoxidase; flavin adenine dinucleotide (FAD); transient kinetics; *Mycoplasma pneumoniae*

Introduction

L-α-glycerophosphate oxidase (GlpO) is a flavoprotein oxidase containing FAD as a cofactor. The enzyme catalyzes the oxidation of L-α-glycerophosphate (Glp)— a metabolic intermediate in lipid biosynthesis, glycolysis, and glycerol metabolism— at the C2 position to yield dihydroxyacetone phosphate (DHAP) as a product. Molecular oxygen (O_2) acts as an electron acceptor in this reaction by receiving two electrons from the substrate to generate hydrogen peroxide (H_2O_2) [1-5]. H_2O_2 is a reactive oxygen species (ROS) that can be converted to more potent reactive oxygen species such as peroxide or hydroxyl radicals and H_2O_2 itself can also serve as a cellular signaling molecule [6]. ROS can affect cell viability by causing lysis of red blood cells, lipid peroxidation, and other oxidative damage [7,8].The GlpO reaction in *Mycoplasma pneumoniae* has been shown to play a role in the virulence of the bacteria, which presents itself as infection of the human respiratory tract [4, 5, 8, 9]. It is thought that H_2O_2 produced from this reaction is involved in the pathogenicity of pneumonia.

GlpO from several bacteria have been studied. Due to its absence in mammalian cells, this enzyme has been proposed as a target for new antibiotic development [10]. Native GlpO from *Trypanosoma brucei*, a human parasite that causes an African sleeping sickness, was isolated, purified and studied with regards to its inhibition. Results indicate that suramin, melarsen oxide, salicylhydroxamic acid, 3-chlorobenzylhydroxamate, 8-hydroxyquinoline, and alkyl esters of 3,4-dihydroxybenzoate are potent inhibitors for GlpO from *T. brucei* [10-14]. GlpO from lactic acid bacteria such as *Streptococcus* sp. and *Streptococcus faecium* ATCC 12755 were also studied [2, 3]. Investigations on the inhibition of the enzyme showed that *S. faecium* GlpO could be inhibited by fructose 6-phosphate [2]. Besides oxygen, the *S. faecium* enzyme can also use other compounds such as ferricyanide and dichlorophenolindolephenol (DCPIP) as electron acceptors [3]. Studies of the recombinant GlpO from *Enterococcus casseliflavus* indicate that the reaction obeys a ping-pong kinetics model and that the flavin reduction step is the rate-limiting step for the overall turnover [15]. In contrast, kinetic studies of the wild-type GlpO from *Streptococcus* sp. and the mutant enzyme in which a flexible surface region was truncated indicate that DHAP release is the rate-limiting step of the reaction [16]. Crystal structures of both wild-type and truncated mutant of *Streptococcus* sp. GlpO at 2.4 and 2.3 Å resolution, respectively were solved. The data indicate that the active site residues in *Streptococcus* sp. GlpO that may be involved in Glp substrate binding are mostly positively charged residues such as Arg346, Lys429, His65, and Arg69 [17, 18].

In this work, the biochemical and catalytic properties of a new GlpO from *Mycoplasma pneumoniae* was investigated using steady-state and transient kinetics, and ligand binding studies. The enzyme shows several unique catalytic properties that have never been reported for other enzymes. It can catalyze a reverse flavin oxidation using the reaction product, DHAP as an electron acceptor. In contrast to previously investigated systems, the rate-limiting step of *Mycoplasma* GlpO is likely the release of H_2O_2 because other reaction steps are faster than the catalytic turnover number. Besides Glp, the enzyme can also use glyceraldehyde 3-phosphate (GAP), an intermediate in the glycolysis pathway, as a substrate, implying that the H_2O_2 generated by the GlpO reaction in *Mycoplasma pneumoniae* can be derived from lipid, glycerol and sugar metabolism.

Objectives

To investigate the kinetic mechanism of L-α-glycerophosphateoxidase (GlpO) from *Mycoplasma pneumoniae*

Experimental Procedures

Chemicals and reagents

Flavin adenine dinucleotide disodium salt hydrate (FAD), horseradish peroxidase, type I (HRP), 2,2'-azino-bis(3-ethylbenzothiazoline-6-sulfonic acid) diammonium salt (ABTS), L-α-glycerophosphatebis(cyclohexylammonium) salt (Glp), DL-glyceraldehyde 3-phosphate solution (GAP), and dihydroxyacetone phosphate dilithium salt (DHAP) were purchased from Sigma-Aldrich (St. Louis, MO, USA).Isopropyl β-D-1-thiogalactopyranoside (IPTG) was purchased from Fermentas Life Sciences (Glen Burnie, MD, USA). All chromatographic media were purchased from GE Healthcare Biosciences (Uppsala, Sweden).

The concentrations of the following compounds were determined using the known extinction coefficients at pH 7.0: ε_{450} = 11.3 $mM^{-1}cm^{-1}$ for FAD, ε_{403} = 100 $mM^{-1}cm^{-1}$ for HRP. The concentrations of Glp in the stock solutions were calculated based on the reducing equivalents in the reduction of the purified recombinant His_6-*Mp*GlpO. A solution (1 mL) of His_6-*Mp*GlpOwas prepared, made anaerobic and the concentration was determined using the molar absorption coefficient at 448 nm of 12.4 $mM^{-1}cm^{-1}$. A solution of Glp was then titrated into the enzyme solution under anaerobic conditions inside an anaerobic glovebox (<5 ppm oxygen; Belle Technology, UK). The absorbance

change at 448 nm (ΔA_{448}) of the enzyme before and after the reduction was used for calculating the concentration of the enzyme that was reduced by Glp which is equivalent to the amount of Glp added. The molar equivalent of Glp was used for calculating the concentration of the stock solution.

Spectroscopic studies

UV-Visible absorbance spectra were recorded with a diode-array spectrophotometer (Hewlett Packard, Palo Alto, CA, USA), a Shimadzu 2501PC (SHIMADZU 2501PC, Shimadzu Corp., Kyoto, Japan)or a Cary 300Bio (Varian Inc., Palo Alto, CA, USA) spectrophotometer. Steady-state and pre-steady-state kinetics studies were carried out using a stopped-flow spectrophotometer (TGK Scientific instruments, model SF-61DX2 or SF-61SX) in both single and double-mixing modes. All instruments were equipped with thermostatic cell compartments.

Enzyme assay

The activity of His_6-*Mp*GlpO was measured by monitoring the amount of H_2O_2 formed using the HRP coupled assay [31, 32]. HRP uses the H_2O_2generated from the His_6-*Mp*GlpO-catalyzed reaction to oxidize reduced ABTS to generate oxidized ABTS, which is dark green with a λ_{max} at 420 nm and a molar absorption coefficient of 42.3 $mM^{-1}cm^{-1}$ (per one mole of Glp consumed). The assay mixture in 50 mM sodium phosphate buffer, pH 7.0 typically contained 15 mM Glp, 1 mM ABTS, and 600 nM HRP. The enzyme activity was measured by monitoring the increase in absorbance at 420 nm which is due to ABTS oxidation. One unit of His_6-*Mp*GlpO activity was defined as the amount of enzyme required to oxidize one micromole of Glp per min.

Expression and purification of His_6-MpGlpO

A single colony of *E. coli* BL21(DE3)harboring the His_6-*Mp*GlpO expression plasmid, pET28a-*mpglpo*, was inoculated into 100 mL of Terrific Broth (in a 500-mL Erlenmeyer flask) containing 30 μg/mL kanamycin, and cultured overnight in a shaking incubator at 37 ^{o}C. An overnight culture with a final ratio of 1% (v/v) was inoculated into 6 × 800 mL of Terrific Broth containing 30 μg/mL kanamycin. A large-scale culture was grown at 37 ^{o}C until the absorbance at 600 nm reached ~1. The culture was then cooled down to 25 ^{o}C and induced by the addition of IPTG at a final concentration of 1 mM and maintained

at this temperature for ~12 h. Cells were harvested by centrifugation and stored at -80 ^{o}C until used.

Unless otherwise indicated, purification of the His_6-*Mp*GlpO was conducted at 4 ^{o}C. Frozen cell paste was thawed and resuspended in 50 mM sodium phosphate buffer, pH 7.0 containing 200 mM NaCl, 10% (v/v) glycerol, 10 mM imidazole, 1 mM DTT, 0.5 mM EDTA, and 100 μM PMSF. Cells were lysed by ultrasonication (Sonic Vibra_cell™ model VCX750). The disrupted cell suspension was then centrifuged at 35,000 ×g for 1 h. The supernatant was additionally clarified by ultracentrifugation at 100,000 ×g for 1.5 h and then loaded onto a Ni-Sepharose (GE Healthcare) column (2.5 × 7.0 cm; volume ~34 mL) pre-equilibrated with 300 mL of 50 mM sodium phosphate buffer, pH 7.0 containing 200 mM NaCl, 10% (v/v) glycerol and 10 mM imidazole. The column was then washed with the same buffer for 300 mL and subsequently eluted with 400 mL of a linear gradient of 10-500 mM imidazole in 50 mM sodium phosphate buffer, pH 7.0 containing 200 mM NaCl, and 10% (v/v) glycerol. Fractions containing the His_6-*Mp*GlpO were identified by measuring the absorbance at 448 nm, pooled, and concentrated using a stirred cell apparatus (Amicon® 8050) equipped with a Millipore membrane YM-10 (10 kDa cut-off). Free FAD was added during the concentration process to make sure that the enzyme fully bound to FAD. An enzyme solution of ~100 mL was then transferred into a dialysis bag (Sigma-Aldrich) and dialyzed against 4 L of 50 mM sodium phosphate buffer, pH 7.0 containing 0.5 mM EDTA for overnight. The dialyzed sample was loaded onto an SP-Sepharose (GE Healthcare) column (2.5 × 13.0 cm; volume ~64 mL) pre-equilibrated with 700 mL of 50 mM sodium phosphate buffer, pH 7.0 containing 0.5 mM EDTA and 150 mM NaCl. The column was washed with 700 mL of the same buffer and then eluted with 800 mL of a linear gradient of 150-800 mM NaCl in 50 mM sodium phosphate buffer, pH 7.0 containing 0.5 mM EDTA. Fractions containing the enzyme were identified, pooled and concentrated as described above. A solution of ~6-8 mL of the purified enzyme was desalted and exchanged into 100 mM Tris-H_2SO_4, pH 7.0 containing 0.5 mM EDTA using a Sephadex G-25 (GE Healthcare) column (1.5 × 60.0 cm; volume ~106 mL). The desalted enzyme was then aliquoted in 500 μL portions in each microcentrifuge tube and kept at -80 ^{o}C until used. The purity of the enzyme was estimated by 12% (w/v) sodium dodecyl sulfate-polyacrylamide gel electrophoresis. The protein amount was determined using a Bradford method and BSA as a standard protein.

Determination of molar extinction coefficients of His_6-MpGlpO-bound FAD

The methods for the determination of the molar absorption coefficients of His_6-*Mp*GlpO-bound FAD were slightly modified from a general procedure [33]. The frozen purified enzyme was quickly thawed and exchanged into 50 mM sodium phosphate buffer, pH 7.0 using a PD-10 column (GE Healthcare). The holoenzyme solution (900 μL) was added 100 μL of 20% (w/v) SDS solution to give a final absorbance value of the enzyme of ~0.25 and a final SDS concentration of 2% (w/v). The same buffer (100 μL) was added to another aliquot of holoenzyme (900 μL). The absorption spectra of both solutions were recorded and compared. The concentration of released FAD was calculated based on the FAD molar extinction coefficient of 11.3 $mM^{-1}cm^{-1}$ at 450 nm. For the holoenzyme, the molar extinction coefficient at 448 nm (λ_{max}) can be determined according to Eqn 1, on the basis that the apoenzyme binds FAD with a ratio of 1:1 mol. A_{enzyme} represents enzyme absorbance while A_{FAD} represents FAD absorbance.

$$\varepsilon_{enzyme} = \frac{A_{enzyme}}{A_{FAD}} x \varepsilon_{FAD} \qquad (1)$$

Steady-State Kinetics

Two-substrate steady-state kinetics of the His_6-*Mp*GlpO was carried out in 50 mM sodium phosphate buffer, pH 7.0 at 4°C using an ABTS coupled-enzyme assay as previously described [34] and monitored by the Hi-Tech Scientific model SF-61DX stopped-flow spectrophotometer in single-mixing mode. The optical pathlength of the observation cell was 1 cm. A mixture of 5.16 nM His_6-*Mp*GlpO, 600 nM HRP, and 1 mM ABTS was mixed against solutions of various concentrations of Glp (4, 8, 16, and 32 mM) and oxygen (0.13, 0.26, 0.44, 0.65, 1.16 mM). The reaction progress was followed by monitoring the increase of absorbance at 420 nm at which the oxidized ABTS absorbs with the molar extinction coefficient of 42.3 $mM^{-1}cm^{-1}$ (per one mole of Glp consumed) [31, 32]. Kinetic traces obtained from each reaction (performed in triplicate) were calculated their initial rates using Program A (developed by Chun-Jen Chiu, Rong Chang, Joel Dinverno, and David P. Ballou at the University of Michigan, Ann Arbor, MI). The initial rates were then analyzed for steady-state kinetic parameters of a bi-substrate enzyme reaction according to either a double-reciprocal plot of a ping-pong mechanism (Eqn 2) [35] or a direct plot (Eqn 3) using the EnzFitter program (BIOSOFT, Cambridge, UK).

Apparent steady-state kinetics of the His_6-*Mp*GlpO reaction was performed in air-saturated (oxygen concentration of ~0.26 mM) 50 mM sodium phosphate buffer, pH 7.0 at 25 ^{o}C at various concentrations of DL-glyceraldehyde 3-phosphate (GAP) (0.025-6.4 mM) using the coupling assay with horseradish peroxidase-coupled assay. The reactions were monitored at 420 nm as described above. The initial rates were calculated and then plotted *versus* GAP concentration. Apparent kinetic parameters were calculated using Marquardt-Lavenberg algorithms in the KaleidaGraph program version 4.0 and compared to the reaction using various concentrations of Glp (0.1-51.2 mM) under the same conditions.

$$\frac{e}{v} = \phi_0 + \frac{\phi_A}{[A]} + \frac{\phi_B}{[B]} \quad (2)$$

$$v = \frac{V[A][B]}{K_B[A] + K_A[B] + [A][B]} \quad (3)$$

Binding of the oxidized His_6-MpGlpO with products

A solution (1 mL) of the oxidized enzyme (A_{448} ~0.3; 24 μM) in 50 mM sodium phosphate buffer, pH 7.0 was placed in both sample and reference cells. Then, a baseline was recorded. Various concentrations of H_2O_2 (0.16-371 mM) or DHAP (0.005-30 mM) were added into the enzyme solution in the sample cell while an equal volume of buffer was added into the reference cell. An absorption spectrum was recorded after each titration using a double-beam spectrophotometer. The changes in absorbance were plotted against the concentrations of each product. Dissociation constants for the binding of products to the oxidized enzyme were determined and analyzed according to the method previously described [36] and Eqn 4, where ΔA represents the absorbance change, ΔA_{max} is the maximum absorbance change, $[L]_{free}$ is a concentration of free ligand, and K_d is a dissociation constant for enzyme-ligand complex. The analysis was done using Marquardt-Lavenberg algorithms in the KaleidaGraph program version 4.0. Similar protocol and data analysis were also applied for spectrophotometric titration of the FAD solution (A_{450} ~0.3) with H_2O_2 using a similar range of concentrations. For the binding of enzyme with other substrate analogues—glycerol, L-lactate, and D,L-malate—the reactions and analysis were performed and carried out as mentioned above, except that the concentrations of glycerol, L-lactate, and D,L-malate used were varied from 0.16-371 mM.

$$\frac{\Delta A}{\Delta A_{max}} = \frac{[L]_{free}}{K_d + [L]_{free}}$$

(4)

Binding and reaction of the reducedHis$_6$-MpGlpO with DHAP

A solution (1 mL) of the oxidized enzyme (A_{448} ~0.3; 24 μM) in 50 mM sodium phosphate buffer, pH 7.0 was placed in an anaerobic glove box in which the oxygen concentration was less than 5 ppm (Belle Technology, UK) to remove trace amounts of oxygen and then reduced by a stoichiometric concentration of dithionite under anaerobic conditions. Various concentrations of DHAP (0.69-4,308 μM) were subsequently added to the reduced enzyme. All concentrations reported above are final concentrations after mixing. A spectrum after each titration was recorded by a GeneQuant1300spectrophotometer (GE Healthcare, UK) residing in the anaerobic glove box. The spectrum of reduced enzyme was subtracted from all the spectra obtained from each titration to give the change in absorbance (ΔA).Analysis was done according to the method previously described [36].

As the results indicate that the reverse reaction of the reduced enzyme and DHAP can occur, the kinetics of the enzyme re-oxidation by DHAP was further explored using stopped-flow spectrophotometry at 4 °C. The reduced enzyme (16 μM) in 50 mM sodium phosphate buffer, pH 7.0 was mixed with various concentrations of DHAP (0.1-12.8 mM) under anaerobic conditions using a single-mixing mode of a stopped-flow apparatus. All concentrations shown above are given as final concentrations after mixing. The reactions were monitored at 448 nm and the final spectra after the reaction were recorded. Kinetic traces were analyzed by Program A and the observed rate constants (k_{obs}) were plotted *versus* DHAP concentrations. The plots were analyzed according to Eqn 5, where k_1 is a bimolecular rate constant for the reduced enzyme re-oxidation.

$$k_{obs} = k_1 \cdot [\mathrm{DHAP}] \qquad (5)$$

Measurement of the standard reduction potential of His$_6$-MpGlpO

Standard reduction potential of His$_6$-*Mp*GlpO was measured in 50 mM sodium phosphate buffer, pH 7.0 at 25 °C by Massey's method using the xanthine/xanthine oxidase reduction system with benzyl viologen as an electron mediator [37]. The reference dye used for measuring the standard reduction potential of His$_6$-*Mp*GlpO was cresyl violet which has a standard reduction potential (E_m^0) value of -166 mV [38]. A

solution mixture of dye (A_{519} ~0.3) and the oxidized enzyme (A_{448} ~0.3; 24 μM), benzyl viologen (5.3 μM), and xanthine (0.5 mM) in 50 mM sodium phosphate buffer, pH 7.0 was placed in an anaerobic cuvette and made anaerobic by purging with oxygen-free nitrogen for 10-12 cycles to evacuate trace amounts of oxygen. The spectrum of the oxidized species was then recorded. The anaerobic solution was then tipped into xanthine oxidase (10 nM) from the cuvette sidearm and the spectral changes were recorded. All concentrations shown above are as after mixing. The enzyme and dye were slowly reduced (>8 hr) so that the reduction process was under equilibrium. The reduction potentials of enzyme (E_e) and dye (E_d) were determined according to Eqns 6 and 7, respectively, in which E_{red} and E_{ox} are the concentrations of the reduced and oxidized enzyme, respectively, D_{red} and D_{ox} are the concentrations of the reduced and oxidized dye, respectively, E_e^0 and E_d^0 are the standard reduction potential values of enzyme and dye, respectively, and n_e and n_d are the numbers of electrons involved in the reduction process. At equilibrium, the value of E_e is equivalent to E_d and Eqns 6and 7 can be rearranged to Eqn8 which can be used for determining the E_e^0 value. After the complete reduction, the absorbance at 407 nm (isobestic point of a reference dye) and 540 nm were used for calculating the concentrations of the oxidized enzyme (E_{ox}) and the reduced dye (D_{red}) during the reduction process, respectively. The concentrations of reduced and oxidized enzyme (E_{red}) and dye (D_{ox}) at different points of the reduction process were analyzed with Eqn 8 to determine the standard reduction potential value (E_e^0) of the enzyme.

$$E_e = E_e^0 - \frac{0.0592}{n_e}\log(E_{red}/E_{ox}) \quad (6)$$

$$E_d = E_d^0 - \frac{0.0592}{n_d}\log(D_{red}/D_{ox}) \quad (7)$$

$$\log(E_{red}/E_{ox}) = \frac{n_e(E_e^0 - E_d^0)}{0.0592} + (n_e/n_d)\log(D_{red}/D_{ox}) \quad (8)$$

Reductive half-reaction of His_6-MpGlpO

A solution of anaerobic oxidized enzyme (~28 μM; A_{448} ~0.35) in 50 mM sodium phosphate buffer, pH 7.0 containing 0.5 mM EDTA, and 1 mM DTT was mixed with various concentrations of Glp (0.2-51.2mM) under anaerobic conditions using the stopped-flow spectrophotometer at 4 ^{o}C. All concentrations shown are as after mixing.

Kinetics of the enzyme reduction was monitored by the absorbance change at 448 nm. The kinetic traces were analyzed by Program A to obtain observed rate constants from each exponential phase. The observed rate constants obtained were plotted *versus* Glp concentrations. The results were then analyzed with Eqn9, where k_{obs} is the observed rate constants, k_{max} is the rate constant for flavin reduction (k_{red}), S is Glp concentration, and K_d is the dissociation constant for substrate binding. The analysis was carried out using Marquardt-Lavenberg algorithms in KaleidaGraph program version 4.0.

$$k_{obs} = \frac{k_{max} \cdot [S]}{K_d + [S]} \qquad (9)$$

Oxidative half-reaction of His_6-MpGlpO

The anaerobically oxidized enzyme (~28 μM; A_{448} ~0.35) in 50 mM sodium phosphate buffer, pH 7.0 containing 0.5 mM EDTA, and 1 mM DTT was titrated stoichiometrically with Glp to yield the reduced enzyme. The reduced enzyme was then mixed with various concentrations of oxygen (0.13, 0.32, 0.61, 1.03 mM) using a stopped-flow spectrophotometer at 4°C. All concentrations shown are as after mixing. The kinetics of enzyme oxidation was monitored by absorbance at 448 nm. The kinetic traces were analyzed by Program A to obtain the observed rate constants. The plots of k_{obs} as a function of oxygen concentrations were analyzed using Eqn9, in which k_{max} is the rate constant for flavin oxidation (k_{ox}), S is oxygen concentration, and K_d is the dissociation constant for oxygen binding. The analysis was carried out using Marquardt-Lavenberg algorithms in KaleidaGraph program version 4.0.

Reactions of the Glp-reduced His_6-MpGlpO with O_2 in a double-mixing mode

Double-mixing stopped-flow experiments were done to evaluate whether the presence of DHAP can affect the oxygen reaction. An anaerobic solution of the oxidized His_6-*Mp*GlpO (91 μM) in Syringe A was mixed first with Glp (91 μM) in Syringe B. The reactions were aged for 100 s to allow the enzyme reduction to proceed. The solution from the first mixing was later mixed with various concentrations of oxygen (0.26, 0.61, 1.03, 2.06 mM) in 50 mM sodium phosphate buffer, pH 7.0 in the second mix. The reactions were monitored at 448 nm with a double-mixing mode stopped-flow spectrophotometer (Hi-Tech Scientific Model SF-61DX). All concentrations shown are initial concentrations before mixing. The kinetic traces were analyzed by Program A and the k_{obs} values of individual phases were plotted *versus* oxygen concentration. The plots

were analyzed according to Eqn 9 using Marquardt-Lavenberg algorithms in KaleidaGraph program version 4.0. Results of this reaction were compared to the results of single-mixing mode oxidative half-reaction experiments previously described.

Reactions of the dithionite-reduced His_6-MpGlpO with O_2 in the presence of DHAP

An anaerobic solution of the dithionite-reduced His_6-*Mp*GlpO (91 μM) in Syringe A was mixed first with DHAP (136.5 μM) in Syringe B at various age times (10, 20, 100, and 200 s). The solution mixture was then mixed with oxygen (0.26 mM) in 50 mM sodium phosphate buffer, pH 7.0 in the second mix. The reactions were monitored at 448 nm by double-mixing mode stopped-flow experiments. All concentrations shown are initial concentrations before mixing. The kinetic traces were analyzed by Program A and the kinetics results at various age times were compared to the results obtained from the oxidative half-reaction in the absence of DHAP.

Results

Preparation and spectroscopic properties of His_6-MpGlpO

Recombinant His_6-*Mp*GlpO was successfully expressed as a soluble enzyme in *E. coli*BL21(DE3) cells cultured in Terrific Broth and induced by IPTG at 25 ^{o}C. The yield of cell paste was about 17 g per 1liter of cell culture. His_6-*Mp*GlpO was purified to homogeneity using Ni-Sepharose affinity and SP-Sepharose cation-exchange chromatography as described in Experimental Procedures. This protocol resulted in ~19 mg of purified enzyme with a specific activity of ~10 U/mg per 1 liter of cell culture (Table 1). A low yield of the enzyme preparation was due to the protein loss during the last step (SP-Sepharose chromatography). This step was used because it could remove impurities that were retained after Ni-Sepharose chromatography. SDS-PAGE (12%) analysis indicated that the enzyme is >95% pure and that the subunit molecular mass was about 43 kDa (data not shown). The purified enzyme exhibited spectral characteristics typical of FAD-bound enzyme with a maximum absorbance at 448 nm (solid line of Fig. 1). The molar absorption coefficient was determined according to the protocol described in Experimental Procedures as 12.40 ± 0.03 $mM^{-1}cm^{-1}$, which is slightly different from a molar absorption coefficient of free-released FAD (11.3 $mM^{-1}cm^{-1}$) (dashed line of Fig. 1).

Steady-state kinetics of His_6-MpGlpO

The two-substrate steady state kinetics of His_6-*Mp*GlpO using Glp and O_2 as substrates was investigated at 4 °C, pH 7.0 using the 2,2'-azino-bis(3-ethylbenzothiazoline-6-sulphonic acid)-horse radish peroxidase (ABTS-HRP) coupled assay system as described in Experimental Procedures. Initial rates of reactions at various concentrations of Glp and O_2were measured. A double-reciprocal plot of initial rates and concentrations, e/V_o *versus* 1/[Glp] (Fig. 2A) or 1/[O_2] (Fig. 2B), showed parallel lines, indicating that the His_6-*Mp*GlpO reaction uses a ping-pong mechanism. Steady-state kinetic parameters of the enzyme reaction that were obtained from reciprocal (Eqn 2) or direct plots (Eqn 3) were similar: K_m^{Glp}, 5.5 ± 0.4 mM; $K_m^{O_2}$, 55±8μM; and k_{cat}, 4.2 ± 0.1 s^{-1} at 4 °C. The results indicated that the steady-state turnover number of GlpO from *M. pneumoniae* is about 4- and 9-fold lower than that of GlpO from *Streptococcus* sp. (18 s^{-1}) and *Enterococcus casseliflavus* (37 s^{-1}), respectively [15, 16].

Standard reduction potential value of His_6-MpGlpO

The standard reduction potential value of His_6-*Mp*GlpO was measured by Massey's method using cresyl violet as a reference dye. Spectra obtained during the reduction (Fig. 1B) indicated that the enzyme was completely reduced via a two-electron reduction process using the benzyl viologen-mediated xanthine/xanthine oxidase system. Concentrations of the oxidized enzyme and the reduced dye were calculated based ontheir absorbance at 407 and 540 nm, respectively. The standard reduction potential value (E_e^0) of the enzyme was calculated from the y-intercept of the plot of log(E_{red}/E_{ox}) *versus* log(D_{red}/D_{ox}) as -167 ± 1 mV (Inset of Fig. 1B).

Kinetics of the reduction of His_6-MpGlpO by Glp

A solution of the oxidized enzyme (~28 μM after mixing) in 50 mM sodium phosphate buffer, pH 7.0 containing 0.5 mM EDTA, and 1 mM DTT was mixed with various concentrations of Glp under anaerobic conditions, and the kinetics of enzyme reduction was monitored by the change in absorbance at 448 nm using a stopped-flow spectrophotometer at 4 °C. Kinetic traces shown in Fig. 3A indicate that flavin reduction shows biphasic kinetics in which the amplitude change of the first (fast) phase varied from 10-70% (relative to total flavin reduction) while the second (slow) phase was from 90-30% upon increasing the concentration of Glp. This indicates that there are two distinct populations of the oxidized enzyme that are slowly interconverted. The k_{obs} values obtained from both phases are hyperbolically dependent on Glp concentration (Figs. 3B and 3C). According to the plots, the reduction rate constants (k_{red}) were

determined as 199 ± 34 and 2.08 ± 0.01 s^{-1}, respectively. Because k_{obs} of both phases were hyperbolically dependent on substrate concentration (Figs. 3B and 3C), the data suggest that each of the oxidized enzyme forms reacts with Glp via a two-step reduction process in which a binary complex of the oxidized enzyme and its substrate is initially formed in the first step, followed by flavin reduction in the second step(Fig. 3E). These data indicate that the substrate binding affinity of the fast reacting species (K_d = 72 ±18mM) is 52-fold lower than that of the slow reacting enzyme (K_d = 1.38 ± 0.02mM).As at the highest concentration of Glp where both populations of enzyme can react with Glp rapidly, the amplitude ratio of fast:slow species is 70:30, the data indicate that a ratio of fast to slow species under equilibrium is 70:30. This conclusion is also supported by the results of the oxidative half-reaction (see the following section). We also noted that a clear amplitude change ratio of 70:30 could only be observed when the k_{obs} value of the fast reacting species is ≥16 s^{-1}. These results also imply that k_f+ k_r of the interconversion process between the fast and slow reacting species is <16 s^{-1}(Fig. 3E).

Kinetics of the reaction of reduced His_6-MpGlpO with O_2

An anaerobic solution of the reduced enzyme (~28 μM after mixing) in 50 mM sodium phosphate buffer, pH 7.0 containing 0.5 mM EDTA, and 1 mM DTT was mixed with buffer containing various concentrations of oxygen. The kinetics of enzyme oxidation was monitored by measuring the absorbance at 448 nm using a stopped-flow spectrophotometer at 4 °C. Kinetic traces for enzyme oxidation are biphasic (Fig. 4A)in which the amplitude change for the first (fast) phase reflects 70% of the total amount of flavin oxidation while the second (slow) phase is about 30%.Some fraction of the fast reacting enzyme was oxidized during the dead-time period. Kinetic analyses indicate that the k_{obs} values of the first phase and second phase *versus* the oxygen concentration are hyperbolic, with rate constant values for the fast and slow reacting species of 627 ± 81 and 85 ± 11 s^{-1}, respectively (Figs. 4B and 4C). The hyperbolic plots obtained for the k_{obs} values *versus* oxygen concentration suggest that the re-oxidation occurs via a two-step process. The reduced enzyme may form a binary complex with O_2prior to flavin re-oxidation in the second step. According to the plots shown in Figs. 4B and 4C,the K_d values for binary complex formation were 1.3 ± 0.2 and 0.5 ± 0.1 mM for the fast and slow reacting enzyme species, respectively. Similar to the reductive half-reaction, the ratio of amplitude of fast to slow reacting species is

70:30. The amplitude changes observed due to the fast and slow reacting species was clearly separated at all oxygen concentrations employed because all k_{obs} values were greater than 16 s^{-1}(the lowest k_{obs} value in Fig. 4C is 17.6 s^{-1}). The kinetic mechanism of the oxidative half-reaction is summarized in Fig. 4D.

Effects of DHAP on the oxidative half-reaction of His_6-MpGlpO

Previous studies of the reductive half-reaction (Fig. 3A) indicated that the reduction of enzyme by Glp is a fast process in which DHAP release cannot be detected in the stopped-flow experiments. In this experiment, we used double-mixing stopped-flow experiments (see Experimental Procedures) to investigate if DHAP can bind to the reduced enzyme by monitoring the influence of DHAP on the oxidative half-reaction. The reduced enzyme was mixed with an equal concentration of Glp and aged for 100 s (to ensure complete reduction) in the first mixing step. The DHAP-bound reduced enzyme was then mixed with various concentrations of O_2 in the second mixing step and the enzyme re-oxidation was followed by monitoring the absorbance at 448 nm, similar to the experiments in Fig. 4A. The kinetic traces obtained from the change in absorbance at 448 nm shown in Fig. 5A display biphasic kinetic and amplitude changes for the first (70%) and second (30%) phases similar to those observed for the oxidative half-reaction carried out using the single-mixing mode in Fig. 4A(Fig. 5A). Kinetic analyses also indicate that the k_{obs}values for both phases and the rate constants for enzyme oxidation (k_{ox} = 524 $\pm$ 34 s^{-1}(Fig. 5B) and 107 $\pm$ 5 s^{-1}(Fig. 5C)), are similar to those obtained from Fig. 4 (627 $\pm$ 81 s^{-1}(Fig. 4B) and 85 $\pm$ 11 s^{-1}(Fig. 4C)). The similarities in the kinetic results obtained by the two different mixing modes suggest that after the enzyme was reduced by Glp, the DHAP formed was quickly released prior to the reaction of the reduced enzyme with oxygen.

To verify our hypothesis, the reduced enzyme (91 μM before mixing) plus DHAP (136.5 μM before mixing) was incubated for various aging times in the first mixing step. The solution was then mixed with buffer containing oxygen at 0.26 mM (before mixing) in the second mixing step to allow the re-oxidation of enzyme to occur while the progression of the reactionwas monitored by measuring the absorbance change at 448 nm. Analyses of the kinetic traces (Fig. 5D) indicated that the k_{obs} values and the amplitude changes obtained from various age times were similar and also similar to those obtained from the previous results (Fig. 5A). These data again suggest that DHAP does not tightly bind to the enzyme but rather, was quickly released after its formation.

All results indicate that the reaction of His_6-*Mp*GlpO occurs via a true ping-pong mechanism.

Product binding and the reverse oxidation of reduced His_6-MpGlpO by DHAP

Both the oxidized and reduced forms of the enzyme were tested for their ability to bind various ligands by detecting their absorbance signal changes (Experimental Procedures). For the binding of the oxidized enzyme and H_2O_2, a solution of oxidized enzyme (24 μM) was titrated in various concentrations of H_2O_2. The difference spectra (data not shown) indicated a maximum absorbance change at 385 nm. The equilibrium dissociation constant (K_d) determined from measurements at 385 nm for the binding of H_2O_2 to the oxidized enzyme was determined as 0.4 $\pm$0.2 mM. The same experiment was also performed using DHAP at various concentrations. The difference spectra obtained did not show any clear signal due to the binding of oxidized enzyme and DHAP. The large absorption increase at shorter wavelengths was likely due to DHAP absorption (data not shown). As H_2O_2 can bind to the oxidized enzyme, H_2O_2 release from the enzyme may be a rate-limiting step for the overall catalytic turnover of the enzyme reaction.

Results from the addition of DHAP at various concentrations to the reduced His_6-*Mp*GlpO (24 μM) indicate that the reduced enzyme can be re-oxidized by DHAP (Fig. 6A), suggesting that the reduction of His_6-*Mp*GlpO by Glp is reversible. Therefore, the kinetics of re-oxidation of the reduced enzyme with DHAP was investigated by monitoring the absorbance change at 448 nm using single-mixing mode stopped-flow spectrophotometry (Experimental Procedures). The kinetic traces at 448 nm (Fig. 6B) showed biphasic kinetics with majority of absorbance increase in the second phase. Kinetic analyses showed that the k_{obs} values obtained from the first phase were independent of DHAP concentration with values ~6 s^{-1}(Fig. 6C), while those obtained from the second phase are linearly dependent on DHAP concentration with a bimolecular rate constant of 56.5 $M^{-1}s^{-1}$(Fig. 6D). As the first reaction of reduced GlpO and DHAP is a bimolecular reaction in which the rate constants should be linearly dependent on DHAP, these results suggest that the rate constant (6 s^{-1}) observed in the first phase likely belongs to the step following the bimolecular reaction. Due to its greater value than the k_{obs} values of the bimolecular reaction of reduced enzyme and DHAP, this step appeared at the first phase even though it in fact occurs after the initial bi-molecular reaction (rate-switching phenomenon, [19]). The kinetic model of the

reaction of reduced enzyme with DHAP to form the oxidized enzyme and Glp is shown in Fig. 6E.

Overall catalytic reaction of His_6-MpGlpO

Based on the results of transient and steady-state kinetic studies shown in Figs. 2-4, the overall reductive and oxidative half-reactions of His_6-*Mp*GlpO can be summarized as shown in Fig 7. Both half-reactions showed evidence supporting the presence of a mixture of fast and slow reacting enzymes, present at a molar ratio of 70:30. As the overall k_{cat} derived from the steady-state kinetic measurements was 4.2 s^{-1} and the k_{red} value of the slow reacting species (upper path, Fig. 7) was 2.08 $\pm$ 0.01 s^{-1}(Fig. 3C), the results indicated that primarily, only the fast reacting species is involved in the reductive half-reaction during the catalytic turnover. Because all of the rate constants measured had greater values than the k_{cat}, we propose that the rate-limiting step is associated with product release. As the results from the double-mixing experiments in Fig. 5 indicated that DHAP release is rapid, we thus propose that the release of H_2O_2 is the rate-limiting step of the overall reaction.

Data obtained from the reverse reaction of His_6-*Mp*GlpO are useful for assigning the rate constants in the reductive half-reaction. The results in Figs. 6C and 6D were used to assign rate constants for the bimolecular reaction between reduced enzyme and DHAP as 56.5 $M^{-1}s^{-1}$ and for the dissociation of Glp from the E_{ox}:Glp binary complex as 6 s^{-1}(red arrows in Fig. 7). As the reverse reaction (Figs. 6) only showed ~80% of the reduced enzyme oxidation at the end, the data imply that only the reaction of fast reacting species was observed (rate 56.5 $M^{-1}s^{-1}$, red arrow of Fig. 7). This suggests that the rate constant of 6 s^{-1} is likely k_2 of the first step in Fig. 7. Therefore, based on aK_d value of 72mM (the first step), k_1 can be calculated as 83.3 $M^{-1}s^{-1}$.

Glyceraldehyde 3-phosphate can be used as a substrate for the His_6-MpGlpO reaction

As the previous report showed that a significant amount of H_2O_2 could be generated in *M. pneumoniae* when glucose (0.1 mM) was used as a sole carbon source [5] and the structure of GAP (an intermediate in the glycolytic pathway) is similar to Glp, we investigated whether GlpO can use GAP as a substrate. Apparent steady state kinetics of the His_6-*Mp*GlpO reaction using GAP as a substrate under air-saturation (0.26 mM) was measured. The reactions were carried out at 25 ^{o}C, pH 7.0 using the same ABTS-HRP assay at various concentrations of GAP (0.025-6.4 mM) (Experimental

Procedures).The results show that GAP can be used as a substrate for His_6-*Mp*GlpO. Initial rates were directly plotted as a function of GAP concentration (Fig. 3D). For comparison, similar reactions with Glp as a substrate were carried out under the same conditions. The results clearly indicate that His_6-*Mp*GlpO can use GAP as a substrate. The apparent steady-state kinetic parameters were as follows: K_m^{GAP}, 1.8 ± 0.2 mM;k_{cat},0.6 s^{-1}, and k_{cat}/K_m, 0.33 $mM^{-1}s^{-1}$. When compared to the kinetic parameters of Glp, it is quite clear that the enzyme prefers to use Glp as a substrate because the k_{cat} and k_{cat}/K_m of the Glp reactions are 100- and 15-fold larger than those of the GAP reactions, respectively (Inset of Fig. 13) (K_m^{Glp}, 12 ± 1 mM; k_{cat},60.1 s^{-1}, and k_{cat}/K_m,5 $mM^{-1}s^{-1}$).Nevertheless, our data imply that in the absence of glycerol, GAP may serve as a substrate in the GlpO reaction to supply H_2O_2 during mycoplasma infection.

Ligand Binding

The bindings of the oxidized enzyme with other ligands (glycerol, L-lactate, and DL-malate) were investigated to gain the understanding on the active site specificity. Results indicate that only the binding of the oxidized enzyme with L-lactate and DL-malate, not glycerol, can give clear spectroscopic changes (data not shown). The K_d values of the binding of the oxidized enzyme and L-lactate calculated from absorbance changes at 401 and 489 nm are 23 ± 4 and 26 ± 4 mM, respectively. For the binding of enzyme and DL-malate, the K_d value determined based on absorbance changes at 440 nmis 10 ± 5 mM. These data suggest that enzyme can bind to these substrate analogues but with low affinity.

Discussion

Our work herein reports on the biochemical and catalytic properties of the recombinant GlpO from *Mycoplasma pneumoniae*. The enzyme is unique among all GlpO enzymes for its ability to catalyze the reverse reaction of reduced enzyme and DHAP. The results also showed that besides Glp, GlpO can also use GAP as a substrate. His_6-*Mp*GlpO was successfully expressed in a soluble form in *E. coli*, giving a protein yield of around 19 mg/L cell culture. The purified enzyme has a specific activity of about 10 U/mg, and exhibits biochemical properties similar to other flavoprotein oxidases. The His_6-*Mp*GlpO-bound FAD has a maximum absorption at 448 nm with a molar extinction coefficient of 12.40 $mM^{-1}cm^{-1}$(Fig. 1A). These values are slightly different from those of free FAD (11.3$mM^{-1}cm^{-1}$ at 450 nm) [20], and GlpO from *Streptococcus faecium* (11.3 $mM^{-1}cm^{-1}$ at 446nm) [3] and *Streptococcus* sp. (11.2 $mM^{-1}cm^{-1}$ at 449 nm) [16].

Unlike other GlpO enzymes previously investigated such as the enzyme from *S. faecium* [3], His_6-*Mp*GlpO can catalyze the reverse reaction of reduced enzyme and DHAP. This catalytic property of His_6-*Mp*GlpO may represent a control mechanism to prevent excessive generation of H_2O_2, which may be harmful to bacterial cells. Based on the rate constants determined in Fig. 7 and Table 2, the data indicate that the rate constants of the forward reaction (black arrows) are much greater than the reverse reaction (red arrows). Therefore, the reverse reaction can only occur at very high DHAP concentrations. Similar to GlpO, another flavoenzyme mandelate dehydrogenase (MDH) was also reported to catalyze the reverse flavin oxidation by the product [21].

The ability of His_6-*Mp*GlpO to accept electrons from DHAP can also be explained by the reduction potential (E_m^0) of enzyme-bound FAD (FAD/$FADH_2$). The E_m^0 value of His_6-*Mp*GlpO (Fig. 1B) was calculated as -167 $\pm$ 1 mV which is lower than the value of GlpO from *Enterococcus casseliflavus* (-118 mV) [15]. With the reduction potential of DHAP/Glp of -190 mV, the change of the standard reduction potential ($\Delta E^{o'}$) for the forward reaction of His_6-*Mp*GlpO (FAD + Glp$\longrightarrow$ $FADH_2$ + DHAP) is +23 mV, which corresponds to a standard free-energy change ($\Delta G^{o'}$) of -4.44 kJ/mol. Based on these parameters, Glp can favorably reduce the His_6-*Mp*GlpO-bound FAD and the reverse reaction can occur at high concentrations of DHAP (such as those used in Fig. 6A). For GlpO from *E. casseliflavus* that has an E_m^0 value of -118 mV, the thermodynamics of the forward reduction reaction of this enzyme is more heavily favored than the reverse reaction. The reverse reaction of FAD oxidation by DHAP would require much higher concentrations of DHAP than those employed in the previous investigation [3].

Steady-state kinetic analysis of the His_6-*Mp*GlpO reaction using Glp and O_2 as substrates indicates that the reaction obeys ping-pong kinetics with a turnover number (k_{cat}) of 4.2 s^{-1}(Fig. 2). This k_{cat} value is 4- and 9-fold lower than those of GlpO from *Streptococcus* sp. (18 s^{-1}) [16] and *E. casseliflavus* (37 s^{-1}) [15] under the same pH (7.0) and temperature (4-5 ^{o}C), respectively. These enzymes also use a ping-pong mechanism for their reactions. The K_m value for Glp in the His_6-*Mp*GlpO reaction is 5.5 mM, which is about 4-fold lower and 3-fold higher those of GlpO from *E. casseliflavus* (24 mM) [15] and *Streptococcus* sp. (2 mM) [16], respectively. However, these enzymes have K_m values of O_2 in the same range. The K_m of oxygen for His_6-*Mp*GlpO is 55 μM while those for the enzymes from *E. casseliflavus* and *Streptococcus* sp. are 35 μM and 52 μM, respectively [15, 16].

As for the relevance of these kinetic parameters under physiological conditions, the K_m value for Glp in the *M. pneumoniae* GlpO reaction (5.5 mM) is much higher than the physiological concentration of Glp in *M. pneumoniae* (~0.1 mM). The K_d value of the fast reacting (72 mM) that was obtained from half-saturation of k_{obs} is also much higher than the range of Glp physiological concentration. We estimated the physiological concentration of Glp based on the concentration of glycerol present in the host blood serum [5, 8] because a previous investigation on glycerol and Glp uptake in *M. mycoides* SC showed that only glycerol, not Glp, could be taken up into the cells. Glycerol can be converted to Glp by intracellular glycerol kinase [22]. Altogether, these data imply that under physiological conditions, GlpO only functions at a slow rate (turnover$\approx$0.72 s^{-1}).

Our investigation also suggests that besides its physiological substrates, His_6-*Mp*GlpO can use GAP as an electron donor (Fig. 3D), although with the k_{cat} value ~100-fold lower than Glp. These results suggest that GAP, a metabolic intermediate in the glycolysis pathway, may also be involved in H_2O_2 production during mycoplasma infection. Therefore, GlpO can be viewed as an enzyme that can employ substrates from three metabolic pathways (the glycerol and lipid metabolic pathways, and glycolysis) for the generation of the reactive oxygen species necessary for the virulence of *M. pneumoniae*. His_6-*Mp*GlpO can use a variety of compounds such as 2,6-dichlorophenol indole phenol (DCPIP), phenazinemethosulfate (PMS) and menadione as electron acceptors (data not shown). This is similar to GlpO from *S. faecium* that can use ferricyanide and DCPIP as electron acceptors [3]. These data imply that if oxygen is not readily available in the cells, the GlpO reactions may mediate the transfer of electrons from Glp or GAP to other mediators such as quinones for cell energy production.

Investigation of binding of His_6-*Mp*GlpO with ligands gives insight into specificity of the active site. Our data indicate that His_6-*Mp*GlpO can bind L-lactate and DL-malate, but not glycerol. Previous study of GlpO from *S. faecium* ATCC12755 also showed that the enzyme could be inhibited by fructose 6-phosphate [2].These results suggest that the interaction between the anionic moiety of ligand with the enzyme active site is important for the ligand anchorage. Previous structural analysis of a truncated form of GlpO from *Streptococcus* sp. (*Ssp*GlpOΔ) [18] indicates that the Glp-binding pocket of *Ssp*GlpOΔ is formed by various positively charged residues such as Lys429, His65, Arg69, and Arg346. The Arg346 in *Ssp*GlpOΔ is equivalent to Arg302 in glycine oxidase (ThiO) and Arg285 in yeast D-amino acid oxidase (DAAO) [18]. The

guanidinium side chain of Arg in these enzymes interacts with a carboxylate group of amino acid substrates. Concurrent with the work in this report, the X-ray structures of His_6-*Mp*GlpO in both oxidized and reduced forms were solved at 2.4 and 2.5 Å resolutions, respectively. More details about His_6-*Mp*GlpO structure and interactions with ligands can be found in[23].The currently available structures suggest that Arg320 of *Mp*GlpO is important for substrate recognition because its guanidinium side chain shows electrostatic interaction with the phosphate moiety of Glp. The data also show that the α-carboxyl moiety of Gly259 and β-hydroxyl moiety of Ser348 can make a hydrogen bond interaction with the C1-OH and C2-OH of Glp, respectively. His51 is located at the position in which it can act as a base to deprotonate the C2-OH of Glp to initiate the hydride transfer for the flavin reduction [23].These residues are also likely to be important for providing the protein-ligand interaction with GAP.

A mixture of fast and slow reacting species observed in the reaction of His_6-*Mp*GlpO was also observed in GlpO from *E. casseliflavus* (*Ec*GlpO) [15] and *Streptococcus* sp. (*Ssp*GlpO) [16]. For *Ec*GlpO reduction, the first (fast) phase was hyperbolically dependent on Glp concentration with a limiting k_{red} value of 48 s^{-1}, while the second (slow) phase was independent of Glp concentration with invariable rate constant values of 3.6-5.4 s^{-1}[15]. In contrast to His_6-*Mp*GlpO and *Ec*GlpO, the first (fast) phase of the *Ssp*GlpO reduction reaction is linearly dependent on the Glp concentration, with a bimolecular rate constant for enzyme reduction of 4900 M^{-1} s^{-1}. On the other hand, the second (slow) phase was independent of Glp concentration with an invariable rate constant value of 11.7 s^{-1} [16]. Similar to His_6-*Mp*GlpO, the reduction rate constant of the slow reacting species of both enzymes is significantly lower than that of their overall turnovers, suggesting that the fast reacting enzymes is primarily responsible for the catalytic reactions.

In contrast to many flavin-dependent enzymes that use oxygen as a substrate, a plot of k_{obs} for the enzyme oxidation *versus* oxygen was hyperbolic. This reaction does not form C4a-hydroperoxyflavin as in the reaction of pyranose 2-oxidase [24, 25] or *p*-hydroxyphenylacetate hydroxylase [26, 27]. The origin of the His_6-*Mp*GlpO hyperbolic dependency on oxygen concentration is not certain. Although a simple kinetic interpretation would allude to the formation of a binary complex of reduced enzyme:oxygen, the current knowledge regarding the specific binding site of oxygen in flavoenzymes are still under debate. A specific oxygen binding site in flavoenzymes is not well defined although a hydrophobic tunnel that may be relevant for oxygen diffusion is found in cholesterol oxidase [28]. Based on structures of flavin-dependent oxidases

and monooxygenases and molecular dynamics simulations, the oxygen approach to the flavin C4a-position is proposed to be “edge-on” for the oxidases and “face-on” for the monooxygenases [29,30]. We could not identify any clear oxygen binding site in the active site of *Mp*GlpO—and the approach for oxygen diffusion in *Mp*GlpO is via the “edge-on” approach [23].

Conclusion

Our results indicate that the kinetic mechanism of His_6-*Mp*GlpO is a ping-pong type in which DHAP leaves before the oxidative half-reaction with oxygen. H_2O_2 release is likely the rate-limiting step for the overall turnover. The rapid kinetics of both half-reactions showed biphasic kinetics which is due to a mixture of fast and slow reacting enzyme species. The enzyme can catalyze the reverse reaction of reduced His_6-*Mp*GlpO and DHAP. It can also use GAP as a substrate, implying its involvement in the glycolysis pathway in addition to the pathways of glycerol and lipid metabolism. Thus, the contributions from this work can serve as the groundwork for future development of inhibitors against GlpO for the prevention of *M. pneumoniae* infection.

References

1. Koditschek LK &Umbreit WW (1969) α-Glycerophosphate oxidase in *Streptococcus faecium*F24.*J Bacteriol*98, 1063-1068.

2. Esders TW &Michrina CA (1979) Purification and properties of α-glycerophosphate oxidase from *Streptococcus faecium* ATCC 12755. *J BiolChem*254, 2710-2715.

3. Claiborne A (1986) Studies on the structure and mechanism of *Streptococcus faecium* L-α-glycerophosphate oxidase. *J BiolChem*261, 14398-14407.

4. Halbedel S, Hames C &Stulke J (2007) Regulation of carbon metabolism in the mollicutes and its relation to virulence. *JMolMicrobiolBiotechnol*12, 147-154.

5. Hames C, Halbedel S, Hoppert M, Frey J &Stulke J (2009) Glycerol metabolism is important for cytotoxicity of *Mycoplasma pneumoniae*. *J Bacteriol*191, 747-753.

6. Veal EA, Day AM & Morgan BA (2007) Hydrogen peroxide sensing and signaling. *Mol Cell*26, 1-14.

7. Almagor M, Kahane I &Yatziv S (1984) Role of superoxide anion in host cell injury induced by *Mycoplasma pneumoniae* infection: a study in normal and trisomy 21 cells. *J Clin Invest*73, 842-847.

8. Pilo P, Vilei EM, Peterhans E, Bonvin-Klotz L, Stoffel MH, Dobbelaere D & Frey J (2005) A metabolism enzyme as a primary virulence factor of *Mycoplasma mycoides* subsp. *mycoides* small colony. *J Bacteriol*187, 6824-6831.

9. Waites KB &Talkington DF (2004) *Mycoplasma pneumoniae* and its role as a human pathogen. *ClinMicrobiol Rev*17, 696-728.

10.Fairlamb AH &Bowman IBR (1977) *Trypanosomabrucei*: suramin and other trypanocidal compounds' effect on *sn*-glycerol-3-phosphate oxidase. *ExpParasitol*43, 353-361.

11. Opperdoes FR, Borst P &Fonck K (1976) The potential use of inhibitors of glycerol-3-phosphate oxidase for chemotherapy of African trypanosomiasis. *FEBS Lett*62, 169-172.

12. Fairlamb AH & Bowman IBR (1977) The isolation and characterisation of particulate *sn*-glycerol-3-phosphate oxidase from *Trypanosomabrucei*. *Int J Biochem*8, 659-668.

13. Fairlamb AH & Bowman IBR (1977) Inhibitor studies on particulate sn-glycerol-3-phosphate oxidase from *Trypanosomabrucei*. *Int J Biochem*8, 669-675.

14. Grady RW, Bienen EJ & Clarkson AB (1986) Esters of 3,4-dihydroxybenzoic acid, highly effective inhibitors of the *sn*-glycerol-3-phosphate oxidase of *Trypanosomabruceibrucei*. *MolBiochemParasitol*21, 55-63.

15. Parsonage D, Luba J, Mallett TC & Claiborne A (1998) The soluble α-glycerophosphate oxidase from *Enterococcus casseliflavus*. *J BiolChem*273, 23812-23822.

16. Charrier V, Luba J, Parsonage D & Claiborne A (2000) Limited proteolysis as a structural probe of the soluble α-glycerophosphate oxidase from *Streptococcus* sp. *Biochemistry* 39, 5035-5044.

17. Finnerty CM, Charrier V, Claiborne A &Karplus PA (2002) Crystallization and preliminary crystallographic analysis of the soluble α-glycerophosphate oxidase from *Streptococcus* sp. *ActaCrystallogr D BiolCrystallogr*D58, 165-166.

18. Colussi T, Parsonage D, Boles W, Matsuoka T, Mallett TC, Karplus PA & Claiborne A (2008) Structure of α-glycerophosphate oxidase from *Streptococcus* sp.: a template for the mitochondrial α-glycerophosphate dehydrogenase. *Biochemistry*47, 965-977.

19.Fersht A (1999) Measurement and magnitude of individualrate constants. In*Structure and Mechanism in Protein Science: A Guide to Enzyme Catalysis and Folding*, pp 132–167. W.H. Freeman & Co., NewYork, NY.

20. Dawson RMC, Elliot DC, Elliot WH & Jones KM (1986) *Data for biochemical research*, 3rd edn. Oxford University Press, New York, NY.

21. Dewanti AR &Mitra B (2003) A transient intermediate in the reaction catalyzed by (*S*)-mandelate dehydrogenase from *Pseudomonas putida*. *Biochemistry*42, 12893-12901.

22. Vilei EM & Frey J (2001) Genetic and biochemical characterization of glycerol uptake in *Mycoplasma mycoides* subsp. *mycoides* SC: its impact on H_2O_2 production and virulence. *ClinDiagn Lab Immunol*8, 85-92.

23. Elkhal CK, Kean K, Parsonage D, Maenpuen S, Chaiyen P, Claiborne A & Karplus PA (2015) Structure and proposed mechanism of α-glycerophosphate oxidase from *Mycoplasma pneumoniae*. *Article in Revision*.

24. Sucharitakul J, Prongjit M, Haltrich D & Chaiyen P (2008) Detection of a C4a-hydroperoxyflavin intermediate in the reaction of a flavoprotein oxidase. *Biochemistry*47, 8485-8490.

25. Wongnate T, Surawatanawong P, Visitsatthawong S, Sucharitakul J, Scrutton NS & Chaiyen P (2014) Proton-coupled electron transfer and adduct configuration are important for C4a-hydroperoxyflavin formation and stabilization in a flavoenzyme. *J Am ChemSoc*136, 241-253.

26. Ruangchan N, Tongsook C, Sucharitakul J & Chaiyen P (2011) pH-dependent studies reveal an efficient hydroxylation mechanism of the oxygenase component of *p*-hydroxyphenylacetate 3-hydroxylase. *J BiolChem*286, 223-233.

27. Thotsaporn K, Chenprakhon P, Sucharitakul J, Mattevi A&Chaiyen P (2011) Stabilization of C4a-hydroperoxyflavin in a two-component flavin-dependent monooxygenase is achieved through interactions at flavin N5 and C4a atoms.*J BiolChem*286, 28170-80.

28. Chen L, Lyubimov AY, Brammer L, Vrielink A & Sampson NS (2008) The binding and release of oxygen and hydrogen peroxide are directed by a hydrophobic tunnel in cholesterol oxidase. *Biochemistry*47, 5368-5377.

29. Baron R, Riley C, Chenprakhon P, Thotsaporn K, Winter RT, Alfieri A, Forneris F, van Berkel WJ, Chaiyen P, Fraaije MW, Mattevi A &McCammon JA (2009) Multiple pathways guide oxygen diffusion into flavoenzyme active sites. *ProcNatlAcadSci USA* 106, 10603-10608.

30. Chaiyen P, Fraaije MW &Mattevi A (2012) The enigmatic reaction of flavins with oxygen. *Trends BiochemSci*37, 373-380.

31. Prongjit M, Sucharitakul J, Wongnate T, Haltrich D & Chaiyen P (2009) Kinetic mechanism of pyranose 2-oxidase from *Trametes multicolor*. *Biochemistry*48, 4170-4180.

32. Pitsawong W, Sucharitakul J, Prongjit M, Tan TC, Spadiut O, Haltrich D, Divne C &Chaiyen P (2010) A conserved active-site threonine is important for both sugar and flavin oxidations of pyranose 2-oxidase. *J BiolChem*285, 9697-9705.

33. Macheroux P (1999) UV-visible spectroscopy as a tool to study flavoproteins, In *Flavoprotein Protocols*,(Chapman, S.K., & Reid, G.A., eds.), pp. 1-7, Humana Press. Totowa, NJ.

34. Daneel HJ, Rossner E, Zeeck A &Giffhorn F (1993) Purification and characterization of a pyranose oxidase from the basidiomycete*Peniophoragigantea* and chemical analyses of its reaction products. *Eur J Biochem*214, 795-802.

35. Dalziel K (1957) Initial steady-state velocities in the evaluation of enzyme-coenzyme-substrate reaction mechanism. *ActaChemScand*11, 1706-1723.

36. Chenprakhon P, Sucharitakul J, Panijpan B & Chaiyen P (2010) Measuring binding affinity of protein-ligand interaction using spectrophotometry: binding of neutral red to riboflavin-binding protein. *J Chem Ed*87, 829-831.

37. Massey V (1991) A simple method for the determination of redox potentials, In *Flavins and Flavoproteins* (Curti, B., Rochi, S., &Zanetti, G., eds.) pp. 59-66, Water DeGruyter&Co., Berlin, Germany.

38. Clark WM (1960) Compilations of data in *oxidation-reduction potentials of organic systems*. pp. 410, Wavery Press, Inc., Baltimore.

Table 1: Purification table of the recombinant His_6-*Mp*GlpO

	Volume (mL)	Total Activity (U)	Total Protein (mg)	Specific Activity (U/mg)	Yield (%)
Crude extract	180	13,968	10,746	1.3	100
Ni-Sepharose	150	2,775	244.5	11.4	20
SP-Sepharose	9	1,638	163.8	10	12

*The data in this table were from the purification of 83 g cell paste (8.8 liters culture).

Table 2: Thermodynamics and kinetic parameters involved in the His_6-*Mp*GlpO reaction

Parameters	Constants
Fast reacting enzyme	
k_1, formation of E_{ox}:Glp complex	83.3 $M^{-1}s^{-1}$
k_2, Glp release	6 s^{-1}
k_3, enzyme reduction	199 $\pm$ 34 s^{-1}
k_4, reverse reaction of E_{red} and DHAP	56.5 $M^{-1}s^{-1}$
k_5, k_6, k_{10}	ND
k_7, re-oxidation of reduced enzyme	627 $\pm$ 81 s^{-1}
k_9, H_2O_2 release	4.2 $\pm$ 0.1 s^{-1}
K_{d1}, dissociation constant for E_{ox}:Glp complex	72 $\pm$ 18 mM
K_{d2}, dissociation constant for E_{red}:O_2 complex	1.3 $\pm$ 0.2 mM
K_{d3}, dissociation constant for E_{red}:H_2O_2 complex	0.4 $\pm$ 0.2 mM
Slow reacting enzyme	
k_1', k_2', k_4', k_5', k_6'	ND
k_3', enzyme reduction	2.08 $\pm$ 0.01 s^{-1}
k_7', re-oxidation of reduced enzyme	85 $\pm$ 11 s^{-1}
$K_{d1'}$, dissociation constant of E^*_{ox}:Glp complex	1.38 $\pm$ 0.02 mM
$K_{d2'}$, dissociation constant of E^*_{red}:O_2 complex	0.5 $\pm$ 0.1 mM
k_{obs} for interconversion of fast and slow reacting enzymes	
$k_f + k_r$	> 6 s^{-1}, <16 s^{-1}

ND = Not determined

Figure legends

Fig. 1. Absorption and reduction properties of His_6-*Mp*GlpO. (A)Absorption spectra of the enzyme-bound FAD (solid line) and the released FAD upon denaturation by 2% (w/v) SDS (dashed line) are overlaid. The molar absorption coefficient of His_6-*Mp*GlpO was determined as12.40 $\pm$ 0.03 $mM^{-1}cm^{-1}$. (B) Standard reduction potential measurement of His_6-*Mp*GlpO at 25 ^{o}C by Massey's method using benzyl viologen-mediated xanthine/xanthine oxidase reaction system.The standard reduction potential value (E_e^0) of the enzyme calculated from the y-intercept of the plot of $\log(E_{red}/E_{ox})$ *versus* $\log(D_{red}/D_{ox})$ is -167 $\pm$ 1 mV (Inset of B).

Fig. 2. Two-substrate steady-state kinetics of the His_6-*Mp*GlpO reaction at 4 ^{o}C. The assay reactions were monitored by the HRP coupled-assay using astopped-flow spectrophotometer. (A) Initial rates obtained from various concentrations of Glp and O_2 were measured and plotted as a double-reciprocal plot of e/V_o*versus* 1/[Glp] at various concentration of O_2 (0.13-1.16 mM from upper to lower lines) or (B) *versus*1/[O_2] at various concentrations of Glp (4-32 mM from upper to lower lines). Both double-reciprocal plots in A and B show a parallel-line pattern, indicating that His_6-*Mp*GlpO uses a ping-pong mechanism.

Fig. 3. Reductive half-reaction of His_6-*Mp*GlpO at 4 ^{o}C. A solution of the oxidized enzyme (~28 μM) was mixed with various concentrations of Glp (0.4-51.2 mM from right to left traces) under anaerobic conditions using a single-mixing mode of the stopped-flow apparatus. (A) The reaction kinetics was monitored by measuring the absorbance change at 448 nm. Kinetic analyses indicate that the enzyme reduction is biphasic. (B-C) Plots of k_{obs} values obtained from both phases *versus*Glp concentrations are hyperbolic with limiting reduction rate constant values of 199 $\pm$ 34 (B) and 2.08 $\pm$ 0.01 s^{-1} for the fast and slow reacting enzyme, respectively. The data suggest that the enzyme reduction involves a two-step process in which one population reacts faster than another. (D) Apparent steady-state kinetics of His_6-*Mp*GlpO using GAP and Glp as substratesat 25 ^{o}C. Initial rates obtained from the reaction usingGAP (0.025-6.4 mM) were directly plotted *versus*GAP concentrations while those obtained from the reaction using Glp (0.1-51.2 mM) as a substrate are shown in the inset. The results indicated that the k_{cat} and $k_{cat}/K_m$of the reaction using Glp as a substrate are 100- and 15-fold

greater than those of GAP, respectively. (E)Proposed kinetic scheme for the reductive half-reaction of His_6-*Mp*GlpO.

Fig. 4. Oxidative half-reaction of the reduced His_6-*Mp*GlpO at 4 ^{o}C. An anaerobic solution of the reduced enzyme was mixed with various concentrations (0.13-1.03 mM from lower to upper traces) of oxygenated buffer using a single-mixing mode of stopped-flow apparatus. (A) The reaction kinetics was monitored by the absorbance change at 448 nm. (B-C) Kinetic analyses indicated that the kinetics of the reaction of the reduced enzyme with O_2 is biphasic and the plots of k_{obs} values of both phases *versus* O_2 concentrations are hyperbolic. The ratio of amplitude change for both phases is 70:30 throughout all oxygen concentrations used. The limiting rate constant values for the reduced enzyme re-oxidation for the fast and slow reacting enzyme are 627 $\pm$ 81 and 85 $\pm$ 11 s^{-1}, respectively. (D)Proposed kinetic scheme for the oxidative half-reaction of His_6-*Mp*GlpO.

Fig. 5. Double-mixing stopped-flow experiments of reduced His_6-*Mp*GlpO reacting with oxygen at 4 ^{o}C. A solution of the oxidized enzyme (91 μM before mixing) was added to Glp (91 μM before mixing) in the first mix and then mixed with various concentrations of O_2 (0.26-2.06 mM before mixing; from lower to upper traces) in the second mix. (A) The reaction kinetics was monitored by changes in the absorbance at 448 nm. Kinetic analyses indicated that all reaction traces display biphasic kinetics and amplitude changes that are similar to those obtained from the oxidative half-reaction performed in the single-mixing mode (Fig. 4A). (B-C) The plots of k_{obs} values *versus* oxygen concentrations are hyperbolic with the rate constant (k_{ox}) values for enzyme re-oxidation of 524 $\pm$ 34 and 107 $\pm$ 5 s^{-1} that are similar to those obtained from the results in Figs. 4B and 4C. The similarity in these kinetic behaviors suggests that DHAP is quickly released after its formation. (D) In another experiment, a solution of the dithionite-reduced enzyme (91 μM before mixing) was added to DHAP (136.5 μM before mixing) for various age times (10, 20, 100, and 200 s) in the first mix and then mixed with the oxygenated buffer (O_2 = 0.26 mM before mixing) in the second mix. All kinetics traces were similar and also similar to the results in (A) and in Fig. 4. Altogether, complex of reduced enzyme and DHAP could not be detected, implying that the DHAP release is fast during the catalytic turnover of His_6-*Mp*GlpO.

Fig. 6. The reaction of the reduced His_6-*Mp*GlpO with DHAP. (A) A solution of the reduced enzyme (24 μM) was mixed with various concentrations of DHAP (0.69-4,308 μM(from lower to upper spectra). The binding signal was measured by spectrophotometry at 25 ^{o}C. Difference spectra showed that binding of DHAP to the reduced enzyme caused enzyme re-oxidation as indicated by the increase of absorbance at 448 nm. (B) Pseudo-first order kinetics for the reaction of the reduced enzyme and various concentrations of DHAP (0.2-12.8 mM from lower to upper traces) was monitored under anaerobic conditions using a single-mixing mode stopped-flow spectrophotometer at 4 ^{o}C. The kinetic traces at 448 nm were recorded. (C-D) Kinetic analysis indicatedthat the reaction is biphasic and the k_{obs} values obtained from the first phase are constant (6 s^{-1}) while those of the second phase are linearly dependent on DHAP concentrations with a bimolecular rate constant of 56.5 $M^{-1}s^{-1}$. (E)Proposed scheme for the reverse reaction of reduced His_6-*Mp*GlpO and DHAP.

Fig. 7. Proposed overall catalytic reaction of His_6-*Mp*GlpO. Two enzyme populations (fast and slow reacting species) react with substrates in both half-reactions. The reverse flavin oxidation is shown as the red arrows (see text for details). Thermodynamics and kinetics parameters are presented in Table 2.

Figures

Fig. 1

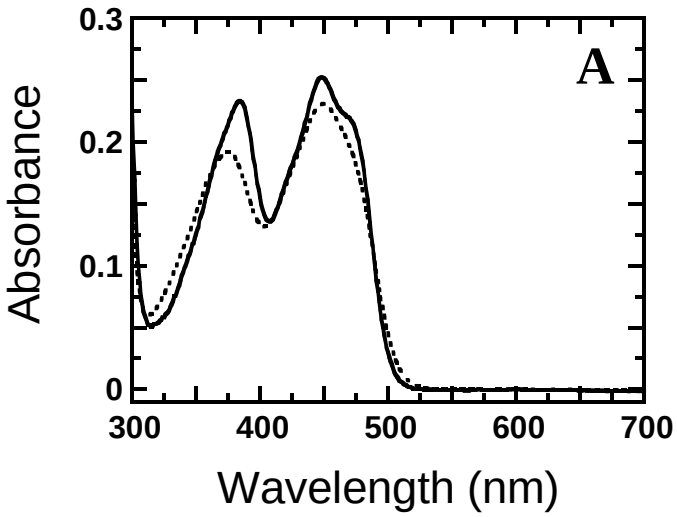

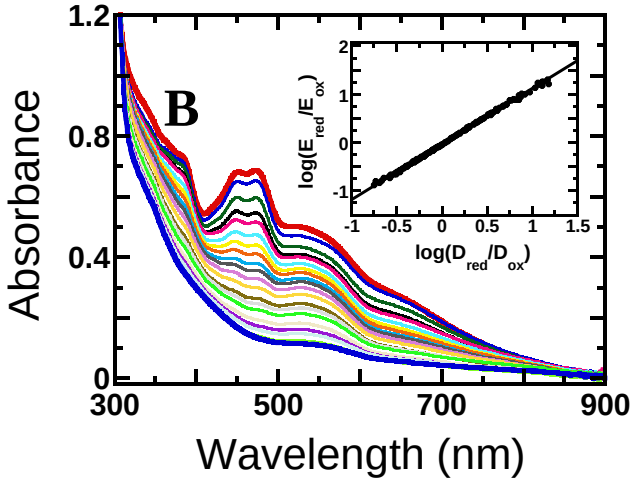

Fig. 2

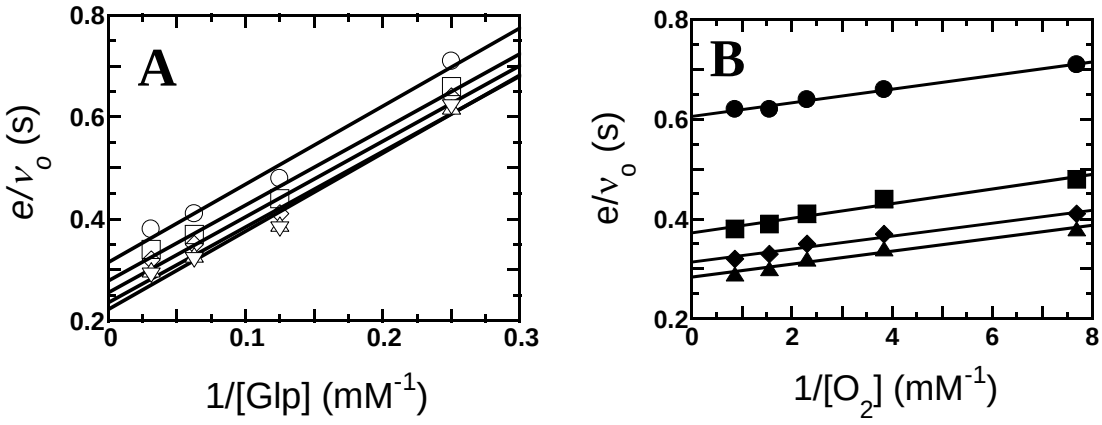

Fig. 3

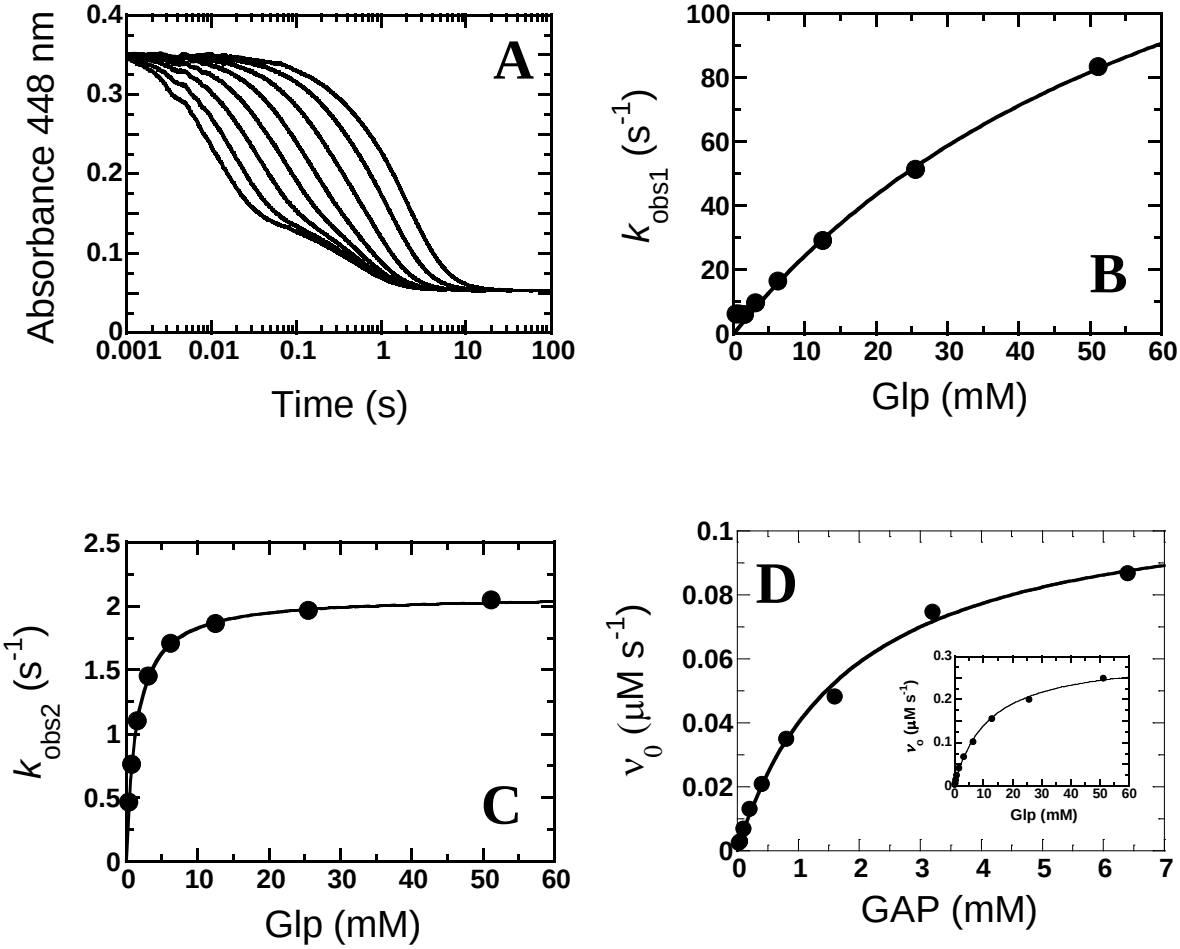
A
Absorbance 448 nm
Time (s)
B
k_{obs1} (s^{-1})
Glp (mM)
C
k_{obs2} (s^{-1})
Glp (mM)
D
v_0 ($\mu M\ s^{-1}$)
GAP (mM)

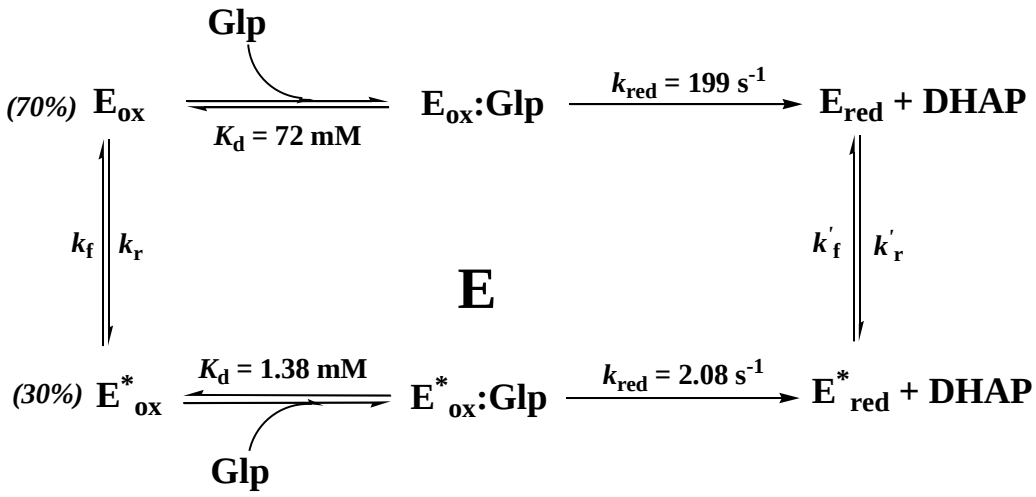
Glp
(70%) E_{ox}
K_d = 72 mM
E_{ox}:Glp
k_{red} = 199 s^{-1}
E_{red} + DHAP
k_f k_r
k'_f k'_r
E
(30%) E^*_{ox}
K_d = 1.38 mM
E^*_{ox}:Glp
k_{red} = 2.08 s^{-1}
E^*_{red} + DHAP
Glp

Fig. 4

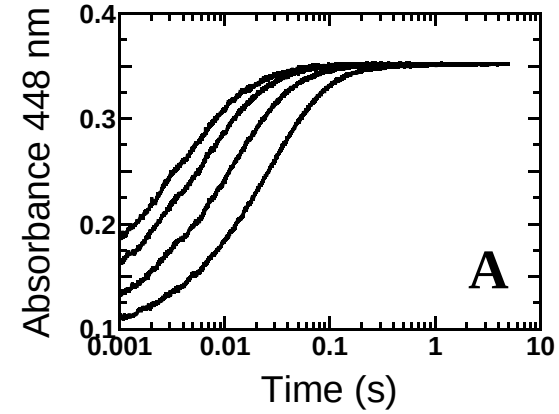
Absorbance 448 nm
0.4
0.3
0.2
0.1
0.001
0.01
0.1
1
10
Time (s)
A

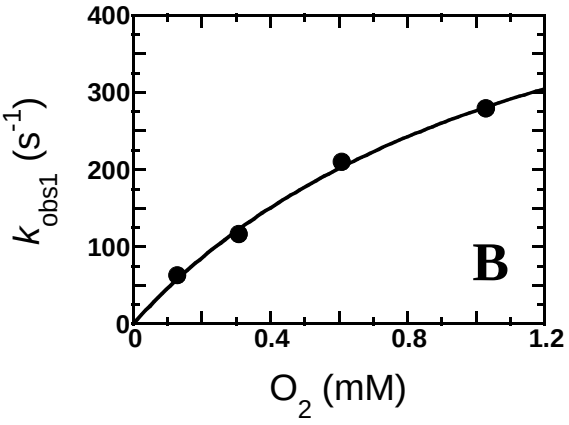
k_{obs1} (s^{-1})
400
300
200
100
0
0
0.4
0.8
1.2
O_2 (mM)
B

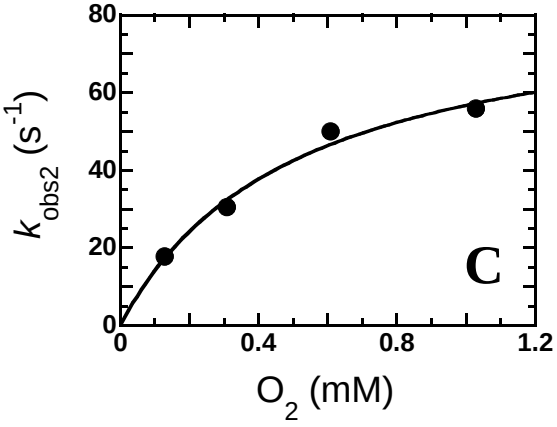
k_{obs2} (s^{-1})
80
60
40
20
0
0
0.4
0.8
1.2
O_2 (mM)
C

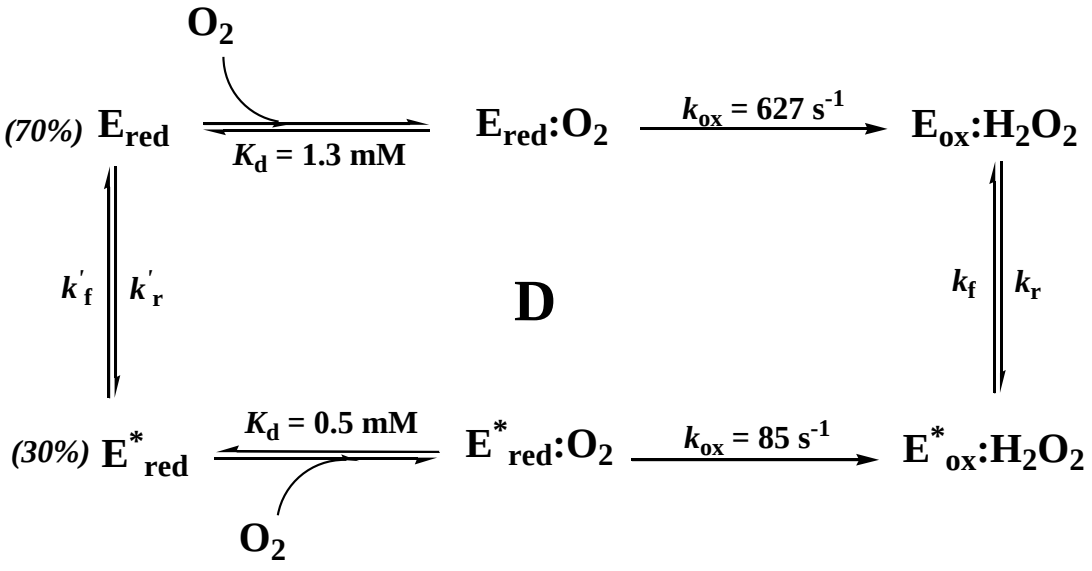
O_2
(70%) E_{red}
K_d = 1.3 mM
E_{red}:O_2
k_{ox} = 627 s^{-1}
E_{ox}:H_2O_2
k'_f
k'_r
D
k_f
k_r
(30%) E^*_{red}
K_d = 0.5 mM
E^*_{red}:O_2
k_{ox} = 85 s^{-1}
E^*_{ox}:H_2O_2
O_2

Fig. 5

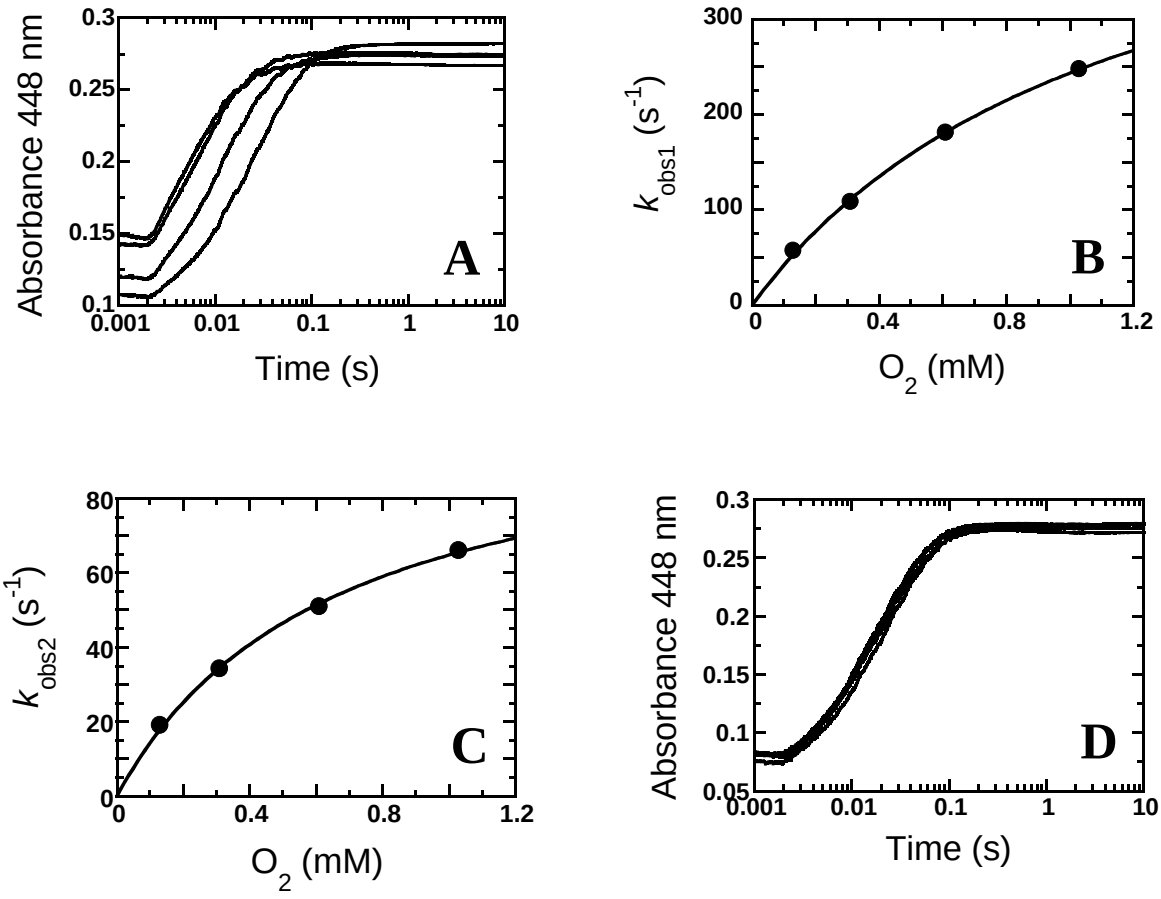
Absorbance 448 nm
0.3
0.25
0.2
0.15
0.1
0.001
0.01
0.1
1
10
Time (s)
A
k_{obs1} (s^{-1})
300
200
100
0
0
0.4
0.8
1.2
O_2 (mM)
B
k_{obs2} (s^{-1})
80
60
40
20
0
0
0.4
0.8
1.2
O_2 (mM)
C
Absorbance 448 nm
0.3
0.25
0.2
0.15
0.1
0.05
0.001
0.01
0.1
1
10
Time (s)
D

Fig. 6

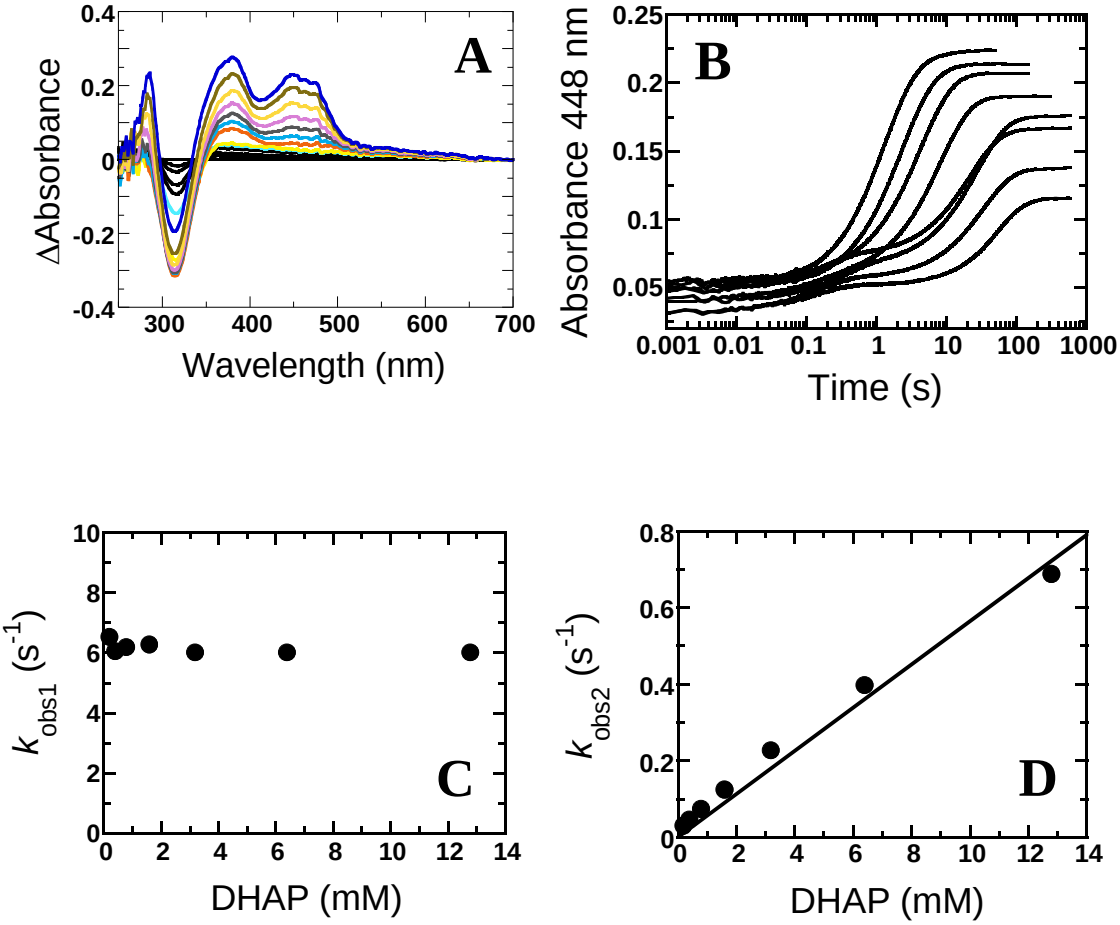
A
ΔAbsorbance
Wavelength (nm)
B
Absorbance 448 nm
Time (s)
C
k_{obs1} (s^{-1})
DHAP (mM)
D
k_{obs2} (s^{-1})
DHAP (mM)

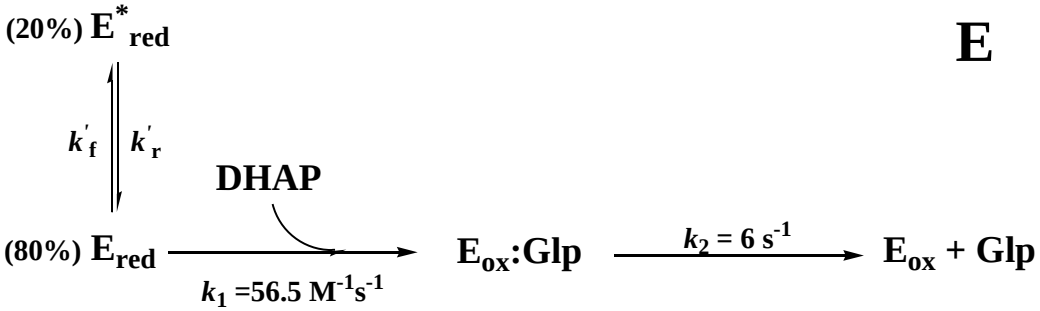
(20%) E^*_{red}
k'_f
k'_r
DHAP
(80%) E_{red}
k_1 =56.5 $M^{-1}s^{-1}$
E_{ox}:Glp
k_2 = 6 s^{-1}
E_{ox} + Glp
E

Fig. 7

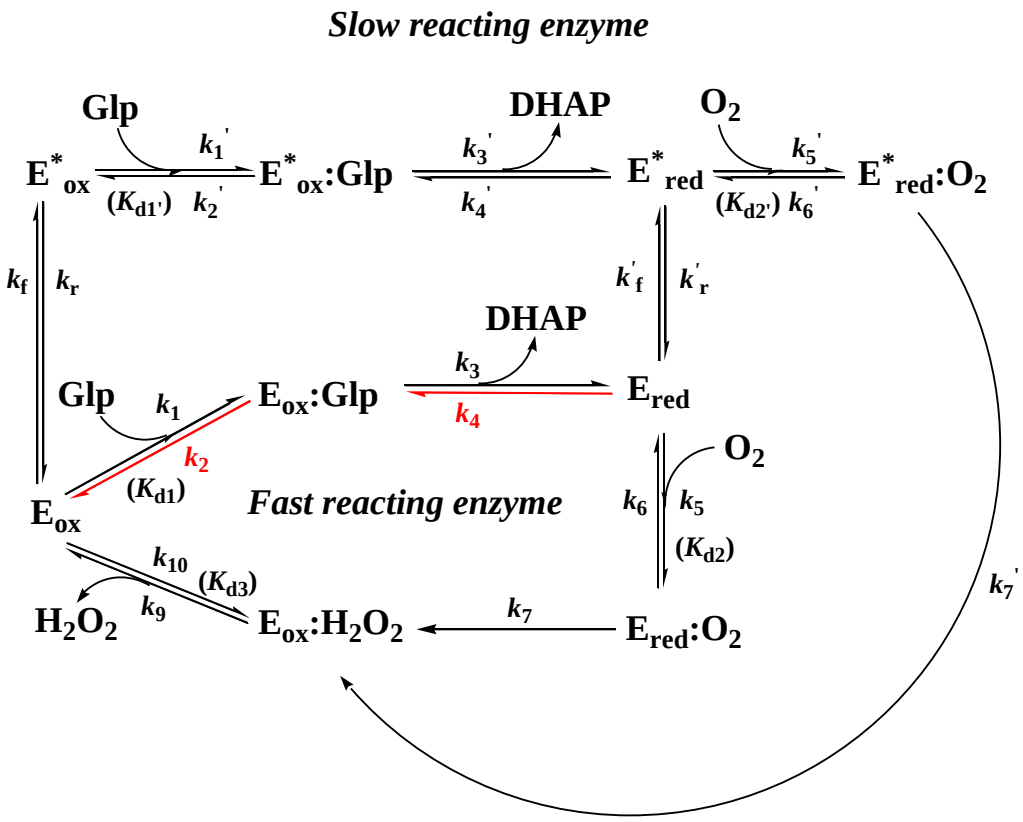
Slow reacting enzyme
Glp
DHAP
O2
E*ox
k1'
E*ox:Glp
k3'
E*red
k5'
E*red:O2
(Kd1')
k2'
k4'
(Kd2')
k6'
kf
kr
k'f
k'r
DHAP
Glp
k1
Eox:Glp
k3
Ered
k2
k4
O2
(Kd1)
Fast reacting enzyme
k6
k5
Eox
(Kd2)
k10
(Kd3)
k9
H2O2
Eox:H2O2
k7
Ered:O2
k7'

Output จากโครงการวิจัยที่ได้รับทุนจาก สกว.

1. ผลงานตีพิมพ์ในวารสารวิชาการนานาชาติ

ระบุชื่อผู้แต่ง : **Maenpuen S**, Watthaisong P, Supon P, Sucharitakul J, Parsonage D, Karplus PA, Claiborne A and Chaiyen P.
ชื่อเรื่อง : Kinetic Mechanism of L-α-Glycerophosphate Oxidase from *Mycoplasma pneumoniae*
ชื่อวารสาร : FEBS J
ปี : 20 February 2015 (Accepted)
เล่มที่ เลขที่ : -
หน้า : -

ระบุชื่อผู้แต่ง : Elkhal CK, Kean K, Parsonage D, **Maenpuen S**, Chaiyen P, Claiborne A, Karplus PA.
ชื่อเรื่อง : Structure and proposed mechanism of α-glycerophosphate oxidase from *Mycoplasma pneumoniae*
ชื่อวารสาร : FEBS J
ปี : 16 February 2015 (Accepted)
เล่มที่ เลขที่ : -
หน้า : -

ระบุชื่อผู้แต่ง : **Maenpuen S**, Amornwatcharapong W, Krasatong P, Sucharitakul J, Palfey BA, Yuthavong Y, Chitnumsub P, Leartsakulpanich U, Chaiyen P.
ชื่อเรื่อง : Kinetic Mechanism and the Rate-Limiting Step of *Plasmodium vivax* Serine Hydroxymethyltransferase.
ชื่อวารสาร : Journal of Biological Chemistry
ปี : 12 February 2015 (In Press)
เล่มที่ เลขที่ : -
หน้า : -

ระบุชื่อผู้แต่ง : Chitnumsub P, Jaruwat A, Riangrungroj P, Ittarat W, Noytanom K, Oonanant W, Vanichthanankul J, Chuankhayan P, **Maenpuen S**, Chen CJ, Chaiyen P, Yuthavong Y, Leartsakulpanich U.

ชื่อเรื่อง : Structures of *Plasmodium vivax* serine hydroxymethyltransferase: implications for ligand-binding specificity and functional control.

ชื่อวารสาร : Acta Crystallographica Section D: Biological Crystallography

ปี : 2014

เล่มที่ เลขที่ : 70(Pt 12)

หน้า : 3177-3186

ระบุชื่อผู้แต่ง : Pinthong C, **Maenpuen S**, Amornwatcharapong W, Yuthavong Y, Leartsakulpanich U, Chaiyen P.

ชื่อเรื่อง : Distinct biochemical properties of human serine hydroxymethyltransferase compared with the *Plasmodium* enzyme: implications for selective inhibition.

ชื่อวารสาร : FEBS J.

ปี : 2014

เล่มที่ เลขที่ : 281(11)

หน้า : 2570-2583

2. การนำผลงานวิจัยไปใช้ประโยชน์

- **เชิงพาณิชย์** : ไม่มี
- **เชิงนโยบาย** : ไม่มี
- **เชิงสาธารณะ** : ไม่มี
- **เชิงวิชาการ** : มีการนำความรู้ที่ได้ไปประยุกต์ใช้ในการเรียนการสอนวิชาเทคนิคทางชีวเคมี 1 และ 2

3. อื่น ๆ (เช่น ผลงานตีพิมพ์ในวารสารวิชาการในประเทศ การเสนอผลงานในที่ประชุมวิชาการ หนังสือ การจดสิทธิบัตร)

Proceedings:

(1). **Maenpuen S**, Sucharitakul J, Claiborne A, Chaiyen P. Characterization of α-glycerophosphate oxidase from *Mycoplasma pneumoniae*. *In* Miller, S., Hille, R., Palfey, B., editors. Flavins and Flavoproteins 2011: Proceedings of the Seventeenth International Symposium; 2011 July 24-29; Lulu: North Carolina, the United States of America; 2013. p. 193-198.

Poster Presentations:

(1). **Maenpuen S**, Sucharitakul J, Claiborne A, Chaiyen P. (2011). "Characterization of α-glycerophosphate oxidase from *Mycoplasma pneumoniae*" in the 17th International Symposium on Flavins and Flavoproteins, University of California, Berkeley, California, USA.

(2). Claiborne A, Parsonage D, **Maenpuen S**, Chaiyen P, Palioca CK, Karplus PA, Sazinsky MH, Hames C, Stulke J, Ross LJ, and White EL. (2012). "Targeting glycerol metabolism in Mycoplasma: α-glycerophosphate oxidase and its contribution to virulence" in 2012 International Conference on Gram-Positive Pathogens, University of Nebraska Medical Center, Nebraska, USA.

(3). **Maenpuen S**, Sucharitakul J, Claiborne A, Chaiyen P. (2012). "Characterization of α-glycerophosphate oxidase from *Mycoplasma pneumoniae*" in the 13th FAOBMB Congress Bangkok, Thailand.

(4). **Maenpuen S**, Sucharitakul J, Claiborne A, Chaiyen P. (2013). "Biochemical properties and kinetics of glycerol 3-phosphate oxidase" in the Enzyme Engineering XXII: Emerging Topics in Enzyme Engineering, Toyama, Japan.

(5). **Maenpuen S**, Watthaisong P, Supon P, Sucharitakul J, Claiborne A, Chaiyen P. (2014). "Thermodynamic properties of glycerol 3-phosphate oxidase from *Mycoplasma pneumoniae*" in the 18th International Symposium on Flavins and Flavoproteins, Petchaburi, Cha-Am, Thailand.

(6). **Maenpuen S**, Amornwatcharapong W, Krasatong P, Sucharitakul J, Palfey BA, Yuthavong Y, Chitnumsub P, Leartsakulpanich U, Chaiyen P. (2014).

“Kinetic mechanism and rate-limiting step in the reaction of *Plasmodium vivax* serine hydroxymethyltransferase” in the 7th AOHUPO Congress and 9th International Symposium of the Protein Society of Thailand, Bangkok, Thailand.

Oral Presentations:

(1). **Maenpuen S**, Amornwatcharapong W, Krasatong P, Sucharitakul J, Palfey BA, Yuthavong Y, Chitnumsub P, Leartsakulpanich U, Chaiyen P. (2014). “Kinetic mechanism and rate-limiting step in the reaction of *Plasmodium vivax* serine hydroxymethyltransferase” in the 7th AOHUPO Congress and 9th International Symposium of the Protein Society of Thailand, Bangkok, Thailand.

KineticMechanism ofL-α-GlycerophosphateOxidase from *Mycoplasma pneumoniae*

Somchart Maenpuen[1], Pratchaya Watthaisong[1], Pacharee Supon[1], Jeerus Sucharitakul[2],Derek Parsonage[3], P. Andrew Karplus[4], Al Claiborne[3]and Pimchai Chaiyen[5]*

[1]Department of Biochemistry, Faculty of Science, Burapha University, 169 Long-HaadBangsaen Road, Chonburi, 20131, Thailand

[2]Department of Biochemistry, Faculty of Dentistry, Chulalongkorn University, Henri-Dunant Road, Patumwan, Bangkok 10330, Thailand

[3]Department of Biochemistry and Center for Structural Biology, Wake Forest School of Medicine, Winston-Salem, North Carolina 27157, United States

[4]Department of Biochemistry and Physics, Oregon State University, Corvallis, Oregon 97331, United States

[5]Department of Biochemistry and Center of Excellence in Protein Structure & Function, Faculty of Science, Mahidol University, Rama 6 Road, Bangkok, 10400, Thailand

*Correspondence to: P. Chaiyen, Department of Biochemistry and Center of Excellence in Protein Structure & Function, Faculty of Science, Mahidol University, Rama 6 Road, Bangkok, 10400, Thailand. Fax: +6623547174, Tel: +6622015596,

Email: pimchai.cha@mahidol.ac.th

Running Title

Catalytic properties of L-α-glycerophosphateoxidase from *Mycoplasma pneumoniae*

Abbreviations

His_6-*Mp*GlpO, six-histidine-tagged *Mycoplasma pneumonia* L-α-glycerophosphateoxidase; FAD, flavin adenine dinucleotide; Glp, L-α-glycerophosphate; DHAP, dihydroxyacetone phosphate; GAP, DL-glyceraldehyde 3-phosphate; H_2O_2, hydrogen peroxide; ABTS, 2,2'-azino-bis(3-ethylbenzothiazoline-6-sulfonic acid) diammonium salt; HRP, horseradish peroxidase.

Enzyme Commission number

L-α-glycerophosphate oxidase, EC 1.1.3.21

Keywords

L-α-glycerophosphate oxidase;flavoprotein oxidase;flavin adenine dinucleotide (FAD);transient kinetics; *Mycoplasma pneumoniae*

Subdivision

Enzymology

Abstract

L-α-glycerophosphate oxidase is an FAD-dependent enzyme that catalyzes the oxidation of L-α-glycerophosphate (Glp) by molecular oxygen to generatedihydroxyacetone phosphate (DHAP) and hydrogen peroxide (H_2O_2). The catalytic properties of the recombinant His_6-GlpO from *Mycoplasma pneumoniae*(His_6-*Mp*GlpO) were investigated withtransient and steady-state kinetics and ligand binding. The results indicate that the reaction mechanism of His_6-*Mp*GlpOfollowsaping-pongmodel. Double-mixing stopped-flow experiments show thatafter flavin-mediate substrate oxidation, DHAP leaves rapidly prior to the oxygen reaction.The values of the individual rate constants and k_{cat}(4.2 s^{-1}at 4 ^{o}C) determined, in addition to the finding that H_2O_2 can bind to the oxidized enzyme suggest that H_2O_2 release is the rate-limiting step for the overall reaction. Resultsindicate that His_6-*Mp*GlpOcontains mixed populations of fast and slow reacting species. Only the fast reacting species predominantlyparticipates in turnovers. Different from other GlpOenzymes previously reported, His_6-*Mp*GlpOcan catalyze the reverse reaction of reduced enzyme and DHAP. This result can be explained by the standard reduction potential value of His_6-*Mp*GlpO(-167 ± 1 mV), which is lower than those of GlpO from other species. We found that DL-glyceraldehyde 3-phosphate(GAP)can be used as a substrate in the His_6-*Mp*GlpO reaction,although it exhibited a~100-fold lower k_{cat} value in comparisonto the reaction of Glp.These results also imply the involvement of GlpO in glycolysis, as well as in lipid and glycerol metabolism. The kinetic models and distinctive properties of His_6-*Mp*GlpOreported here should be useful for future studies of drug development against *Mycoplasma pneumonia* infection.

Introduction

L-α-glycerophosphate oxidase (GlpO) is a flavoprotein oxidase containing FAD as a cofactor. The enzymecatalyzes the oxidation of L-α-glycerophosphate (Glp)− a metabolic intermediate in lipid biosynthesis, glycolysis, and glycerol metabolism−at the C2 position to yielddihydroxyacetone phosphate (DHAP) as a product. Molecular oxygen (O_2) acts as an electron acceptor in this reaction by receiving two electrons from the substrate to generate hydrogen peroxide (H_2O_2) [1-5]. H_2O_2 is a reactive oxygen species (ROS) that can be converted to more potent reactive oxygen species such as peroxide or hydroxyl radicals and H_2O_2 itself can also serve as a cellular signaling molecule [6]. ROS can affect cell viability by causing lysis of red blood cells, lipid peroxidation, and other oxidative damage [7,8].The GlpO reaction in *Mycoplasma pneumonia* has been shown to play a role in the virulence of the bacteria, which presents itself as infection of the human respiratory tract[4, 5, 8, 9]. It is thought that H_2O_2 produced from this reaction is involved in the pathogenicity of pneumonia.

GlpO from several bacteria have been studied. Due to its absence in mammaliancells, this enzyme has been proposed as a target for new antibiotic development [10].Native GlpO from *Trypanosomabrucei*, a human parasite that causes an African sleeping sickness,was isolated, purified and studied with regards to its inhibition. Results indicate thatsuramin, melarsen oxide, salicylhydroxamic acid, 3-chlorobenzylhydroxamate, 8-hydroxyquinoline, and alkyl esters of 3,4-dihydroxybenzoate are potent inhibitors for GlpO from *T. brucei*[10-14]. GlpO from lactic acid bacteria such as *Streptococcus*sp.and *Streptococcus faecium* ATCC 12755were also studied[2, 3]. Investigations on the inhibition of the enzymeshowed that *S. faecium*GlpOcould be inhibited by fructose 6-phosphate [2]. Besides oxygen, the*S.*

faecium enzyme can also use other compoundssuch as ferricyanide and dichlorophenolindolephenol (DCPIP)as electron acceptors[3].Studies of the recombinant GlpOfrom *Enterococcus casseliflavus*indicate that the reaction obeys aping-pong kinetics model andthat the flavin reduction step is the rate-limiting step for the overall turnover [15]. In contrast, kinetic studies of the wild-typeGlpO from *Streptococcus* sp.and the mutant enzyme in which a flexible surface regionwas truncated indicate that DHAP release is the rate-limiting step of the reaction[16].Crystal structures of both wild-type and truncated mutant of *Streptococcus* sp. GlpOat 2.4 and 2.3 Å resolution, respectively were solved. The data indicate that the active site residues in *Streptococcus* sp. GlpO that may be involved in Glp substrate binding aremostly positively charged residues such as Arg346, Lys429, His65, and Arg69 [17, 18].

In this work, the biochemical and catalytic properties of a new GlpOfrom*Mycoplasma pneumonia* was investigated using steady-state and transient kinetics, and ligand binding studies. The enzyme shows several unique catalytic properties that have never been reported for other enzymes. It can catalyze a reverse flavin oxidation using the reaction product, DHAP as an electron acceptor. In contrast to previously investigated systems, the rate-limiting step of*Mycoplasma*GlpOis likely the release of H_2O_2because other reaction steps are faster than the catalytic turnover number. Besides Glp, the enzyme can also use glyceraldehyde 3-phosphate (GAP), an intermediate in the glycolysis pathway, as a substrate, implying that the H_2O_2 generated by the GlpO reaction in *Mycoplasma pneumoniae* can be derived from lipid, glycerol and sugar metabolism.

Results

Preparation and spectroscopic properties of His_6-MpGlpO

Recombinant His_6-*Mp*GlpO was successfully expressed as a soluble enzyme in *E. coli*BL21(DE3) cells cultured in Terrific Broth and induced by IPTG at 25 ^{o}C.The yield of cell paste was about 17 g per 1liter of cell culture. His_6-*Mp*GlpO was purified to homogeneity using Ni-Sepharose affinity and SP-Sepharosecation-exchange chromatography as described in Experimental Procedures. This protocol resulted in ~19 mg of purified enzyme with a specific activity of ~10 U/mg per 1 liter of cell culture (Table 1). A low yield of the enzyme preparation was due to the protein loss during the last step (SP-sepharose chromatography). This step was used because it could remove impurities that were retained after Ni-Sepharose chromatography.SDS-PAGE (12%) analysis indicatedthat the enzyme is >95% pure and thatthesubunit molecular mass was about 43 kDa(data not shown). The purified enzyme exhibited spectral characteristics typical of FAD-bound enzyme with a maximum absorbance at 448 nm (solid line of Fig. 1). The molar absorption coefficient was determined according to the protocol described in Experimental Procedures as 12.40 ± 0.03 $mM^{-1}cm^{-1}$, which is slightly different from a molar absorption coefficient of free-released FAD (11.3 $mM^{-1}cm^{-1}$) (dashed line of Fig. 1).

Steady-state kinetics of His_6-MpGlpO

The two-substrate steady state kinetics of His_6-*Mp*GlpO using Glp and O_2 as substrates was investigated at 4 ^{o}C, pH 7.0 using the 2,2'-azino-bis(3-ethylbenzothiazoline-6-sulphonic acid)-horse radish peroxidase (ABTS-HRP) coupled

assay system as described in Experimental Procedures. Initial rates of reactions at various concentrations of Glpand O_2were measured. A double-reciprocal plot of initial rates and concentrations,e/v_o *versus*1/[Glp] (Fig. 2A) or 1/[O_2] (Fig. 2B),showed parallellines, indicating that the His_6-*Mp*GlpO reaction uses a ping-pong mechanism. Steady-state kinetic parameters of the enzyme reaction that were obtained from reciprocal (Eqn 2)ordirect plots(Eqn 3)weresimilar: K_m^{Glp}, 5.5 ± 0.4 mM; $K_m^{O_2}$, 55±8μM; and k_{cat}, 4.2 ± 0.1 s^{-1} at 4 ^oC.The results indicated that the steady-state turnover number of GlpOfrom *M. pneumoniae* is about 4- and 9-fold lower than that of GlpO from*Streptococcus* sp. (18 s^{-1}) and *Enterococcus casseliflavus*(37 s^{-1}), respectively[15, 16].

Standard reduction potential value of His_6-MpGlpO

The standard reduction potential value of His_6-*Mp*GlpO was measured by Massey's method using cresyl violet as a reference dye. Spectra obtained during the reduction(Fig. 1B) indicated that the enzyme was completely reduced via a two-electron reduction process using the benzyl viologen-mediated xanthine/xanthine oxidase system. Concentrations of the oxidized enzyme and the reduced dye were calculated based ontheir absorbance at 407 and 540 nm, respectively. The standard reduction potential value (E_e^0)of the enzyme was calculated from the y-intercept of the plot of log(E_{red}/E_{ox}) *versus*log(D_{red}/D_{ox}) as -167 ± 1 mV (Inset of Fig. 1B).

Kinetics of the reduction of His_6-MpGlpO by Glp

A solution of the oxidized enzyme (~28 μM after mixing) in 50 mM sodium phosphate buffer, pH 7.0 containing 0.5 mM EDTA, and 1 mM DTT was mixed with

various concentrations of Glpunder anaerobic conditions, and the kinetics of enzyme reduction was monitored by the change in absorbance at 448 nm using a stopped-flow spectrophotometer at 4 ^{o}C. Kinetic traces shown inFig. 3A indicate that flavin reductionshows biphasic kinetics in which the amplitude change of the first (fast) phase variedfrom 10-70% (relative to total flavin reduction) while the second (slow) phase was from 90-30% uponincreasing the concentration of Glp. This indicates that there are two distinct populations of the oxidized enzymethat are slowly interconverted. The k_{obs} values obtained from both phases are hyperbolically dependent on Glp concentration (Figs. 3B and 3C). According to the plots, the reduction rate constants (k_{red}) were determined as 199 ± 34 and 2.08 ± 0.01 s^{-1}, respectively. Because $k_{obs}$of both phases were hyperbolically dependent on substrate concentration (Figs. 3B and 3C), the data suggest that each of the oxidized enzyme forms reacts with Glpvia a two-step reduction process in which a binary complex of the oxidized enzyme and its substrate is initially formed inthe first step, followed by flavin reduction in the second step(Fig. 3E). Thesedata indicate that the substrate binding affinity of the fast reacting species (K_d = 72 ±18mM) is 52-fold lower than that of the slow reacting enzyme (K_d = 1.38 ± 0.02mM).As at the highest concentration of Glpwhere both populations of enzyme can react with Glp rapidly, the amplitude ratio of fast:slow species is 70:30, the data indicate that a ratio of fast to slow species under equilibrium is 70:30. This conclusion is also supported by the results of the oxidative half-reaction (see the following section). We also noted that a clear amplitude change ratio of 70:30 could only be observed when the k_{obs} value of the fast reacting species is ≥16 s^{-1}. These results also imply that k_f+ k_r of the interconversionprocess between the fast and slow reacting species is <16 s^{-1}(Fig. 3E).

Kinetics of the reaction of reduced His_6-MpGlpO with O_2

An anaerobic solution of the reduced enzyme (~28 μM after mixing) in 50 mM sodium phosphate buffer, pH 7.0 containing 0.5 mM EDTA, and 1 mM DTT was mixed with buffer containing various concentrations of oxygen. The kinetics of enzyme oxidation was monitored by measuring the absorbance at 448 nm using a stopped-flow spectrophotometer at 4 ^{o}C. Kinetic traces for enzyme oxidation are biphasic (Fig. 4A)in which the amplitude change for the first (fast) phase reflects 70% of the total amount of flavinoxidation while the second (slow) phase is about 30%.Some fraction of the fast reacting enzyme was oxidized during the dead-time period. Kinetic analyses indicate that the k_{obs} values of the first phase and second phase *versus* the oxygenconcentration are hyperbolic,with rate constant values for the fast and slow reacting species of 627 ± 81 and 85 ± 11 s^{-1}, respectively (Figs. 4B and 4C). The hyperbolic plotsobtained for the k_{obs} values *versus*oxygen concentration suggest that the re-oxidation occurs via a two-step process. The reduced enzyme may form a binary complex with O_2prior to flavin re-oxidation in the second step. According to the plots shown in Figs. 4B and 4C,the K_d values for binary complex formation were 1.3 ± 0.2 and 0.5 ± 0.1 mM for the fast and slow reacting enzyme species, respectively. Similar to the reductive half-reaction, the ratio of amplitude of fast toslow reacting species is 70:30. The amplitude changesobserved due to the fast and slow reacting species was clearly separatedatall oxygen concentrations employed because all k_{obs} values were greater than 16 s^{-1}(the lowest k_{obs} value in Fig. 4C is 17.6 s^{-1}). The kinetic mechanism of the oxidative half-reaction is summarized in Fig. 4D.

Effects of DHAP on the oxidative half-reaction of His_6-MpGlpO

Previous studiesof the reductive half-reaction (Fig. 3A) indicated that thereduction of enzyme by Glpis a fast process in which DHAP release cannot be detectedin the stopped-flow experiments. In this experiment, we used double-mixing stopped-flow experiments (see Experimental Procedures) to investigate if DHAP can bind to the reduced enzyme by monitoring the influence of DHAP on the oxidative half-reaction. The reduced enzyme was mixed with an equal concentration of Glp and aged for 100 s (to ensure complete reduction) in the first mixing step. The DHAP-bound reduced enzyme was then mixed with various concentrations of O_2 in the second mixing step and the enzyme re-oxidation was followed by monitoring the absorbance at 448 nm,similar to the experiments in Fig. 4A. The kinetic traces obtained from the change in absorbance at 448 nm shown in Fig. 5A display biphasic kinetic and amplitude changes for the first (70%) and second (30%) phases similar to those observed for the oxidative half-reaction carried out using the single-mixing mode in Fig. 4A(Fig. 5A). Kinetic analyses also indicate that the k_{obs}values for both phases and the rate constants for enzyme oxidation (k_{ox} = 524 ± 34 s^{-1}(Fig. 5B) and 107 ± 5 s^{-1}(Fig. 5C)), are similar to those obtained from Fig. 4 (627 ± 81 s^{-1}(Fig. 4B) and 85 ± 11 s^{-1}(Fig. 4C)). The similarities in the kinetic results obtained by the two different mixing modes suggest that after the enzyme was reduced by Glp, the DHAP formed was quickly released prior to the reaction of the reduced enzyme with oxygen.

To verify our hypothesis, the reduced enzyme (91 μM before mixing) plus DHAP (136.5 μM before mixing) was incubated for various aging times in the first mixing step. The solution was then mixed with buffer containing oxygen at 0.26 mM (before mixing)

in the second mixing step to allow the re-oxidation of enzyme to occur while the progression of the reactionwas monitored by measuring the absorbance change at 448 nm. Analyses of the kinetic traces (Fig. 5D) indicated that the k_{obs} values and the amplitude changes obtained from various age times were similar and also similar to those obtained from the previous results (Fig. 5A). These data again suggest that DHAP does not tightly bind to the enzyme but rather, was quickly released after its formation. All results indicate that the reaction of His_6-*Mp*GlpO occurs via a true ping-pong mechanism.

Product binding and the reverse oxidation of reduced His_6-MpGlpO by DHAP

Both the oxidized and reduced forms of the enzyme were tested for their ability to bind various ligands by detecting their absorbance signal changes (Experimental Procedures). For the binding of the oxidized enzyme and H_2O_2, a solution of oxidized enzyme (24 μM) was titrated invarious concentrations of H_2O_2. The difference spectra (data not shown) indicated a maximum absorbance change at 385 nm. The equilibrium dissociation constant (K_d) determined from measurements at 385 nm for the binding of H_2O_2 to the oxidized enzyme was determined as 0.4 ±0.2 mM. The same experiment was also performed using DHAP at various concentrations. The difference spectra obtained did not show any clear signal due to the binding of oxidized enzyme and DHAP. The large absorption increase at shorter wavelengths was likely due to DHAP absorption (data not shown). As H_2O_2 can bind to the oxidized enzyme, H_2O_2 release from the enzyme may be a rate-limiting step for the overall catalytic turnover of the enzyme reaction.

Results from the addition of DHAP at various concentrations to the reduced His_6-*Mp*GlpO (24 µM) indicate that the reduced enzyme can be re-oxidized by DHAP (Fig. 6A), suggesting that the reduction of His_6-*Mp*GlpO by Glpis reversible. Therefore, the kinetics of re-oxidation of the reduced enzyme with DHAP was investigated by monitoring the absorbance change at 448 nm using single-mixing mode stopped-flow spectrophotometry (Experimental Procedures). The kinetic traces at 448 nm (Fig. 6B) showed biphasic kinetics with majority of absorbance increase in the second phase. Kinetic analyses showed that the k_{obs} values obtained from the first phase were independent of DHAP concentration with values ~6 s^{-1}(Fig. 6C), while those obtained from the second phase are linearly dependent on DHAP concentration with a bimolecular rate constant of 56.5 $M^{-1}s^{-1}$(Fig. 6D). As the first reaction of reduced GlpO and DHAP is a bimolecular reaction in which the rate constants should be linearly dependent on DHAP, these results suggest that the rate constant (6 s^{-1}) observed in the first phase likely belongs to the step following the bimolecular reaction.Due to its greater value than the k_{obs} values of the bimolecular reaction of reduced enzyme and DHAP, this step appearedat the first phase even though it in fact occurs after the initial bi-molecular reaction(rate-switching phenomenon, [19]). The kinetic model of the reaction of reduced enzyme with DHAP to form the oxidized enzyme and Glp is shown in Fig. 6E.

Overall catalytic reaction of His_6-MpGlpO

Based on the results of transient and steady-statekinetic studies shownin Figs. 2-4, the overall reductive and oxidative half-reactions of His_6-*Mp*GlpO can be summarized as shown in Fig 7. Both half-reactions showed evidence supporting the presence of a

mixture of fast and slow reacting enzymes, present at a molar ratio of 70:30. As the overall k_{cat}derived from the steady-state kinetic measurementswas 4.2 s^{-1} and the k_{red}value of the slow reacting species (upper path, Fig. 7)was 2.08 ± 0.01 s^{-1}(Fig. 3C), the results indicated that primarily, only the fast reacting species is involved inthe reductive half-reaction during the catalytic turnover.Because all of the rate constants measured hadgreater values than the k_{cat}, we propose that the rate-limiting step is associated with product release. As the results from the double-mixing experiments in Fig. 5 indicated thatDHAP release is rapid, we thus propose that the release of H_2O_2 is the rate-limiting step of the overall reaction.

Data obtained from the reverse reaction of His_6-*Mp*GlpO are useful for assigning the rate constants in the reductive half-reaction. The results in Figs. 6C and 6D were used to assign rate constants for the bimolecular reaction between reduced enzyme and DHAP as 56.5 $M^{-1}s^{-1}$ and for the dissociation of Glp from the E_{ox}:Glp binary complex as 6 s^{-1}(red arrows in Fig. 7). As the reverse reaction (Figs. 6) only showed ~80% of the reduced enzyme oxidation at the end, the data imply that only the reaction of fast reacting species was observed (rate 56.5 $M^{-1}s^{-1}$, red arrow ofFig. 7). This suggests that the rate constant of 6 s^{-1} is likely k_2 of the first step in Fig. 7. Therefore, based on aK_d value of 72mM (the first step), k_1 can be calculated as 83.3 $M^{-1}s^{-1}$.

Glyceraldehyde 3-phosphate can be used as a substrate for the His_6-MpGlpO reaction

As the previous report showed thata significant amount of H_2O_2 could be generated in *M. pneumoniae* when glucose (0.1 mM) was used as a sole carbon source [5]and the structure of GAP (an intermediate in the glycolytic pathway) is similar toGlp,

we investigated whetherGlpO can use GAP as a substrate. Apparent steady state kinetics of the His_6-*Mp*GlpO reaction usingGAPas a substrate under air-saturation (0.26 mM) was measured. The reactions were carried out at 25 ^{o}C, pH 7.0 using the same ABTS-HRP assay at various concentrations of GAP (0.025-6.4 mM) (Experimental Procedures).The results show that GAP can be used as a substrate for His_6-*Mp*GlpO. Initial rates were directly plotted as a function of GAP concentration (Fig. 3D). For comparison, similar reactions with Glp as a substrate were carried out under the same conditions.The results clearly indicate that His_6-*Mp*GlpO can use GAP as a substrate. The apparent steady-state kinetic parameters were as follows: K_m^{GAP} , 1.8 ± 0.2 mM;k_{cat},0.6 s^{-1}, and k_{cat}/K_m, 0.33 $mM^{-1}s^{-1}$. When compared to the kinetic parameters of Glp, it is quite clear that the enzyme prefers to use Glp as a substrate because thek_{cat} and k_{cat}/K_m of the Glp reactions are 100- and 15-fold larger than those of the GAP reactions, respectively (Inset of Fig. 13) (K_m^{Glp} , 12 ± 1 mM; k_{cat},60.1 s^{-1}, and k_{cat}/K_m,5 $mM^{-1}s^{-1}$).Nevertheless, our data imply that in the absence of glycerol, GAP may serve as a substrate in the GlpO reaction to supply H_2O_2 during mycoplasmainfection.

Ligand Binding

The bindings of the oxidized enzyme with other ligands (glycerol, L-lactate, and DL-malate) were investigated to gain the understanding on the active site specificity. Results indicate that only the binding of the oxidized enzyme with L-lactateand DL-malate, not glycerol, can give clear spectroscopic changes (data not shown). The $K_d$values of the binding of the oxidized enzyme and L-lactate calculated from absorbance changes at 401 and 489 nm are 23 ± 4 and 26 ± 4 mM, respectively. For the binding of

318 enzyme and DL-malate, the K_d value determined based on absorbance changes at 440
319 nmis 10 ± 5 mM. These data suggest that enzyme can bind to these substrate analogues
320 but with low affinity.
321
322 **Discussion**
323 Our work herein reports on the biochemical and catalytic properties of the recombinant
324 GlpO from *Mycoplasma pneumoniae*. The enzyme is unique among all GlpOenzymes for
325 its ability to catalyze the reverse reaction of reduced enzyme and DHAP. The results also
326 showed that besides Glp, GlpOcan also use GAP as a substrate. His_6-*Mp*GlpO was
327 successfully expressed in a soluble form in *E. coli*, giving a protein yield of around 19
328 mg/L cell culture. The purified enzyme has a specific activity of about 10 U/mg, and
329 exhibits biochemical properties similar to other flavoprotein oxidases. The His_6-*Mp*GlpO-
330 bound FAD has a maximum absorption at 448 nm with a molar extinction coefficient of
331 12.40 $mM^{-1}cm^{-1}$(Fig. 1A). These valuesareslightly different from thoseof free FAD
332 (11.3$mM^{-1}cm^{-1}$ at 450 nm) [20],and GlpO from *Streptococcus faecium* (11.3 $mM^{-1}cm^{-1}$ at
333 446nm) [3] and *Streptococcus* sp. (11.2 $mM^{-1}cm^{-1}$ at 449 nm) [16].
334 Unlike other GlpOenzymes previously investigated such as the enzyme from *S.*
335 *faecium*[3], His_6-*Mp*GlpO can catalyze the reverse reaction of reduced enzyme and
336 DHAP. This catalytic property of His_6-*Mp*GlpO may represent a control mechanism to
337 prevent excessive generation of H_2O_2,which may be harmful to bacterial cells. Based on
338 the rate constants determined in Fig. 7 and Table 2, the data indicate that the rate
339 constants of the forward reaction (black arrows) are much greater than the reverse
340 reaction (red arrows). Therefore, the reverse reaction can only occur at very high DHAP

concentrations. Similar toGlpO, another flavoenzymemandelate dehydrogenase (MDH) was also reported to catalyze the reverse flavin oxidation by the product[21].

The ability of His_6-*Mp*GlpO to accept electrons from DHAP can also be explained by the reduction potential (E_m^0) of enzyme-bound FAD (FAD/$FADH_2$). The E_m^0 value of His_6-*Mp*GlpO(Fig. 1B) was calculated as -167 ± 1 mV which is lower than the value ofGlpO from *Enterococcuscasseliflavus* (-118 mV) [15]. With the reduction potential of DHAP/Glp of -190 mV, the change of the standard reduction potential ($\Delta E^{o'}$) for the forward reaction of His_6-*Mp*GlpO (FAD + Glp$\rightarrow$ $FADH_2$ + DHAP) is +23 mV, which corresponds to a standard free-energy change ($\Delta G^{o'}$) of -4.44 kJ/mol. Based on these parameters, Glp can favorably reduce the His_6-*Mp*GlpO-bound FAD and the reverse reaction can occur at high concentrations of DHAP (such as those used in Fig. 6A). ForGlpO from *E. casseliflavus*that has anE_m^0 value of -118 mV, the thermodynamics of the forward reduction reaction of this enzyme is more heavily favored than the reverse reaction. The reverse reaction of FAD oxidation by DHAP would require much higher concentrations of DHAP than those employed in the previous investigation [3].

Steady-state kinetic analysis of the His_6-*Mp*GlpO reaction using Glp and O_2 as substrates indicates that the reaction obeys ping-pong kinetics with a turnover number (k_{cat}) of 4.2 s^{-1}(Fig. 2). This k_{cat} value is 4- and 9-fold lower than those of GlpO from*Streptococcus* sp. (18 s^{-1}) [16] and *E.casseliflavus* (37 s^{-1}) [15]under the same pH (7.0) and temperature (4-5 ^{o}C), respectively. These enzymes also use a ping-pong mechanism for their reactions. The K_m value for Glp in the His_6-*Mp*GlpO reaction is 5.5 mM, which is about 4-fold lower and 3-fold higher those of GlpO from *E.casseliflavus* (24 mM) [15] and *Streptococcus* sp. (2 mM) [16], respectively. However, these enzymes

have $K_m$values of O_2 in the same range. The K_m of oxygen for His_6-*Mp*GlpO is 55 μM while those for the enzymes from *E.casseliflavus* and *Streptococcus* sp. are 35 μM and 52 μM, respectively [15, 16].

As for the relevance of these kinetic parameters under physiological conditions, theK_m value for Glpin the *M. pneumoniae*GlpO reaction (5.5 mM) is much higher than thephysiological concentration ofGlp in *M. pneumoniae*(~0.1 mM). The Kd value of the fast reacting (72 mM) that was obtained from half-saturation of kobs is also much higher than the range of Glp physiological concentration. We estimated thephysiological concentration of Glpbased onthe concentration of glycerolpresent in the host blood serum [5, 8] becausea previousinvestigation on glycerol and Glp uptake in *M.mycoides* SC showed that only glycerol, not Glp, could be taken up into the cells. Glycerol can beconverted to Glp by intracellular glycerol kinase [22]. Altogether, these data imply that under physiological conditions, GlpO only functions at a slow rate(turnover≈0.72 s^{-1}).

Our investigation also suggests that besides its physiological substrates, His_6-*Mp*GlpO can use GAP as an electron donor (Fig. 3D),although withthe k_{cat} value ~100-fold lower than Glp. These results suggest that GAP, a metabolic intermediate in the glycolysis pathway, may also be involved in H_2O_2 production during mycoplasma infection. Therefore, GlpOcan be viewed as an enzyme that can employ substrates from three metabolic pathways (the glycerol and lipid metabolic pathways, and glycolysis) for the generation of the reactive oxygen species necessary for the virulence of *M. pneumoniae*. His_6-*Mp*GlpO can use a variety of compounds such as 2,6-dichlorophenol indole phenol (DCPIP), phenazinemethosulfate (PMS) and menadione as electron acceptors (data not shown). This is similar to GlpO from *S.faecium* that can use

ferricyanide and DCPIP as electron acceptors [3]. These data imply that if oxygen is not readily available in the cells, theGlpO reactions may mediate the transfer of electrons from Glp or GAP to other mediators such as quinones for cell energy production.

Investigation of binding of His_6-*Mp*GlpO with ligands gives insight into specificity of the active site. Our data indicate that His_6-*Mp*GlpO can bind L-lactate and DL-malate, but not glycerol. Previous study of GlpO from *S. faecium* ATCC12755 also showed that the enzyme could be inhibited by fructose 6-phosphate [2].These results suggest that the interaction between the anionic moiety of ligand with the enzyme active site is important for the ligand anchorage. Previous structural analysis of a truncated form of GlpO from *Streptococcus* sp. (*Ssp*GlpOΔ) [18] indicates that the Glp-binding pocket of *Ssp*GlpOΔ is formed by various positively charged residues such as Lys429, His65, Arg69, and Arg346. The Arg346 in *Ssp*GlpOΔ is equivalent to Arg302 in glycine oxidase (ThiO) and Arg285 in yeast D-amino acid oxidase (DAAO) [18]. The guanidinium side chain of Arg in these enzymes interacts with a carboxylate group of amino acid substrates. Concurrent with the work in this report, the X-ray structures of His_6-*Mp*GlpO in both oxidized and reduced forms were solved at 2.4 and 2.5 Å resolutions, respectively. More details about His_6-*Mp*GlpO structure and interactions with ligands can be found in[23].The currently available structures suggest that Arg320 of *Mp*GlpO is important for substrate recognition because its guanidinium side chain shows electrostatic interaction with the phosphate moiety of Glp. The data also show that the α-carboxyl moietyof Gly259 and β-hydroxyl moiety of Ser348 can make a hydrogen bond interaction with the C1-OH and C2-OH of Glp, respectively. His51 is located at the position in which it can act as a base to deprotonate the C2-OH of Glp to initiate the hydride transfer for the

410 flavin reduction [23].These residues are also likely to be important for providing the
411 protein-ligand interaction with GAP.

412 A mixture of fast and slow reacting species observed in the reaction of His_6-
413 *Mp*GlpO was also observed in GlpO from *E. casseliflavus* (*Ec*GlpO) [15]and
414 *Streptococcus* sp. (*Ssp*GlpO) [16]. For *Ec*GlpO reduction, the first (fast) phase was
415 hyperbolically dependent on Glp concentration with a limiting k_{red} value of 48 s^{-1}, while
416 the second (slow) phase was independent of Glp concentration with invariable rate
417 constant values of 3.6-5.4 s^{-1}[15]. In contrast to His_6-*Mp*GlpO and *Ec*GlpO, the first (fast)
418 phase of the *Ssp*GlpOreduction reaction is linearly dependent on theGlp concentration,
419 with a bimolecular rate constant for enzyme reduction of 4900 M^{-1} s^{-1}. On the other hand,
420 the second (slow) phase was independent of Glp concentration with an invariable rate
421 constant value of 11.7 s^{-1}[16]. Similar to His_6-*Mp*GlpO, the reduction rate constant of the
422 slow reacting species of both enzymes is significantly lower than that of their overall
423 turnovers, suggesting that the fast reacting enzymesis primarily responsible for
424 thecatalytic reactions.

425 In contrast to many flavin-dependent enzymes that use oxygen as a substrate, a
426 plot of k_{obs} for the enzyme oxidation *versus* oxygen was hyperbolic. This reaction does
427 not form C4a-hydroperoxyflavin as in the reaction of pyranose 2-oxidase [24, 25] or *p*-
428 hydroxyphenylacetate hydroxylase [26, 27]. The origin of the His_6-*Mp*GlpO hyperbolic
429 dependency on oxygen concentration is not certain. Although a simple kinetic
430 interpretation would allude tothe formation of a binary complex of reduced
431 enzyme:oxygen, the current knowledge regarding the specific binding site of oxygen in
432 flavoenzymes are still under debate. A specific oxygen binding site in flavoenzymes is

not well defined although a hydrophobic tunnel that may be relevant for oxygen diffusion is found in cholesterol oxidase[28]. Based on structures of flavin-dependent oxidases and monooxygenases and molecular dynamics simulations, the oxygen approach to the flavin C4a-position is proposed to be "edge-on" for the oxidases and "face-on" for the monooxygenases [29,30]. We could not identify any clear oxygen binding site in the active site of *Mp*GlpO–and the approach for oxygen diffusion in *Mp*GlpO is via the "edge-on" approach [23].

In conclusion, our results indicate that the kinetic mechanism of His_6-*Mp*GlpO is a ping-pongtype in which DHAP leaves before the oxidative half-reaction with oxygen. H_2O_2 release is likely the rate-limiting step for the overall turnover. The rapid kinetics of both half-reactions showed biphasic kinetics whichis due to a mixture of fast and slow reacting enzyme species. The enzyme can catalyze the reverse reaction of reduced His_6-*Mp*GlpO and DHAP. It can also use GAP as a substrate, implying its involvement in the glycolysis pathway in addition to the pathways of glycerol and lipid metabolism.Thus, the contributions from this work can serve as the groundwork for future development of inhibitors against GlpO forthe prevention of *M. pneumonia* infection.

Experimental Procedures

Chemicals and reagents

Flavin adenine dinucleotide disodium salt hydrate (FAD), horseradish peroxidase, type I (HRP), 2,2'-azino-bis(3-ethylbenzothiazoline-6-sulfonic acid) diammonium salt (ABTS), L-α-glycerophosphatebis(cyclohexylammonium) salt (Glp), DL-glyceraldehyde 3-phosphate solution (GAP), and dihydroxyacetone phosphate dilithium salt (DHAP)

were purchased from Sigma-Aldrich (St. Louis, MO, USA).Isopropyl β-D-1-thiogalactopyranoside (IPTG) was purchased from Fermentas Life Sciences (Glen Burnie, MD, USA). All chromatographic media were purchased from GE Healthcare Biosciences (Uppsala, Sweden).

The concentrations of the following compounds were determined using the known extinction coefficients at pH 7.0: ε_{450} = 11.3 $mM^{-1}cm^{-1}$ for FAD, ε_{403} = 100 $mM^{-1}cm^{-1}$ for HRP. The concentrations of Glp in the stock solutions were calculated based on the reducing equivalents in the reduction of the purified recombinant His_6-*Mp*GlpO. A solution (1 mL) of His_6-*Mp*GlpOwas prepared, made anaerobic and the concentration was determinedusing the molar absorption coefficient at 448 nm of 12.4 $mM^{-1}cm^{-1}$. Asolution of Glp was then titrated into the enzyme solution under anaerobic conditions insidean anaerobic glovebox (<5 ppm oxygen; Belle Technology, UK). The absorbance change at 448 nm (ΔA_{448}) of the enzyme before and after the reduction was used for calculating the concentration of the enzyme that was reduced by Glp which is equivalent to the amount of Glp added. The molarequivalent of Glpwas used for calculating the concentration of the stock solution.

Spectroscopic studies

UV-Visible absorbance spectra were recorded with a diode-array spectrophotometer (Hewlett Packard, Palo Alto, CA, USA), a Shimadzu 2501PC (SHIMADZU 2501PC, Shimadzu Corp., Kyoto, Japan)or a Cary 300Bio (Varian Inc., Palo Alto, CA, USA) spectrophotometer. Steady-stateand pre-steady-state kinetics studies were carried out using a stopped-flow spectrophotometer (TGK Scientific

instruments, model SF-61DX2 or SF-61SX) in both single and double-mixing modes. All instruments were equipped with thermostatic cell compartments.

Enzyme assay

The activity of His_6-*Mp*GlpO was measured by monitoring the amount of H_2O_2 formed using the HRP coupled assay[31, 32]. HRP uses the H_2O_2generated from the His_6-*Mp*GlpO-catalyzed reaction to oxidize reduced ABTS to generate oxidized ABTS, which is dark green with a λ_{max} at 420 nm and amolar absorption coefficient of 42.3 $mM^{-1}cm^{-1}$ (per one mole of Glp consumed). The assay mixture in 50 mM sodium phosphate buffer, pH 7.0 typically contained 15 mMGlp, 1 mM ABTS, and 600 nM HRP. The enzyme activity was measured by monitoring the increase inabsorbance at 420 nmwhichisdue to ABTS oxidation. One unit of His_6-*Mp*GlpO activity was defined as the amount of enzyme required to oxidize one micromole of Glp per min.

Expression and purification of His_6-MpGlpO

A single colony of *E. coli* BL21(DE3)harboring the His_6-*Mp*GlpO expression plasmid, pET28a-*mpglpo*, was inoculated into 100 mL of Terrific Broth (in a 500-mL Erlenmeyer flask) containing 30 μg/mL kanamycin, and cultured overnight in a shaking incubator at 37 ^oC. An overnight culture with a final ratio of 1% (v/v) was inoculated into 6 × 800 mL of Terrific Broth containing 30 μg/mL kanamycin. A large-scale culture was grown at 37 ^oC until the absorbance at 600 nm reached ~1. The culture was then cooled down to 25 ^oC and induced by the addition of IPTG at a final concentration of 1 mM and

maintained at this temperature for ~12 h. Cells were harvested by centrifugation and stored at -80 ^{o}C until used.

Unless otherwise indicated, purification of the His_6-*Mp*GlpO was conducted at 4 ^{o}C. Frozen cell paste was thawed and resuspended in 50 mM sodium phosphate buffer, pH 7.0 containing 200 mMNaCl, 10% (v/v) glycerol, 10 mM imidazole, 1 mM DTT, 0.5 mM EDTA, and 100 μM PMSF. Cells were lysed by ultrasonication (Sonic Vibra_cell™ model VCX750). The disrupted cell suspension was then centrifuged at 35,000 ×g for 1 h. The supernatant was additionally clarified by ultracentrifugation at 100,000 ×g for 1.5 h and then loaded onto a Ni-Sepharose (GE Healthcare) column (2.5 × 7.0 cm; volume ~34 mL) pre-equilibrated with 300 mL of 50 mM sodium phosphate buffer, pH 7.0 containing 200 mMNaCl, 10% (v/v) glycerol and 10 mM imidazole. The column was then washed with the same buffer for 300 mL and subsequently eluted with 400 mL of a linear gradient of 10-500 mM imidazole in 50 mM sodium phosphate buffer, pH 7.0 containing 200 mMNaCl, and 10% (v/v) glycerol. Fractions containing the His_6-*Mp*GlpO were identified by measuring the absorbance at 448 nm, pooled, and concentrated using a stirred cell apparatus (Amicon® 8050) equipped with a Millipore membrane YM-10 (10 kDa cut-off). Free FAD was added during the concentration process to make sure that the enzyme fully bound to FAD. An enzyme solution of ~100 mL was thentransferred into a dialysis bag (Sigma-Aldrich) and dialyzed against 4 L of 50 mM sodium phosphate buffer, pH 7.0 containing 0.5 mM EDTA for overnight. The dialyzed sample was loaded onto an SP-Sepharose (GE Healthcare) column (2.5 × 13.0 cm; volume ~64 mL) pre-equilibrated with 700 mL of 50 mM sodium phosphate buffer, pH 7.0 containing 0.5 mM EDTA and 150 mMNaCl. The column was washed with 700 mL of the same buffer and

524 then eluted with 800 mL of a linear gradient of 150-800 mMNaCl in 50 mM sodium
525 phosphate buffer, pH 7.0 containing 0.5 mM EDTA. Fractions containing the enzyme
526 were identified, pooled and concentrated as described above. A solution of ~6-8 mL of
527 the purified enzyme wasdesalted and exchanged into 100 mM Tris-H_2SO_4, pH 7.0
528 containing 0.5 mM EDTA using a Sephadex G-25 (GE Healthcare) column (1.5 × 60.0
529 cm; volume ~106 mL). The desalted enzyme was then aliquotedin500 μL portionsin each
530 microcentrifuge tube and kept at -80 ^{o}C until used. The purity of the enzyme was
531 estimated by 12% (w/v) sodium dodecyl sulfate-polyacrylamide gel electrophoresis. The
532 protein amount was determined using a Bradford method and BSA as a standard protein.
533
534 *Determination of molar extinction coefficients of His_6-MpGlpO-bound FAD*
535 The methods for the determination of the molar absorption coefficients of His_6-
536 *Mp*GlpO-bound FAD wereslightly modified from a general procedure [33]. The frozen
537 purified enzyme was quickly thawed and exchanged into 50 mM sodium phosphate
538 buffer, pH 7.0 using a PD-10 column (GE Healthcare). The holoenzyme solution (900
539 μL) was added 100 μL of 20% (w/v) SDS solution to givea final absorbance value of the
540 enzyme of ~0.25 and afinal SDS concentration of 2% (w/v). The same buffer (100 μM)
541 was added to another aliquot of holoenzyme(900 μL). The absorption spectra of both
542 solutions were recorded and compared. The concentration of released FAD was
543 calculated based onthe FAD molar extinction coefficient of 11.3 $mM^{-1}cm^{-1}$at 450 nm. For
544 the holoenzyme, the molar extinction coefficient at 448 nm (λ_{max}) can be determined
545 according to Eqn1, on the basis that the apoenzyme binds FAD with a ratio of
546 1:1mol.A_{enzyme} represents enzyme absorbance while A_{FAD} represents FAD absorbance.

$$\varepsilon_{enzyme} = \frac{A_{enzyme}}{A_{FAD}} x \varepsilon_{FAD} \qquad (1)$$

Steady-State Kinetics

Two-substrate steady-state kinetics of the His_6-*Mp*GlpO was carried out in 50 mM sodium phosphate buffer, pH 7.0 at 4^{o}C using an ABTS coupled-enzyme assay as previously described [34] and monitored by the Hi-Tech Scientific model SF-61DX stopped-flow spectrophotometer in single-mixing mode. The optical pathlength of the observation cell was 1 cm. A mixture of 5.16 nM His_6-*Mp*GlpO, 600 nM HRP, and 1 mM ABTS was mixed against solutions of various concentrations of Glp (4, 8, 16, and 32 mM) and oxygen (0.13, 0.26, 0.44, 0.65, 1.16 mM). The reaction progress was followed by monitoring the increase of absorbance at 420 nm at which the oxidized ABTS absorbs with the molar extinction coefficient of 42.3 $mM^{-1}cm^{-1}$ (per one mole of Glp consumed) [31, 32]. Kinetic traces obtained from each reaction (performed in triplicate) were calculated their initial rates using Program A (developed by Chun-Jen Chiu, Rong Chang, Joel Dinverno, and David P. Ballou at the University of Michigan, Ann Arbor, MI). The initial rates were then analyzed for steady-state kinetic parameters of a bi-substrate enzyme reaction according to either a double-reciprocal plot of a ping-pong mechanism (Eqn 2)[35] or a direct plot (Eqn 3) using the EnzFitter program (BIOSOFT, Cambridge, UK).

Apparent steady-state kinetics of the His_6-*Mp*GlpO reaction was performed in air-saturated (oxygen concentration of ~0.26 mM)50 mMsodium phosphate buffer, pH 7.0 at 25 ^{o}C at various concentrations of DL-glyceraldehyde 3-phosphate (GAP) (0.025-6.4 mM) using thecoupling assay with horseradish peroxidase-coupled assay. The reactions

were monitored at 420 nm as described above. The initial rates were calculated and then plotted *versus*GAP concentration. Apparent kinetic parameters werecalculated using Marquardt-Lavenberg algorithms in the KaleidaGraph program version 4.0 and compared to the reaction using various concentrations of Glp (0.1-51.2 mM) under the same conditions.

$$\frac{e}{v} = \phi_0 + \frac{\phi_A}{[A]} + \frac{\phi_B}{[B]} \quad (2)$$

$$v = \frac{V[A][B]}{K_B[A] + K_A[B] + [A][B]} \quad (3)$$

Binding of the oxidized His$_6$-MpGlpO with products

A solution (1 mL) of the oxidized enzyme (A_{448} ~0.3; 24 μM) in 50 mM sodium phosphate buffer, pH 7.0 was placed in both sample and reference cells.Then, a baseline was recorded.Various concentrations of H_2O_2 (0.16-371 mM) or DHAP (0.005-30 mM) were added into the enzyme solution in the sample cell while an equal volume of buffer was added into the reference cell.An absorption spectrum was recorded after each titration using a double-beam spectrophotometer. The changes in absorbance were plotted against the concentrations of each product.Dissociation constants for the binding of products to the oxidized enzyme were determined and analyzed according to the method previously described [36]andEqn 4, where ΔA represents the absorbance change, ΔA_{max} is the maximum absorbance change, $[L]_{free}$ is a concentration of free ligand, and K_d is a dissociation constant for enzyme-ligand complex. The analysis was done using Marquardt-Lavenberg algorithms in the KaleidaGraph program version 4.0. Similar

protocol and data analysis were also applied for spectrophotometric titration of the FAD solution (A_{450} ~0.3) with H_2O_2 using a similar range of concentrations. For the binding of enzyme with other substrate analogues–glycerol, L-lactate, and D,L-malate– the reactions and analysis were performed and carried out as mentioned above, except that the concentrations of glycerol, L-lactate, and D,L-malate used were varied from 0.16-371 mM.

$$\frac{\Delta A}{\Delta A_{max}} = \frac{[L]_{free}}{K_d + [L]_{free}} \qquad (4)$$

Binding and reaction of the reducedHis$_6$-MpGlpO with DHAP

A solution (1 mL) of the oxidized enzyme (A_{448} ~0.3; 24 μM) in 50 mM sodium phosphate buffer, pH 7.0 was placed in an anaerobic glove box in which the oxygen concentration was less than 5 ppm (Belle Technology, UK) to remove trace amounts of oxygen and then reduced by a stoichiometric concentration of dithionite under anaerobic conditions. Various concentrations of DHAP (0.69-4,308 μM) were subsequently added to the reduced enzyme. All concentrations reported above are final concentrations after mixing. A spectrum after each titration was recorded by a GeneQuant1300spectrophotometer (GE Healthcare, UK) residing in the anaerobic glove box. The spectrum of reduced enzyme was subtracted from all the spectra obtained from each titration to give the change in absorbance (ΔA).Analysis was done according to the method previously described [36].

As the results indicate that the reverse reaction of the reduced enzyme and DHAP can occur, the kinetics of the enzyme re-oxidation by DHAP was further explored using

stopped-flow spectrophotometry at 4 ^{o}C. The reduced enzyme (16 μM) in 50 mM sodium phosphate buffer, pH 7.0 was mixed with various concentrations of DHAP (0.1-12.8 mM) under anaerobic conditions using a single-mixing mode of a stopped-flow apparatus. All concentrations shown above are given as final concentrations after mixing. The reactions were monitored at 448 nm and the final spectra after the reaction were recorded. Kinetic traces were analyzed by Program A and the observed rate constants (k_{obs}) were plotted *versus* DHAP concentrations. The plots were analyzed according to Eqn 5, where k_1 is a bimolecular rate constant for the reduced enzyme re-oxidation.

$$k_{obs} = k_1 \cdot [\text{DHAP}] \qquad (5)$$

Measurement of the standard reduction potential of His$_6$-MpGlpO

Standard reduction potential of His$_6$-*Mp*GlpO was measured in 50 mM sodium phosphate buffer, pH 7.0 at 25 ^{o}C by Massey's method using the xanthine/xanthine oxidase reduction system with benzyl viologen as an electron mediator [37]. Thereference dye used for measuring the standard reduction potential of His$_6$-*Mp*GlpO was cresyl violet which has a standard reduction potential (E_m^0) value of -166 mV [38]. A solution mixture of dye (A_{519} ~0.3) and the oxidized enzyme (A_{448} ~0.3; 24 μM), benzyl viologen (5.3 μM), and xanthine (0.5 mM) in 50 mM sodium phosphate buffer, pH 7.0 was placed in an anaerobic cuvette and made anaerobic by purging with oxygen-free nitrogen for 10-12 cycles to evacuate trace amounts of oxygen. The spectrum of the oxidized species was then recorded. The anaerobic solution was then tipped into xanthine oxidase (10 nM) from the cuvette sidearm and the spectral changes were recorded. All

concentrations shown above are as after mixing. The enzyme and dye were slowly reduced (>8 hr) so that the reduction process was under equilibrium. The reduction potentials of enzyme (E_e) and dye (E_d) were determined according to Eqns 6and 7, respectively, in which E_{red} and E_{ox} are the concentrations of the reduced and oxidized enzyme, respectively, D_{red} and D_{ox} are the concentrations of the reduced and oxidized dye, respectively, E_e^0 and E_d^0 are the standard reduction potential values of enzyme and dye, respectively, and n_e and n_d are the numbers of electrons involved in the reduction process. At equilibrium, the value of E_e is equivalent to E_d and Eqns 6and 7 can be rearranged to Eqn8 which can be used for determining the E_e^0 value. After the complete reduction, the absorbance at 407 nm (isobestic point of a reference dye) and 540 nm were used for calculating the concentrations of the oxidized enzyme (E_{ox}) and the reduced dye (D_{red}) during the reduction process, respectively. The concentrations of reduced and oxidized enzyme (E_{red}) and dye (D_{ox}) at different points of the reduction process were analyzed with Eqn 8 to determine the standard reduction potential value (E_e^0) of the enzyme.

$$E_e = E_e^0 - \frac{0.0592}{n_e}\log(E_{red}/E_{ox}) \quad (6)$$

$$E_d = E_d^0 - \frac{0.0592}{n_d}\log(D_{red}/D_{ox}) \quad (7)$$

$$\log(E_{red}/E_{ox}) = \frac{n_e(E_e^0 - E_d^0)}{0.0592} + (n_e/n_d)\log(D_{red}/D_{ox}) \quad (8)$$

Reductive half-reaction of His_6-MpGlpO

A solution of anaerobic oxidized enzyme (~28μM; A_{448} ~0.35) in 50 mM sodium phosphate buffer, pH 7.0 containing 0.5 mM EDTA, and 1 mM DTT was mixed with various concentrations of Glp (0.2-51.2mM) under anaerobic conditions using the stopped-flow spectrophotometer at 4 ^{o}C.All concentrations shown are as after mixing. Kinetics of the enzyme reduction was monitored by the absorbance change at 448 nm. The kinetic traces were analyzed by Program A to obtain observed rate constants from each exponential phase. The observed rate constants obtained were plotted *versus* Glpconcentrations. The results were then analyzed with Eqn9, where k_{obs} is the observed rate constants, k_{max} is the rate constant for flavin reduction (k_{red}), S is Glp concentration, and K_d is the dissociation constant for substrate binding. The analysis was carried out using Marquardt-Lavenberg algorithms in KaleidaGraph program version 4.0.

$$k_{obs} = \frac{k_{max} \cdot [S]}{K_d + [S]} \qquad (9)$$

Oxidative half-reaction of His_6-MpGlpO

The anaerobically oxidized enzyme (~28μM; A_{448} ~0.35) in 50 mM sodium phosphate buffer, pH 7.0 containing 0.5 mM EDTA, and 1 mM DTT was titrated stoichiometrically with Glp to yield the reduced enzyme. The reduced enzyme was then mixed with various concentrations of oxygen (0.13, 0.32, 0.61, 1.03mM) using a stopped-flow spectrophotometer at 4^{o}C. All concentrations shown are as after mixing. The kinetics of enzyme oxidation was monitored by absorbance at 448 nm. The kinetic traces were analyzed by Program A to obtain the observed rate constants. The plots of k_{obs} as a

682 function of oxygen concentrations were analyzed using Eqn9, in which k_{max} is the rate
683 constant for flavinoxidation (k_{ox}), S is oxygen concentration, and K_d is the dissociation
684 constant for oxygen binding. The analysis was carried out using Marquardt-Lavenberg
685 algorithms in KaleidaGraph program version 4.0.
686
687 *Reactions of the Glp-reduced His$_6$-MpGlpO with O_2 in a double-mixing mode*
688 Double-mixing stopped-flow experiments were doneto evaluate whetherthe
689 presence of DHAP can affect the oxygen reaction. An anaerobic solution of the oxidized
690 His$_6$-*Mp*GlpO (91 μM) in Syringe A was mixed first with Glp (91 μM) in Syringe B. The
691 reactions were aged for 100 s to allow the enzyme reduction to proceed. The solution
692 from the first mixing was later mixed with various concentrations of oxygen (0.26, 0.61,
693 1.03, 2.06 mM) in 50 mM sodium phosphate buffer, pH 7.0 in the second mix. The
694 reactions were monitored at 448 nm with a double-mixing mode stopped-flow
695 spectrophotometer (Hi-Tech Scientific Model SF-61DX). All concentrations shown are
696 initial concentrationsbefore mixing. The kinetic traces were analyzed by Program A and
697 the k_{obs} values of individual phases were plotted *versus* oxygen concentration. The plots
698 were analyzed according to Eqn 9 using Marquardt-Lavenberg algorithms in
699 KaleidaGraph program version 4.0. Results of this reaction were compared to the results
700 of single-mixing mode oxidative half-reaction experiments previously described.
701
702 *Reactions of the dithionite-reduced His$_6$-MpGlpO with O_2 in the presence of DHAP*
703 An anaerobic solution of the dithionite-reduced His$_6$-*Mp*GlpO (91 μM) in Syringe
704 A was mixed first with DHAP (136.5 μM) in Syringe B at various age times (10, 20, 100,

and 200 s). The solution mixture was then mixed with oxygen (0.26 mM) in 50 mM sodium phosphate buffer, pH 7.0 in the second mix. The reactions were monitored at 448 nm by double-mixing mode stopped-flow experiments. All concentrations shown are initial concentrations before mixing. The kinetic traces were analyzed by Program A and the kinetics results at various age times were compared to the results obtained from the oxidative half-reaction in the absence of DHAP.

Acknowledgements

This work was supported by grants from The Thailand Research Fund MRG5580066 (to SM) and RTA5680001 (to PC), the Faculty of Science, Burapha University (to SM) and the Faculty of Science, Mahidol University (to PC).We would like to thank Dr. RuchanokTinikul(MahidolUniversity Nakhonsawan Campus)for her help with the molecular biology work. We are grateful for Professor Dr. David P. Ballou (University of Michigan, Ann Arbor) for helpful discussion.

728 **References**

729 1. Koditschek LK &Umbreit WW (1969) α-Glycerophosphate oxidase in *Streptococcus*
730 *faecium*F24.*J Bacteriol***98**, 1063-1068.

731 2. Esders TW &Michrina CA (1979) Purification and properties of α-glycerophosphate
732 oxidase from *Streptococcus faecium* ATCC 12755. *J BiolChem***254**, 2710-2715.

733 3. Claiborne A (1986) Studies on the structure and mechanism of *Streptococcus faecium*
734 L-α-glycerophosphate oxidase. *J BiolChem***261**, 14398-14407.

735 4. Halbedel S, Hames C &Stulke J (2007) Regulation of carbon metabolism in the
736 mollicutes and its relation to virulence. *JMolMicrobiolBiotechnol***12**, 147-154.

737 5. Hames C, Halbedel S, Hoppert M, Frey J &Stulke J (2009) Glycerol metabolism is
738 important for cytotoxicity of *Mycoplasma pneumoniae*. *J Bacteriol***191**, 747-753.

739 6. Veal EA, Day AM & Morgan BA (2007) Hydrogen peroxide sensing and signaling.
740 *Mol Cell***26**, 1-14.

741 7. Almagor M, Kahane I &Yatziv S (1984) Role of superoxide anion in host cell injury
742 induced by *Mycoplasma pneumoniae* infection: a study in normal and trisomy 21 cells. *J*
743 *Clin Invest***73**, 842-847.

744 8. Pilo P, Vilei EM, Peterhans E, Bonvin-Klotz L, Stoffel MH, Dobbelaere D & Frey J
745 (2005) A metabolism enzyme as a primary virulence factor of *Mycoplasma mycoides*
746 subsp. *mycoides* small colony. *J Bacteriol***187**, 6824-6831.

747 9. Waites KB &Talkington DF (2004) *Mycoplasma pneumoniae* and its role as a human
748 pathogen. *ClinMicrobiol Rev***17**, 696-728.

749 10.Fairlamb AH &Bowman IBR (1977) *Trypanosomabrucei*: suramin and other
750 trypanocidal compounds' effect on *sn*-glycerol-3-phosphate oxidase. *ExpParasitol***43**,
751 353-361.
752 11. Opperdoes FR, Borst P &Fonck K (1976) The potential use of inhibitors of glycerol-
753 3-phosphate oxidase for chemotherapy of African trypanosomiasis. *FEBS Lett***62**, 169-
754 172.
755 12. Fairlamb AH & Bowman IBR (1977) The isolation and characterisation of particulate
756 *sn*-glycerol-3-phosphate oxidase from *Trypanosomabrucei*. *Int J Biochem***8**, 659-668.
757 13. Fairlamb AH & Bowman IBR (1977) Inhibitor studies on particulate sn-glycerol-3-
758 phosphate oxidase from *Trypanosomabrucei*. *Int J Biochem***8**, 669-675.
759 14. Grady RW, Bienen EJ & Clarkson AB (1986) Esters of 3,4-dihydroxybenzoic acid,
760 highly effective inhibitors of the *sn*-glycerol-3-phosphate oxidase of
761 *Trypanosomabruceibrucei*. *MolBiochemParasitol***21**, 55-63.
762 15. Parsonage D, Luba J, Mallett TC & Claiborne A (1998) The soluble α-
763 glycerophosphate oxidase from *Enterococcus casseliflavus*. *J BiolChem***273**, 23812-
764 23822.
765 16. Charrier V, Luba J, Parsonage D & Claiborne A (2000) Limited proteolysis as a
766 structural probe of the soluble α-glycerophosphate oxidase from *Streptococcus* sp.
767 *Biochemistry* **39**, 5035-5044.
768 17. Finnerty CM, Charrier V, Claiborne A &Karplus PA (2002) Crystallization and
769 preliminary crystallographic analysis of the soluble α-glycerophosphate oxidase from
770 *Streptococcus* sp. *ActaCrystallogr D BiolCrystallogr***D58**, 165-166.

771 18. Colussi T, Parsonage D, Boles W, Matsuoka T, Mallett TC, Karplus PA & Claiborne
772 A (2008) Structure of α-glycerophosphate oxidase from *Streptococcus* sp.: a template for
773 the mitochondrial α-glycerophosphate dehydrogenase. *Biochemistry***47**, 965-977.
774 19.Fersht A (1999) Measurement and magnitude of individualrate constants. In*Structure*
775 *and Mechanism in Protein Science: A Guide to Enzyme Catalysis and Folding*, pp
776 132−167. W.H. Freeman & Co., NewYork, NY.
777 20. Dawson RMC, Elliot DC, Elliot WH & Jones KM (1986) *Data for biochemical*
778 *research*, 3rd edn. Oxford University Press, New York, NY.
779 21. Dewanti AR &Mitra B (2003) A transient intermediate in the reaction catalyzed by
780 (*S*)-mandelate dehydrogenase from *Pseudomonas putida*. *Biochemistry***42**, 12893-12901.
781 22. Vilei EM & Frey J (2001) Genetic and biochemical characterization of glycerol
782 uptake in *Mycoplasma mycoides* subsp. *mycoides* SC: its impact on H_2O_2 production and
783 virulence. *ClinDiagn Lab Immunol***8**, 85-92.
784 23. Elkhal CK, Kean K, Parsonage D, Maenpuen S, Chaiyen P, Claiborne A & Karplus
785 PA (2015) Structure and proposed mechanism of α-glycerophosphate oxidase from
786 *Mycoplasma pneumoniae*. *Article in Revision*.
787 24. Sucharitakul J, Prongjit M, Haltrich D & Chaiyen P (2008) Detection of a C4a-
788 hydroperoxyflavin intermediate in the reaction of a flavoprotein oxidase. *Biochemistry***47**,
789 8485-8490.
790 25. Wongnate T, Surawatanawong P, Visitsatthawong S, Sucharitakul J, Scrutton NS &
791 Chaiyen P (2014) Proton-coupled electron transfer and adduct configuration are
792 important for C4a-hydroperoxyflavin formation and stabilization in a flavoenzyme. *J Am*
793 *ChemSoc***136**, 241-253.

794 26. Ruangchan N, Tongsook C, Sucharitakul J & Chaiyen P (2011) pH-dependent studies
795 reveal an efficient hydroxylation mechanism of the oxygenase component of *p*-
796 hydroxyphenylacetate 3-hydroxylase. *J BiolChem***286**, 223-233.
797 27. Thotsaporn K, Chenprakhon P, Sucharitakul J, Mattevi A&Chaiyen P (2011)
798 Stabilization of C4a-hydroperoxyflavin in a two-component flavin-dependent
799 monooxygenase is achieved through interactions at flavin N5 and C4a atoms.*J*
800 *BiolChem***286**, 28170-80.
801 28. Chen L, Lyubimov AY, Brammer L, Vrielink A & Sampson NS (2008) The binding
802 and release of oxygen and hydrogen peroxide are directed by a hydrophobic tunnel in
803 cholesterol oxidase. *Biochemistry***47**, 5368-5377.
804 29. Baron R, Riley C, Chenprakhon P, Thotsaporn K, Winter RT, Alfieri A, Forneris F,
805 van Berkel WJ, Chaiyen P, Fraaije MW, Mattevi A &McCammon JA (2009) Multiple
806 pathways guide oxygen diffusion into flavoenzyme active sites. *ProcNatlAcadSci USA*
807 **106**, 10603-10608.
808 30. Chaiyen P, Fraaije MW &Mattevi A (2012) The enigmatic reaction of flavins with
809 oxygen. *Trends BiochemSci***37**, 373-380.
810 31. Prongjit M, Sucharitakul J, Wongnate T, Haltrich D & Chaiyen P (2009) Kinetic
811 mechanism of pyranose 2-oxidase from *Trametes multicolor*. *Biochemistry***48**, 4170-4180.
812 32. Pitsawong W, Sucharitakul J, Prongjit M, Tan TC, Spadiut O, Haltrich D, Divne C
813 &Chaiyen P (2010) A conserved active-site threonine is important for both sugar and
814 flavin oxidations of pyranose 2-oxidase. *J BiolChem***285**, 9697-9705.

33. Macheroux P (1999) UV-visible spectroscopy as a tool to study flavoproteins, In *Flavoprotein Protocols*,(Chapman, S.K., & Reid, G.A., eds.), pp. 1-7, Humana Press. Totowa, NJ.

34. Daneel HJ, Rossner E, Zeeck A &Giffhorn F (1993) Purification and characterization of a pyranose oxidase from the basidiomycete*Peniophoragigantea* and chemical analyses of its reaction products. *Eur J Biochem***214**, 795-802.

35. Dalziel K (1957) Initial steady-state velocities in the evaluation of enzyme-coenzyme-substrate reaction mechanism. *ActaChemScand***11**, 1706-1723.

36. Chenprakhon P, Sucharitakul J, Panijpan B & Chaiyen P (2010) Measuring binding affinity of protein-ligand interaction using spectrophotometry: binding of neutral red to riboflavin-binding protein. *J Chem Ed***87**, 829-831.

37. Massey V (1991) A simple method for the determination of redox potentials, In *Flavins and Flavoproteins* (Curti, B., Rochi, S., &Zanetti, G., eds.) pp. 59-66, Water DeGruyter&Co., Berlin, Germany.

38. Clark WM (1960) Compilations of data in *oxidation-reduction potentials of organic systems*. pp. 410, Wavery Press, Inc., Baltimore.

Table 1: Purification table of the recombinant His_6-*Mp*GlpO

	Volume (mL)	Total Activity (U)	Total Protein (mg)	Specific Activity (U/mg)	Yield (%)
Crude extract	180	13,968	10,746	1.3	100
Ni-Sepharose	150	2,775	244.5	11.4	20
SP-Sepharose	9	1,638	163.8	10	12

*The data in this table were from the purification of 83 g cell paste (8.8 liters culture).

855 **Table 2:** Thermodynamics and kinetic parameters involvedin the His_6-*Mp*GlpO reaction

Parameters	Constants
Fast reacting enzyme	
k_1, formation of E_{ox}:Glp complex	83.3 $M^{-1}s^{-1}$
k_2, Glp release	6 s^{-1}
k_3, enzyme reduction	199 ± 34 s^{-1}
k_4, reverse reaction of E_{red} and DHAP	56.5 $M^{-1}s^{-1}$
k_5, k_6, k_{10}	ND
k_7, re-oxidation of reduced enzyme	627 ± 81 s^{-1}
k_9, H_2O_2 release	4.2 ± 0.1 s^{-1}
K_{d1}, dissociation constant for E_{ox}:Glp complex	72 ± 18 mM
K_{d2}, dissociation constant for E_{red}:O_2 complex	1.3 ± 0.2 mM
K_{d3}, dissociation constant for E_{red}:H_2O_2 complex	0.4 ± 0.2 mM
Slow reacting enzyme	
k_1', k_2', k_4', k_5', k_6'	ND
k_3', enzyme reduction	2.08 ± 0.01 s^{-1}
k_7', re-oxidation of reduced enzyme	85 ± 11 s^{-1}
$K_{d1'}$, dissociation constant of E^*_{ox}:Glp complex	1.38 ± 0.02 mM
$K_{d2'}$, dissociation constant of E^*_{red}:O_2 complex	0.5 ± 0.1 mM
k_{obs} for interconversion of fast and slow reacting enzymes	
$k_f + k_r$	> 6 s^{-1}, <16 s^{-1}

856 ND = Not determined

857 **Figure legends**

858 **Fig. 1.** Absorption and reduction properties of His_6-*Mp*GlpO. (A)Absorption spectra of
859 the enzyme-bound FAD (solid line) and the released FAD upon denaturation by 2% (w/v)
860 SDS (dashed line) are overlaid. The molar absorption coefficient of His_6-*Mp*GlpO was
861 determined as12.40 ± 0.03 $mM^{-1}cm^{-1}$. (B) Standard reduction potential measurement of
862 His_6-*Mp*GlpO at 25 ^{o}C by Massey's method using benzyl viologen-mediated
863 xanthine/xanthine oxidase reaction system.The standard reduction potential value (E_e^0) of
864 the enzyme calculated from the y-intercept of the plot of $\log(E_{red}/E_{ox})$ *versus*
865 $\log(D_{red}/D_{ox})$ is -167 ± 1 mV (Inset of B).

866

867 **Fig. 2.** Two-substrate steady-state kinetics of the His_6-*Mp*GlpO reaction at 4 ^{o}C. The
868 assay reactions were monitored by the HRP coupled-assay using astopped-flow
869 spectrophotometer. (A) Initial rates obtained from various concentrations of Glp and O_2
870 were measured and plotted as a double-reciprocal plot of e/v_o *versus* 1/[Glp] at various
871 concentration of O_2 (0.13-1.16 mM from upper to lower lines) or (B) *versus*1/[O_2] at
872 various concentrations of Glp (4-32 mM from upper to lower lines). Both double-
873 reciprocal plots in A and B show a parallel-line pattern, indicating that His_6-*Mp*GlpO
874 uses a ping-pong mechanism.

875

876 **Fig. 3.** Reductive half-reaction of His_6-*Mp*GlpO at 4 ^{o}C. A solution of the oxidized
877 enzyme (~28 μM) was mixed with various concentrations of Glp (0.4-51.2 mM from
878 right to left traces) under anaerobic conditions using a single-mixing mode of the
879 stopped-flow apparatus. (A) The reaction kinetics was monitored by measuring the

absorbance change at 448 nm. Kinetic analyses indicate that the enzyme reduction is biphasic. (B-C) Plots of k_{obs} values obtained from both phases *versus*Glp concentrations are hyperbolic with limiting reduction rate constant values of 199 ± 34 (B) and 2.08 ± 0.01 s^{-1} for the fast and slow reacting enzyme, respectively. The data suggest that the enzyme reduction involves a two-step process in which one population reacts faster than another. (D) Apparent steady-state kinetics of His_6-*Mp*GlpO using GAP and Glp as substratesat 25 ^oC. Initial rates obtained from the reaction usingGAP (0.025-6.4 mM) were directly plotted *versus*GAP concentrations while those obtained from the reaction using Glp (0.1-51.2 mM) as a substrate are shown in the inset. The results indicated that the k_{cat} and $k_{cat}/K_m$of the reaction using Glp as a substrate are 100- and 15-fold greater than those of GAP, respectively. (E)Proposed kinetic scheme for the reductive half-reaction of His_6-*Mp*GlpO.

Fig. 4. Oxidative half-reaction of the reduced His_6-*Mp*GlpO at 4 ^oC. An anaerobic solution of the reduced enzyme was mixed with various concentrations (0.13-1.03 mM from lower to upper traces) of oxygenated buffer using a single-mixing mode of stopped-flow apparatus. (A) The reaction kinetics was monitored by the absorbance change at 448 nm. (B-C) Kinetic analyses indicated that the kinetics of the reaction of the reduced enzyme with O_2 is biphasic and the plots of k_{obs} values of both phases *versus* O_2 concentrations are hyperbolic. The ratio of amplitude change for both phases is 70:30 throughout all oxygen concentrations used. The limiting rate constant values for the reduced enzyme re-oxidation for the fast and slow reacting enzyme are 627 ± 81 and 85 ± 11 s^{-1}, respectively. (D)Proposed kinetic scheme for the oxidative half-reaction of His_6-

903 *Mp*GlpO.

904

905 **Fig. 5.** Double-mixing stopped-flow experiments of reduced His_6-*Mp*GlpO reacting with
906 oxygen at 4 ^{o}C. A solution of the oxidized enzyme (91 μM before mixing) was added to
907 Glp (91 μM before mixing) in the first mix and then mixed with various concentrations of
908 O_2 (0.26-2.06 mM before mixing; from lower to upper traces) in the second mix. (A) The
909 reaction kinetics was monitored by changes in the absorbance at 448 nm. Kinetic
910 analyses indicated that all reaction traces display biphasic kinetics and amplitude changes
911 that are similar to those obtained from the oxidative half-reaction performed in the single-
912 mixing mode (Fig. 4A). (B-C) The plots of k_{obs} values *versus* oxygen concentrations are
913 hyperbolic with the rate constant (k_{ox}) values for enzyme re-oxidation of 524 ± 34 and
914 107 ± 5 s^{-1} that are similar to those obtained from the results in Figs. 4B and 4C. The
915 similarity in these kinetic behaviors suggests that DHAP is quickly released after its
916 formation. (D) In another experiment, a solution of the dithionite-reduced enzyme (91
917 μM before mixing) was added to DHAP (136.5 μM before mixing) for various age times
918 (10, 20, 100, and 200 s) in the first mix and then mixed with the oxygenated buffer (O_2 =
919 0.26 mM before mixing) in the second mix. All kinetics traces were similar and also
920 similar to the results in (A) and in Fig. 4. Altogether, complex of reduced enzyme and
921 DHAP could not be detected, implying that the DHAP release is fast during the catalytic
922 turnover of His_6-*Mp*GlpO.

923

924 **Fig. 6.** The reaction of the reduced His_6-*Mp*GlpO with DHAP. (A) A solution of the
925 reduced enzyme (24 μM) was mixed with various concentrations of DHAP (0.69-4,308

μM(from lower to upper spectra). The binding signal was measured by spectrophotometry at 25 ^{o}C. Difference spectra showed that binding of DHAP to the reduced enzyme caused enzyme re-oxidation as indicated by the increase of absorbance at 448 nm. (B) Pseudo-first order kinetics for the reaction of the reduced enzyme and various concentrations of DHAP (0.2-12.8 mM from lower to upper traces) was monitored under anaerobic conditions using a single-mixing mode stopped-flow spectrophotometer at 4 ^{o}C. The kinetic traces at 448 nm were recorded. (C-D) Kinetic analysis indicatedthat the reaction is biphasic and the k_{obs} values obtained from the first phase are constant (6 s^{-1}) while those of the second phase are linearly dependent on DHAP concentrations with a bimolecular rate constant of 56.5 $M^{-1}s^{-1}$. (E)Proposed scheme for the reverse reaction of reduced His_6-*Mp*GlpO and DHAP.

Fig. 7. Proposed overall catalytic reaction of His_6-*Mp*GlpO. Two enzyme populations (fast and slow reacting species) react with substrates in both half-reactions. The reverse flavin oxidation is shown as the red arrows (see text for details). Thermodynamics and kinetics parameters are presented in Table 2.

Figures

Fig. 1

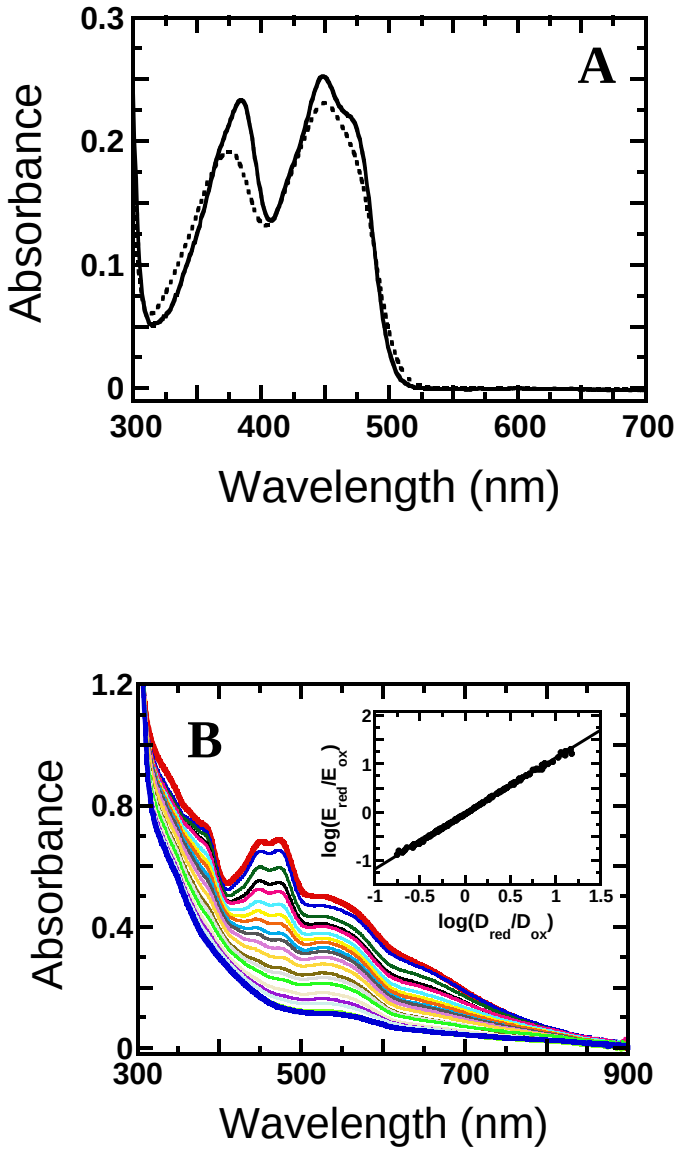

Fig. 2

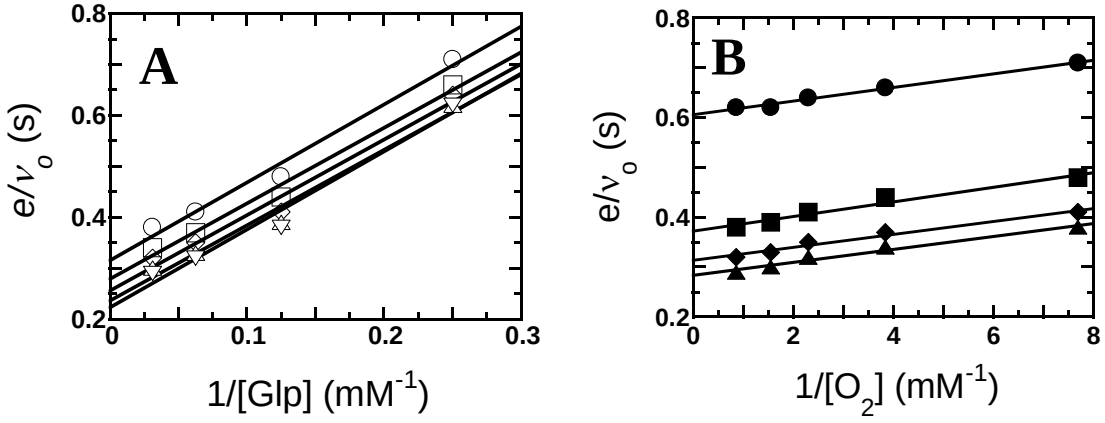

Fig. 3

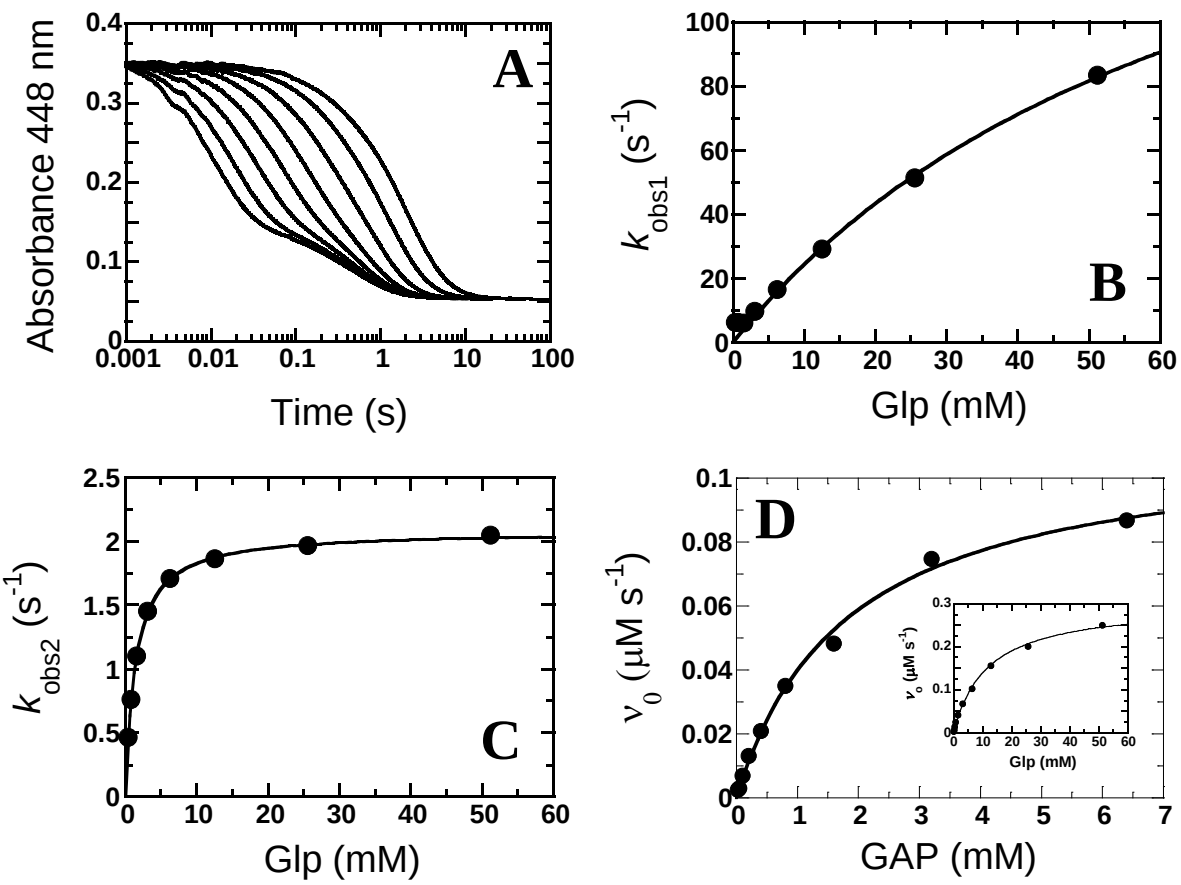
A
Absorbance 448 nm
Time (s)
B
k_{obs1} (s^{-1})
Glp (mM)
C
k_{obs2} (s^{-1})
Glp (mM)
D
v_0 (μM s^{-1})
GAP (mM)
Glp
(70%) E_{ox}
K_d = 72 mM
E_{ox}:Glp
k_{red} = 199 s^{-1}
E_{red} + DHAP
k_f k_r
E
k'_f k'_r
(30%) E^*_{ox}
K_d = 1.38 mM
E^*_{ox}:Glp
k_{red} = 2.08 s^{-1}
E^*_{red} + DHAP
Glp

Fig. 4

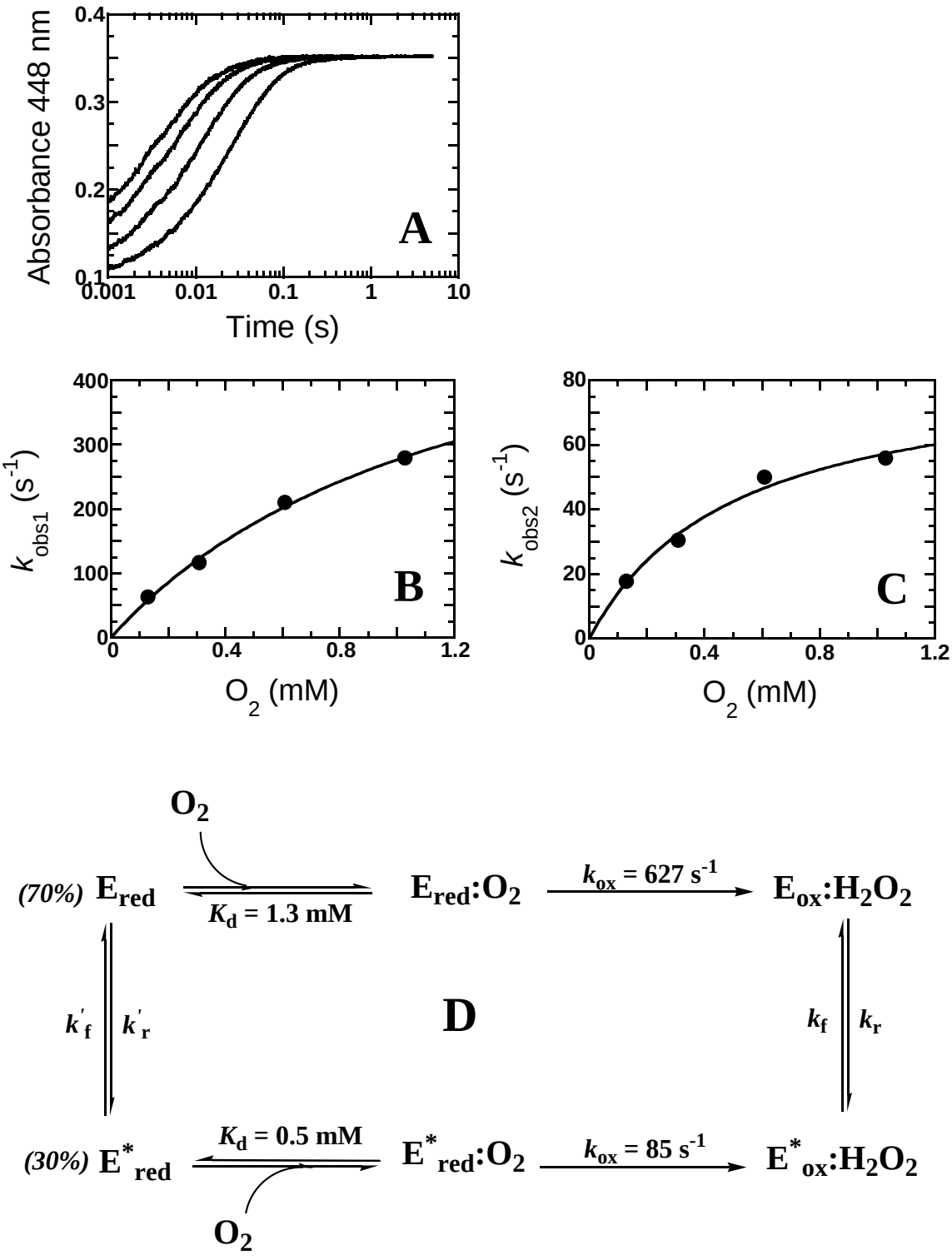
Absorbance 448 nm
Time (s)
A
k_{obs1} (s^{-1})
O_2 (mM)
B
k_{obs2} (s^{-1})
O_2 (mM)
C
O_2
(70%) E_{red}
K_d = 1.3 mM
$E_{red}:O_2$
k_{ox} = 627 s^{-1}
$E_{ox}:H_2O_2$
k'_f
k'_r
D
k_f
k_r
(30%) E^*_{red}
K_d = 0.5 mM
$E^*_{red}:O_2$
k_{ox} = 85 s^{-1}
$E^*_{ox}:H_2O_2$
O_2

Fig. 5

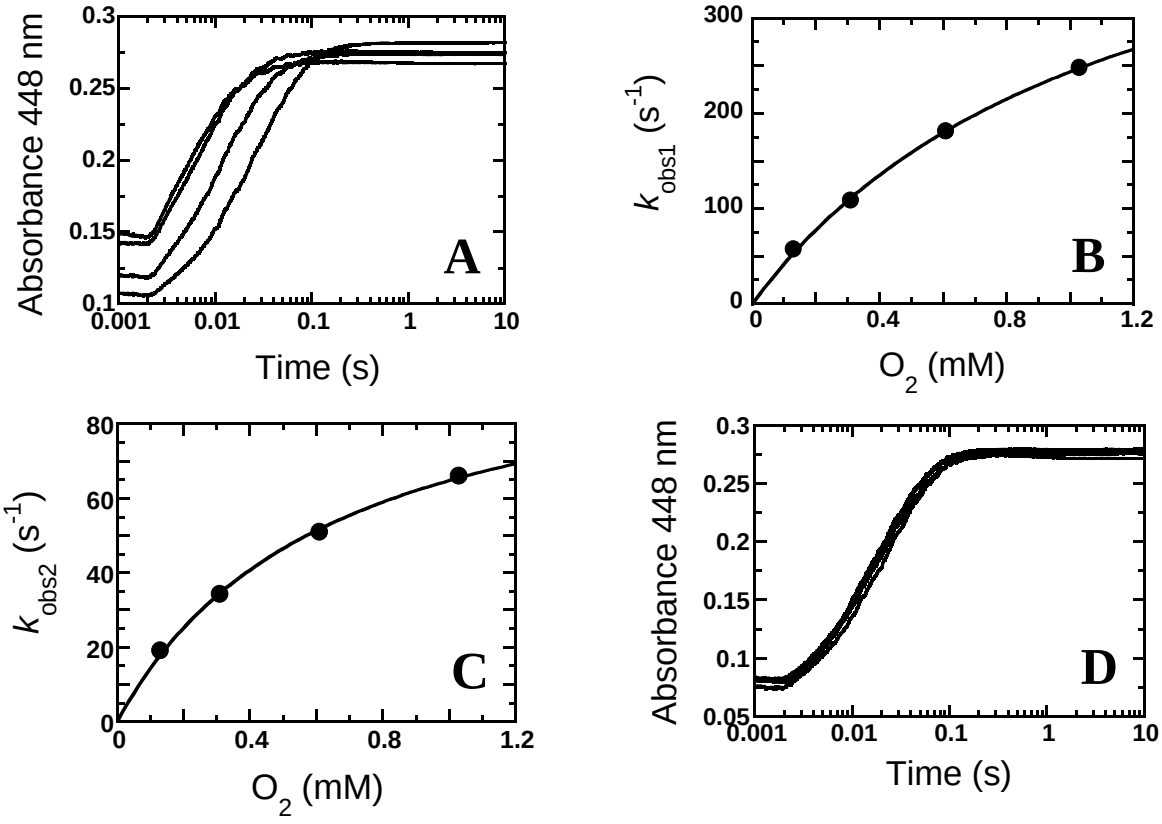
A
Absorbance 448 nm
Time (s)
B
k_{obs1} (s^{-1})
O_2 (mM)
C
k_{obs2} (s^{-1})
O_2 (mM)
D
Absorbance 448 nm
Time (s)

Fig. 6

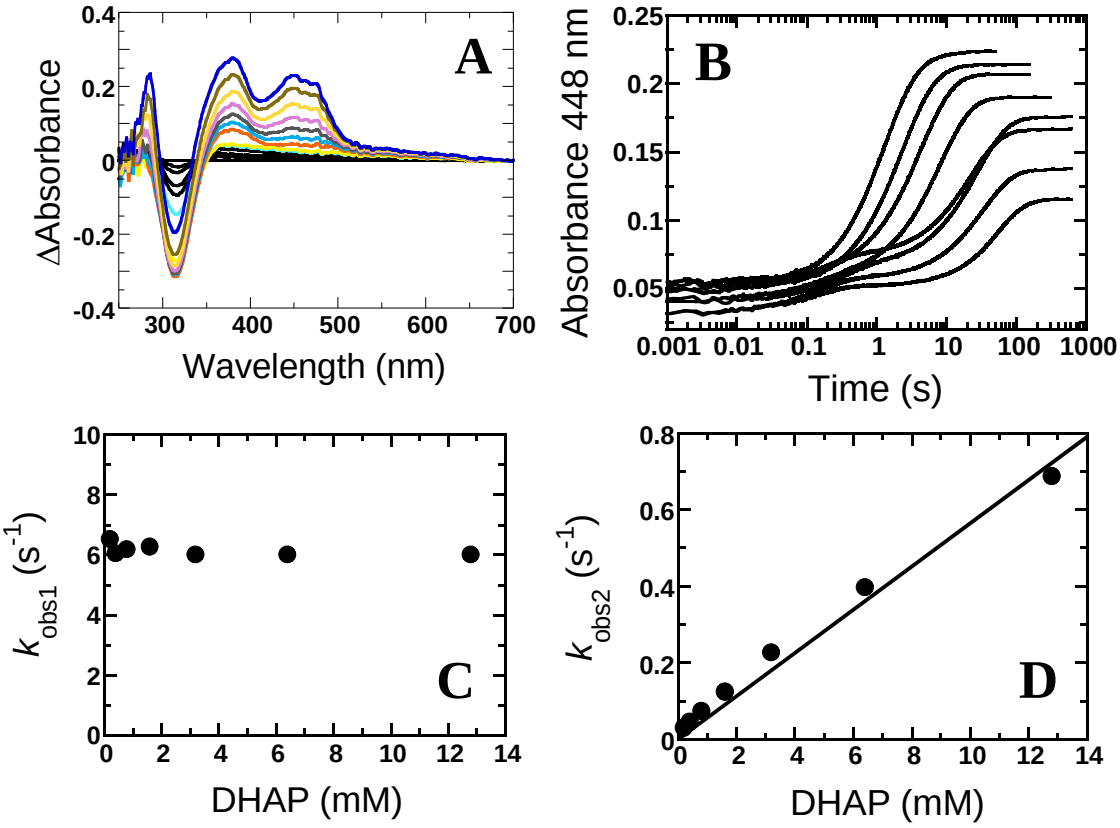
A
ΔAbsorbance
Wavelength (nm)
B
Absorbance 448 nm
Time (s)
C
k_{obs1} (s^{-1})
DHAP (mM)
D
k_{obs2} (s^{-1})
DHAP (mM)

E

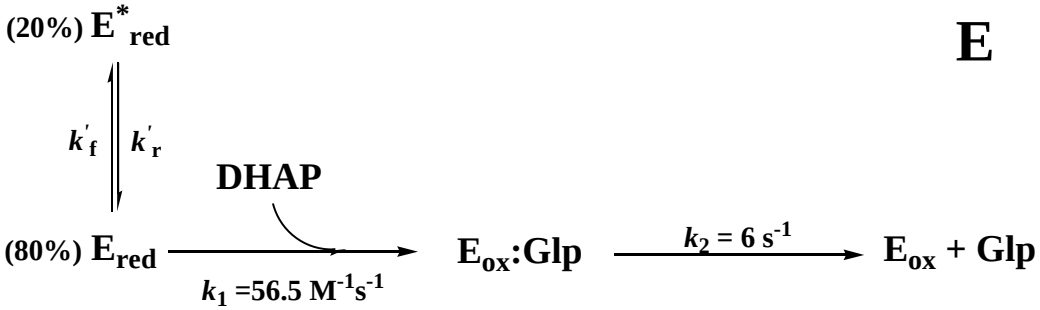
(20%) E*red
k'f
k'r
DHAP
(80%) Ered
k1 =56.5 M-1s-1
Eox:Glp
k2 = 6 s-1
Eox + Glp

Fig. 7

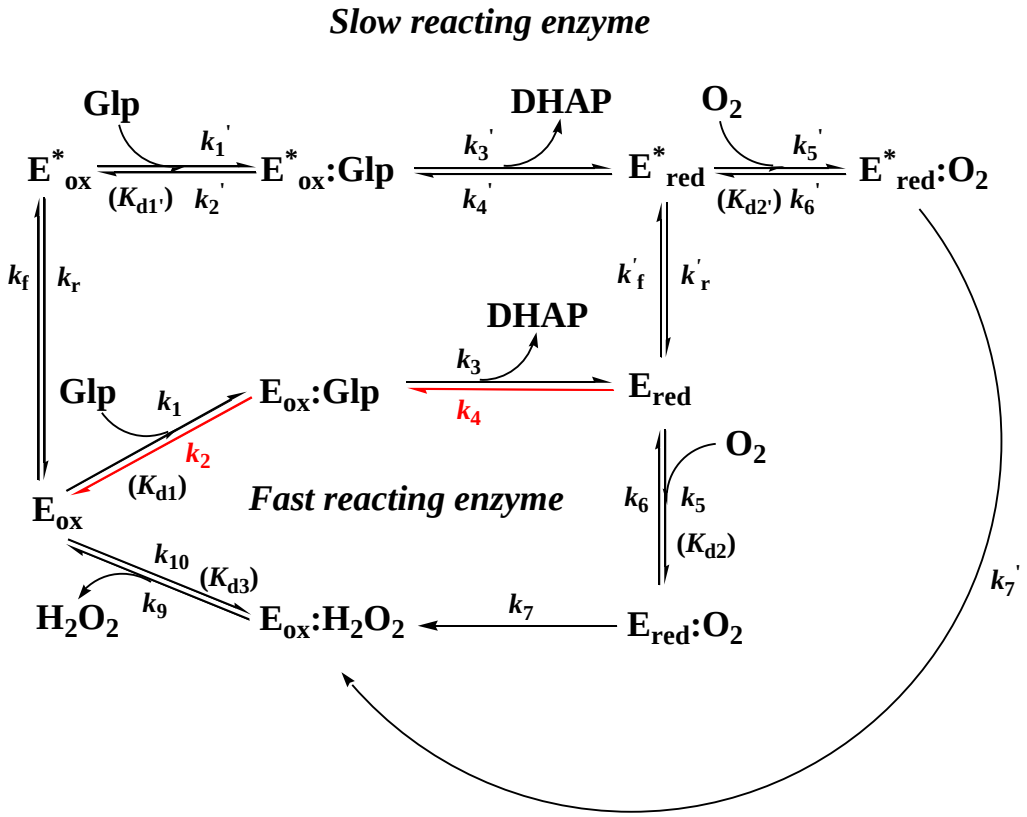
Slow reacting enzyme
Glp
DHAP
O2
E*ox
k1'
E*ox:Glp
k3'
E*red
k5'
E*red:O2
(Kd1')
k2'
k4'
(Kd2')
k6'
kf
kr
k'f
k'r
DHAP
k3
Glp
k1
Eox:Glp
Ered
k4
k2
O2
(Kd1)
Fast reacting enzyme
k6
k5
Eox
(Kd2)
k10
(Kd3)
k7'
H2O2
k9
k7
Eox:H2O2
Ered:O2

Structure and proposed mechanism of α-glycerophosphate oxidase from *Mycoplasma pneumoniae*

Callia K. Elkhal,[1#] *Kelsey Kean,*[1#] *Derek Parsonage,*[2] *Somchart Maenpuen,*[3] *Pimchai Chaiyen,*[4] *Al Claiborne,*[2,*] and *P. Andrew Karplus*[1 *]

[1]Department of Biochemistry and Biophysics, Oregon State University, Corvallis, Oregon 97331

[2]Center for Structural Biology, Wake Forest School of Medicine, Winston-Salem, North Carolina 27157

[3]Department of Biochemistry, Faculty of Science, Burapha University, Chonburi, Thailand

[4]Department of Biochemistry and Center of Excellence in Protein Structure and Function, Faculty of Science, Mahidol University, Bangkok, Thailand

[*] To whom correspondence should be addressed: e-mail: karplusp@science.oregonstate.edu, alc@csb.wfu.edu

[#] These two authors contributed equally to this work.

Article type : Original Article

Contact information for editorial correspondence: Andrew Karplus; 2011 ALS Bldg, Dept. of Biochemistry, Oregon State University, Corvallis, OR 97331; ph: 541-737-3200; Fax: 541-737-0481; email: karplusp@science.oregonstate.edu

Running Title: α-glycerophosphate oxidase structure and mechanism

Database: Structural data are available in PDB database under the accession number(s) **4x9m** (oxidized) and **4x9n** (reduced).

Abbreviations: Glp – L-α-glycerophosphate; DHAP – dihydroxyacetone phosphate; GlpO - L-α-glycerophosphate oxidase; DH - L-α-glycerophosphate dehydrogenase; *Mp – Mycoplasma pneumoniae*; *Bp – Bordetella pertussis*; *Sp – Streptococcus pneumonia*; *Ssp – Streptococcus* sp.

Enzyme Commission number: L-α-glycerophosphate oxidase – EC 1.1.3.21

This article has been accepted for publication and undergone full peer review but has not been through the copyediting, typesetting, pagination and proofreading process, which may lead to differences between this version and the Version of Record. Please cite this article as doi: 10.1111/febs.13233

Keywords: flavoenzyme, drug design, protein evolution, GlpA, hydride transfer

ABSTRACT

The formation of hydrogen peroxide (H_2O_2) by the FAD-dependent α-glycerophosphate oxidase (GlpO), is important for the pathogenesis of *Streptococcus pneumoniae* and *Mycoplasma pneumoniae*. The structurally known GlpO from *Streptococcus* sp. (*Ssp*GlpO) is similar to the pneumococcal protein (*Sp*GlpO) and provides a guide for drug design against that target. However, *M. pneumoniae* GlpO (*Mp*GlpO), having <20% sequence identity with structurally known GlpOs, appears to represent a second type of GlpO we designate as Type II GlpOs. Here, the recombinant His-tagged *Mp*GlpO structure is described at ~2.5 Å resolution, solved by molecular replacement using as a search model the *Bordetella pertussis* protein 3253 (*Bp*3253) a protein of unknown function solved by structural genomics efforts. Recombinant *Mp*GlpO is an active oxidase with a turnover number of ~580 min^{-1} while *Bp*3253 showed no GlpO activity. No substantial differences exist between the oxidized and dithionite-reduced *Mp*GlpO structures. Although, no liganded structures were determined, a comparison with the tartrate-bound *Bp*3253 structure and consideration of residue conservation patterns guided the construction of a model for α-glycerophosphate (Glp) recognition and turnover by *Mp*GlpO. The predicted binding mode also appears relevant for the type I GlpOs (such as *Ssp*GlpO) despite differences in substrate recognition residues, and it implicates a histidine conserved in type I and II Glp oxidases and dehydrogenases as the catalytic acid/base. This work provides a solid foundation for guiding further studies of the mitochondrial Glp dehydrogenases as well as for continued studies of *M. pneumoniae* and *S. pneumoniae* glycerol metabolism and the development of novel therapeutics targeting *Mp*GlpO and *Sp*GlpO.

INTRODUCTION

Mycoplasma pneumoniae is a human respiratory tract pathogen that causes 40% or more of community-acquired pneumonias [1], with the typical syndrome being tracheobronchitis in children. This pathogen initiates colonization of the host airway mucosal epithelium *via* a special attachment organelle [2], which also provides an important gliding function. Among other distinctive features of *M. pneumoniae* are a small genome, the lack of a rigid cell wall, and

limited metabolic capabilities. As in the Gram-positive streptococci from which the mycoplasmas diverged ca. 600 million years ago [1], the tricarboxylic acid cycle, electron transport chain, and respiratory cytochromes are absent. However, glycerol metabolism appears to be an important pathogenicity factor for *M. pneumoniae* [3-6] and thus the enzymes involved provide potential drug targets for combating respiratory infectious diseases.

Of particular interest in this context is the *M. pneumoniae glpD* gene (MPN051) that is annotated as encoding a glycerol-3-phosphate dehydrogenase [4], and based on its sequence can be identified as a member of the D-amino acid oxidase (DAAO) superfamily [7] of FAD-dependent enzymes combining a 'glutathione-reductase-2' type FAD-binding domain and an antiparallel β-sheet based substrate-binding domain. Despite the annotation as a dehydrogenase, the encoded enzyme has been shown to be a constitutively expressed cytosolic FAD-dependent α-glycerophosphate oxidase [4], using O_2 as the final electron acceptor and producing dihydroxyacetone phosphate (DHAP) and H_2O_2:

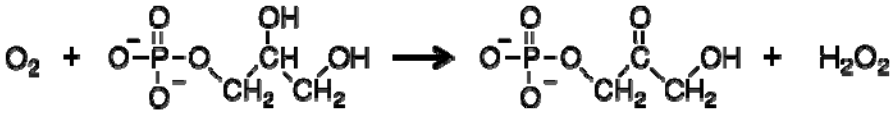

We therefore refer here to the encoded protein as *M. pneumoniae* GlpO (*Mp*GlpO), rather than GlpD. The gene is tightly linked with that for glycerol kinase (*glpK*), and together these enzymes can catalyze the ATP-dependent conversion of glycerol to the glycolytic intermediate dihydroxyacetone phosphate [4]. The peroxide produced by *Mp*GlpO has been shown to be crucial for pathogenicity, and the ortholog from the animal pathogen, *Mycoplasma mycoides* subsp. *mycoides* SC, has also been implicated as a primary virulence factor [3]. Similarly, Mahdi *et al.* [8] have shown that *Streptococcus pneumoniae* GlpO (*Sp*GlpO) is responsible for H_2O_2-mediated cytotoxicity against human brain microvascular endothelial cells and for promoting pneumococcal meningitis.

Given the clinical significance of *M. pneumoniae* and *S. pneumoniae* and the importance of *Mp*GlpO and *Sp*GlpO in cytotoxicity and virulence, structural studies of these enzymes would provide a valuable foundation for drug design. A good understanding of the *Sp*GlpO structure is in hand because it is quite similar (~62% sequence identity) to the structurally known *Streptococcus* sp. GlpO (*Ssp*GlpO) [9]. However, insufficient information exists for modeling the 43 kD *Mp*GlpO enzyme, as it is surprisingly divergent from the higher molecular weight (~65 kD) streptococcal enzymes: it is not only missing a C-terminal α-helical domain, but it has

only ~20% sequence identity with *Ssp*GlpO and is actually more sequence similar to other DAAO superfamily enzymes, such as glycine oxidase, than it is to *Ssp*GlpO. To provide a foundation for understanding catalysis and guiding drug design against *Mp*GlpO, we report here its crystal structure. As part of this work, we also carried out some functional characterizations of the protein encoded by *Bordetella pertussis* gene 3253 (*Bp*3253), which is a related protein of unknown function solved by the NorthEast Structural Genomics group (PDB entry 3DME, deposited 2008). It became of interest because it is the structurally known protein most similar to *Mp*GlpO (27% sequence identity).

RESULTS and DISCUSSION

Expression and biochemical properties of MpGlpO and the B. pertussis protein Bp*3253*. Previously published studies of *Mp*GlpO were carried out with an N-terminal His-tagged protein derived from *M. pneumoniae* M129 [4]. In the present study, the pET28a vector introduces a 34-residue His-tag in-frame with the codon-optimized synthetic gene, and this tag was present in all studies. The characterization of *B. pertussis Bp*3253 was carried out using the same N-terminally His-tagged construct used in the crystal structure determination of PDB entry 3DME. Both recombinant *Mp*GlpO and *Bp*3253 were expressed and purified (yielding ~5 and ~60 mg/L culture respectively), and the visible absorption spectra for the purified proteins are characteristic of properly folded flavoenzymes (Figure 1). The native molecular weight for His-tagged *Mp*GlpO as determined by gel filtration, at 41.7 kD, is reasonably close to the value of 46.3 kD calculated for His-tagged *Mp*GlpO indicating that the recombinant protein is a monomer in solution.

Although the oxidase activity of *Mp*GlpO was documented previously [4], we assayed the recombinant His-tagged *Mp*GlpO purified here and found a specific activity of 12.8 U/mg at 25 ˚C with 200 mM D/L-Glp and ca. 260 μM O_2 (the saturating concentration in water at 25 ºC). This is equivalent to a k_{cat} of 9.7 s^{-1} (i.e. 580 min^{-1}). This level of activity is reasonable for an oxidase even though it is somewhat lower than was seen for native and recombinant GlpOs from *E. casseliflavus* (*Ecass*GlpO) [10] and *Streptococcus* sp. (*Ssp*GlpO) [11] which gave k_{cat} values of 70-90 s^{-1} at 25 ºC. When *Bp*3253 was tested using the same assay, it showed no ability to catalyze the Glp-dependent formation of H_2O_2.

Many flavoprotein oxidases show a pronounced reactivity with sulfite to form a reversible adduct at the flavin N5-position [12]. The *Ecass*GlpO and *Ssp*GlpO giving similar values of K_d = 0.82 mM and 1.5 mM [10, 11], and we here performed similar sulfite titrations with freshly prepared *Mp*GlpO and *Bp*3253 (Figure 1A). For *Mp*GlpO, the measured K_d was 3.0 mM, but flavin absorbance was only partially bleached with about half of the *Mp*GlpO flavin being refractory to sulfite adduct formation, even after an incubation of 30 min at 48 mM sulfite. A parallel experiment with the *Bp*3253 protein (Figure 1B) shows a monophasic sulfite titration giving essentially complete bleaching of the flavin absorbance spectrum with a K_d of 0.42 mM, about seven-fold more favorable than that for *Mp*GlpO. We do not have any good proposals at this time for why only roughly half of the *Mp*GlpO reacts with sulfite.

Structure determination of oxidized and reduced Mp*GlpO*. Crystals obtained of recombinant His-tagged *Mp*GlpO yielded diffraction data to ~2.5 Å resolution. Attempts to solve the structure by molecular replacement with a structure of *Ssp*GlpOΔ (PDB entry 2RGH) as the search model were unsuccessful, which was not surprising given the low ~20% sequence identity between *Mp*GlpO and *Ssp*GlpO. A PDB database query for better search models, led to the identification of the *B. pertussis* protein *Bp*3253 (PDB entry 3DME; 27% identity) as the known structure with the highest sequence similarity. Using this as a search model, molecular replacement was successful and led to ~2.5 Å resolution structures with acceptable statistics (Table 1) for both oxidized and dithionite-reduced *Mp*GlpO.

The refined models contain a single *Mp*GlpO chain in the asymmetric unit including residues 1-384, the FAD cofactor, ordered water sites, and a Ni^{2+} atom. The $2F_o$-F_c map for the FAD cofactor and some of its environment illustrates the quality of electron density in well-ordered regions of the protein (Figure 2). Missing from the models and presumed mobile are all 34 residues of the N-terminal His-tag and two side-chains; also, a few residues are modeled with alternate conformations (see Experimental Procedures). The Ni^{2+} ion, identified using an X-ray fluorescence scan and presumably introduced during Ni-affinity chromatography, is situated at a crystallographic three-fold packing interface where it is coordinated by three His59-side chains. As the gel filtration result described above shows that the recombinant His-tagged *Mp*GlpO is a monomer, this three-fold interface and a two-fold crystal packing interaction involving strand

β15 and burying ca. 1600 Å^2 of surface area are not physiologically relevant. So the nickel, possibly picked up during purification, can be considered a fortuitous crystallization aid.

Overall structure. As expected for a DAAO superfamily member, the *Mp*GlpO chain is organized into an FAD-binding domain with a predominantly parallel, six-stranded β-sheet and a substrate-binding domain with a core antiparallel, eight-stranded β-sheet (Figure 3). The two domains are discontinuous, with the FAD-binding domain including residues 1-87, 149-219, and 330-364, and the substrate-binding domain formed by residues 86-148 and 227-323.

A search using the DALI server [13] to identify structural homologs of *Mp*GlpO, confirms that there are no highly similar known structures. The most similar structure is that of the molecular replacement search model *Bp*3253 (PDB code 3DME; Z-score=44, 26% sequence identity and 2.0 Å rmsd over 352 residues), and a bit less similar is a glycine oxidase from *Bacillus subtilis* (PDB code 1NG4; Z-score=42; 20% sequence identity and 1.9 Å rmsd over 340 residues). An overlay with these proteins shows the high similarity extends throughout the protein chains (Figure 4A). Remarkably, the enzymes with more similarity in function, *Ssp*GlpO (PDB codes 2RGO) and *E. coli* GlpD (PDB code 2QCU), are structurally less similar, giving *Z*-scores of only 28 and 36, respectively (with higher rmsd values of 2.9 and 3.7 Å), and showing only ~17% sequence identity over the ~350 residues that are in the two domains common to the proteins. Visually, the overlay of *Mp*GlpO with *Ssp*GlpO and *E. coli* GlpD shows their greater divergence (Figure 4B). A structure-based sequence alignment of these proteins (Figure 4C) provides further details of the comparisons, and also is useful for tracking the similarities and differences in active site residues that will be discussed in the active site section.

That *Mp*GlpO is more similar to other DAAO superfamily enzymes than it is to *Ssp*GlpO led us to consider that whether GlpO activity may have independently evolved twice in the DAAO superfamily. To explore this possibility further we generated a relatedness tree of structurally known proteins similar to *Mp*GlpO (Figure 5). In this tree, despite the DALI scores, the *Mp*GlpO and *Ssp*GlpO and *E. coli* GlpD actually do come out as being more closely-related to each other than to other functionally characterized DAAO superfamily members. The *Ssp*GlpO-like enzymes that cluster together include both GlpOs and the mitochondrial/bacterial GlpD dehydrogenases [14]. They represent a very widely distributed group that we are designating as 'Type I GlpO/DH' enzymes. In contrast, the *Mp*GlpO-like enzymes, which we are designating

'Type II GlpO/DH' enzymes, are more narrowly distributed, being found only bacteria of the class mollicutes (including *M. pneumoniae*) and the closely related low G+C Gram-positive anaerobic bacteria of the class Erysipelotrichia [15].

Interestingly, the Type II GlpO/DHs from anaerobic bacteria appear to all have an additional ca. 85 residue C-terminal domain that is not closely related to any known structure but includes two segments with conserved pairs of Cys residues (CxCE and CQxGFC) and has some similarity (e-value $4x10^{-10}$) with the Pfam family of bacterioferritin-associated ferredoxin-like [2Fe-2S] domains (Pfam04324). The one biochemically studied Type II GlpO/DH containing such a C-terminal domain is the *E. coli glpA* gene product that is expressed under anaerobic conditions (replacing GlpD); and consistent with the assignment of the additional domain having an iron-sulfur center is the report that *E. coli* GlpA binds both FAD and non-heme iron [16]. Our proposal based on these observations is that these Type II GlpO/DHs with the additional C-terminal domain are all dehydrogenases for which the Type II GlpO/DH module converts Glp to DHAP, and the C-terminal domain serves as a conduit to receive electrons from the flavin and pass them on to a further (anaerobic) acceptor.

Flavin binding and active site. General features of FAD binding to DAAO superfamily enzymes have been well-described [7], so we will not detail those here but will focus in on the flavin and the substrate binding site. In *Mp*GlpO, the bound flavin is slightly twisted with a 3_{10}-helix involving residues Thr42 - Asn46 closely covering its *si* face, and Ser47 – Val49 interacting with the N5, O4, and N3 atoms of the flavin (Figure 2). Optimizing the hydrogen-bond between flavin-N3 and Val49-O appears to be a cause of the flavin twist. Above the flavin (on the *si* side), there is open space above and in front of atom N5, creating a cavity lined by His51, Arg320, and Ser348 (Figure 2). Interestingly, we do not see any substantive differences between the active sites of oxidized and reduced *Mp*GlpO structures at this resolution, even though the pale color of the reduced *Mp*GlpO crystals provided visual evidence that they truly were reduced. Given the lack of differences, in the remaining discussion of the active site features, we will focus solely on the somewhat higher resolution oxidized structure.

Unfortunately, attempts to obtain an *Mp*GlpO structure with a substrate or substrate analog bound were unsuccessful (see methods), as was also true for our earlier structural work on *Ssp*GlpO [9]. However, the protein structure that is the most similar to *Mp*GlpO, that of *Bp*3253,

fortuitously has a ligand – L-tartrate – bound in its active site. Although the function of *Bp*3253 is not yet known, it binds tartrate similarly to how glycine oxidase [17, 18] and DAAO [19] bind their substrate analogs (overlays not shown), implying that the *Bp*3253:tartrate complex is an informative one. Specifically, one tartrate α-carbon (i.e. alpha to one of the carboxylates) is placed just 3.7 Å from flavin N5 and with excellent geometry for hydride transfer (Figure 6).

An overlay of *Mp*GlpO with *Bp*3253 (Figure 6) shows that the flavins and most nearby peptide backbone segments align well. In the *Bp*3253 complex there are just six side chains (and no backbone atoms) making van der Waals or hydrogen-bond contacts with the tartrate. Starting with the key Arg sitting above the flavin C7 and C8 methyl groups, the *Bp*3253 residues, with their *Mp*GlpO equivalents in parentheses, are Arg316(Arg320), Pro272(Pro274), His259(Ile261), Tyr248(Phe250), His52(His51), and Ser350(Ser348). Hydrogen bonds connect Arg316 with the C1-carboxylate, His259 via a water molecule with the C3 hydroxyl, and Tyr248, His52, and Ser350 with the C4-carboxylate (Figure 6). Four of these positions are perfectly conserved in *Mp*GlpO, both in identity and potential placement, recognizing that Arg320 in *Mp*GlpO could easily shift to match the position seen for the equivalent *Bp*3253 residue. The conserved placement of Ser350(Ser348) projecting over the flavin depends on a conserved *cis*-peptide bond between the Ser and Pro351(Pro349). Notable differences in the active sites are the Tyr248->Phe replacement in *Mp*GlpO and the His259->Ile261 replacement that is compounded by a large difference in the path of the β12-β13 loop, with the backbone of *Mp*GlpO Gly259 occupying the space filled by the His259 side chain in *Bp*3253.

Regarding this β12-β13 loop difference, a key question is why the path of *Mp*GlpO residues 256-261 is different. Are they adopting an arbitrary conformation in this crystal form or a conformation that reliably represents the chain path of the Type II GlpO/DHs? Three evidences suggest it is representative rather than arbitrary: first, the *Mp*GlpO path is similar to the paths seen in broader superfamily members such as glycine oxidase meaning that it is the *Bp*3253 path that is unusual; second, the distinct *Bp*3253 path appears to be directly related to it having a proline (Pro249) at the end of strand β12 that disrupts the normal β-sheet hydrogen bonding (Figure 6) and is not present in *Mp*GlpO (Figure 4C); and third, the loop is well ordered and not involved in crystal contacts.

Modeling Glp binding to type II GlpO/DHs. Given the reliability of the β12-β13 loop conformation, we can now consider how *Mp*GlpO binds substrate (Figure 7A). Compared with

*Bp*3253, the presence of Phe250 and the Gly259 methylene make the pocket above the pyrimidyl portion of the flavin less polar, leading us to speculate that this region would recognize the C1-end of Glp and the region near Arg320 would accommodate the negatively charged phosphoryl group. As to what could provide additional recognition of the phosphoryl, the side chains of Arg230, Lys258 and Lys347 are nearby and appear adjustable (B-factors at the side-chain tips being ~20 $Å^2$ higher than at the backbone). These side chains are also well conserved among the 70 sequences having >40% sequence identity with *Mp*GlpO (i.e. BLAST e-value $<10^{-80}$): Lys258 is fully conserved; Lys347 is conserved as either a Lys or a Gln; and Arg230 is Arg or Lys in all but four sequences, but in these it is a Leu implying a lesser importance. Given these insights, we created a model for docked Glp guided by the constraints that the C2-hydrogen be oriented for transfer to the flavin-N5, that either the C1- or C2-hydroxyl replaces the water binding to His51 and Ser348 (see Figure 2), and the phosphate interacts with Arg320. The binding mode obtained (Figure 7A) fortuitously places His51 ideally for serving as a catalytic base that could deprotonate the C2-hydroxyl in the forward reaction.

Extrapolation of Glp binding to type I GlpO/DHs. Interestingly, this proposed mode of substrate binding differs from those proposed previously for the type I GlpO/DHs *Ssp*GlpO [9] and *Ec*GlpD [14], neither of which were very satisfactory. For *Ssp*GlpO, we had proposed that the substrate would be oriented the other way, with the 3'-phosphoryl moiety near the equivalent of *Mp*GlpO His51 and the C1-hydroxyl interacting with the equivalent of *Mp*GlpO Arg320 [9]. We had also noted that the equivalent of His51 seemed the only potential base, but how this could be achieved was not clear. For *Ec*GlpD [14], a phosphate bound in the native crystal structure interacted with Arg317 (equivalent of *Mp*GlpO Arg320), Arg54 and Tyr55, but ligand soaks were taken to indicate binding modes that placed the substrate C2-atom far from flavin-N5.

Given the unsatisfactory nature of those proposals, we explored whether the mode of binding we predict for *Mp*GlpO could also work for the Type I enzymes. An overlay of *Ec*GlpD onto *Mp*GlpO with its docked Glp shows a remarkable compatibility, with the predicted position of the phosphoryl of Glp matching closely with the experimentally observed phosphate of *Ec*GlpD (Figure 7B). The ligand fits reasonably into the *Ec*GlpD active site, and it can be seen that the functionality of key *Mp*GlpO residues that are not conserved in *Ec*GlpD appears to be fulfilled by substitutions of residues often from different parts of the chain: with Lys354 replacing Ser348

in interacting with the C2-hydroxyl, Arg54 and Tyr55 replacing Lys258 and Lys347 in interacting with the phosphoryl, and Phe257 replacing Phe250 in providing a non-polar environment for the C1-methylene (Figure 7B). These functional substitutions are most easily seen in schematic drawings of the interactions (Figure 8). We emphasize that whereas the general features associated with this rough placement of Glp are plausible and have explanatory power, the details are not reliably defined because the side chain and backbone positions of protein groups are expected to shift during ligand binding from the positions they adopt in the unliganded *Mp*GlpO structure used to guide the modeling.

Catalytic mechanism and outlook. Given the predicted mode of Glp binding to the *Mp*GlpO (Figure 8A) and the *SSp*GlpO (Figure 8B) active sites, how the electrons flow during catalysis and how the forward reaction is enhanced by base catalysis become readily apparent. As indicated by the arrows in the Figure 8A schematic, in *Mp*GlpO the substrate is well-aligned for His51 to deprotonate the C2-hydroxyl, promoting its electrons to fold in to form a carbonyl, and facilitating loss of the C2-hydrogen as a hydride that can attack the flavin N5; the ensuing shifting of flavin electrons would lead to the formation of the reduced flavin N1-anionic form, with the negative charge at the N1/O2 locus stabilized by three hydrogen bonds donated by the Leu351 and Thr352 backbone amides and the Thr352 hydroxyl. The geometries of the interactions are also stereoelectronically reasonable, in that the His51 interaction with the C2-hydroxyl has a roughly "anti" orientation with respect to the hydride leaving group. The Ser47 hydroxyl – supported by its interactions with Tyr234 – is well-placed to help stabilize the protonated N5 of the reduced flavin through minor shifts in its position in association with flavin reduction. A set of equivalent interactions exist in the *SSp*GlpO active site (Figure 8B).

A full kinetic analysis of *Mp*GlpO has recently been completed (Maenpuen et al; submitted for publication in the same issue), and our structural results allow us to propose explanations for some of the observations made in that study. One such area is the redox potential difference between the *Mp*GlpO flavin, which at -167 mV is much lower than those seen for type I GlpOs (e.g. *Enterococcus casseliflavus* GlpO at -118 mV; [10]). While many subtle factors can influence redox potential, we note that one very clear difference in the flavin electrostatic environment consistent with this shift is that the Type I GlpO/DH enzymes conserve an active site lysine (equivalent to Lys354 in *Ec*GlpD; Figure 8B, 7B, 4C) having its amino group just at

van der Waals distance above the flavin N1/O2 locus, whereas the type II enzymes have a conserved neutral serine side chain in that place (equivalent to Ser348 in *Mp*GlpO). The additional local positive charge in the type I enzymes would make them more easily reduced. As was pointed out by Maenpuen et al, the difference in redox potential may be the reason that *Mp*GlpO can catalyze the reverse reaction (i.e. DHAP oxidation of the reduced flavin) whereas those type I enzymes tested cannot.

Another very interesting result of the kinetics study was the observation of two enzyme populations, partitioning as 70:30 with 70% of the oxidized enzyme reacting rapidly with Glp, and 70% of the reduced enzyme reacting slowly with DHAP in the reverse reaction, but reacting rapidly with O_2. Based on the structure, a plausible single explanation for all of these observations is that the two populations are defined by the protonation state of the catalytic acid/base His-51, with 70% being deprotonated and 30% protonated at the pH of 7 at which the studies were done. For the reaction with Glp, the deprotonated form of His51 is required for abstracting the C2-hydroxyl proton, so 70% of the enzyme would react rapidly. The slower population would reasonably be limited by the rate of deprotonation of His51 in the ligand bound form. For the reaction of the reduced flavin with DHAP, the deprotonated 70% of the enzyme reacts poorly (in bimolecular limited fashion at 56 M^{-1} s^{-1}), while the protonated 30% reacts rapidly enough that the k_{off} of the Glp produced (at 6 s^{-1}) is rate limiting. In terms of the O_2 reactivity of the reduced enzyme, it is reasonable that the His51-protonated/charged and the His51-deprotonated/neutral active sites would react differently and our proposal implies that the deprotonated 70% reacts rapidly with oxygen (at ~600 s^{-1}) while the protonated 30% reacts more slowly (at ~100 s^{-1}). This explanation predicts that the enzyme will be more active above pH=7, and a set of assays looking at the enzymes pH dependence at a single high substrate concentration shows the pH optimum is near 8. More extensive studies of k_{cat} and K_M as a function of pH are now planned to test these ideas and better define the enzyme mechanism.

The proposed binding mode of Glp also implies the importance of the negatively charged phosphoryl group for substrate recognition, as both the Type I and Type II enzymes have 3 to 4 positively charged side chains involved in its recognition (Figure 8). The importance of the phosphoryl is consistent with the binding studies reported by Maenpuen et al (submitted) showing that *Mp*GlpO effectively binds the negatively charged glyceraldehyde-3-phosphate, lactate, and malate, but not the neutral glycerol. While much remains to be done, we see the most

influential contributions of these analyses are two-fold: first, is the recognition of the Type I and Type II GlpO/DH enzymes as distinct variants with striking active site differences that were not predicted from sequence alignments; and second, is the plausible concrete predicted mode for substrate recognition and catalysis that is relevant not only for bacterial GlpO enzymes, but also for the widespread mitochondrial GlpD dehydrogenases, and that will guide mutational studies that test the proposed mechanism and dissect the roles of specific active site residues. Also, the distinction between the Type I and Type II GlpO/DH active sites raises the encouraging possibility that it will be possible to design inhibitors that may selectively block activity of bacterial Type II enzymes such as *Mp*GlpO while not inhibiting the mitochondrial GlpD dehydrogenase of the host.

EXPERIMENTAL PROCEDURES

Expression and Purification of Mp*GlpO and* Bp*3253.* The codon-optimized MPN051 gene encoding *Mp*GlpO was synthesized by GenScript (Piscataway, NJ, USA) and subcloned into the expression plasmid pET28a (Novagen, Darmstadt, Germany). *Mp*GlpO was expressed with an N-terminal His-tag in *E. coli* B834(DE3) cells using autoinduction medium at 28ºC. All steps of purification were conducted at 4ºC. Harvested cells were resuspended in 50 mM potassium phosphate, pH 7.0, containing 200 mM NaCl, 20 mM imidazole, 0.5 mM 4-(2-aminoethyl)benzenesulfonyl fluoride (AEBSF) protease inhibitor and 10 % glycerol. Cells were disrupted using an Avestin EmulsiFlex-C5 homogenizer, and centrifuged (27,000 g for 60 min). The clarified extract was loaded onto a 25 mL Co Sepharose High Performance column (GE Healthcare, Piscataway, NJ, USA), and *Mp*GlpO protein was eluted with 0.5 M imidazole after washing with 20 mm imidazole. The pooled yellow fractions were dialyzed overnight against 50 mM potassium phosphate, pH 7.0, containing 0.5 mM EDTA. FAD (0.25 mM) was added to the enzyme and incubated for 45 min on ice before loading on a 75-mL SP-Sepharose HP column (GE Healthcare). The column was washed with 50 mM potassium phosphate, pH 7.0, 0.5 mM EDTA, 100 mM NaCl before *Mp*GlpO was eluted with a 100 mM to 1 M NaCl gradient. Fractions were analyzed by SDS-PAGE, pooled, buffer-exchanged into 50 mM potassium phosphate, pH 7.0, 0.5 mM EDTA and concentrated to 10 mg/mL before freezing in aliquots at -80ºC.

The pET21_NESG clone for expression of His-tagged *Bp*3253 (corresponding to PDB entry 3DME) was purchased from the DNASU Plasmid Repository, and its expression and purification followed the protocol described above for *Mp*GlpO, with the following modifications. Recombinant *E. coli* B834(DE3) cells were grown in TYP medium, prior to induction with 0.5 mM IPTG and overnight protein expression at 16 °C. The cells were broken in a solution containing 50 mM Tris-Cl, pH 8.0 (4 °C). Nucleic acids were removed by adding 2% (w/v) streptomycin sulfate and centrifugation. Crude extract was loaded to the Co column in 50 mM sodium phosphate pH 8.0, 300 mM NaCl, 20 mM imidazole, the column was washed with more buffer, and pure *Bp*3253 was eluted with 500 mM imidazole. *Bp*3253 protein was concentrated to 10 mg/ml in an Amicon ultrafiltration cell with a YM30 membrane and for freezing was buffer-exchanged into 50 mM potassium phosphate, pH 7.0, containing 0.5 mM EDTA.

Biochemical characterizations. Extinction coefficients for His-tagged *Mp*GlpO and *Bp*3253 were determined by standard methods, using an Agilent model 8453 diode-array spectrophotometer. The specific activities of the two proteins were measured as described earlier for *Ssp*GlpO [11], using the standard spectrophotometric assay with a Cary 50 spectrophotometer (Varian) thermostatted at 25ºC. The native M_r for recombinant His-tagged *Mp*GlpO was determined by gel filtration at 25ºC, in a pH 7 phosphate buffer with 150 mM NaCl, using a Sephadex G-200 medium HR 10/30 column calibrated with six standard proteins covering the range 15,600 to 440,000. Titrations of both MpGlpO and Bp3253 proteins with sulfite followed established protocols [10, 11].

Crystallization and Data Collection. Thawed aliquots of wild-type His-tagged *Mp*GlpO were subjected to a variety of crystal screens at 4 ˚C and the most promising crystal leads grew using a reservoir of 2.68 M NaCl, 3.35% v/v isopropanol, and 0.1 M HEPES pH 7.5 (Wizard Precipitant Synergy Screen Block 1 condition B7). Optimization at 4 ºC using hanging-drops led to yellow, trigonal-pyramidal crystals measuring approximately 0.3 x 0.3 x 0.3 mm^3 growing within one week using drops made from 1 µL protein at 5 mg/ml plus 2 µL of a reservoir solution as above but containing 2% (v/v) isopropanol. For data collection, crystals in an artificial mother liquor (AML) of 3 M NaCl in 0.1 M Bis-Tris, pH 7.0 were placed for 3 minutes in AML with 15% glycerol as a cryoprotectant before being flash-frozen by plunging into liquid nitrogen. Data sets to first 2.50 Å and then 2.40 Å resolution were collected at beamline 5.0.3 at the Advanced Light Source synchrotron. For analyses of additional forms of *Mp*GlpO, crystals were soaked in either

10 mM dithionite, 10 mM L-Glp, 10 mM L-tartrate, 10 mM 2-phosphoglycerate, or 10 mM phosphoenolpyruvate (PEP) in AML for 1 h prior to freezing and data collection. Two experiments with dithionite-soaked crystals gave a complete merged data set to 2.50 Å. Data sets at between 2.5 and 3.0 Å resolution were collected for the ligand soaks.

Mp*GlpO Phasing and Structure Refinement.* Diffraction data for oxidized *Mp*GlpO were processed with iMOSFLM [20] and with SCALA in the CCP4 suite [21, 22]. *Mp*GlpO crystallizes in space group *P*23, and there is one molecule per asymmetric unit. Attempts to solve the structure by molecular replacement using AMoRe with the *Ssp*GlpO coordinates were not successful. However, using chain A of PDB entry 3DME – annotated as the "conserved exported protein (BP3253) from *Bordetella pertussis*" – as a search model gave a solution using the 2.50 Å data set and AutoMR [23]. Manual rebuilding of the initial model was carried out in COOT [24], and this model was refined with the PHENIX software suite [25]. Six rounds of simulated annealing and minimization refinement gave a partially refined model with R/R_{free} of 32%/45%, respectively. At this point, the improved 2.40 Å resolution *Mp*GlpO data were used, and six rounds of refinement with BUSTER [26] led to an R_{free} of 28%. Water molecules were added, as indicated by both electron density peak height and hydrogen-bonding interactions, and refinement continued with REFMAC [27]. A nickel ion (see "Results") was introduced late in the process and was confirmed by X-ray fluorescence, and further manual modeling and refinement led to the final oxidized *Mp*GlpO structure with R/R_{free} 15.8%/16.4%. The model does not include the Lys79 and Lys298 side chains beyond -CB, as these surface residues have little-or-no side chain density. Alternate side chain and/or backbone conformations are included for Gln40, His244, and the Trp375-Asn376-Gly377 backbone.

The 2.50 Å refinement of the dithionite-reduced GlpO structure began from the oxidized structure. Rounds of manual modeling and REFMAC refinement gave a model with only minor changes, and with R/R_{free} values of 16.4%/22.6%. Of the soaks with Glp, 2-phosphoglycerate, PEP, and tartrate, no substantive interpretable density differences were observed in the vicinity of the isoalloxazine and so these structural analyses were not pursued further.

ACKNOWLEDGEMENTS

We thank Dale Tronrud for helpful guidance with the crystallographic work. This work was supported by North Carolina Biotechnology Center Grant 2011-MRG-1116 (to A.C.), by Thailand Research Fund MRG5580066 (to S.M.), by Thailand Research Fund RTA5680001 (to P.C.), and Howard Hughes Medical Institute grant 52005883 (to C.K.E.). Synchrotron data were collected at the Advanced Light Source, supported by contract DE-AC02-98CH10886 from the Office of Basic Energy Sciences of the U.S. Department of Energy.

AUTHOR CONTRIBUTIONS

CKE Planned and performed experiments and analyzed data; KK Analyzed data and wrote the paper; DP Planned and performed experiments, contributed reagents, and analyzed data; SM and PC Planned and performed experiments and analyzed data; AC and PAK Planned experiments, analyzed data and wrote the paper.

REFERENCES

1. Waites, KB & Talkington, DF (2004) Mycoplasma pneumoniae and its role as a human pathogen. *Clin Microbiol Rev* **17**, 697-728.
2. Prince, OA, Krunkosky, TM & Krause, DC (2014) In vitro spatial and temporal analysis of Mycoplasma pneumoniae colonization of human airway epithelium. *Infect Immun* **82**, 579-86.
3. Pilo, P, Vilei, EM, Peterhans, E, Bonvin-Klotz, L, Stoffel, MH, Dobbelaere, D & Frey, J (2005) A metabolic enzyme as a primary virulence factor of Mycoplasma mycoides subsp. mycoides small colony. *J Bacteriol* **187**, 6824-31.
4. Hames, C, Halbedel, S, Hoppert, M, Frey, J & Stulke, J (2009) Glycerol metabolism is important for cytotoxicity of Mycoplasma pneumoniae. *J Bacteriol* **191**, 747-53.
5. Schmidl, SR, Otto, A, Lluch-Senar, M, Pinol, J, Busse, J, Becher, D & Stulke, J (2011) A trigger enzyme in Mycoplasma pneumoniae: impact of the glycerophosphodiesterase GlpQ on virulence and gene expression. *PLoS Pathog* **7**, e1002263.

6. Grosshennig, S, Schmidl, SR, Schmeisky, G, Busse, J & Stulke, J (2013) Implication of glycerol and phospholipid transporters in Mycoplasma pneumoniae growth and virulence. *Infect Immun* **81**, 896-904.
7. Dym, O & Eisenberg, D (2001) Sequence-structure analysis of FAD-containing proteins. *Protein Sci* **10**, 1712-28.
8. Mahdi, LK, Wang, H, Van der Hoek, MB, Paton, JC & Ogunniyi, AD (2012) Identification of a novel pneumococcal vaccine antigen preferentially expressed during meningitis in mice. *J Clin Invest* **122**, 2208-20.
9. Colussi, T, Parsonage, D, Boles, W, Matsuoka, T, Mallett, TC, Karplus, PA & Claiborne, A (2008) Structure of alpha-glycerophosphate oxidase from Streptococcus sp.: a template for the mitochondrial alpha-glycerophosphate dehydrogenase. *Biochemistry* **47**, 965-77.
10. Parsonage, D, Luba, J, Mallett, TC & Claiborne, A (1998) The soluble alpha-glycerophosphate oxidase from Enterococcus casseliflavus. Sequence homology with the membrane-associated dehydrogenase and kinetic analysis of the recombinant enzyme. *J Biol Chem* **273**, 23812-22.
11. Charrier, V, Luba, J, Parsonage, D & Claiborne, A (2000) Limited proteolysis as a structural probe of the soluble alpha-glycerophosphate oxidase from Streptococcus sp. *Biochemistry* **39**, 5035-44.
12. Massey, V, Muller, F, Feldberg, R, Schuman, M, Sullivan, P A, Howell, LG, Mayhew, SG, Matthews, RG & Foust, GP (1969) The reactivity of flavoproteins with sulfite: Possible relevance to the problem of oxygen reactivity. *J Biol Chem* **244**, 3999-4006.
13. Holm, L & Rosenstrom, P (2010) Dali server: conservation mapping in 3D. *Nucleic Acids Res* **38**, W545-9.
14. Yeh, JI, Chinte, U & Du, S (2008) Structure of glycerol-3-phosphate dehydrogenase, an essential monotopic membrane enzyme involved in respiration and metabolism. *Proc Natl Acad Sci USA* **105**, 3280-5.
15. Davis, JJ, Xia, F, Overbeek, RA & Olsen, GJ (2013) Genomes of the class Erysipelotrichia clarify the firmicute origin of the class Mollicutes. *Int J Syst Evol Microbiol* **63**, 2727-41.
16. Schryvers, A & Weiner, JH (1981) The anaerobic sn-glycerol-3-phosphate dehydrogenase of Escherichia coli. Purification and characterization. *J Biol Chem* **256**, 9959-65.

17. Mortl, M, Diederichs, K, Welte, W, Molla, G, Motteran, L, Andriolo, G, Pilone, MS & Pollegioni, L (2004) Structure-function correlation in glycine oxidase from Bacillus subtilis. *J Biol Chem* **279**, 29718-27.
18. Settembre, EC, Dorrestein, PC, Park, JH, Augustine, AM, Begley, TP & Ealick, SE (2003) Structural and mechanistic studies on ThiO, a glycine oxidase essential for thiamin biosynthesis in Bacillus subtilis. *Biochemistry* **42**, 2971-81.
19. Umhau, S, Pollegioni, L, Molla, G, Diederichs, K, Welte, W, Pilone, MS & Ghisla, S (2000) The x-ray structure of D-amino acid oxidase at very high resolution identifies the chemical mechanism of flavin-dependent substrate dehydrogenation. *Proc Natl Acad Sci USA* **97**, 12463-8.
20. Battye, TG, Kontogiannis, L, Johnson, O, Powell, HR & Leslie, AG (2011) iMOSFLM: a new graphical interface for diffraction-image processing with MOSFLM. *Acta Crystallogr D Biol Crystallogr* **67**, 271-81.
21. Winn, MD, Ballard, CC, Cowtan, KD, Dodson, EJ, Emsley, P, Evans, PR, Keegan, RM, Krissinel, EB, Leslie, AG, McCoy, A, McNicholas, SJ, Murshudov, GN, Pannu, NS, Potterton, EA, Powell, HR, Read, RJ, Vagin, A & Wilson, KS (2011) Overview of the CCP4 suite and current developments. *Acta Crystallogr D Biol Crystallogr* **67**, 235-42.
22. Evans, PR (2006) Scaling and assessment of data quality. *Acta Crystallogr D Biol Crystallogr* **62**, 72-82.
23. McCoy, AJ, Grosse-Kunstleve, RW, Adams, PD, Winn, MD, Storoni, LC & Read, RJ (2007) Phaser crystallographic software. *J Appl Crystallogr* **40**, 658-674.
24. Emsley, P, Lohkamp, B, Scott, WG & Cowtan, K (2010) Features and development of Coot. *Acta Crystallogr D Biol Crystallogr* **66**, 486-501.
25. Adams, PD, Afonine, PV, Bunkoczi, G, Chen, VB, Davis, IW, Echols, N, Headd, JJ, Hung, LW, Kapral, GJ, Grosse-Kunstleve, RW, McCoy, AJ, Moriarty, NW, Oeffner, R, Read, RJ, Richardson, DC, Richardson, JS, Terwilliger, TC & Zwart, PH (2010) PHENIX: a comprehensive Python-based system for macromolecular structure solution. *Acta Crystallogr D Biol Crystallogr* **66**, 213-21.
26. Bricogne, G, Blanc, E, Brandl, M, Flensburg, C, Keller, P, Paciorek, W, Roversi, P, Sharff, A, Smart, OS, Vonrhein, C & Womack, TO (2011) BUSTER version 2.11.2 in Global Phasing Ltd., Cambridge, UK.

27. Murshudov, GN, Vagin, AA & Dodson, EJ (1997) Refinement of macromolecular structures by the maximum-likelihood method. *Acta Crystallogr D Biol Crystallogr* **53**, 240-55.
28. Guindon, S, Dufayard, JF, Lefort, V, Anisimova, M, Hordijk, W & Gascuel, O (2010) New algorithms and methods to estimate maximum-likelihood phylogenies: assessing the performance of PhyML 3.0. *Systematic Biology* **59**, 307-21.

Scheme 1

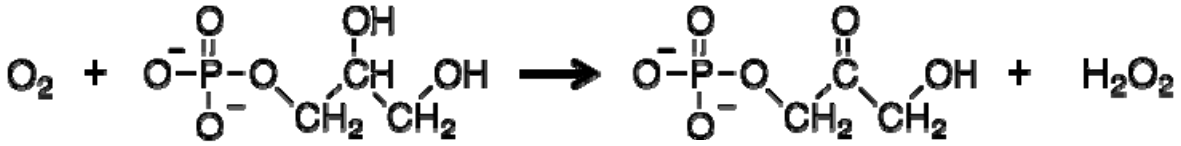

Table 1. Data Collection and Refinement Statistics for *Mp*GlpO structures. Numbers in parentheses represent data for the high-resolution shell.

	oxidized	reduced
PDB entry code	**4X9M**	**4X9N**
Data quality statistics		
Wavelength (Å)	0.9765	0.9765
Space group	*P*23	*P*23
Cell dimensions, $a = b = c$ (Å)	111.59	111.61
Resolution range (Å)	50-2.4 (2.53-2.4)	60-2.5 (2.64-2.5)
Reflections	430,576	836,296
Unique reflections	18,401	16,368
Completeness (%)	100 (99)	100 (100)
Multiplicity	23.4 (23.6)[a]	51.1 (28.6)
R_{pim}	0.022 (0.19)	0.072 (0.28)

R_{meas}	0.109 (0.90)	0.533 (1.51)
I/σ	22.7 (4.4)	19.9 (3.0)
Refinement statistics		
R_{work} (%)	14.8 (21.9)	14.7 (23.5)
R_{free} (%)	20.4 (25.3)	21.1 (34.3)
No. amino acid residues	384	384
No. solvent atoms	200	200
No. non-hydrogen atoms	3301	3313
<*B*> protein (Å^2)	35	39

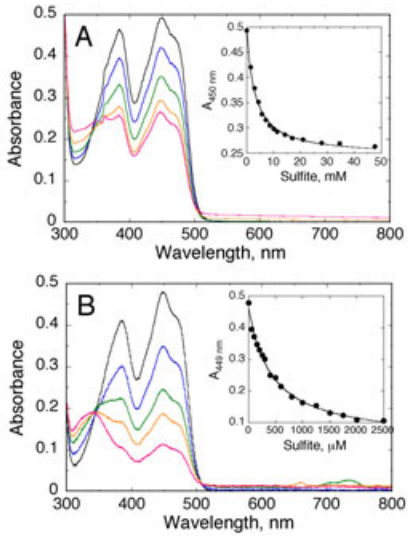

Figure 1. Sulfite titrations of *Mp*GlpO and *Bp*3253. **A.** MpGlpO [35.4 μM in 0.8 mL of 50 mM potassium phosphate, 0.5 mM EDTA, pH 7.0] was titrated aerobically with a 1 M sodium sulfite solution. The spectra shown correspond to the addition of 0 (black), 1.43 (blue), 4.27 (green), 11.3 (orange) and 47.6 mM (red) total sulfite. The inset shows the absorbance at 450 nm as a function of added sulfite. **B.** The titration of *Bp*3253 (36.2 μM in 1 mL) was carried out as described in (A), with 25 and 100 mM solutions of sodium sulfite. The spectra shown are with 0 (black), 0.15 (blue), 0.50 (green), 0.80 (orange) and 2.0 mM (red) total sulfite. The inset shows the absorbance changes at 449 nm as sulfite is added.

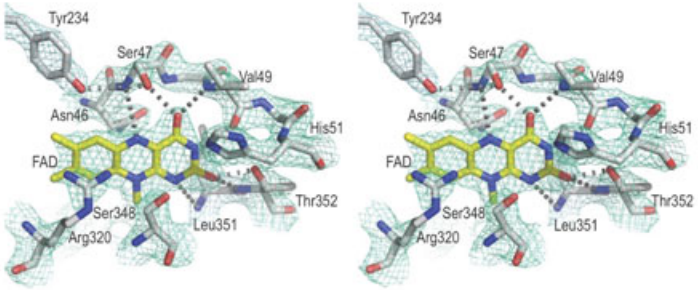

Figure 2. Electron density quality for the flavin and nearby side chains. Stereoview of the final $2F_o$-F_c electron density map (cyan; contoured at $2.0\rho_{rms}$) for the *Mp*GlpO flavin (yellow carbons) and the adjacent protein atoms (off-white carbons) and one water (red sphere). Hydrogen bonds (dashed lines) to the flavin and the water are indicated. Residues are labeled.

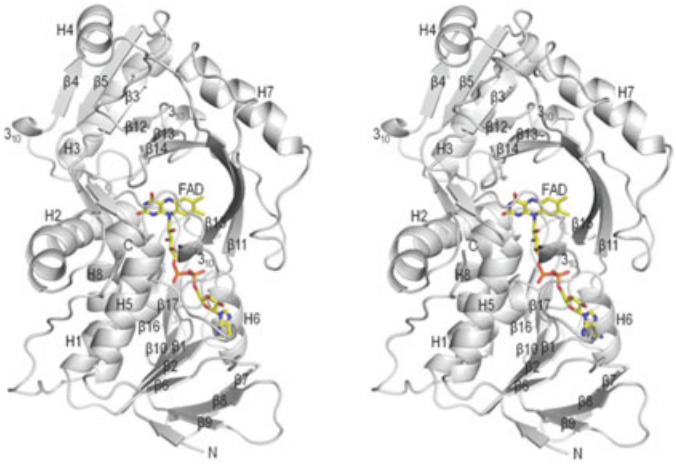

Figure 3. Tertiary structure of the *Mp*GlpO monomer. Stereo ribbon diagram of the *Mp*GlpO monomer showing the FAD (sticks with yellow carbons) and labeling the secondary structural elements. The FAD-binding domain is at the bottom and the substrate-binding domain is at the top.

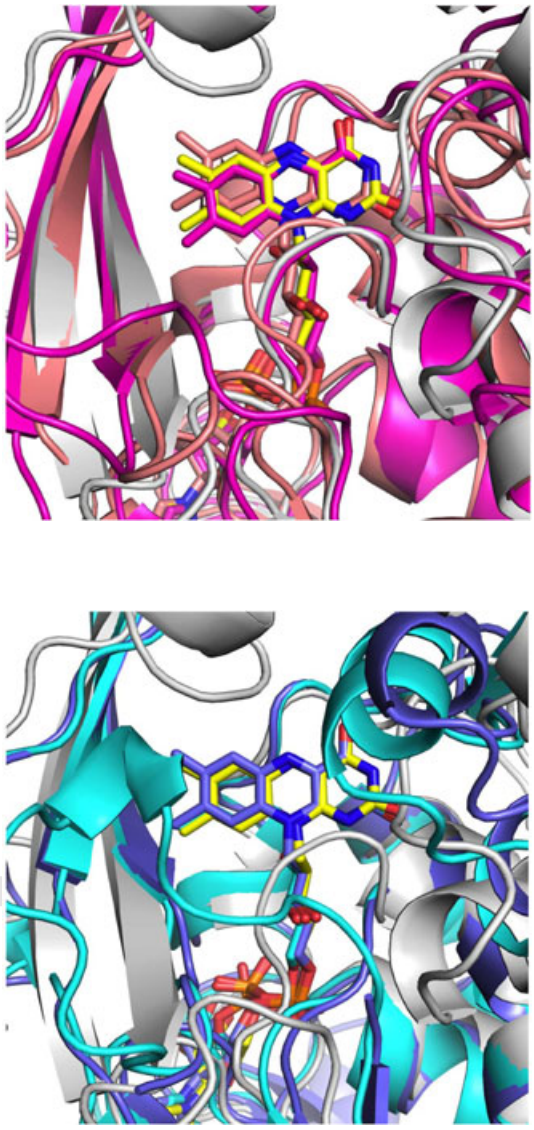

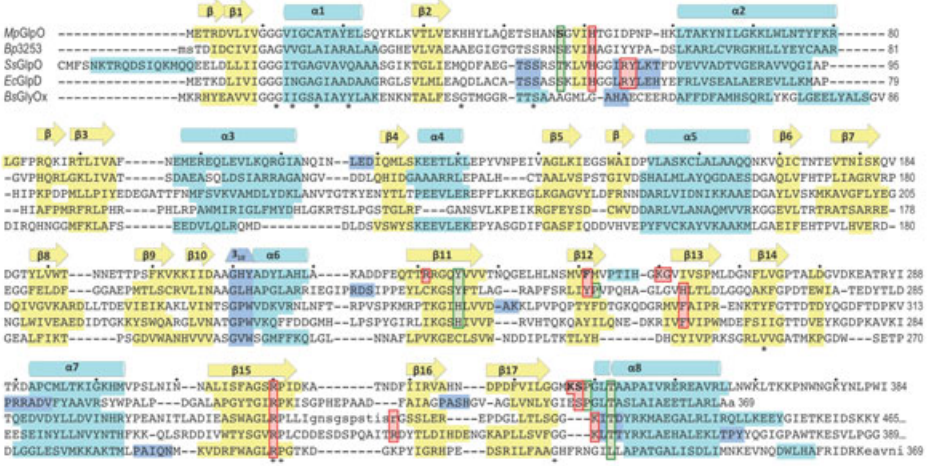

Figure 4. Comparisons of the *Mp*GlpO structure and sequence with select homologs. **A.** The flavin region in an overlay of *Mp*GlpO (off-white protein and yellow FAD) on *Bp*3253 (violet; PDB entry 3DME) and glycine oxidase (salmon; PDB entry 1RYI; [17]). For this view the Figure 3 molecule was rotated 180˚ around a vertical axis (i.e. this view is from the back of that image). Note the similar paths of the loop in front of the flavin, in *Mp*GlpO containing Ser 348. **B.** Same as (A) but overlaying *Mp*GlpO (colored as in A) with a form of *Ssp*GlpO missing a 50 residue segment (blue; PDB entry 2RGH; [9]) and *Ec*GlpD (cyan; PDB entry 2QCU; [14]). Note the different paths of the loop in front of the flavin of the type I enzymes compared with *Mp*GlpO. **C.** Structure-based sequence alignment of the five enzymes shown in panels (A) and (B). Conserved residues (*) and residues involved in β-strands (yellow), α-helices (cyan) and 3_{10}-helices (blue) are indicated. Also highlighted are residues discussed as important for in flavin binding (green boxes; and including the *cis*-Pro in *Mp*GlpO and *Bp*3253) and substrate binding (red boxes). Dots above the *Mp*GlpO sequence mark its every 10^{th} residue, and at the end of each line is a numbered residue for each of the sequences.

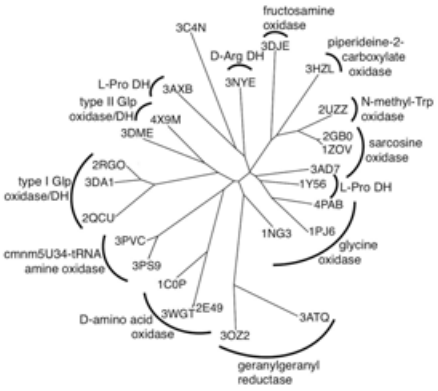

Figure 5. Relatedness tree of structurally known DAAO superfamily members most similar to *Mp*GlpO. A DALI [13] search in November 2014 using the PDB90 database option and oxidized *Mp*GlpO as the search model, provided a gap-removed alignment for hits with Z-scores higher than 20. These were used to generate a tree with PhyML [28]. Branches are labeled with individual PDB entry names and known enzyme types are indicated.

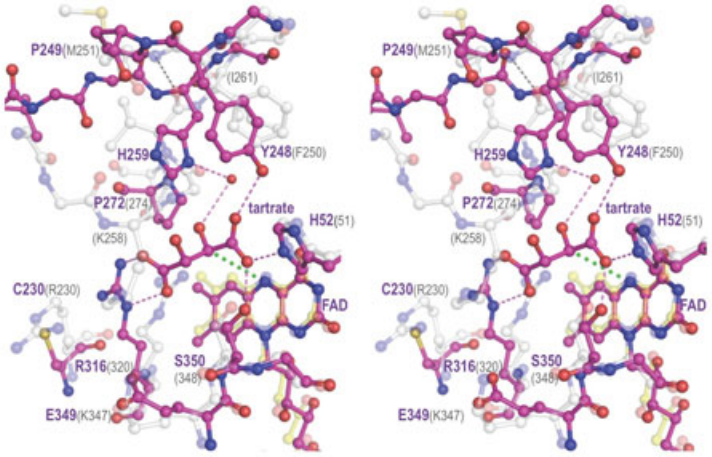

Figure 6. Comparison of the *Bp*3253 tartrate binding pocket and *Mp*GlpO. Stereoview shown of the *Bp*3253-tartrate complex (violet carbons) overlaid on the equivalent region of *Mp*GlpO (semi-transparent off-white carbons for protein and yellow for flavin). Also indicated are H-bonds (grey dashed lines for *Mp*GlpO, violet dashed lines for *Bp*3253-tartrate complex) and the close approach of the tartrate C3 atom to the flavin N5 (green thick dotted line). Select residues in *Bp*3253-tartrate complex (violet) and *Mp*GlpO (grey) are identified. H259 in the *Bp*3253-tartrate complex and I261 in *Mp*GlpO are equivalent residues, but their labels are placed near their respective side chains.

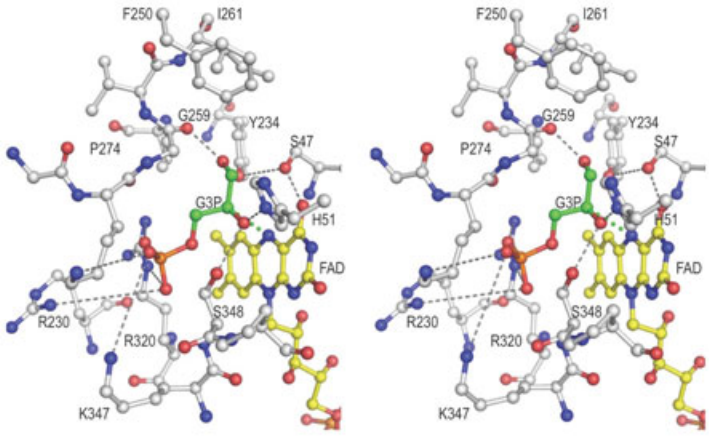

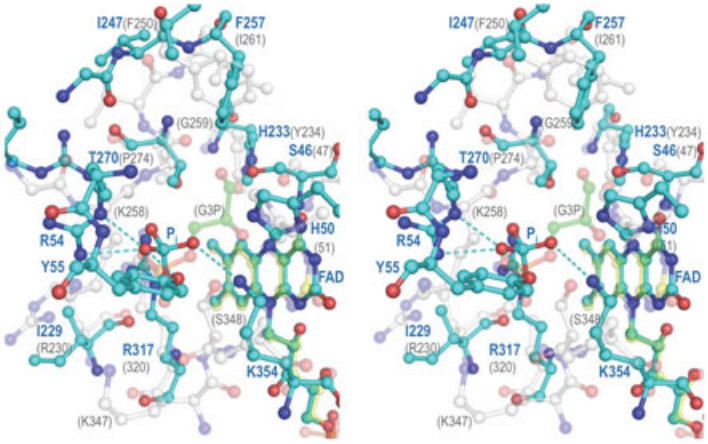

Figure 7. A predicted *Mp*GlpO-Glp complex and its comparison with *Ec*GlpD. **A.** Stereoview of the *Mp*GlpO active site with a roughly positioned Glp-bound (off-white carbons for protein, yellow for flavin, and green for Glp). H-bonds (grey dashed lines) and the close approach of the modeled Glp C2 atom to the flavin N5 (green thick dotted line) are also shown. Criteria used for placing the Glp are described in the text. **B.** Stereoview of the *Mp*GlpO (colored as in A, but semitransparent and without H-bonds shown) overlaid on the equivalent region of *Ec*GlpD (cyan carbons) with its bound inorganic phosphate (cyan phosphorus) and H-bonds (cyan dashed lines). Select residues in *Ec*GlpD (cyan) and *Mp*GlpO (grey) are identified.

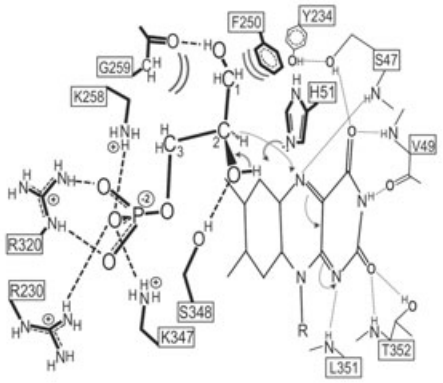

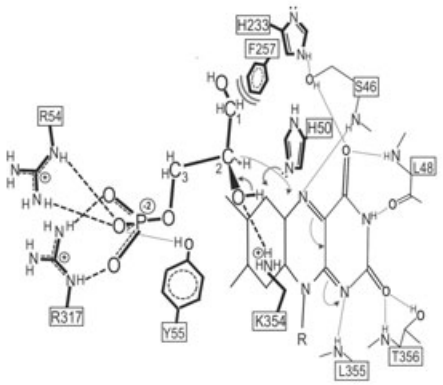

Figure 8. Schematic drawings of residues involved in substrate binding and catalysis in *Mp*GlpO and *Ec*GlpD. **A.** The *Mp*GlpO active site atoms roughly in the plane of the flavin are shown smaller and with thinner bonds and hydrogen bonds (dashed), and atoms in front of the flavin are shown with thicker bonds and hydrogen bonds (dashed). Residues shown interacting with the flavin and the Glp are in Figure 4C highlighted in red and green boxes, respectively,. Curved arrows indicate the proposed flow of electrons during the reductive half-reaction. **B.** The same except for showing the *Ec*GlpD active site as a representative of a Type I GlpO.

Enzymology:

Kinetic Mechanism and the Rate-Limiting Step of Plasmodium vivax Serine Hydroxymethyltransferase

Somchart Maenpuen, Watcharee Amornwatcharapong, Pasupat Krasatong, Jeerus Sucharitakul, Bruce A. Palfey, Yongyuth Yuthavong, Penchit Chitnumsub, Ubolsree Leartsakulpanich and Pimchai Chaiyen

J. Biol. Chem. *published online February 12, 2015*

Access the most updated version of this article at doi: 10.1074/jbc.M114.612275

This article cites 0 references, 0 of which can be accessed free at
http://www.jbc.org/content/early/2015/02/12/jbc.M114.612275.full.html#ref-list-1

JBC Papers in Press. Published on February 12, 2015 as Manuscript M114.612275
The latest version is at http://www.jbc.org/cgi/doi/10.1074/jbc.M114.612275

Kinetic Mechanism and the Rate-Limiting Step of *Plasmodium vivax* Serine Hydroxymethyltransferase*

Somchart Maenpuen[1,2], Watcharee Amornwatcharapong[1], Pasupat Krasatong[2], Jeerus Sucharitakul[3], Bruce A. Palfey[4], Yongyuth Yuthavong[5], Penchit Chitnumsub[5], Ubolsree Leartsakulpanich[5] and Pimchai Chaiyen[1]

[1]Department of Biochemistry and Center of Excellence in Protein Structure and Function, Faculty of Science, Mahidol University, Bangkok, Thailand 10400.
[2]Department of Biochemistry, Faculty of Science, Burapha University, Chonburi, Thailand 20131.
[3]Department of Biochemistry, Faculty of Dentistry, Chulalongkorn University, Bangkok, Thailand 10300.
[4]Department of Biological Chemistry, University of Michigan, Ann Arbor, Michigan, United States of America 48109.
[5]National Center for Genetic Engineering and Biotechnology, National Science and Technology Development Agency, Pathumthani, Thailand 12120.

*Running title: *Kinetic Mechanism of Plasmodium vivax Serine Hydroxymethyltransferase*

To whom correspondence should be addressed: Pimchai Chaiyen, Department of Biochemistry and Center of Excellence in Protein Structure and Function, Faculty of Science, Mahidol University, Bangkok, Thailand 10400. Rama 6 Rd., Ratchatewi, Bangkok, Thailand, Tel.: (66) 2201-5596; Fax: (66) 2354-7174; Email: pimchai.cha@mahidol.ac.th
and Ubolsree Leartsakulpanich, National Center for Genetic Engineering and Biotechnology, National Science and Technology Development Agency, Pathumthani, Thailand 12120. 113 Paholyothin Rd., Klong 1, Klong Luang, Pathumthani, Thailand, Tel.: (66) 2564-6700 ext 3483; Fax: (66) 2564-6707; Email: ubolsree@biotec.or.th

Keywords: Pyridoxal 5'-phosphate-dependent enzyme; *Plasmodium vivax* serine hydroxymethyltransferase (PvSHMT); random-order mechanism; deoxythymidylate (dTMP) cycle

Background: *Plasmodium vivax* serine hydroxymethyltransferase (PvSHMT) catalyzes formation of glycine from L-serine and tetrahydrofolate .
Results: Results indicate that PvSHMT can bind to either substrate first. The rate constant of glycine formation is similar to k_{cat}.
Conclusion: PvSHMT reaction occurs via a random-order mechanism and glycine formation is the rate-limiting step.
Significance: The data are useful for future investigation on inhibition of SHMT for antimalarial drug development.

ABSTRACT

Serine hydroxymethyltransferase (SHMT) is a pyridoxal 5'-phosphate (PLP)-dependent enzyme that catalyzes a hydroxymethyl group transfer from L-serine to tetrahydrofolate (H_4folate) to yield glycine and 5,10-methylenetetrahydrofolate (CH_2-H_4folate). SHMT is crucial for dTMP biosynthesis and a target for antimalarial drug development. Our previous studies indicate that PvSHMT catalyzes the reaction via a ternary-complex mechanism. In order to define the kinetic mechanism of this catalysis, we explored the PvSHMT reaction by employing various methodologies including ligand binding, transient, and steady-state kinetics as well as product analysis by rapid-quench and HPLC/MS techniques. The results indicate that PvSHMT can bind first to either L-serine or H_4folate. The dissociation constants for the enzyme:L-serine and enzyme:H_4folate complexes were determined as 0.18 ± 0.08 mM and 0.35 ± 0.06 mM, respectively. The amounts of glycine formed after single turnovers of different preformed binary complexes were similar, indicating that the reaction proceeds via a random-order binding mechanism. In addition, the rate constant of glycine formation

measured by rapid-quench and HPLC/MS analysis is similar to the k_{cat} value (1.09 ± 0.05 s^{-1}) obtained from the steady-state kinetics, indicating that glycine formation is the rate-limiting step of SHMT catalysis. This information will serve as a basis for future investigation on species-specific inhibition of SHMT for antimalarial drug development.

Serine hydroxymethyltransferase (SHMT) (L-serine:tetrahydrofolate 5,10-hydroxymethyl transferase; EC. 2.1.2.1) is a pyridoxal 5'-phosphate (PLP)-dependent enzyme that catalyzes the reversible transfer of a hydroxymethyl group from L-serine to tetrahydrofolate (H_4folate), yielding glycine and 5,10-methylenetetrahydrofolate (CH_2-H_4folate) as products (1,2). The enzyme is involved in the deoxythymidylate (dTMP) synthesis cycle, as CH_2-H_4folate is a substrate for thymidylate synthase, which synthesizes dTMP, a precursor for DNA biosynthesis (3). In addition to the physiological H_4folate-dependent SHMT reaction, SHMT from many organisms can also catalyze various other reactions such as H_4folate-independent retro-aldol cleavage of β-hydroxy amino acids including L-threonine, L-*allo*-threonine, (D,L)- β-phenylserine, and L-*threo*-phenylserine, transaminations, racemization, decarboxylation, and condensation (2, 4-7). Therefore, SHMT has been an enzyme of interest not only because of its important physiological function, but also for its reaction promiscuity (2, 8-10).

Plasmodium SHMT has been shown to be essential for parasite growth and development, making it a prime target for antimalarial drug chemotherapy development (11). The recombinant expression and purification of *Plasmodium falciparum* (PfSHMT) and *Plasmodium vivax* SHMT (PvSHMT) as well as their biochemical characterizations have been reported (5,12-14). In general, both of these enzymes are similar in their enzymatic properties. The crystal structure of PfSHMT has been recently solved, revealing the unique function of a cysteine pair at the folate binding pocket in regulating enzyme function through variation of the redox states of these cysteines. This regulation is different from the mammalian and bacterial SHMTs (15). Moreover, it has been shown that *Plasmodium* SHMTs display several properties that are distinct from the human enzyme, including the inactivation kinetics towards thiosemicarbazide (16). This implies that it is possible to design species-specific inhibitors for anti-malarial drug development. An in-depth understanding of *Plasmodium* SHMT kinetics and mechanism is therefore needed so that the differences in reaction details among SHMTs can be understood and used for the development of specific inhibitors.

Although the reaction of SHMT from various species has been investigated, many of these studies focused on the non-physiological reaction, or the reverse reaction of glycine and CH_2-H_4folate (2,7,8,17,18). The pre-steady state kinetics of the H_4folate-dependent SHMT reaction has never been investigated. Double-reciprocal plots of bi-substrate kinetics of SHMT from rabbit liver cytosol, *P. vivax*, and *P. falciparum* display intersecting lines, suggesting that the reaction occurs via a ternary-complex mechanism in which the formation of an enzyme:serine:H_4folate complex is required for catalysis (5,12,17). However, it was unclear whether the substrates bind in a compulsory or random order. While the binding of L-serine or other amino acids to SHMT can be clearly monitored by spectroscopic detection based on the formation of an external aldimine, up to now, evidence supporting direct binding between SHMT and H_4folate has not been demonstrated.

In this study, we employed various methodologies including ligand binding measurements, as well as transient and steady-state kinetics to investigate the PvSHMT reaction. Upon anaerobic titration of H_4folate into the enzyme solution, a spectroscopic signal resulting from the direct binding of PvSHMT and H_4folate was detected. Results from rapid-quench and HPLC/MS analysis and steady-state kinetics have clearly established glycine formation as the rate-limiting step for the overall reaction of PvSHMT.

EXPERIMENTAL PROCEDURES

Reagents–All chemicals and reagents used were analytical grade and of the highest purity commercially available as described previously (5). An expression plasmid for hexa-histidine tagged FAD-dependent NAD(P)H:5,10-methylenetetrahydrofolate oxidoreductase (His_6-tagged MTHFR) was kindly provided by Dr.

Elitzabeth E. Trimmer, Grinnell College (IA, USA). Concentrations of (6*S*)-tetrahydrofolate (H_4folate) were determined based on its reaction with formic acid according to the protocol described previously (5,19,20). In brief, a solution of H_4folate was added to formic acid (99%) containing 0.5 mM EDTA and 1 mM DTT and the reaction mixture was incubated in boiling water for 5 min. The solution was allowed to cool, and the absorption of the resulting stable compound, 5,10-methenyltetrahydrofolate (CH^+-H_4folate; ε_{350} = 26 $mM^{-1}cm^{-1}$) was measured. Based on the assumption that all of the H_4folate is converted to CH^+-H_4folate, the determined concentration of CH^+-H_4folate is equivalent to the concentration of H_4folate. Concentrations of PvSHMT and NADH were determined using their molar absorption coefficients: NADH, ε_{340} = 6.22 $mM^{-1}cm^{-1}$; PvSHMT, ε_{422} = 6.37 $mM^{-1}cm^{-1}$ (5).

PvSHMT preparation and activity assay– The expression and purification of recombinant PvSHMT were performed as previously reported (5,14). In brief, the expression plasmid containing pET17b-*pvshmt* was transformed into *E. coli* BL21 (DE3) and induced by auto-induction method to express native PvSHMT without tag at 16 °C in ZYP-5052 rich medium (5 mM Na_2SO_4, 2 mM $MgSO_4$, 1X NPS (25 mM Na_2HPO_4, 25 mM KH_2PO_4, 50 mM NH_4Cl), 1X 5052 (0.5%(w/v) glycerol, 0.05%(w/v) D-glucose, and 0.2%(w/v) α-lactose) containing 50 μg/mL of ampicillin for overnight (~16-18 h). Cells were disrupted by ultrasonication and then centrifuged to obtain crude extract. The enzyme was purified to homogeneity using polyethyleneimine precipitation DEAE- and SP-Sepharose chromatography. The activity of purified PvSHMT was assayed at 25 °C under anaerobic conditions by coupling its reaction with the reaction of His_6-tagged MTHFR (5,21,22). In brief, a mixture of enzyme solution containing PvSHMT (1 μM) and His_6-tagged MTHFR (3 μM) in 50 mM HEPES, pH 7.0 containing 0.5 mM EDTA, and 1 mM DTT was mixed with a substrate solution containing NADH (100 μM), L-serine (2 mM), and H_4folate (400 μM) at 25 °C under anaerobic conditions by using a stopped flow-spectrophotometer (TgK Scientific instruments, models SF-61DX2 or SF-61SX). Stopped-flow machine was used for steady-state assays to maintain anaerobic conditions of the experiments. The anaerobic condition was achieved by rinsing the flow circuits with O_2-scrubbing solution (dithionite). Before experiments, the flow system was washed with anaerobic buffer. All reagents were prepared in anaerobic glovebox (<5 ppm O_2). The reaction was measured by following the consumption of NADH, for which the absorbance at 375 nm was monitored in order to avoid interference from absorbance of H_4folate. Slopes of the kinetic traces were analyzed by Program A (developed by Chun-Jen Chiu, Rong Chang, Joel Dinverno, and David P. Ballou from the University of Michigan, Ann Arbor) and the initial velocities of PvSHMT were calculated using a molar extinction coefficient of 1.92 $mM^{-1}cm^{-1}$ at 375 nm. One unit of PvSHMT was defined as the amount of the enzyme used for oxidizing 1 μmol of NADH per minute at 25 °C under pH 7.0.

Steady-state kinetics of the PvSHMT reaction at pH 8.0–Two-substrate steady-state kinetics was performed and analyzed according to a protocol similar to that described in a previous report (5), except the reactions were investigated at pH 8.0 instead of pH 7.0. The study was carried out at pH 8.0 since PvSHMT was found to have the highest activity at this pH (5). Substrate solutions containing NADH (100 μM), various concentrations of L-serine (200-6400 μM), and H_4folate (25-400 μM) in 50 mM HEPES, pH 8.0 containing 0.5 mM EDTA, and 1 mM DTT were mixed with an enzyme solution containing PvSHMT (1 μM) and His_6-tagged MTHFR (3 μM) in the same buffer at 25 °C under anaerobic conditions using a stopped flow-spectrophotometer. Initial rates were analyzed according to a rate equation (Equation 1) using the Enzfitter program (BIOSOFT, Cambridge, UK). Data are displayed according to Dalziel's equation (double-reciprocal) (Equation 2) for a two-substrate reaction.

$$v = \frac{V[\mathrm{A}][\mathrm{B}]}{K_{\mathrm{iA}}K_{\mathrm{B}} + K_{\mathrm{B}}[\mathrm{A}] + K_{\mathrm{A}}[\mathrm{B}] + [\mathrm{A}][\mathrm{B}]} \quad (1)$$

$$\frac{e}{v} = \phi_0 + \frac{\phi_{\mathrm{A}}}{[\mathrm{A}]} + \frac{\phi_{\mathrm{B}}}{[\mathrm{B}]} + \frac{\phi_{\mathrm{AB}}}{[\mathrm{A}][\mathrm{B}]} \quad (2)$$

Binding of L-serine to PvSHMT at pH 8.0–The titration protocol of PvSHMT (~31 μM; OD_{422} ~0.2) with L-serine (0.16-145 mM) in 50 mM HEPES, pH 8.0 containing 0.5 mM EDTA and 1 mM DTT and data analysis were carried out as described earlier (5,12).

Binding of H_4folate to PvSHMT–In order to determine whether PvSHMT can directly bind H_4folate without requiring prior binding of L-serine, we investigated the binding of PvSHMT and H_4folate under anaerobic conditions to avoid interference signals from H_4folate oxidation. An anaerobic solution (1 mL) of PvSHMT (~47 μM; OD_{422} ~0.3) in 50 mM HEPES, pH 8.0 containing 0.5 mM EDTA and 1 mM DTT prepared inside the anaerobic glove box (<5ppm oxygen; Belle Technology, UK) was first scanned to record an enzyme spectrum before adding various concentrations of H_4folate (0.050-2.954 mM). After adding each concentration of H_4folate, the mixture was thoroughly mixed and left for 5 min before recording a spectrum again. The spectrum of free enzyme was subtracted from all spectra obtained from each titration to determine the absorbance changes (ΔA). The ΔA values were plotted against the H_4folate concentration and the K_d for the binding of H_4folate to PvSHMT was determined according to Equation 3**,** where ΔA represents the absorbance change, ΔA_{max} is the maximum absorbance change, $[L]_{free}$ is a concentration of free ligand, and K_d is a dissociation constant of the enzyme-ligand complex. The analysis was done using Marquardt-Lavenberg algorithms in the KaleidaGraph program version 4.0.

$$\frac{\Delta A}{\Delta A_{max}} = \frac{[L]_{free}}{K_d + [L]_{free}} \qquad (3)$$

Kinetics for the binding of PvSHMT with L-serine–A solution of 31 μM PvSHMT was mixed with various concentrations of L-serine (0.4-12.8 mM) in 50 mM HEPES, pH 8.0 containing 0.5 mM EDTA and 1 mM DTT at 25 °C using a single-mixing mode stopped-flow spectrophotometer. The binding reaction was monitored at 435 nm where it gives a large absorbance change due to the formation of the external aldimine of the serine-PLP complex. All kinetic traces were analyzed using Program A. Observed rate constants (k_{obs}) associated with each kinetic phase were plotted against the concentrations of L-serine and analyzed according to Equation 4 and 5. k_f and k_r are the forward and reverse rate constants for the free enzyme isomerization prior to the ligand binding according to the conformational selection model (23), k_{max} is the maximum observed rate constant, $k_{intercept}$ is the rate constant at an ordinate intercept, K_S represents a concentration of substrate that is a half value of k_{max}.

$$k_{obs} = \frac{k_{max} \cdot S}{K_S + S} + k_{intercept} \qquad (4)$$

$$k_{obs} = k_f + \left(\frac{K_S}{K_S + S} \right) k_r \qquad (5)$$

Single-turnover reactions of PvSHMT with L-serine and H_4folate under different mixing conditions–Three different mixing set-ups were performed to identify the sequence of substrate binding as follows: (i) a solution of pre-equilibrated binary complex of PvSHMT (45 μM)-L-serine (30 μM) was mixed with various concentrations of H_4folate (0.2-6.4 mM), (ii) a solution of pre-equilibrated binary complex of PvSHMT (45 μM) with either 0.4 or 3.2 mM H_4folate was mixed with L-serine (30 μM), and (iii) a solution of PvSHMT (45 μM) was mixed with solution mixtures of L-serine (30 μM) and various concentrations of H_4folate (0.2-6.4 mM). All reactions were carried out under anaerobic conditions at 25 °C in 50 mM HEPES, pH 8.0 containing 0.5 mM EDTA, and 1 mM DTT. Because the largest signal change was observed at 496 nm, the reaction progression was monitored at this wavelength using a stopped-flow spectrophotometer (single-mixing mode) to detect the formation of quinonoid species. Kinetic traces were analyzed by Program A. All concentrations specified are final mixing concentrations.

Detection of glycine product formation in single-turnover reactions of PvSHMT using rapid acid-quenched flow and HPLC/UV or HPLC/MS analysis–An anaerobic solution of pre-equilibrated binary complex of PvSHMT (45 μM):L-serine (30 μM) was mixed with 0.4 or 3.2 mM H_4folate in 50 mM HEPES, pH 8.0 containing 0.5 mM EDTA, 1

mM DTT and 3 mM palatinose (as internal control) using a rapid-quenched flow (RQF) apparatus (TgK Scientific, UK), equipped inside an anaerobic glove box in which the oxygen concentration is <5ppm oxygen (Belle Technology, UK). The reactions were quenched at various time points (0.03-6.30 s) by addition of a HCl solution (0.15 M), and the acid-quenched reaction mixtures were then collected for analysis.

Detection of glycine and serine was carried out either via phenylisothiocyanate (PITC) amino acid derivatization and monitored by HPLC/UV (Agilent 1100) or directly detected by HPLC/MS analysis (Agilent 1260 equipped with Agilent 6120 single quadrupole mass spectrometer). Samples from rapid quench flow (RQF) experiments were transferred into a Microcon ultrafiltration unit and then centrifuged at 10,000 rpm, 4 ^{o}C for 20 min to separate the small molecules from the macromolecules. The derivatization method and HPLC/UV analysis were performed according to the protocol described previously with slight modifications (24). For HPLC analysis, the dried samples were redissolved in 50 µL of solvent A (0.14 M sodium acetate, pH 6.4 containing 0.05% TEA) and centrifuged at 15,000 rpm at room temperature for 30 min to clarify the samples. A clear supernatant was injected onto a C18 column (Waters®; 3.9 x 150 mm) which was pre-equilibrated with 100% solvent A with a flow rate of 1 mL/min. The column was washed with 100% solvent A for 15 min, and then a gradient of 0-53% of solvent B (60% acetonitrile/H_2O) was applied, in which B was gradually increased over the course of 10-min and maintained at the highest concentration for 5 more minutes. A gradient of 53-100% solvent B was applied over the next 5 min and held for another 5 min before re-equilibrating the column in 100% solvent A. Under these conditions, derivatized serine and glycine can be clearly separated and showed retention times of 7.9 and 9.1 min, respectively. Similar amino acid derivatization as described was applied to standard glycine and L-serine solutions (1-30 µM) and a standard curve was generated by plotting the averaged peak areas as a function of glycine or L-serine concentrations.

For the direct sample analysis using HPLC/MS, samples collected from RQF experiments were filtered through a Microcon ultrafiltration unit by centrifugation at 10,000 rpm for 20 min. The filtrate was injected onto a Zorbax-NH_2 column (Agilent Technology; 4.6 x 250 mm, 5 µm) which was pre-equilibrated with 80% solvent C (acetonitrile + 0.1% (v/v) formic acid) with a flow rate of 0.5 mL/min for 60 min. The column was then washed with 80% solvent C for 2 min before the eluent was gradually changed to 60% solvent C over the course of 3 min and further held at this condition for 15 min. The percentage of solvent C was then gradually increased to 80% over 22 min and held at this condition for 10 more minutes to re-equilibrate the column for new injections. HPLC chromatograms of glycine and serine showed retention times of 14.2 and 15.2 min, respectively. The eluent from the HPLC column was continuously flowed into the mass spectrometer equipped with an API-electrospray ionizer (ESI). Conditions for mass spectrometric detection were as follows. Nebulizer pressure was set at 35 psi. The capillary source voltage was set at 3 kV. The drying gas temperature was maintained at 350 ^{o}C. Drying gas flow was 12 L·min^{-1}. Scan mode was from 50-150 m/z. The polarity was set in a positively selected ion mode (SIM) in which glycine and serine were detected separately at 76 m/z and 106 m/z, respectively. The peak area for glycine and serine was quantified based on glycine and serine standard curves, for which the amino acid was treated with the same condition as those from the rapid-quenched flow experiments. The amounts of glycine product formed at different time points were analyzed using a single exponential equation as shown in Equation 6, where A is the amount of glycine at any time, A_0 is the total amount of glycine that can be produced from the reaction, k_{obs} is the observed rate constant for the glycine formation and t is the reaction time.

$$A = A_0(1 - e^{-k_{obs}t}) \qquad (6)$$

For analysis of the products resulting from the different types of mixing set-ups previously described, similar reactions as those performed in the stopped-flow experiments were carried out in a RQF machine, and the reactions were quenched at 10 s to measure glycine formation and to quantify the remaining L-serine. Measurement of L-serine and glycine was carried out as described above.

RESULTS

Bi-substrate steady-state kinetics of PvSHMT reaction at pH 8.0–As PvSHMT activity is the highest at pH 8.0 (5), we decided to re-investigate steady-state kinetics of PvSHMT at this pH. A solution of PvSHMT and His_6-tagged MTHFR was mixed with various concentrations of L-serine and H_4folate using the stopped-flow spectrophotometer under anaerobic conditions at pH 8.0 (Experimental Procedures). A double-reciprocal plot of *e/v versus* 1/L-serine shows a series of convergent lines at various concentrations of H_4folate, indicating that the reaction proceeds via a ternary-complex mechanism as the reaction that takes place at pH 7.0 (Fig. 1). Steady-state kinetic parameters for the PvSHMT reaction at pH 8.0 are similar to those at pH 7.0 (5): K_m of L-serine (pH 8.0 = 0.26 ± 0.04 mM, pH 7.0 = 0.18 ± 0.03 mM), K_m of H_4folate (pH 8.0 = 0.11 ± 0.01 mM, pH 7.0 = 0.14 ± 0.02 mM), and k_{cat} (pH 8.0 = 1.09 ± 0.05 s^{-1}, pH 7.0 = 0.98 ± 0.06 s^{-1}).

Thermodynamics and kinetics of binding of PvSHMT with L-serine–Various concentrations of L-serine (0.16-145 mM) were added to a solution of PvSHMT (31 μM), pH 8.0 and the absorption changes were monitored. Results indicated that the enzyme binds L-serine and forms an external aldimine as an increase in absorbance at 435 nm could be observed (Fig. 2). The data analysis yielded a thermodynamic dissociation constant (K_d) of 2.2 ± 0.5 mM for the PvSHMT:L-serine complex (Inset of Fig. 2).

In order to gain insights into the binding mechanisms, stopped-flow spectrophotometry was used for investigating the kinetics of binding of L-serine to the enzyme. Kinetic traces of the absorption changes at 435 nm (Fig. 3) resulting from formation of the PvSHMT and L-serine complex showed three phases. The traces were analyzed to obtain the observed rate constants (k_{obs}) of each phase. k_{obs} of the first phase (0.001-10 s) was hyperbolically dependent on the L-serine concentration (Inset of Fig. 3), consistent with the maximum limiting rate constant of 0.38 ± 0.02 s^{-1} and L-serine concentration that gives a half-saturation value of 0.86 ± 0.16 mM (Inset of Fig. 3). k_{obs} of the second phase (10-100 s) was independent of the L-serine concentration, with a rate constant of ~0.015 s^{-1}. For the third phase (100-2500 s), k_{obs} values hyperbolically decreased upon increasing the L-serine concentration, with the apparent lowest rate constant of 0.0020 ± 0.0001 s^{-1} and the L-serine concentration that gives a half-minimum value of 2 ± 1 mM (data not shown). Altogether, the data suggest that binding of PvSHMT and L-serine proceeds through three phases with the second and third phases not involved in the catalytic reaction because they are much slower than the k_{cat} value (1.09 ± 0.05 s^{-1}, Fig. 1). The first phase is likely the binding of L-serine to PvSHMT to form a PvSHMT:L-serine complex (ES) which then isomerizes to form the ES* complex with a rate constant of 0.30 ± 0.04 s^{-1} and an overall K_d value for the ES* complex formation was determined as 0.18 ± 0.08 mM (Fig. 8A). This K_d value is different from the value obtained from the plot in Inset of Fig. 2 (2.2 mM) which obtained from absorption signal changes after 15 min. The observed discrepancy between the K_d values obtained from the two techniques implies that the equilibrium K_d value (2.2 mM, Inset of Fig. 2) does not represent the binding event that is involved in the productive pathway. It is likely that in the absence of H_4folate, after the first step of binary complex formation the PvSHMT:L-serine complex proceeds to the unproductive path or promiscuous activity to give a large absorbance signal change (second and third phases of Fig. 3).

Binding of PvSHMT and H_4folate–While the binding of L-serine and SHMT to form an external aldimine complex (as demonstrated in the previous section) is clearly evident, the interaction of SHMT with H_4folate has never been documented. We therefore investigated the binding of PvSHMT and H_4folate under anaerobic conditions by titrating PvSHMT (47 μM) with various concentrations of H_4folate (0.050-2.954 mM) at pH 8.0. The results indicated that the enzyme can also bind to H_4folate to form a binary complex of PvSHMT:H_4folate because spectra (Fig. 4) of solutions of PvSHMT plus H_4folate and free PvSHMT are clearly different, especially around 477 nm (Inset A of Fig. 4). The data were analyzed as described in Experimental Procedures to yield a K_d value of 0.35 ± 0.06 mM (Inset B of Fig. 4).

The binding experiment was also carried out using stopped-flow spectrophotometry under

anaerobic conditions to monitor the kinetics of PvSHMT and H_4folate binding. Due to the very small change in signal, reliable kinetic data could not be obtained (data not shown). Nonetheless, the final spectral changes and the K_d value of H_4folate binding (0.25 ± 0.13 mM) obtained from the stopped-flow experiment are similar to that from the static titration experiments (Inset B of Fig. 4). These data clearly indicate that L-serine and H_4folate can independently bind to PvSHMT and form a PvSHMT:L-serine or PvSHMT:H_4folate binary complex, suggesting that the kinetic mechanism of PvSHMT is a random-order type.

Single-turnover reaction of PvSHMT:L-serine binary complex and H_4folate–When a pre-equilibrated complex of PvSHMT (45 μM):L-serine (30 μM) was mixed with various concentrations of H_4folate (0.2-6.4 mM) and the absorbance was monitored at 496 nm, the reactions showed five kinetic phases (Fig. 5A). The first phase (0.004-0.07 s) was the phase with a large increase in absorbance at 496 nm, while the second phase (0.07-0.2 s) showed a small absorbance decrease, indicating the formation and decay of a quinonoid species, respectively. The third phase (0.2-0.6 s) was a small lag phase that had no significant absorbance change. The fourth phase (0.6-4.0 s) was the phase where the re-formation of a quinonoid species occurred. Interestingly, two different phenomena were observed for the fifth phase depending on the concentration of H_4folate. For the reaction carried out in the presence of 0.2-0.8 mM H_4folate, the fifth phase (4.0-300 s) was a slow decay of the quinonoid species, while for the reaction with 1.6-6.4 mM H_4folate, the intermediate was stabilized until 1000 s. The final spectra for the various concentrations of H_4folate were also recorded (data not shown).

All kinetic traces were analyzed as described in the Experimental Procedures and the observed rate constants (k_{obs}) of each phase were plotted against H_4folate concentrations. The plot in Fig. 5B showed that the k_{obs} of the first phase decreased upon increasing the concentration of H_4folate. This result may be explained according to a model in which an isomerization of the enzyme-L-serine complex exists and only one form of the complex reacts with H_4folate (23,25). This explanation agrees well with the results found in the previous section, showing that a binary complex of PvSHMT:L-serine can be isomerized into several forms of complexes. According to Equation 5, the forward and reverse rate constants for the enzyme isomerization were determined to be 17 ± 1 and 258 ± 180 s^{-1} 275 ± 180 s^{-1}, respectively (Fig. 5B). A decreasing trend upon increasing the H_4folate concentration gives a half-saturation value of 0.033 ± 0.025 mM (Fig. 5B). Observed rate constants of the second phase (~11 s^{-1}) and the third phase (~1 s^{-1}) were independent of H_4folate concentration (Fig. 5A). The third phase was later assigned as the formation of glycine (a dotted line with filled circles of Fig. 5A). The last two phases showed a decrease in k_{obs} upon increasing the H_4folate concentration. Based on the currently available data, the identities of the intermediates formed during the fourth and fifth phases cannot be unequivocally assigned. Since their rate constants (<0.3 s^{-1}) are significantly less than the k_{cat} value (1.09 ± 0.05 s^{-1}), these phases clearly are not relevant to the catalytic turnovers. They may belong to the binding of H_4folate to free PvSHMT or PvSHMT:glycine after product formation.

Detection of glycine product formation using rapid acid-quenched flow/HPLC-UV or HPLC-MS techniques–Although the stopped-flow experiments in the previous section showed the kinetics of quinonoid species formation, the data could not identify the step involved with glycine formation. Therefore, a rapid quench experiment was employed to elucidate the step that is involved in the C_α-C_β bond cleavage in L-serine to form glycine. A solution of PvSHMT (45 μM):L-serine (30 μM) binary complex was mixed with a low or high concentration of H_4folate (0.4 or 3.2 mM) using rapid acid-quenched flow-HPLC/UV or HPLC/MS analysis as described in Experimental Procedures. Glycine (retention time of 14.2 min) and serine (retention time of 15.2 min) were clearly identified and well separated in the HPLC/MS chromatograms (Inset of Fig. 6). Glycine concentrations measured from reactions quenched at different time points were plotted against age times (Fig. 6) and analyzed according to a single-exponential equation (Equation 6) as described in Experimental Procedure. The observed rate constants (k_{obs}) for glycine formation derived from reactions carried out at different H_4folate concentrations are similar, 1.02 ± 0.09 s^{-1} and 1.24 ± 0.14 s^{-1} for 0.4 and 3.2 mM H_4folate,

respectively. It was noted that the total amount of glycine product formed in the reaction with 3.2 mM H_4folate and detected by PITC derivatization was less than that produced from the reaction with 0.4 mM H_4folate (data not shown). This might be due to low efficiency of glycine derivatization when H_4folate is present in high amount.

In order to confirm if the rapid-quench experiment detected all glycine formed either in the free form or in the E:Gly:H_4folate complex, we measured the amount of glycine detected under the rapid-quench condition in both forms (data not shown). The results indicate that H_4folate does not have significant influence on the amount of glycine detected and that under the rapid-quench experiment detected all glycine formed.

When the rapid-quench results were compared to the kinetics of the stopped-flow experiments, the data indicated that the glycine formation phase can be correlated with a small lag period detected as the third phase (~0.2-0.6 s) in Fig. 5A. Furthermore, these k_{obs} values are similar to the catalytic rate constant (k_{cat}) of the PvSHMT reaction (1.09 ± 0.05 s^{-1}) measured from steady-state kinetics (Fig. 1). These results have therefore, for the first time, unambiguously identified the glycine product formation as the rate-limiting step of the H_4folate-dependent SHMT reaction.

Reaction of PvSHMT with L-serine and H_4folate under different mixing conditions–The binding studies revealed that PvSHMT can independently bind L-serine or H_4folate (Fig. 2 to Fig. 4), implying that the enzyme binds both substrates in random-order fashion. However, whether the random-order binding mechanism is relevant to the PvSHMT catalysis or whether the enzyme requires a specific pathway to form the product was not known. Three different types of stopped-flow mixing set-ups (see Experimental Procedures) were employed to pre-form different binary complexes and the absorbance was monitored at 496 nm to follow the formation of a quinonoid species. The appearance of quinonoid absorption was used as an indicative signal for detecting the ternary complex that was committed to catalysis (Fig. 5 and 7) because the quinonoid species has been proposed to be part of the SHMT catalytic cycle (1,2). The absorbance change at 435 nm was also monitored, but the signal change was too small to obtain reliable kinetic data.

Results from the first type of mixing set-up (mixing PvSHMT:L-serine with H_4folate, solid lines with filled circles in Fig. 7A and 7B) were similar to that shown in Fig. 5A discussed earlier, but different from the other two experiments. For the second experiment in which a solution of PvSHMT:H_4folate binary complex (0.4 and 3.2 mM, solid lines with filled rectangles in Fig. 7A and 7B, respectively) was mixed with L-serine, the reactions showed four phases in which all phases displayed an increase in absorbance. The first phase (0.005-0.2 s) of the reaction showed less amplitude change than that of the mixing of PvSHMT:L-serine with H_4folate. k_{obs} values of the reactions with 0.4 and 3.2 mM H_4folate are 11 and 6 s^{-1}, respectively. Although the kinetics of this phase is slower than the first kinetic phase from the mixing of PvSHMT:L-serine with H_4folate, these values are still significantly faster than the rate-limiting step of the reaction (~1 s^{-1}, Fig. 5A). The following kinetic phase (0.2-0.6 s) showed an increase in absorbance at 496 nm and is likely to be the glycine formation step that is the rate-limiting step in the overall reaction. The latter part of the reaction (2-1000 s) occurs much slower than the turnover number (~1 s^{-1}), and thus is not relevant to catalysis. For the third experiment in which the free enzyme was mixed with a solution of L-serine and 0.4 and 3.2 mM H_4folate (solid lines with filled triangles in Fig. 7A and 7B), k_{obs} values for quinonoid formation in the first phase (0.005-0.2 s) in the reactions of 0.4 and 3.2 mM H_4folate were 14.7 and 8 s^{-1}, respectively. The second phase of the reaction (0.2-0.6 s) showed an increase of absorbance; this step likely corresponds to the glycine formation step. Other phases following this step (2-1000 s) are slower than the catalytic turnover.

Although k_{obs} values for initial quinonoid formation in these three experiments are different, this step was faster than the glycine formation step (0.2-0.6 s) for all of the reaction setup conditions tested. Moreover, all reactions yielded similar amounts of product (see next section). Therefore, we conclude that all types of mixings can lead to a productive path for the SHMT reaction. As the mixing of free PvSHMT with a mixture of L-serine and H_4folate resulted in kinetics and amplitude changes that are different from the reactions of either preformed complexes, the data imply that when providing the two substrates

simultaneously, the free enzyme binds randomly to both substrates, agreeing with the data shown in Fig. 3 and Fig. 4. Based on this study, the overall reaction catalyzed by PvSHMT can be described by the scheme displayed in Fig. 8B.

Comparison of glycine generated from different reaction set ups –The amount of glycine generated from the three mixing reactions (Fig. 7) was analyzed using rapid-quench and LC-MS techniques. Samples at the reaction times of 10 s were collected and analyzed. Similar amounts of glycine product (~22 μM) were obtained from all types of mixing reactions (Table 1). Since the conditions employed only allow for a single turnover of the reactions to proceed, these data indicated that all mixing set-ups resulted in similar amount of product after the glycine formation step, suggesting that all mixing set-ups led to a productive pathway and the PvSHMT reaction occurs via a random-order mechanism (Fig. 8B).

Kinetic mechanism of PvSHMT–Based on currently available data, the reaction of PvSHMT can be summarized as shown in Fig. 8. PvSHMT binds to either L-serine or H_4folate as a first substrate. The binary complex then binds to another substrate and proceeds to form glycine. In principle, glycine or CH_2-H_4folate should also be released in random order. All data also imply that under steady-state enzyme turnovers in which L-serine is in excess, the glycine release is quick and the rate-limiting step is the glycine formation. However, in the presence of excess H_4folate such as in Figs. 5 and 7, once glycine forms, it is trapped in the form of the enzyme:Gly:H_4folate complex as noted by high absorbance at 496 nm (Fig. 8B).

DISCUSSION

Our investigation based on transient kinetics, thermodynamics and steady-state kinetics provides insight into the reaction mechanism of PvSHMT and has identified glycine formation as the rate-limiting step of this enzyme reaction. Direct binding experiments under anaerobic conditions has shown for the first time that the free enzyme can independently bind to H_4folate and that the reaction of PvSHMT obeys a random-order mechanism in which the enzyme can bind either to L-serine or H_4folate as the first substrate (Fig. 8B).

Using rapid-quench and HPLC/UV/MS experiments, the rate constant of glycine formation was measured as ~1 s^{-1} which is similar to the k_{cat} value of the PvSHMT reaction obtained from steady-state kinetics under the same condition. The data indicate that the C_α-C_β bond cleavage of L-serine to result in glycine formation is the rate-limiting step for the physiological H_4folate-dependent reaction of PvSHMT. Recently, quantum mechanics calculation of H_4folate-independent retro-aldol cleavage of *β*-hydroxyamino acids via the *β*-hydroxyl proton abstraction based on the structure of *Bacillus stearothermophilus* (bs) SHMT in complex with L-*allo*-threonine suggests that the rate-limiting step for the aldolase activity of bsSHMT reaction is also the C_α-C_β bond cleavage (26). Since the formation of E:L-serine:H_4folate ternary complex (evidenced by formation of a quinonoid intermediate, Figs. 5 and 7) occurs before the glycine formation step (Fig. 7), it implies that the presence of H_4folate is required for the C-C bond breakage. These results agree with the findings of our previous investigation that free formaldehyde could not be detected in the absence of H_4folate (5). The results here also support the mechanism suggested (2,18), which proposes that the binding of H_4folate may cause a conformational change that facilitates the glycine product formation.

Transient kinetics and direct binding experiments suggest that PvSHMT binds L-serine and H_4folate via a random-order mechanism because the enzyme can bind to each ligand independently. The K_d value for the H_4folate binding is 0.35 ± 0.06 mM (Fig. 4), while a K_d value for L-serine binding relevant to catalysis is 0.18 ± 0.08 mM (Fig. 8A). A key experimental setup that allowed us to directly observe the binary complex of PvSHMT:H_4folate for the first time was conducting the reaction under anaerobic conditions. As H_4folate can be readily oxidized, resulting in an absorbance increase at the 330-360 nm regions (5,27,28), it is impossible to aerobically monitor the interaction of H_4folate and protein interaction without any background interference. Previously, most of the binding studies of SHMT and H_4folate were only monitored in the presence of amino acid substrates, especially in the presence of glycine, for which an intense band of quinonoid signal could be observed (29-31). Different mixing set-ups–in which either PvSHMT:L-serine or

PvSHMT:H_4folate was preformed–resulted in the same amount of glycine product at the end of a single turnover, supporting the conclusion that both paths of ligand binding lead to the productive pathway (Fig. 8B). The previous study of the rabbit cytosolic SHMT using equilibrium isotope-exchange of L-serine and CH_2-H_4folate also showed that the rate of isotope exchange under equilibrium conditions was not affected by increasing glycine concentrations, implying that the ordered preference for dissociation of both products, glycine and CH_2-H_4folate, is not required (17). All results support that the kinetic mechanism of PvSHMT conforms to a random order model (Fig. 8B).

The binding of PvSHMT and L-serine is complicated and a multi-step process in which the PvSHMT:L-serine complex is in equilibrium of several forms (Fig. 8A). After the initial binding to form a Michaelis complex of PvSHMT:L-serine, the complex must proceed to form the gem-diamine and then the external aldimine complex. When the preformed PvSHMT-L-serine was mixed with various concentrations of H_4folate, the k_{obs} was decreased. These data suggest that the isomerization step preceding the bi-molecular reaction with H_4folate exists. Based on our current data, we cannot distinguish if this isomerization step is caused by the enzyme conformational change or the equilibrium of gem-diamine and external aldimine complexes. In the presence of H_4folate, it is possible that a PvSHMT:H_4folate complex can readily bind and facilitate the formation of the external aldimine complex.

The random-order binding mechanism of PvSHMT implies that each ligand binds to the enzyme via separate binding pockets and that access to each pocket is independent. Currently, there are seven X-ray structures of SHMT ternary complexes with amino acid and folate analogues ((PDB # 1EQB) (32), (PDB # 1DFO) (33), (PDB # 1KL2) (34), (PDB # 2VGW) (35), (PDB # 2W7H and PDB # 2W7M) (36), (PDB # 2VMS) (37)) including the recently published structure of PvSHMT in complex with D-serine and H_4folate analogue (6*R*-5-CHO-H_4folate) at 2.4 Å resolution (PDB # 4OYT) (38) (Fig. 9). The crystal structure reveals defined binding pockets for amino acid and folate that could support the independent binding of each substrate via a random-order mechanism as proposed (Fig. 8B).

In conclusion, we have shown for the first time direct evidence supporting that the kinetic mechanism of PvSHMT occurs via a random-order model and that glycine formation is the rate-limiting step of SHMT. This information will serve as a basis for future investigation for other SHMTs. The comparative studies of SHMTs from parasite and host will pave the way for the design of species-specific inhibitors for antimalarial drug development.

REFERENCES

1. Schirch, V. (1982) Serine hydroxymethyltransferase. In Meister, A., editor. *Adv. Enzymol. Relat. Areas Mol. Biol*. John Wiley & Sons, Inc., NY. **53**, 83-112
2. Schirch, V., and Szebenyi, D. M. E. (2005) Serine hydroxymethyltransferase revisited. *Curr. Opin. Chem. Biol.* **9**, 482-487
3. Kappes, B., Tews, I., Binter, A., and Macheroux, P. (2011) PLP-dependent enzymes as potential drug targets for protozoan diseases. *Biochim. Biophys. Acta.* **1814**, 1567-1576
4. Schirch, L. V. (1984) Folates in serine and glycine metabolism. In Blakely, R. L., and Benkovic, S. J., Eds. *Folates and Pterins*. Wiley, NY. **1**, 399-431
5. Sopitthummakhun, K., Maenpuen, S., Yuthavong, Y., Leartsakulpanich, U., and Chaiyen, P. (2009) Serine hydroxymethyltransferase from *Plasmodium vivax* is different in substrate specificity from its homologues. *FEBS J*. **276**, 4023-4036
6. Toney, M. D. (2011) Controlling reaction specificity in pyridoxal phosphate enzymes. *Biochim. Biophys. Acta*. **1814**, 1407-1418
7. Angellaccio, S. (2013) Extremophilic SHMTs: from structure to biotechnology. *BioMed. Res. Int.* **2013**, 1-10
8. Matthews, R. G., and Drummond, J. T. (1990) Providing one-carbon units for biological methylations: mechanistic studies on serine hydroxymethyltransferase, methylenetetrahydrofolate reductase, and methyltetrahydrofolate-homocysteine methyltrasferase. *Chem. Rev*. **90**, 1275-1290
9. Schirch, V. (1998) Mechanism of folate requiring enzymes in one-carbon metabolism. In Sinnott, M., editor. *Comprehensive Biological Catalysis: A mechanistic reference*. Academic Press Limited, 223-224
10. Florio, R., di Salvo, M. L., Vivoli, M., and Contestabile, R. (2011) Serine hydroxymethyltransferase: a model enzyme for mechanistic, structural, and evolutionary studies. *Biochim. Biophys. Acta.* **1814**, 1489-1496
11. Pornthanakasem, W., Kongkasuriyachai, D., Uthaipibull, C., Yuthavong, Y., and Leartsakulpanich, U. (2012) *Plasmodium* serine hydroxymethyltransferase: indispensability and display of distinct localization. *Malar. J.* **11**, 387-395.
12. Maenpuen, S., Sopitthummakhun, K., Yuthavong, Y., Chaiyen, P., and Leartsakulpanich, U. (2009) Characterization of *Plasmodium falciparum* serine hydroxymethyltransferase-a potential antimalarial target. *Mol. Biochem. Parasitol*. **168**, 63-73
13. Pang, C. K. T, Hunter, J. H., Gujjar, R., Podutoori, R., Bowman, J., Mudeppa, D. G., and Rathod, P. K. (2009) Catalytic and ligand-binding characteristics of *Plasmodium falciparum* serine hydroxymethyltransferase. *Mol. Biochem. Parasitol*. **168**, 74-83
14. Sopitthummakhun, K., Thongpanchang, C., Vilaivan, T., Yuthavong, Y., Chaiyen, P., and Leartsakulpanich, U. (2012) *Plasmodium* serine hydroxymethyltransferase as a potential anti-malarial target: inhibition studies using improved methods for enzyme production and assay. *Malar. J*. **11**, 194-205
15. Chitnumsub, P., Ittarat, W., Jaruwat, A., Noytanom, K., Amornwatcharapong, W., Pornthanakasem, W., Chaiyen, P., Yuthavong, Y., and Leartsakulpanich, U. (2014) The structure of *Plasmodium falciparum* serine hydroxymethyltransferase reveals a novel redox switch that regulates its activities. *Acta Crystallogr. D Biol. Crystallogr.* **70**, 1517-1527
16. Pinthong, C., Maenpuen, S., Amornwatcharapong, W., Yuthavong, Y., Leartsakulpanich, U., and Chaiyen, P. (2014) Distinct biochemical properties of human serine hydroxymethyltransferase compared with the *Plasmodium* enzyme: implications for selective inhibition. *FEBS J.* **281**, 2570-2583
17. Schirch, L. V., Tatum, C. M., and Benkovic, S. J. (1977) Serine transhydroxymethylase: evidence for a sequential random mechanism. *Biochemistry* **16**, 410-419

18. Szebenyi, D. M., Musayev, F. N., di Salvo, M. L., Safo, M. K., and Schirch, V. (2004) Serine hydroxymethyltransferase: role of Glu75 and evidence that serine is cleaved by a retroaldol mechanism. *Biochemistry* **43**, 6865-6876
19. Rosenthal, S., Smith, L. C., and Buchanan, J. M. (1965) Enzymatic synthesis of the methyl group of methionine: IX. Transmethylation from S-adenosylmethionine and 5-methyltetrahydrofolate to 2-mercaptoethanol and homocysteine. *J. Biol. Chem.* **240**, 836-843
20. Scrimgeour, K. G. (1980) Methods for reduction, stabilization, and analyses of folates. In McCowick, D. B., and Wright, L. D., editors. *Methods. Enzymol*. Academic Press, NY. **66**, 517-523
21. Matthews, R. G., Ross, J., Baugh, C. M., Cook, J. D., and Davis, L. (1982) Interactions of pig liver serine hydroxymethyltransferase with methyltetrahydropteroylpolyglutamate inhibitors and with tetrahydropteroylpolyglutamate substrates. *Biochemistry* **21**, 1230-1238
22. Trimmer, E. E., Ballou, D. P., and Matthews, R. G. (2001) Methylenetetrahydrofolate reductase from *Escherichia coli*: elucidation of the kinetic mechanism by steady-state and rapid-reaction studies. *Biochemistry* **40**, 6205-6215
23. Vogt, A. D., and di Cera, E. (2012) Conformational selection or induced fit? A critical appraisal of the kinetic mechanism. *Biochemistry* **51**, 5894-5902
24. Harris, E. L. V. (1988) Amino acid analysis by precolumn derivatization. In Walker, J. M., editor. *Methods Mol. Biol*. Humana Press, Clifton, NJ. **3**, 33-47
25. Hiromi, K. (1979) Kinetics of fast enzyme reactions: theory and practice. Halsted Press, NY.
26. Chiba, Y., Terada, T., Kameya, M., Shimizu, K., Arai, H., Ishii, M., and Igarashi, Y. (2012) Mechanism for folate-independent aldolase reaction catalyzed by serine hydroxymethyltransferase. *FEBS J*. **279**, 504-514
27. Wahba, A. J., and Friedkin, M. (1961) Direct spectrophotometric evidence for the oxidation of tetrahydrofolate during the enzymatic synthesis of thymidylate. *J. Biol Chem.* **236**, 11-12
28. Dawson, R. M. C., Elliot, D. C., Elliot, W. H., and Jones, K. M. (1986) Data for biochemical research. 3rd Ed., Oxford University Press, NY.
29. Schirch, L. V., and Jenkins, W. T. (1964) Serine transhydroxymethylase: properties of the enzyme-substrate complexes of D-alanine and glycine. *J. Biol. Chem.* **239**, 3801-3807
30. Schirch, L. V., and Peterson, D. (1980) Purification and properties of mitochondrial serine hydroxymethyltransferase. *J. Biol. Chem.* **255**, 7801-7806
31. Strong, W. B., Cook, R., and Schirch, V. (1989) Interaction of tetrahydropteroylpolyglutamates with two enzymes from mitochondria. *Biochemistry* **28**, 106-114
32. Contestabile, R., Angelaccio, S., Bossa, F., Wright, H. T., Scarsdale, N., Kazanina, G., and Schirch, V. (2000) Role of tyrosine 65 in the mechanism of serine hydroxymethyltransferase. *Biochemistry* **39**, 7492-7500
33. Scarsdale, J. N., Radaev, S., Kazanina, G., Schirch, V., and Wright, H. T. (2000) Crystal structure at 2.4 Å resolution of *E. coli* serine hydroxymethyltransferase in complex with glycine substrate and 5-formyl tetrahydrofolate. *J. Mol. Biol.* **296**, 155-168
34. Trivedi, V., Gupta, A., Jala, V. R., Saravanan, P., Rao, G. S., Rao, N. A., Savithri, H. S., and Subramanya, H. S. (2002) Crystal structure of binary and ternary complexes of serine hydroxymethyltransferase from *Bacillus stearothermophilus*: insights into the catalytic mechanism. *J. Biol. Chem.* **277**, 17161-17169
35. Rajaram, V., Bhavani, B. S., Kaul, P., Prakash, V., Appaji, R. N., Savithri, H. S., and Murthy, M. R.N. (2007) Structure determination and biochemical studies on *Bacillus stearothermophilus* E53Q serine hydroxymethyltransferase and its complexes provide insights on function and enzyme memory. *FEBS J.* **274**, 4148-4160
36. Bhavani, B. S., Rajaram, V., Bisht, S., Kaul, P., Prakash, V., Murthy, M. R. N., Appaji, R. N., and Savithri, H. S. (2008) Importance of tyrosine residues of *Bacillus stearothermophilus* serine hydroxymethyltransferase in cofactor binding and L-*allo*-threonine cleavage. *FEBS J.* **275**, 4606-4619

37. Pai, V. R., Rajaram, V., Bisht, S., Bhavani, B. S., Rao, N. A., Murthy, M. R. N., and Savithri, H. S. (2009) Structural and functional studies of *Bacillus stearothermophilus* serine hydroxymethyltransferase: the role of Asn (341), Tyr (60) and Phe (351) in tetrahydrofolate binding. *Biochem. J.* **418**, 635-642
38. Chitnumsub, P., Jaruwat, A., Riangrungroj, P., Ittarat, W., Noytanom, K., Oonanant, W., Vanichthanankul, J., Chuankhayan, P., Maenpuen, S., Chen, C. J., Chaiyen, P., Yuthavong, Y., and Leartsakulpanich, U. (2014) Structures of *Plasmodium vivax* serine hydroxymethyltrasnferase with implications on enzyme activity and functional control. *Acta Crystallogr. D Biol. Crystallogr.* **70**, 3177-3186

Acknowledgements–We thank Prof. David P. Ballou for valuable suggestions and Merck Eprova AG (Schafhausen Switzerland) for providing high quality folate compounds.

FOOTNOTES

*This work was supported by grants from Cluster and Program Management office, NSTDA (P-13-00835) to UL, PC and PCC, and The Thailand Research Fund (RTA5680001) and the Faculty of Science, Mahidol University (to PC) and The Thailand Research Fund (MRG5580066) and the Faculty of Science, Burapha University (to SM).

[1]To whom correspondence may be addressed: Department of Biochemistry and Center of Excellence in Protein Structure and Function, Faculty of Science, Mahidol University, Bangkok, 10400, Thailand, Tel.: (66) 2201-5607; Fax: (66) 2354-7174; Email: pimchai.cha@mahidol.ac.th

[2]National Center for Genetic Engineering and Biotechnology, National Science and Technology Development Agency, Pathumthani, 1212 Thailand, Tel.: (66) 256-46700 ext 3483; Fax: (66) 256-46707; Email: ubolsree@biotec.or.th

[3]The abbreviations used are: SHMT, serine hydroxymethyltransferase; H_4folate, tetrahydrofolate; CH_2-H_4folate, methylenetetrahydrofolate; CH^+-H_4folate, methenyltetrahydrofolate; CHO-H_4folate, formyltetrahydrofolate; PLP, pyridoxal 5'-phosphate; EQ, enzyme-quinonoid complex; RQF, rapid-quench flow; MTHFR, methylenetetrahydrofolate reductase

TABLE LEGENDS

TABLE 1. Amount of glycine resulting from three types of mixing experiments analyzed by rapid-quench and HPLC-MS techniques.

FIGURE LEGENDS

FIGURE 1. A double-reciprocal plot of bi-substrate kinetics of PvSHMT at pH 8.0. A solution of PvSHMT (1 μM) and His_6-tagged MTHFR (3 μM) was mixed with solutions of NADH (100 μM), L-serine (0.2, 0.4, 0.8, 1.6 and 6.4 mM) and H_4folate (0.025 (filled circles), 0.5 (filled squares), 0.1 (filled diamonds), 0.2 (empty circle), and 0.4 mM (empty squares)) at 25 ^oC and pH 8.0 under anaerobic conditions using a stopped-flow spectrophotometer. The plot of e/v and 1/L-serine shows a series of convergent lines indicating ternary complex kinetics. Symbols are represented for reciprocal initial velocities at given concentrations of both substrates. Insets are the secondary plots of slopes (A) and ordinate intercepts (B) of the primary plot as a function of 1/H_4folate. The data analysis yielded the kinetic parameters as K_m for L-serine = 0.26 ± 0.04 mM, K_m for H_4folate = 0.11 ± 0.01 mM, and the turnover number (k_{cat}) = 1.09 ± 0.05 s^{-1}.

FIGURE 2. Difference spectra for the binding of PvSHMT with various concentrations of L-serine at pH 8.0. The sample cuvette contained a solution of PvSHMT (~31 μM) in 50 mM HEPES, pH 8.0 containing 0.5 mM EDTA and 1 mM DTT and various concentrations of L-serine (0.16-145 mM, lower to upper spectra) while the reference cuvette contained only the enzyme solution and buffer. A difference spectrum was recorded after each addition. Inset shows the determination of K_d for the binding of L-serine as 2.2 ± 0.5 mM.

FIGURE 3. Transient kinetics for the binding of PvSHMT with L-serine determined by stopped-flow spectrophotometry. A solution of PvSHMT (~31 μM) was mixed with various concentrations of L-serine (0.4-12.8 mM from lower to upper traces) and the change in absorbance was monitored at 435 nm. The results indicate the formation of an external aldimine complex with L-serine. The kinetic traces show three phases. Observed rate constants of the first phase were hyperbolically dependent on L-serine concentrations with the L-serine concentration that gives the half-saturation value (K_S) of 0.86 ± 0.16 mM

and the maximum rate constant of 0.38 ± 0.02 s^{-1} (Inset). While observed rate constants of the second and third phases are not involved with catalytic reaction because they are much lower than the k_{cat} value.

FIGURE 4. Binding of PvSHMT with H_4folate. A solution of PvSHMT (~47 μM) was mixed with various concentrations of H_4folate (0.050-2.954 mM from lower to upper spectra) under anaerobic conditions. The free enzyme spectrum was subtracted from the spectra obtained after each titration to obtain difference spectra (Inset A). The increase of absorbance around 477 nm indicates the ability of PvSHMT to bind H_4folate. Based on the plot of absorbance changes at 477 nm *versus* H_4folate concentrations, the K_d values obtained from both measurements using conventional and stopped-flow spectrophotometry were determined as 0.35 ± 0.06 (filled circles) and 0.25 ± 0.13 mM (filled rectangles), respectively (Inset B).

FIGURE 5. Single-turnover reaction of PvSHMT:L-serine binary complex with H_4folate. A solution of the PvSHMT-L-serine complex (45 μM PvSHMT and 30 μM L-serine) was mixed with various concentrations of H_4folate (0.2, 0.4, 0.8, 1.6, 3.2, and 6.4 mM from lower to upper traces) under anaerobic conditions using a stopped-flow spectrophotometer. The kinetic traces monitored at 496 nm showed five phases (solid line) (A). The first phase (0.004-0.07 s) was a large increase of absorbance 496 nm and the k_{obs} values were decreased upon the increasing concentration of H_4folate (B). The second and the third phases are independent of H_4folate concentrations. Based on rapid-quench data, the third phase (~1 s^{-1}) is the formation of glycine (dashed line with filled circles in (A)).

FIGURE 6. Detection and kinetic analysis of glycine product formation using rapid acid-quenched flow/HPLC-UV or HPLC-MS technique. A pre-mixed solution of PvSHMT (45 μM) and L-serine (30 μM) was mixed with H_4folate (0.4 mM) under anaerobic conditions using a rapid-quench flow apparatus in an anaerobic glove box and the glycine product formed was quantified by HPLC/UV or HPLC/MS. The plot shows the amount of glycine formed at various times. (Inset) HPLC/MS chromatograms of glycine (retention time of 14.2 min) and serine (retention time of 15.2 min), respectively.

FIGURE 7. Comparison of kinetic traces for the reaction of PvSHMT with L-serine and H_4folate under three different types of mixings. The first experiment (solid lines with filled circles) is a mixing of preformed binary complex of PvSHMT (45 μM):L-serine (30 μM) with 0.4 (A) and 3.2 (B) mM H_4folate. The second experiment (solid lines with filled rectangles) is a mixing of preformed binary complex of PvSHMT (45 μM) and 0.4 (A) or 3.2 (B) mM H_4folate with L-serine (30 μM). The third experiment (solid lines with filled triangles) is a mixing of free PvSHMT with mixtures of L-serine (30 μM) and 0.4 (A) or 3.2 (B) mM H_4folate. All reactions were monitored by the absorption changes at 496 nm using the stopped-flow spectrophotometer in single-mixing mode.

FIGURE 8. A proposed model for the PvSHMT reaction. (A) Binding of L-serine to PvSHMT is a multi-step process. An initial Michaelis complex of PvSHMT and L-serine (a) is isomerized and transformed to a gem-diamine intermediate and subsequently external aldimine complex (b-d). (B) A random-order model describing the overall reaction of PvSHMT mechanism. PvSHMT binds randomly either to L-serine or H_4folate to form an active E:Ser or E:H_4folate binary complex. The binding of enzyme and L-serine is a multi-step process as described in A. Only a relevant form of the external aldimine complex can bind to H_4folate to form the ternary complex of E:Ser:H_4folate. Glycine is generated with a rate constant of 1 s^{-1}. Both products are randomly released. The current data suggest that, in the presence of high concentration of H_4folate, the E:Gly complex can be trapped in the dead-end E:Gly:H_4folate complex.

FIGURE 9. Crystal structure of the homodimeric PvSHMT in complex with D-serine and formyltetrahydrofoalte (6*R*-5-CHO-H_4folate) (PDB # 4OYT) shows two individual pockets on the surface representative for serine (yellow) and folate (white) (38).

Table 1

Mixing conditions	Glycine (μM)
E + Ser *vs.* H_4folate (0.4 mM)	18 ± 3
E + Ser *vs.* H_4folate (3.2 mM)	21 ± 3
E + H_4folate (0.4 mM) *vs.* Ser	22 ± 4
E + H_4folate (3.2 mM) *vs.* Ser	22 ± 2
E *vs.* Ser + H_4folate (0.4 mM)	12 ± 3
E *vs.* Ser + H_4folate (3.2 mM)	22 ± 8

Figure 1

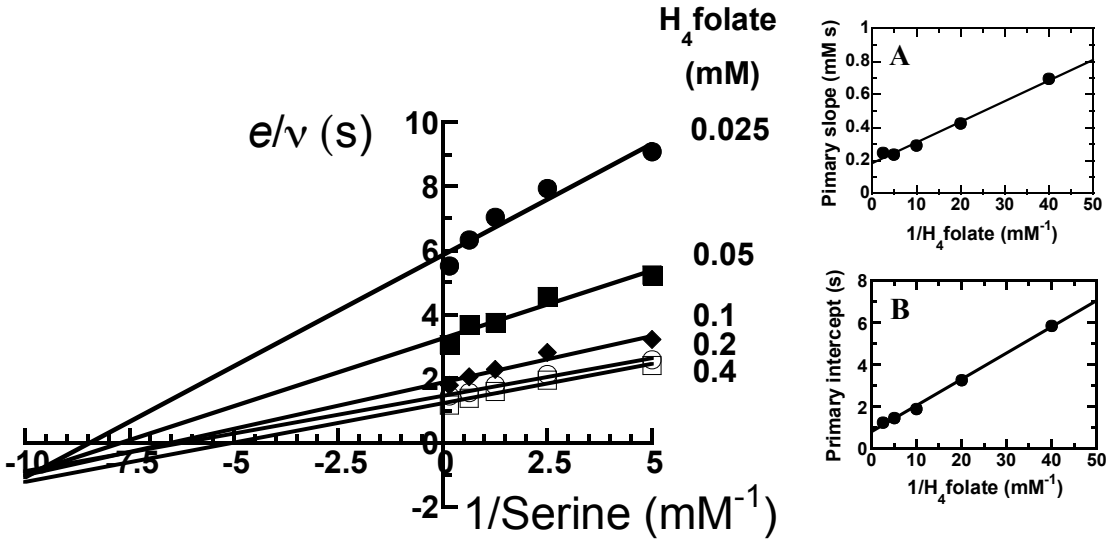

Figure 2

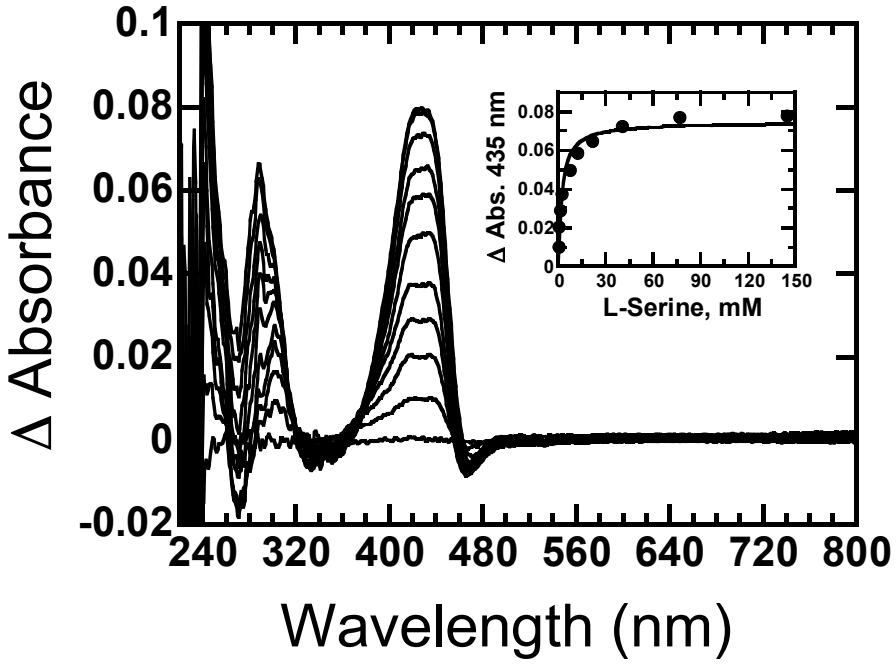

Figure 3

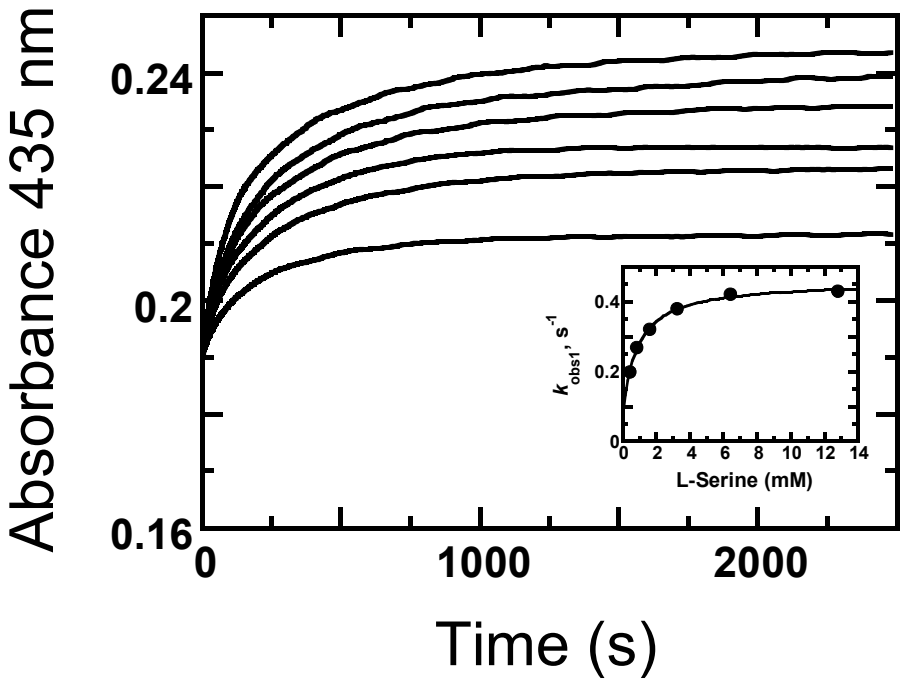

Figure 4

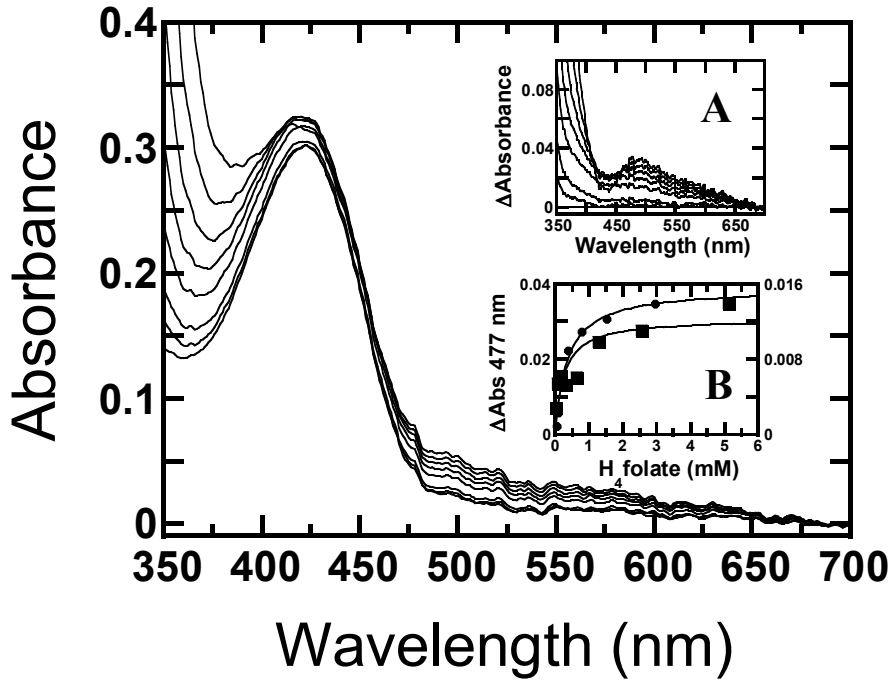

Figure 5

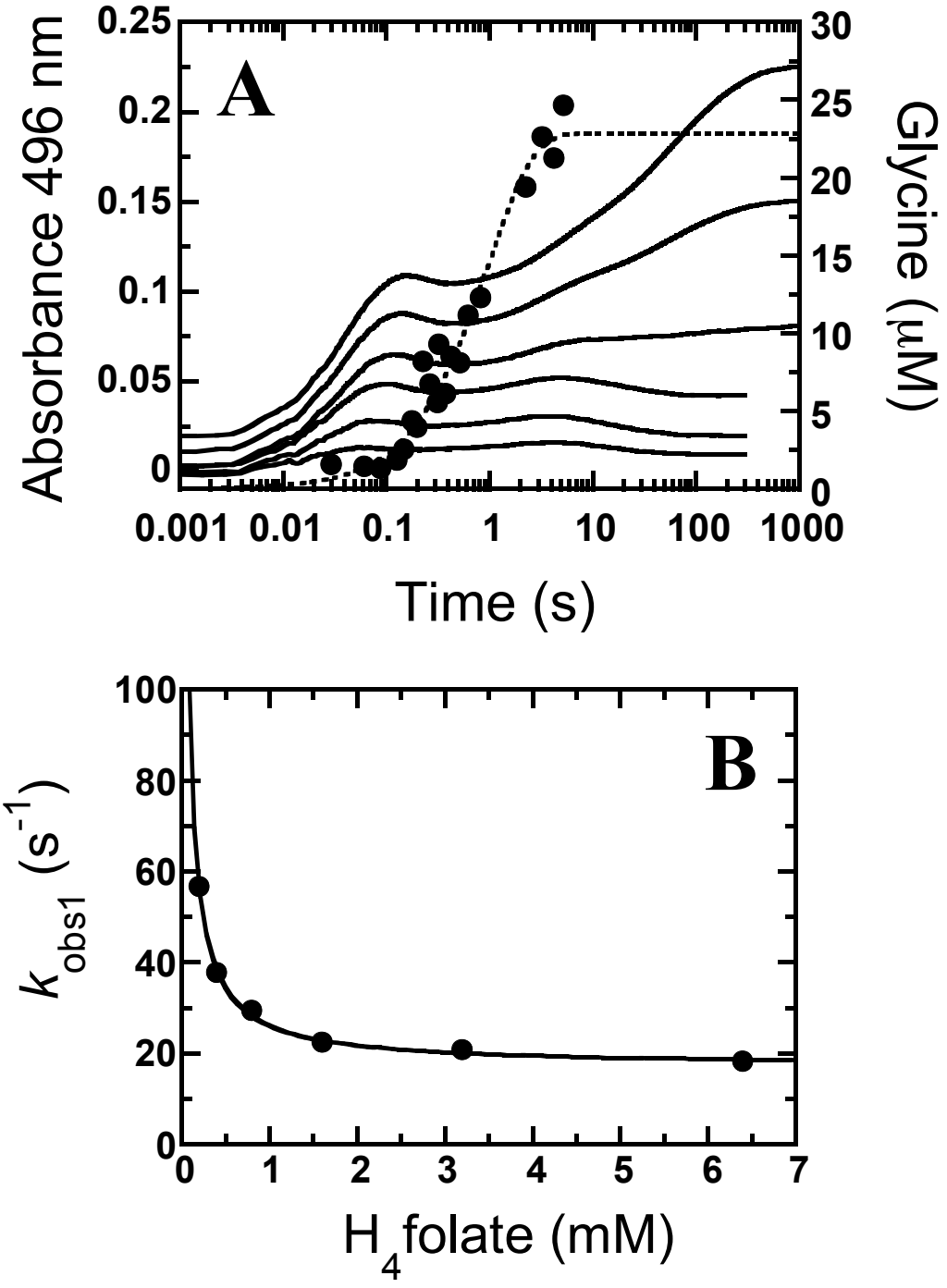

Figure 6

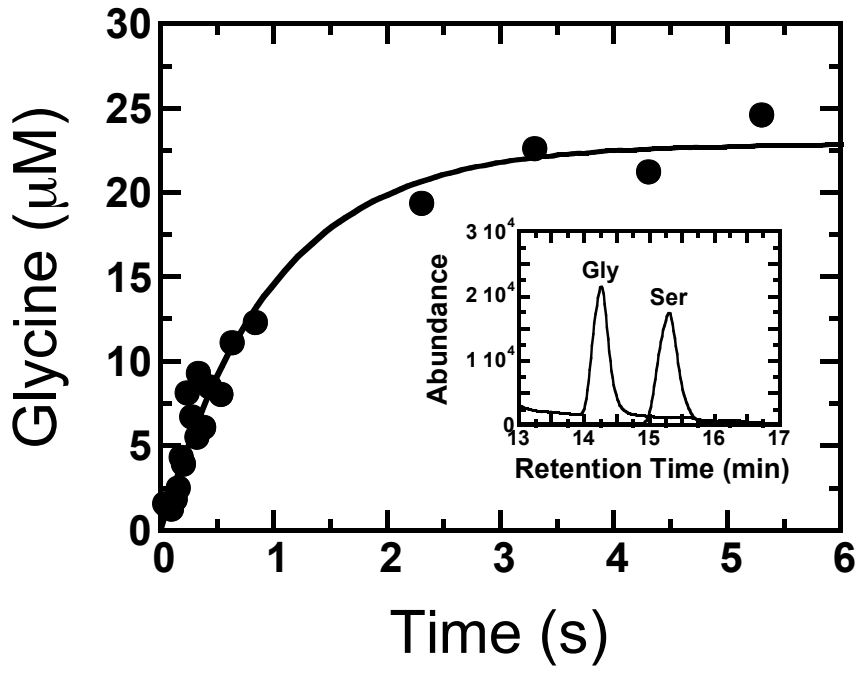

Figure 7

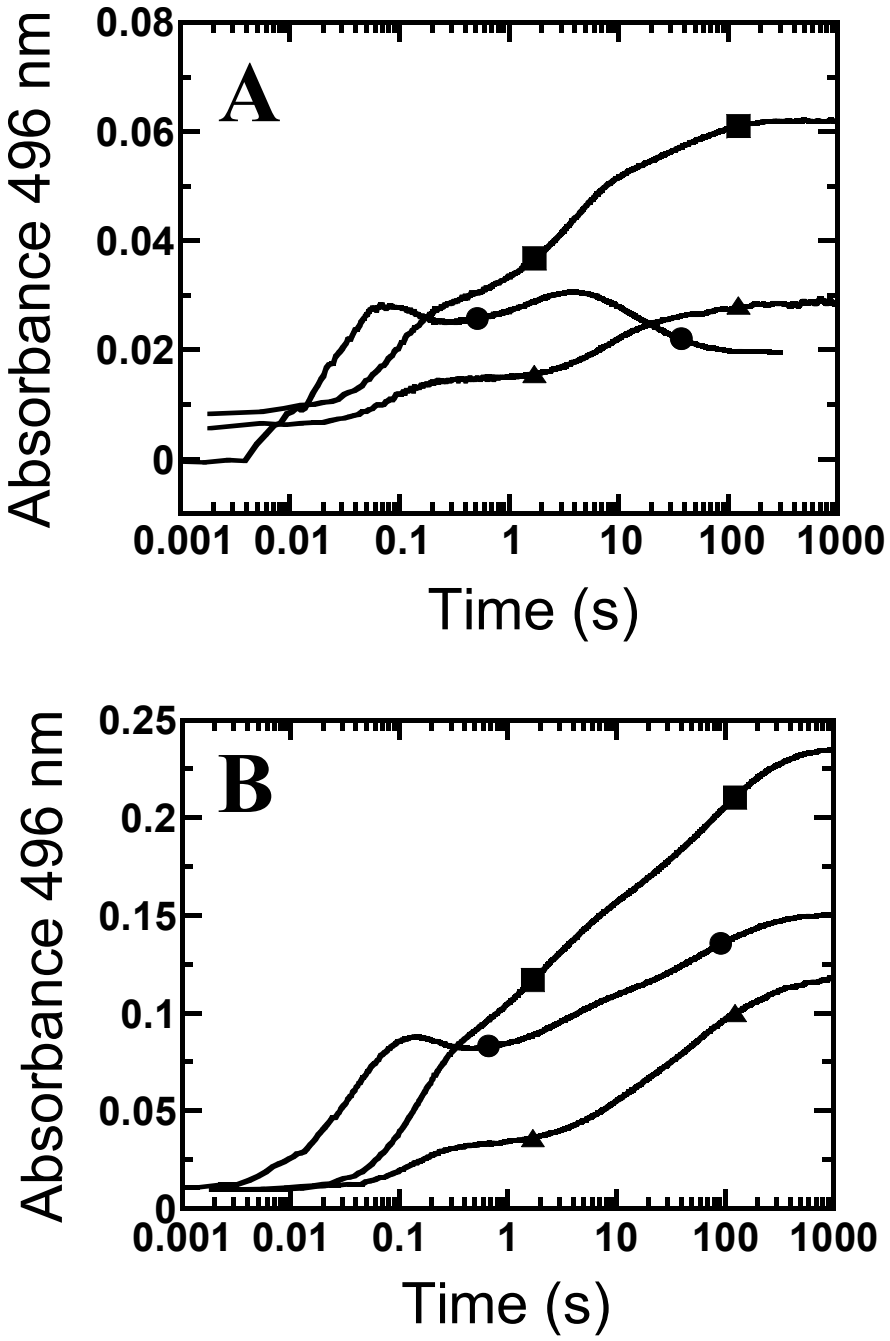

Figure 8

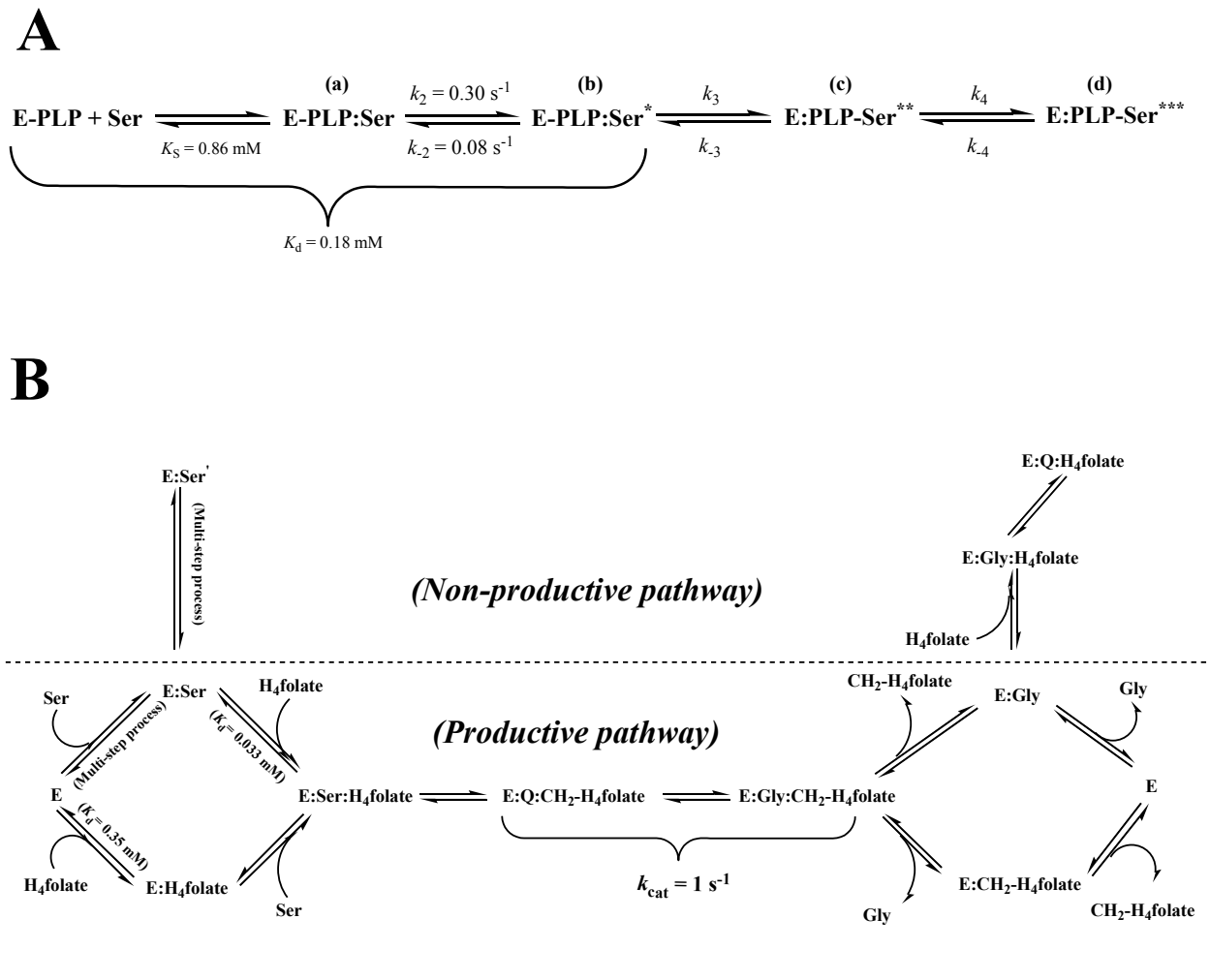

Figure 9

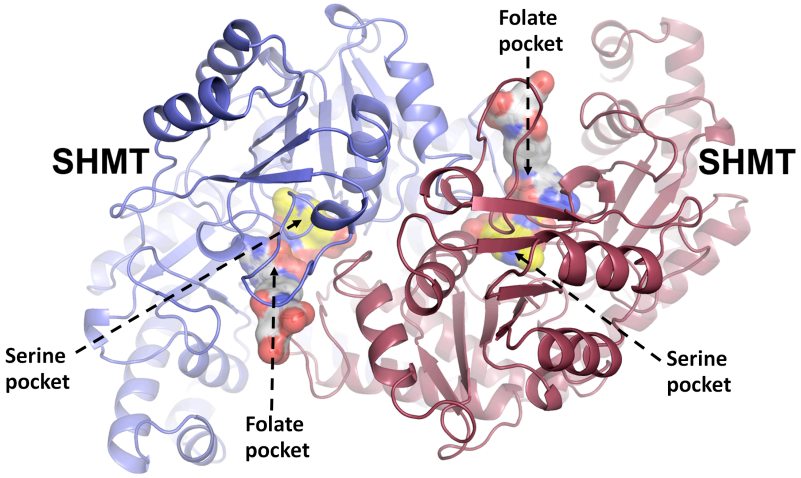

the FEBS Journal

Distinct biochemical properties of human serine hydroxymethyltransferase compared with the *Plasmodium* enzyme: implications for selective inhibition

Chatchadaporn Pinthong[1], Somchart Maenpuen[2], Watcharee Amornwatcharapong[1], Yongyuth Yuthavong[3], Ubolsree Leartsakulpanich[3] and Pimchai Chaiyen[1]

1 Department of Biochemistry and Center of Excellence in Protein Structure and Function, Mahidol University, Bangkok, Thailand
2 Department of Biochemistry, Burapha University, Chonburi, Thailand
3 National Center for Genetic Engineering and Biotechnology, National Science and Technology Development Agency, Pathumthani, Thailand

Keywords
dTMP cycle; folate metabolism; PLP-dependent enzyme; pyridoxal-5′-phosphate; serine hydroxymethyltransferase

Correspondence
P. Chaiyen, Department of Biochemistry and Center of Excellence in Protein Structure and Function, Faculty of Science, Mahidol University, Rama 6 Road, Bangkok 10400, Thailand
Fax: +6623547174
Tel: +6622015596
E-mail: pimchai.cha@mahidol.ac.th
U. Leartsakulpanich, National Center for Genetic Engineering and Biotechnology, National Science and Technology Development Agency, 113 Paholyothin Road, Pathumthani 12120, Thailand
Fax: +6625646707
Tel: +6625646700 ext 3487
E-mail: ubolsree@biotec.or.th

(Received 17 December 2013, revised 25 March 2014, accepted 31 March 2014)

doi:10.1111/febs.12803

Serine hydroxymethyltransferase (SHMT) catalyzes the transfer of a hydroxymethyl group from L-serine to tetrahydrofolate to yield glycine and 5,10-methylenetetrahydrofolate. Our previous investigations have shown that SHMTs from *Plasmodium* spp. (*P. falciparum*, Pf; *P. vivax*, Pv) are different from the enzyme from rabbit liver in that *Plasmodium* SHMT can use D-serine as a substrate. In this report, the biochemical and biophysical properties of the *Plasmodium* and the human cytosolic form (hcSHMT) enzymes including ligand binding and kinetics were investigated. The data indicate that, similar to *Plasmodium* enzymes, hcSHMT can use D-serine as a substrate. However, hcSHMT displays many properties that are different from those of the *Plasmodium* enzymes. The molar absorption coefficient of hcSHMT-bound pyridoxal-5′-phosphate (PLP) is much greater than PvSHMT-bound or PfSHMT-bound PLP. The binding interactions of hcSHMT and *Plasmodium* SHMT with D-serine are different, as only the *Plasmodium* enzyme undergoes formation of a quinonoid-like species upon binding to D-serine. Furthermore, it has been noted that hcSHMT displays strong substrate inhibition by tetrahydrofolate (THF) (at THF > 40 μM), compared with SHMTs from *Plasmodium* and other species. The pH–activity profile of hcSHMT shows higher activities at lower pH values corresponding to a pK_a value of 7.8 ± 0.1. Thiosemicarbazide reacts with hcSHMT following a one-step model [k_1 of 12 ± 0.6 $M^{-1}{\cdot}s^{-1}$ and k_{-1} of (1.0 ± 0.6) × 10^{-3} s^{-1}], while the same reaction with PfSHMT involves at least three steps. All data indicated that the ligand binding environment of SHMT from human and *Plasmodium* are different, indicating that it should be possible to develop species-selective inhibitors in future studies.

Database
serine hydroxymethyltransferase, EC 2.1.2.1; 5,10-methylenetetrahydrofolate dehydrogenase, EC 1.5.1.5

Abbreviations
DTT, dithiothreitol; GdnHCl, guanidine hydrochloride; hc, human cytosolic; hm, human mitochondrial; MTHFD, 5,10-methylenetetrahydrofolate dehydrogenase; Pf, *Plasmodium falciparum*; PLP, pyridoxal-5′-phosphate; Pv, *P. vivax*; SHMT, serine hydroxymethyltransferase; THF, tetrahydrofolate; TSCB, thiosemicarbazide.

Introduction

Serine hydroxymethyltransferase (SHMT, EC 2.1.2.1) is one of the three enzymes involved in the thymidylate synthesis cycle. It is an attractive target for anti-cancer and anti-malarial drug development due to its important role in DNA synthesis for cell replication in both human and *Plasmodium* spp. (*P. falciparum*, Pf; *P. vivax*, Pv) [1–4]. SHMT catalyzes the transfer of a hydroxymethyl group from L-serine to tetrahydrofolate (THF) to yield glycine and 5,10-methylenetetrahydrofolate (5,10-CH_2-THF). Two isoforms – cytosolic (c) and mitochondrial (m) enzymes – have been found in many organisms, including human (h) and *Plasmodium* parasites. Besides SHMT, two other enzymes, dihydrofolate reducase (DHFR) and thymidylate synthase (TS), are also required to complete a one-carbon redox balance of this thymidylate cycle [5]. Structure–function properties of DHFR and TS have been extensively studied as they are critical for the development of new effective anti-cancer and anti-malarial agents which are much needed due to the resistance towards current clinical drugs [5–10]. In addition to DHFR and TS, results from several investigations indicate that hcSHMT is a potential target for cancer treatment [11,12]. For malaria parasites, a molecular biological study of *Plasmodium* SHMT indicates that the enzyme is essential for parasite viability [4].

SHMT contains pyridoxal-5′-phosphate (PLP) as a cofactor and belongs to the α class of PLP-dependent enzymes [13,14]. It can catalyze a wide range of reactions and has a broad range of substrate specificity [14,15]. SHMTs from many sources such as sheep and rabbit liver, *Escherichia coli* and *Bacillus stearothermophilus* have been isolated and studied [16–19]. X-ray structures of SHMT from sheep and rabbit liver [20,21], *E. coli* [22], *B. stearothermophilus* [23] and human [24,25] are available. Our previous investigation has shown that the cytosolic SHMT from *Plasmodium* spp. can use D-serine as a substrate [1,2] while the enzyme from rabbit liver was reported to lack this activity [26]. Therefore, this difference in the biochemical properties between the *Plasmodium* and human enzymes should be explored in order to pave the way for future development of species-specific inhibition that can be useful for anti-malarial and anti-cancer therapy.

The genes encoding hcSHMT and hmSHMT are located on chromosomes 17p11.2 and 12q13.2, respectively. The cytosolic enzyme was overexpressed in *E. coli* and purified to homogeneity [27,28]. In addition to these two forms, a pseudogene of SHMT (SHMT-ps1) was also found to be located on chromosome 1p32.3-p33 [29]. Studies have shown that hmSHMT is responsible for maintaining the glycine supply in cells because knockout of hmSHMT in cells resulted in a glycine auxotroph phenotype. The level of hmSHMT expression is also steady throughout different stages of the cell cycle. In contrast, the expression of hcSHMT increases significantly in rapidly dividing cells such as cancer cells [30,31], suggesting that hcSHMT is a more relevant cancer drug target than hmSHMT [3,32]. Therefore, in our studies, hcSHMT was chosen for a comparative study of its biochemical properties with *Plasmodium* enzymes.

In this report, hcSHMT was overexpressed in *E. coli* and purified to homogeneity. Biochemical and biophysical properties such as ligand binding and kinetics were investigated. Contrary to the previous report on rabbit SHMT, we found that hcSHMT can use D-serine as a substrate. Nevertheless, hcSHMT displays many properties that are distinct from the *Plasmodium* enzymes including the kinetics of inactivation by thiosemicarbazide (TSCB). The results reported here highlight the differences of SHMTs from various species that should be useful for development of hcSHMT-specific (anti-cancer) or *Plasmodium*-specific (anti-malarial) inhibitors in the future.

Results and discussion

Expression and purification of the recombinant human cytosolic SHMT (hcSHMT)

The recombinant hcSHMT was expressed in *E. coli* BL21(DE3) using an auto-induction media system according to the protocol mentioned in Experimental procedures. Expression of hcSHMT was found in both soluble and insoluble forms in which the soluble form expresses about 10% of the total proteins. A typical total cell mass obtained from the auto-induction culture was about 20 $g \cdot L^{-1}$. hcSHMT was purified to homogeneity using 0.1% (w/v) polyethyleneimine precipitation, Q-Sepharose anion exchange chromatography and Sephacryl S-200 size exclusion chromatography according to the protocol described in Experimental procedures. This protocol resulted in 37 mg of purified hcSHMT per liter of culture (Table 1), which is greater than the yield obtained from the protocol previously reported for His_6-tagged hcSHMT of 15 $mg \cdot L^{-1}$ cell culture [24].

Determination of subunit and native molecular masses of hcSHMT

The subunit molecular mass of hcSHMT was calculated as 52.02 kDa, based on the amino acid sequence

Table 1. Purification table of recombinant hcSHMT. This purification table is from a 7.8 L culture.

Step	Volume (mL)	Total activity (units)	Total protein (mg)	Yield (%)	Purification fold
Crude extract	114	1276	4105	100	1
Q-Sepharose	6	1220	489	96	8
Sephacryl S-200	5.8	1002	288	79	11.2

using the PROTPARAM program of ExPASy Proteomics Server. This is in agreement with the results of 12% SDS/PAGE analysis, which indicated a subunit molecular mass of purified hcSHMT of ~ 53 kDa (data not shown). The native molecular mass of hcSHMT was determined to be 195 kDa using Superdex S200 HR 10/30 gel filtration chromatography (Experimental procedures), indicating that the enzyme is a tetramer as previously reported [25]. Based on the crystal structure, the tetrameric hcSHMT has four discrete active sites. Each active site is located at the dimer interface and is constituted of amino acids from two subunits [25].

Spectroscopic properties of hcSHMT

While free PLP has absorption peaks at 330 and 388 nm, hcSHMT holoenzyme displays a maximum peak at 429 nm (Fig. 1). The molar absorption coefficient of hcSHMT was determined according to the protocol described in Experimental procedures as 8.00 ± 0.14 mM^{-1}·cm^{-1} at 429 nm. This value is significantly higher than the value of free PLP in 50 mM HEPES pH 7.0 ($^{388}\varepsilon_{PLP} = 4.97$ mM^{-1}·cm^{-1}) and in 4 M guanidine hydrochloride ($^{393}\varepsilon_{PLP} = 4.83 \pm 0.04$ mM^{-1}·cm^{-1}), as well as in the PvSHMT-bound ($^{422}\varepsilon_{PvSHMT\text{-}PLP} = 6.37 \pm 0.05$ mM^{-1}·cm^{-1}) and PfSHMT-bound ($^{420}\varepsilon_{PfSHMT\text{-}PLP} = 5.4 \pm 0.2$ mM^{-1}·cm^{-1}) forms [1,2], implying that the binding environment of PLP in human and *Plasmodium* enzymes is significantly different.

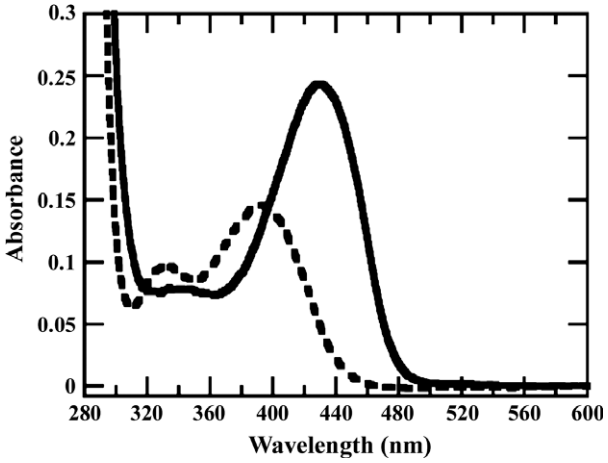

Fig. 1. Determination of the molar extinction coefficient of holo-hcSHMT. The absorption spectra in the absence (solid line) and presence (dashed line) of 4 M guanidine hydrochloride (GdnHCl) with 1 mM DTT and 0.5 mM EDTA were recorded. The molar absorption coefficient of hcSHMT under these conditions was calculated to be 8.00 ± 0.14 mM^{-1}·cm^{-1} at 429 nm.

Dissociation constant (K_d) for the binding of PLP with hcSHMT

The binding of PLP to apo-hcSHMT was investigated using an ultrafiltration method which uses a Centricon device to separate the free PLP (in the filtrate) from the enzyme-bound PLP (in the retentate). The respective concentrations of the free and bound forms of PLP were calculated by UV-visible absorbance with the molar absorption coefficient of PLP ($\varepsilon_{388} = 4.83$ mM^{-1}·cm^{-1}) and hcSHMT ($\varepsilon_{429} = 8.00$ mM^{-1}·cm^{-1}). The K_d of hcSHMT at equilibrium was calculated as 0.010 ± 0.005 μM, which is significantly lower than the K_d for the binding of PvSHMT and PLP determined by the same protocol (10.9 ± 0.1 μM). These results indicate that hcSHMT binds to PLP strongly and has a binding affinity ~ 1090-fold greater than PvSHMT.

Binding of hcSHMT to amino acids

The interactions of hcSHMT with D- and L-serine were examined to determine whether these interactions are different from those of *Plasmodium* SHMTs. We previously investigated the binding of *Plasmodium* SHMTs with D-serine, which showed the formation of an enzyme-quinonoid intermediate [1,2]. However, the existence of the quinonoid species could not be observed for the binding of L-serine with the *Plasmodium* enzymes. In this study, investigation of the binding of hcSHMT with D- and L-serine showed an increase in absorbance due to the formation of external aldimine complexes at 435 and 412 nm, respectively. No absorption at ~ 500 nm was observed (Fig. 2A,B), indicating that formation of quinonoid species under this condition (starting enzyme concentration of ~ 34 μM) could not be detected. The K_d values for the enzyme–ligand complexes of D- and L-serine in this buffer system were measured as 39 ± 6 mM and 0.96 ± 0.08 mM, respectively (Fig. 2A, B, insets). We also repeated the binding experiment of

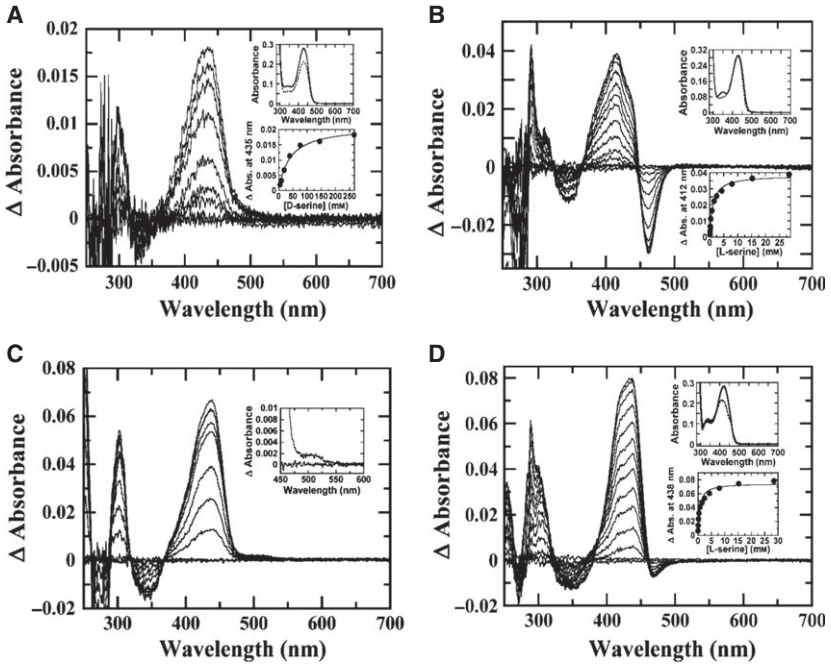

Fig. 2. Changes in the absorbance spectra of (A), (B) hcSHMT and (C), (D) PvSHMT upon titration with (A), (C) D-serine or (B), (D) L-serine. Solid and dashed lines in the upper insets in (A), (B) and (D) represent the absorption spectra of enzymes before and after addition of D- or L-serine, respectively. The lower insets in (A), (B) and (D) show plots of the absorbance changes at the wavelength where maximum signal change was observed (435 nm for D-serine and 412 for L-serine of hcSHMT and 438 nm for L-serine of PvSHMT) versus amino acid concentration. The inset in (C) shows an enlargement of the spectra in the region of 450–600 nm (enlarged insets are available in Figs S1–S7).

PvSHMT under the same condition as used in Fig. 2A,B. The results were indeed different from those of hcSHMT, but similar to the previous report [1,2] in that the binding of D-serine to PvSHMT caused an increase in absorbance around 500 nm (Fig. 2C) while binding of L-serine to PvSHMT did not cause any change in absorbance around 500 nm (Fig. 2D). These results suggest that the binding interactions of D-serine with hcSHMT and *Plasmodium* SHMTs are different.

Effects of buffer on SHMT stability and activity

During purification, we noticed that upon transferring the enzyme into 50 mM HEPES, pH 7.0, protein precipitation was observed. However, precipitation disappeared when NaCl (100 mM) was added into the same solution. Therefore, in order to keep hcSHMT soluble, all experiments reported in this study were performed in 10 mM HEPES pH 7.5, 100 mM NaCl, 0.5 mM EDTA and 1 mM dithiothreitol (DTT).

Steady-state kinetics parameters of hcSHMT in HEPES as mentioned above and in potassium phosphate buffer as used in the previous report [28] were measured and are summarized in Table 2. The absorption characteristics of hcSHMT in both systems are similar in that the protein showed a maximum absorption peak at 429 nm. The K_d values for the enzyme-bound PLP complex in both systems are very low and not significantly different within experimental certainty. The K_m values for L-serine and (6*S*)-THF in the hcSHMT reactions in both buffers are similar, whereas the k_{cat} determined from the assay carried out in phosphate buffer is about 50% less than that in HEPES buffer. Therefore, the enzyme was kept in the HEPES system with NaCl (10 mM HEPES pH 7.5, 100 mM NaCl, 0.5 mM EDTA and 1 mM DTT) throughout this study.

Steady-state kinetics of the recombinant hcSHMT and inhibition by THF

Two-substrate steady-state kinetics of hcSHMT were studied using a coupled assay with the 5,10-methylenetetrahydrofolate dehydrogenase (MTHFD) reaction under aerobic conditions as described in Experimental procedures. The initial velocities of reactions at various concentrations of L-serine and (6*S*)-THF were measured. When THF concentrations were > 40 μM, the initial rates were lower than the values at lower concentrations of THF. These results indicate that

Table 2. Kinetic and thermodynamic parameters of hcSHMT when L- and D-serine were used as substrates and comparison of the parameters with other enzymes. The K_m and k_{cat} values were determined from assays carried out by the stopped-flow techniques described in Fig. 4. The K_d value was determined from binding titrations (Fig. 2).

	Kinetic parameters					
Organism	$K_m^{L-serine}$ (mM)	$K_m^{(6S)-THF}$ (μM)	k_{cat} (s^{-1})	$K_d^{L-serine}$ (mM)	$k_{cat}/K_m^{L-serine}$ ($mM^{-1}·s^{-1}$)	References
Human (cytosolic)						
HEPES	0.18 ± 0.03	5.2 ± 0.6	28.0 ± 0.1	0.96 ± 0.08	156	Present study
Phosphate	0.17 ± 0.03	7.0 ± 1.0	15.0 ± 0.1	–	88	Present study
P. vivax	0.18 ± 0.03	140 ± 20	0.98 ± 0.06	17.0 ± 4.7	5.4	[2]
	–	–	–	0.62 ± 0.12	–	Present study
P. falciparum	0.37 ± 0.05	190 ± 20	0.74 ± 0.03	–	2	[1]
Rabbit (liver cytosolic)	0.3	20	14.17	–	47	[18]
Sheep (liver cytosolic)	1	820	–	–	–	[16]
B. stearothermophilus	0.90 ± 0.03	–	5.0 ± 0.6	–	5.56	[17]
E. coli	0.3	–	10.67	–	35.56	[19]
	$K_m^{D-serine}$ (mM)	$K_m^{(6S)-THF}$ (μM)	k_{cat} (s^{-1})	$K_d^{D-serine}$ (mM)	$k_{cat}/K_m^{D-serine}$ ($mM^{-1}·s^{-1}$)	
Human (cytosolic)	55 ± 12	21 ± 3	9.46 ± 0.03	39 ± 6	0.172	Present study
P. vivax	47 ± 6	–	0.26 ± 0.01	–	0.006	[2]
P. falciparum	71 ± 3	–	0.246 ± 0.003	–	0.003	[1]

high concentrations of THF cause substrate inhibition (Fig. 3). In contrast, high concentrations of L-serine did not show any signs of inhibition (Fig. 3, inset). Therefore, only the data from reactions with THF concentrations < 40 μM were used for further analysis.

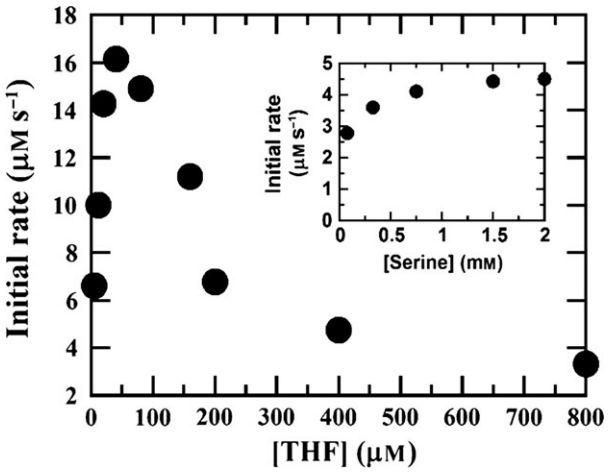

Fig. 3. Inhibition of the activity of hcSHMT by THF (substrate inhibition). The assay reactions contained 250 μM $NADP^+$, 3 mM L-serine, 10 μM MTHFD, 1.0 μM hcSHMT and various concentrations of THF (5, 11.7, 20, 40, 80,160, 200, 400 and 800 μM). The inset shows the activity of hcSHMT versus serine concentration (see the enlarged figure in Fig. S8). The assay reactions contained 250 μM $NADP^+$, 400 μM THF, 10 μM MTHFD, 1.0 μM hcSHMT and various concentrations of L-serine (0.075, 0.15, 0.375, 0.75, 1.5 and 2 mM).

A plot of e/v (reciprocal of activity) versus 1/[L-serine] at various THF concentrations shows a series of convergent lines (Fig. 4A), suggesting that the reaction proceeds via a ternary complex mechanism. Analysis of direct-plot data using the ENZFITTER program yields the following kinetic parameters: $K_m^{L-serine} = 0.18 \pm 0.03$ mM, $K_m^{(6S)-THF} = 5.2 \pm 0.6$ μM and $k_{cat} = 28.0 \pm 0.1\ s^{-1}$. The data in Fig. 3 demonstrate strong THF inhibition on hcSHMT. For *Plasmodium* SHMTs, THF inhibition was observed only at THF concentrations > 400 μM (data not shown). Based on the data available, it is likely that SHMT from *Leishmania donovani* and *Crithidia fasciculata* possess THF inhibition (at > 1 mM) [33,34].

Steady-state kinetics of the recombinant hcSHMT with D-serine

Reports of the differences between the *Plasmodium* and rabbit liver enzymes in their abilities to use D-serine as a substrate for the THF-dependent reaction prompted us to investigate whether hcSHMT can use D-serine as a substrate [1,2,26]. The reaction of THF and D-serine catalyzed by hcSHMT was monitored by coupling the reaction with MTHFD. In this study, D-serine concentrations were varied from 10 to 1280 mM, while other components were similar to those used for the reaction containing L-serine. In contrast to the previous report on rabbit liver enzyme [26], the results

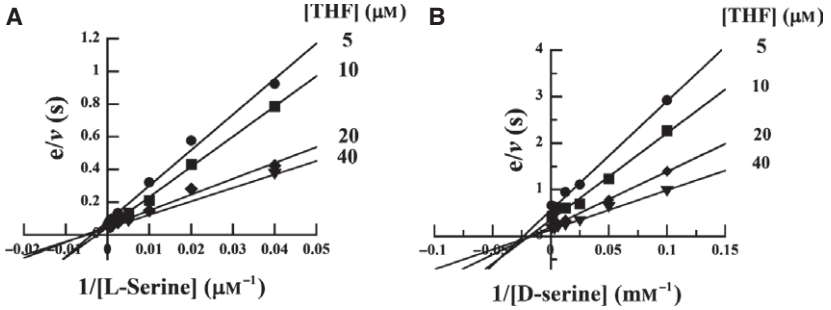

Fig. 4. Double reciprocal plots of two-substrate steady-state kinetics of hcSHMT. The assay reactions were carried out in 50 mM HEPES pH 7.0 containing 250 μM $NADP^+$, 10 μM MTHFD and 0.05 μM hcSHMT with various concentrations of (6*S*)-THF (5–40 μM) and either (A) L-serine (25–3000 μM) or (B) D-serine (10–1280 mM).

clearly showed that hcSHMT can use D-serine as a substrate. However, less catalytic efficiency was shown for D-serine than L-serine (Fig. 4B and Table 2). The kinetic constants of the reaction are as follows: $K_m^{D-serine} = 55 \pm 12$ mM, $K_m^{(6S)-THF} = 21 \pm 3$ μM and $k_{cat} = 9.46 \pm 0.03\ s^{-1}$.

pH-activity profile of hcSHMT

The effect of pH on hcSHMT activity was investigated by measuring the initial velocities of the hcSHMT reactions at pH 6.5–9.8 using hcSHMT/MTHFD coupled assays monitored by a stopped-flow instrument under a single-mixing mode at 25 °C. The results in Fig. 5 show that the rate of the reaction catalyzed by hcSHMT decreased significantly when the pH of the reaction was increased. The reaction solution was turbid at pH values lower than 6.5. This shape of the plot is significantly different from the bell-shaped pH-activity profile of PfSHMT that was previously reported (overlaid) (Fig. 5). The data for hcSHMT were analyzed according to the protocol described in Experimental procedures and the pK_a value of the group that has to be protonated in order to achieve the higher activities was obtained as 7.8 ± 0.1. The data in Fig. 5 display the difference in active site environment of the two enzymes. They cannot be used for in-depth mechanistic interpretation. The comprehensive pH-activity profile and pre-steady-state kinetics of hcSHMT are currently being investigated to obtain insights into the reaction mechanism of SHMT. Recent pH-activity studies of Thr254 mutants of rabbit cytosolic SHMT also showed an increase in activity at lower pH (pK_a value of 6.8) [35], similar to the behavior of hcSHMT reported here.

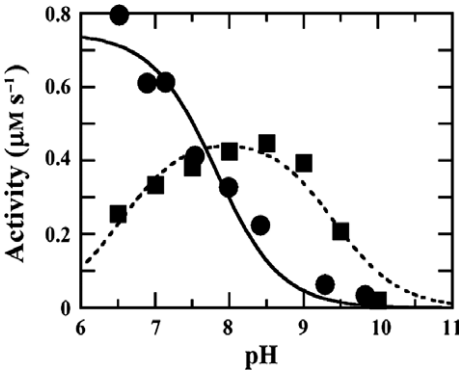

Fig. 5. The pH-activity profiles at 25 °C of PfSHMT (dashed line) and hcSHMT (solid line) show an overlap.

Effect of temperature on the hcSHMT reaction

The effect of temperature on hcSHMT was investigated by measuring the enzyme activity at various temperatures from 3 to 50 °C. However, the enzyme activities decrease at temperatures higher than 43 °C, possibly due to protein denaturation. Therefore, only the data from 3 to 43 °C were used in the analysis. The activities were plotted against temperature (°C) (Fig. 6). The plot shows a transition temperature at 18 °C, which is similar to the *Plasmodium* enzymes that exhibit a transition temperature at 19 °C [1,2]. Activation energies of the reaction below and above the transition temperature were calculated from the slopes ($-E_a/R$) of the Arrhenius plot (Experimental procedures) as 86.5 and 38.6 $kJ \cdot mol^{-1}$, respectively. A nonlinear Arrhenius plot of apparent catalytic constant versus reciprocal of the absolute temperature suggests that the rate-limiting step for the overall reaction is altered upon the change of temperature. These results may be due to the enzyme conformation change upon change in temperature. At low temperature, the enzyme is much less active than at a temperature above the breakpoint. Although the Arrhenius plots of

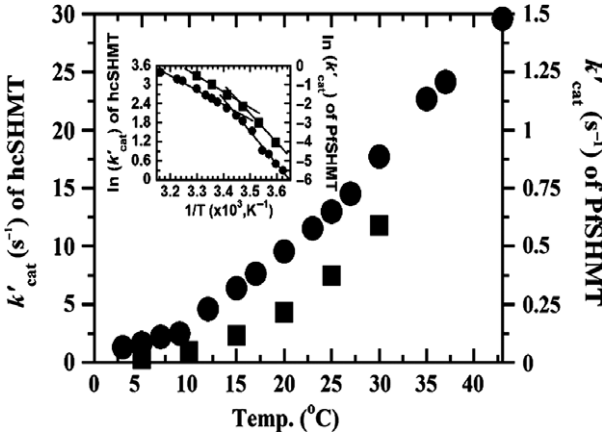

Fig. 6. Effect of temperature on the activity of hcSHMT (circles) and PfSHMT (squares). Apparent catalytic constants of hcSHMT in the temperature range 3–43 °C were measured. The inset is the Arrhenius plot of ln(k'_{cat}) versus the reciprocal of the absolute temperature showing a transition temperature at 18 °C for hcSHMT and 19 °C for PfSHMT [2] (see the enlarged inset in Fig. S9).

hcSHMT and PfSHMT look qualitatively similar, the human enzyme has a less abrupt breaking point. These data imply that, unlike *Plasmodium* enzymes in which the activity is almost abolished at lower temperatures, the activity of hcSHMT still remains active below the temperature breakpoint.

Inhibition of hcSHMT and PfSHMT by thiosemicarbazide (TSCB)

TSCB is a known inhibitor of PLP-dependent enzymes including PvSHMT and PfSHMT [36,37]. In this study, we explored whether TSCB can inactivate hcSHMT by incubating the enzyme with TSCB at various time periods before measuring SHMT activity to quantify the remaining amount of free enzyme. The experiment was carried out using a stopped-flow instrument in double-mixing mode. Syringe A contained 0.05 μM hcSHMT with 10 μM MTHFD or 1 μM PfSHMT with 5 μM MTHFD; syringe B contained various concentrations of TSCB (50–500 μM for the hcSHMT experiments and 20–1000 μM for the PfSHMT experiments); syringe C contained 250 μM $NADP^+$, 2 mM L-serine and 0.04 mM THF for the hcSHMT experiment and 0.4 mM THF for the PfSHMT experiment; syringe D only contained buffer (50 mM HEPES pH 7.0 containing 0.5 mM EDTA and 1 mM DTT). The time-dependent inactivation experiment was initiated by mixing the solutions in syringes A (SHMT) and B (TSCB) and incubating for various time periods (0.01–480 s) in the first mixing. The buffer in syringe D was then pushed through the solution of first mixing to react with the solution in syringe C (assay reagents). All reactions were carried out in 50 mM HEPES pH 7.0 containing 0.5 mM EDTA and 1 mM DTT at 25 °C. With this experimental set-up, the incubation time of the enzyme and TSCB is limited by the age time of the stopped-flow instrument (0.01–500 s).

The observed rate constant (k_{obs}) of the inactivation reaction at each TSCB concentration was calculated from the exponential value associated with the decrease of enzyme activity or from the slope of ln (V/V_0) versus time (Fig. 7A). The k_{obs} values were then plotted against the inhibitor concentrations (Fig. 7B). k_{obs} from the hcSHMT reaction increased linearly with the TSCB concentration, while k_{obs} of the PfSHMT reaction reached saturation at higher TSCB concentrations (Fig. 7D). However, due to the limitations of the detection time period (0.01–500 s) in this experiment, the kinetics of the decrease in free enzyme upon incubation with TSCB (Fig. 7A) could not be used for analysis of k_{obs} over a wide range of TSCB concentrations. Therefore, in the next section, direct binding kinetics of TSCB and PfSHMT were monitored by absorbance changes. Nevertheless, the data in Fig. 7B,D show that the kinetics of TSCB inhibition of hcSHMT and PfSHMT are different.

Kinetics of TSCB reaction with hcSHMT and PfSHMT based on spectroscopic changes monitored by rapid-mixing techniques

Changes in spectroscopic signals due to the binding of hcSHMT or PfSHMT to TSCB were monitored using a rapid-mixing apparatus attached to a diode-array spectrophotometer. The reactions were initiated by mixing the solution in syringe A (2.5 μM hcSHMT or 4 μM PfSHMT) with solutions in syringe B that contained various concentrations of TSCB (30–2000 μM for hcSHMT and 50–2000 μM for PfSHMT). All reactions were performed in 50 mM HEPES pH 7.0 containing 0.5 mM EDTA and 1 mM DTT at 25 °C. With this type of measurement, the early detection limit is 2–4 s while the end point of detection is not limited. Therefore it allows longer monitoring of the enzyme and TSCB reactions. The reaction of hcSHMT resulted in an absorbance increase at 469 nm while that of PfSHMT resulted in an increase at 478 nm. Observed rate constants (k_{obs}) were obtained by fitting the changes in absorbance over time with exponential equations using KALEIDAGRAPH software (Synergy Software, Reading, PA, USA).

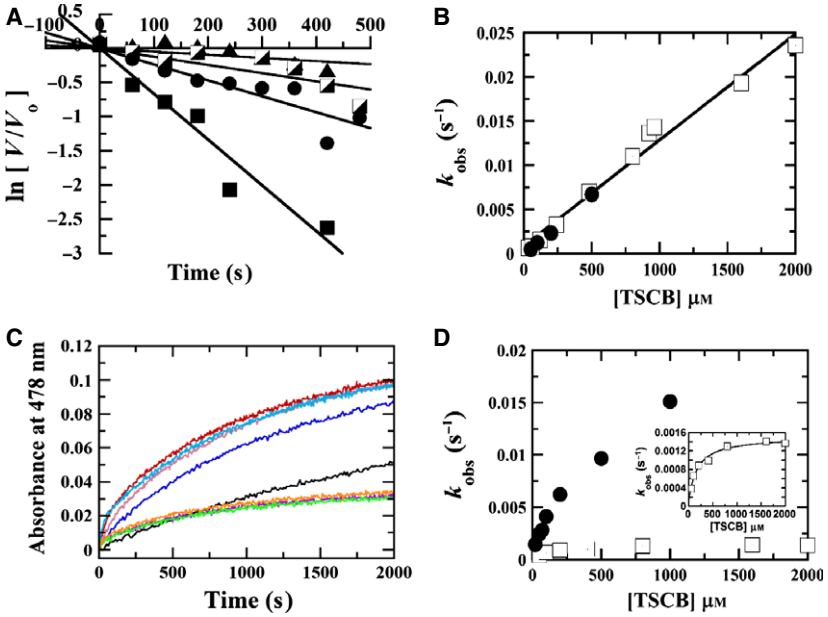

Fig. 7. Inactivation of hcSHMT and PfSHMT by TSCB. (A) A plot of ln V/V_0 (the remaining activity of hcSHMT) at various incubation times and concentrations of TSCB. (B) Observed rate constants (k_{obs}) calculated from the slopes in (A) (filled circles) and k_{obs} obtained from the spectroscopic change of hcSHMT upon mixing with TSCB (empty squares) are plotted as a function of inhibitor concentration. For the reaction of hcSHMT and TSCB, k_1 and k_{-1} were calculated as 12.0 ± 0.6 $M^{-1}{\cdot}s^{-1}$ and 0.0010 ± 0.0006 s^{-1}, respectively, corresponding to a K_I value of 75 ± 45 μM. (C) Absorbance change of PfSHMT upon mixing with TSCB monitored by a rapid-mixing apparatus. (D) Observed rate constants (k_{obs}) calculated from the slopes of ln V/V_0 (PfSHMT) versus incubation time (filled circles) and k_{obs} obtained from the spectroscopic change of PfSHMT upon mixing with TSCB (empty squares) are plotted as a function of inhibitor concentration. The inset in (D) is a close-up plot of the empty squares on a smaller *y*-axis scale.

Similar to the previous section, a plot of k_{obs} for the hcSHMT reaction versus TSCB concentration is linear, and the values are in the same range as those from the inhibition experiment (Fig. 7B). The linear plot in Fig. 7B indicates that the inactivation kinetics of hcSHMT by TSCB is a one-step process (Scheme 1 and Eqn 1) or involves more than one step but, under the TSCB concentrations employed, the saturating concentration cannot be reached. According to a one-step reaction model, a forward (k_1) and reverse (k_{-1}) rate constant for complex formation and an equilibrium dissociation constant of the complex (K_I) can be calculated based on Eqn (2). The analysis yielded k_1 and k_{-1} values for the hcSHMT reaction as 12.0 ± 0.6 $M^{-1}{\cdot}s^{-1}$ and 0.001 ± 0.0006 s^{-1}, respectively. These values correspond to a calculated K_I value of 75 ± 45 μM (Eqn 2). Based on spectroscopic titration experiments of TSCB and hcSHMT, performed similar to those shown in Fig. 2, the K_d value for the hcSHMT:TSCB complex was found to be 33 ± 5 μM, which is in the same range as the value obtained from the kinetics experiment. Taken together, the data indicate that the reaction of TSCB and hcSHMT is a one-step process and can be summarized as shown in Scheme 1.

$$k_{obs} = k_1[S] + k_{-1} \quad (1)$$

$$K_I = \frac{k_{-1}}{k_1} \quad (2)$$

For the PfSHMT and TSCB reaction, the observed binding kinetics were different from those observed for the enzyme inhibition experiments (Fig. 7D and inset). These data suggest that the reaction of PfSHMT and TSCB is a multi-step process (Scheme 2). The initial

Scheme 1. Kinetics model for hcSHMT inactivation by TSCB.

Scheme 2. Kinetics model for PfSHMT inactivation by TSCB.

phase (decrease of E or formation of E – I) could only be observed by double-mixing stopped-flow assays to measure the decrease of free PfSHMT activity (previous section). The PfSHMT-TSCB isomerization step that resulted in the absorbance increase at 478 nm (E – I*) showed much slower kinetics (Fig. 7C). As a plot of k_{obs} value versus TSCB concentration obtained from the inhibition experiments in Fig. 7D is hyperbolic, the data indicate that there is a bi-molecular step of TSCB binding (E:I) preceding the E – I formation [38,39]. These data indicate that the reaction of PfSHMT and TSCB involves at least three steps (Scheme 2). Comprehensive analysis of three-step reactions is complicated and should also be analyzed by kinetic simulations [40,41]. Due to the lack of measurable spectroscopic signals in the first two steps, individual rate constants associated with the reaction of PfSHMT and TSCB are difficult to obtain. Nevertheless, all data clearly show that the reactions of hcSHMT with TSCB and PfSHMT with TSCB are different. These results as well as other evidence reported herein suggest that the ligand binding environments in hcSHMT and *Plasmodium* SHMTs are different and it should be possible in the future to design inhibitors that are specific for SHMT from each of the various organisms.

Conclusion

Our findings have clearly shown that the ligand binding properties of hcSHMT are distinct from those of the *Plasmodium* enzymes. The molar absorption coefficient of hcSHMT-bound PLP is much greater than for PvSHMT- and PfSHMT-bound PLP. Although hcSHMT can use D-serine as a substrate similar to the *Plasmodium* enzymes, the binding interactions of hcSHMT and *Plasmodium* SHMTs with D-serine are not alike. Only the *Plasmodium* enzymes are able to catalyze the formation of quinonoid-like species upon binding to D-serine. hcSHMT displays strong substrate inhibition by THF compared with enzymes from *Plasmodium* or other species. pH-activity profiles of hcSHMT show higher activities at lower pH values while those of the *Plasmodium* enzymes are bell-shaped. TSCB reacts with hcSHMT according to a one-step model, while the same reaction with PfSHMT involves at least three steps. Results reported herein clearly demonstrate different ligand binding environments between human and *Plasmodium* enzymes, implying that it should be possible to develop inhibitors specific for hcSHMT (anti-cancer drug) or *Plasmodium* SHMTs (anti-malarial drug) in the future.

Experimental procedures

Chemicals and reagents

L-Serine, D-serine (98%), β-$NADP^+$, PLP, D-glucose and α-lactose were purchased from Sigma Chemicals Co. (St Louis, MO, USA). DTT, phenylmethanesulfonyl fluoride, ampicillin and yeast extract were purchased from Bio Basic Inc. (Allentown, PA, USA). HEPES was purchased from USB Corporation (Cleveland, OH, USA). EDTA, 85% (v/v) glycerol, sodium chloride (NaCl), sodium hydroxide (NaOH), sodium dihydrogen phosphate (NaH_2PO_4), ammonium sulfate ($(NH_4)_2SO_4$), potassium dihydrogen phosphate (KH_2PO_4), methanol and ethanol were purchased from Merck (Gibbstown, NJ, USA). Agar was from Scharlau Chemie S.A. (Barcelona, Spain). Bacteriological peptone was from Laboratorios Conda S.A. (Madrid, Spain). Q-Sepharose fast flow anion exchange, Sephacryl S-200 and PD10 chromatographic materials were purchased from GE Healthcare (Uppsala, Sweden). (6*S*)-THF was received as a gift from Merck Eprova AG (Schauffhausen, Switzerland). All chemicals and reagents used in this study were analytical grade and of the highest purity available.

The (6*S*)-THF stock solution was prepared in an anaerobic glove box (Belle Technology, Weymouth, UK). The concentration of (6*S*)-THF was determined by converting to 5,10-methenyl-THF. An aliquot of (6*S*)-THF solution containing 0.5 mM EDTA and 1 mM DTT was added with formic acid (99%) in an appropriate dilution (~ 1000-fold). The mixture was incubated in boiling water for 5 min and then cooled and its absorption spectrum was measured. The absorbance at 350 nm was used for calculating 5,10-methenyl-THF concentrations with a molar absorption coefficient of 26 000 $M^{-1}\cdot cm^{-1}$ [2].

Spectroscopic instrument

UV-visible absorbance spectra were collected with a diode-array spectrophotometer (Hewlett Packard, Palo Alto, CA, USA) or a double-beam spectrophotometer (Shimadzu 2501PC, Shimadzu Corp., Kyoto, Japan). Steady-state kinetic studies were carried out using a stopped-flow spectrophotometer (model SF-61DX2; TgK Scientific Instruments, Bradford-on-Avon, UK) in single-mixing mode. Inhibition by TSCB was investigated using a stopped-flow spectrophotometer in double-mixing mode. The kinetics of TSCB binding to SHMT were investigated using a rapid-mixing apparatus attached to the diode-array spectrophotometer. These instruments are equipped with a thermostat sample compartment.

Gene cloning and expression

Plasmids pET100D/TOPO-hSHMTΔH and pET23b-MTHFD were used for expression of hcSHMT and

MTHFD, respectively. Total RNA of human white blood cells was prepared using TRIzol® (Invitrogen™, Carlsbad, CA, USA) according to the manufacturer's protocol. The cDNA was prepared using oligo-dT primer in the presence of ImProm-II™ reverse transcriptase (Promega, Madison, WI, USA) and was used to PCR amplify *hcshmt*. The sense and antisense primers were 5′NdeI_hshmt (CACCCATATGACGATGCCAGTCAACGGGG) and 3′BamHI_hshmt (TTGGAATTCTTAGAAGTCAGGCAGGCCAGGCAG). The resulting 1.4 kb amplicon was cloned into pET100D/TOPO (Invitrogen™) and designated pET100D/TOPO-hSHMT. To generate pET100D/TOPO-hSHMTΔH plasmid for expressing native hcSHMT protein, pET100D-hSHMT was digested with *Nde*I to remove 5′ sequences encoding the N-terminus including the hexahistidine sequences derived from pET100D/TOPO, and the digested DNA was re-ligated. The sequence of *hcshmt* was analyzed by an automated DNA sequencer (1st BASE, Selangor DarulEhsan, Malaysia).

E. coli BL21(DE3) carrying pET100D/TOPO-hSHMTΔH plasmid was inoculated into ZYM-5052 auto-induction medium (100 mL) [42] containing 0.5% yeast extract, 1% peptone, 0.05% glucose, 2 mM $MgSO_4$, 5 mM Na_2SO_4, 1× NPS (50 mM NH_4Cl, 25 mM KH_2PO_4 and 25 mM Na_2HPO_4) and 50 $\mu g \cdot mL^{-1}$ ampicillin at 37 °C. The culture was maintained overnight to produce a starter culture and was used to inoculate into fresh ZYP-5052 medium (0.5% or 3 mL : 600 mL) containing 0.5% (w/v) glycerol, 0.2% (w/v) α-lactose and 0.05% (w/v) D-glucose and 50 $\mu g \cdot mL^{-1}$ ampicillin. The culture was maintained at 37 °C until the A_{600} of the culture reached 1.0, after which the temperature was lowered to 16 °C. The culture was maintained overnight before harvesting by centrifugation at 4420 *g* for 15 min at 4 °C. Cells were stored at −80 °C until used. The yield of the cell paste was ~ 20 $g \cdot L^{-1}$ culture.

Purification of recombinant hcSHMT

Frozen cell paste (35 g) was thawed and resuspended in a lysis buffer (50 mM HEPES buffer pH 7.0 containing 1 mM DTT, 0.5 mM EDTA, 100 μM phenylmethanesulfonyl fluoride and 10 μM PLP). Cells were disrupted by ultrasonication (model VCX750; Sonic Vibra-cellTM, Sonics & Materials, Inc, Newtown, CT, USA.). The cell debris was removed by centrifugation at 35 000 ***g***, 4 °C, and then ultracentrifugation at 100 000 ***g***, 4 °C for 1 h. The resulting supernatant was defined as crude extract.

Nucleic acid and nucleic acid binding proteins in the crude extract were precipitated by 0.1% (w/v) of polyethyleneimine (PEI) (final concentration) and ultracentrifuged at 100 000 ***g*** for 1 h at 4 °C. The supernatant was dialyzed against 4 L of 10 mM HEPES buffer pH 7.5 containing 1 mM DTT and 0.5 mM EDTA at 4 °C overnight.

The dialyzed protein after the PEI precipitation was loaded onto a Q-Sepharose column (2.5 × 14 cm) pre-equilibrated with 10 mM HEPES buffer pH 7.5 containing 1 mM DTT and 0.5 mM EDTA. The column was then washed with the same buffer for 10 column volumes. A linear gradient of 0–150 mM NaCl in 10 mM HEPES buffer pH 7.5 containing 1 mM DTT and 0.5 mM EDTA was used to elute the column. Fractions with a ratio of absorbances at 280 and 429 nm ≤ 18 were pooled and concentrated using a stirred-cell concentrator (10 kDa cut-off membrane) followed by a Centriprep® YM-30 centrifugal filter unit (30 kDa cut-off membrane; EMD Millipore, Billerica, MA, USA.).

The enzyme solution was applied onto a Sephacryl S-200 gel filtration column (2.5 × 80 cm) pre-equilibrated with 10 mM HEPES buffer pH 7.5 containing 100 mM NaCl, 1 mM DTT and 0.5 mM EDTA. The same buffer was used to elute the column. The purified protein was then stored at −80 °C until used.

Molecular mass determination

The native molecular mass of hcSHMT was determined using a Superdex S200 HR 10/30 (GE Healthcare) gel filtration column operated by an AKTA FPLC system (GE Healthcare). The protein standards used were ferritin (440 kDa), aldolase (158 kDa), BSA (65.4 kDa), ovalbumin (48.9 kDa), chymotrypsinogen A (22.8 kDa) and ribonuclease A (15.6 kDa). All proteins were eluted with 50 mM sodium phosphate buffer pH 7.0 containing 150 mM NaCl at 25 °C with a flow rate of 0.5 $mL \cdot min^{-1}$. The molecular mass of hcSHMT was determined from a plot of the elution volume versus the logarithm of standard molecular weight values.

The subunit molecular mass of hcSHMT was determined by SDS/PAGE (12% w/v) and was also calculated using the PROTPARAM program from the ExPASy Proteomics Server, from which the calculation is based on the amino acid sequence.

Determination of the molar extinction coefficient of free PLP and recombinant hcSHMT

The absorption of the free PLP solution (A_{388} ~ 0.22) in 50 mM HEPES buffer pH 7.0 containing 1 mM DTT and 0.5 mM EDTA at 25 °C was recorded, and the concentration was calculated based on the known molar absorption coefficient value of free PLP (ε_{388} = 4900 $M^{-1} \cdot cm^{-1}$) [43]. Guanidine hydrochloride (GdnHCl, 8 M) was then added into the PLP solution at a final concentration of 4 M, and the mixture was incubated for 10 min at 25 °C. The absorption spectrum of the reaction mixture was read in triplicate and the molar absorption coefficient of PLP under this condition was calculated based on the value in buffer.

A similar experiment was performed to determine the molar absorption coefficient of hcSHMT. Absorption spectra of holo-hcSHMT in buffer (A_{429} ~ 0.24) and in 4 M

GdnHCl were recorded. The molar absorption coefficient of PLP in 4 M GdnHCl (from the above experiment) was used to calculate the concentration of the released PLP. The concentration of holoenzyme is assumed to be equivalent to that of the released PLP. The molar absorption coefficient of hcSHMT was calculated based on the holo-hcSHMT concentration and the absorbance at 429 nm.

Determination of the dissociation constant (K_d) for the binding of PLP to hcSHMT

The binding experiment was performed using an ultrafiltration technique using a Centriprep® YM-10 filter (10 kDa cut-off). Initially, the spectrum of hcSHMT ($A_{429} \sim 0.2$) in 10 mM HEPES buffer pH 8.0 with 100 mM NaCl containing 1 mM DTT and 0.5 mM EDTA was recorded and the concentration of holoenzyme was calculated based on the holoenzyme molar absorption coefficient. The protein solution (11 mL) was subjected to ultrafiltration at 1380 ***g*** at 25 °C for 7 min to obtain ~ 1 mL filtrate. The absorption of the filtrate was recorded and used for calculating the concentration of the released free PLP.

Determination of dissociation constants for binding of hcSHMT and amino acids

In order to examine the interaction between hcSHMT and the different ligands, hcSHMT was mixed with various amino acids and the changes in the absorption characteristics were monitored using a double-beam spectrophotometer. In brief, a solution of hcSHMT (~ 34 μM) in 10 mM HEPES pH 8 with 100 mM NaCl containing 1 mM DTT and 0.5 mM EDTA was added into the sample and reference cells (1 mL each). A solution of amino acid was added into the sample cell while an equal volume of buffer was added into the reference cell. For each titration, the mixture was incubated for 10 min before the absorption spectrum was recorded. The final concentrations of L-serine and D-serine used were 0.025–28.47 mM and 4.98–266 mM, respectively. The change in absorption was plotted against the concentration of amino acids and the dissociation constant was calculated according to Eqn (3), where ΔA represents the absorbance change, ΔA_{max} is the maximum absorbance change, $[L]_{free}$ is the concentration of free ligand and K_d is a dissociation constant for the enzyme–ligand complex. $[L]_{free}$ was determined from Eqns (4) and (5), respectively. $[L]_{total}$, [PL] and $[P]_{total}$ are the concentrations of total ligand, ligand bound protein and total protein, respectively. Similar experiments and analysis as described above were performed for PvSHMT, but the concentrations of L- and D-serine were 0.025–28.47 mM and 4.98–386 mM, respectively.

$$\frac{\Delta A}{\Delta A_{max}} = \frac{[L]_{free}}{K_d + [L]_{free}} \quad (3)$$

$$[PL] = \frac{\Delta A}{\Delta A_{max}} [P]_{total} \quad (4)$$

$$[L]_{free} = [L]_{total} - [PL] \quad (5)$$

Enzyme activity assay

The activity of hcSHMT was measured by following the protocol previously described [37]. The coupled assay was performed under aerobic conditions in 50 mM HEPES buffer pH 7.0 containing 1 mM DTT, 0.5 mM EDTA, 2 mM L-serine, 250 μM $NADP^+$, 40 μM THF, 10 μM MTHFD and 0.05 μM hcSHMT enzyme. Assays were measured using the diode-array spectrophotometer. The enzyme activity was calculated from the initial slopes of the coupled assays using the molar extinction coefficient of NADPH at 375 nm of 1.92 $mM^{-1} \cdot cm^{-1}$. One unit of enzyme is equivalent to the formation of 1 μmol NADPH per minute at pH 7.0, 25 °C.

Steady-state kinetics of the recombinant hcSHMT

The kinetics of hcSHMT were measured by coupling the reaction with MTHFD. Assay reactions contained 50 mM HEPES pH 7.0, 1 mM DTT, 0.5 mM EDTA, 250 μM $NADP^+$, 10 μM MTHFD, 0.05 μM hcSHMT and various concentrations of L-serine (25–3000 μM) and (6*S*)-THF (5–160 μM). The enzyme solution was mixed with an equal volume of a substrate solution using the stopped-flow instrument in single-mixing mode. The reaction progression was monitored by the increase of NADPH at 375 nm, 25 °C. Double-reciprocal plots of the data were used to identify whether the reaction occurs with ping-pong or ternary-complex type kinetics according to Dalziel's equation (Eqn 6). The ENZFITTER program (Biosoft, Cambridge, UK) was used to determine the kinetic parameters according to Eqn (7).

$$\frac{e}{v} = \varphi_0 + \frac{\varphi_A}{[A]} + \frac{\varphi_B}{[B]} + \frac{\varphi_{AB}}{[A][B]} \quad (6)$$

$$v = \frac{V_{max}[A][B]}{K_{iA}K_B + K_A[B] + K_B[A] + [A][B]} \quad (7)$$

Optimum pH for the reaction of hcSHMT

The initial rates of hcSHMT reactions at various pH values (6.5–9.8) were measured. The assays contained 0.05 μM hcSHMT, 10 μM MTHFD, 2 mM L-serine, 40 μM (6*S*)-THF and 250 μM $NADP^+$ in buffers at various pH values. Stock solutions of hcSHMT and MTHFD were in 10 mM HEPES buffer pH 8.0 with 100 mM NaCl while other components

were prepared in buffers at various pH values. The buffers used were NaH_2PO_4 (50 mM) for pH 6.5, HEPES (50 mM) for pH 6.9, 7.1, 7.5, 8.0 and 8.4, and carbonate (15 mM) for pH 9.0, 9.3 and 9.8. The ionic strength of the buffers was kept constant at 100 mM by adjusting with NaCl. A plot of the apparent rate constants as a function of pH was analyzed according to Eqn (8), where Y is the apparent maximum velocity, C is the pH-independent value of V'_{max} and K_a is the dissociation constant for the ionizable group.

$$Y = \frac{C}{1 + 10^{-pK_a}/10^{-pH}} \quad (8)$$

Effect of temperature on hcSHMT activity

The effect of temperature on the hcSHMT activity was investigated by following the protocol previously described [1,2]. The coupled assay was performed under aerobic conditions in 50 mM HEPES buffer pH 7.0 containing 1 mM DTT, 0.5 mM EDTA, 2 mM serine, 40 μM (6*S*)-THF, 250 μM $NADP^+$, 0.05 μM hcSHMT and 10 μM MTHFD at various temperatures ranging from 3 to 50 °C. The catalytic rate constant (k'_{cat}) was determined using the Arrhenius equation and the activation energy was calculated from the slope ($-E_a/R$) of the Arrhenius plot ($\ln(k'_{cat})$ versus $1/T$).

$$k'_{cat} = Ae^{-E_a/RT} \quad (9)$$

Acknowledgements

This work was supported by grants from the Cluster Program and Management Office, National Science and Technology Development Agency (BT-B-02-MG-BC-5006/CPMO-P-00-20029 and CPMO-P-13-00835) to U.L. and P.C., the Cluster Program and Management Office for Discovery based Development Grants (CPMO-DD/P-10-11274) to U.L., the Thailand Research Fund (RTA5680001) and Faculty of Science, Mahidol University, to P.C. C.P. and W.A. are recipients of scholarships from Thailand Graduate Institute of Science and Technology (TGIST). S.M. received research support from the Thailand Research Fund (MRG5580066) and the Faculty of Science, Burapha University. We thank Dr Martino di Salvo (Università di Roma) and Merck Eprova AG (Schaffhausen Switzerland) for providing the plasmid for MTHFD expression and high quality folate compounds, respectively. We also thank Dr Wichai Pornthanakasem, Ms Sasithorn Sivanuntakorn and Ms Herlina for technical support on construction of the plasmids used in the study. We thank Ms. Rachawan Nuchsiri for her assistance for temperature dependence experiments.

Author contribution

C.P. planned experiments, performed experiments, analyzed data and wrote the paper; S.M. planned experiments and performed experiments; W.A. performed experiments and analyzed data; Y.Y. wrote the paper; U.L. planned experiments, performed experiments and wrote the paper; P.C. planned experiments, analyzed data and wrote the paper.

References

1 Maenpuen S, Sopitthummakhun K, Yuthavong Y, Chaiyen P & Leartsakulpanich U (2009) Characterization of *Plasmodium falciparum* serine hydroxymethyltransferase-A potential antimalarial target. *Mol Biochem Parasitol* **168**, 63–73.

2 Sopitthummakhun K, Maenpuen S, Yuthavong Y, Leartsakulpanich U & Chaiyen P (2009) Serine hydroxymethyltransferase from *Plasmodium vivax* is different in substrate specificity from its homologues. *FEBS J* **276**, 4023–4036.

3 Agrawal S, Kumar A, Srivastava V & Mishra BN (2003) Cloning, expression, activity and folding studies of serine hydroxymethyltransferase: a target enzyme for cancer chemotherapy. *J Mol Microbiol Biotechnol* **6**, 67–75.

4 Pornthanakasem W, Kongkasuriyachai D, Uthaipibull C, Yuthavong Y & Leartsakulpanich U (2012) *Plasmodium* serine hydroxymethyltransferase: indispensability and display of distinct localization. *Malar J* **11**, 387.

5 Yuthavong Y, Kamchonwongpaisan S, Leartsakulpanich U & Chitnumsub P (2006) Folate metabolism as a source of molecular targets for antimalarials. *Future Microbiol* **1**, 113–125.

6 Bertino JR (2009) Cancer research: from folate antagonism to molecular targets. *Best Pract Res Clin Haematol* **22**, 577–582.

7 Chen CY, Chang YL, Shih JY, Lin JW, Chen KY, Yang CH, Yu CJ & Yang PC (2011) Thymidylate synthase and dihydrofolate reductase expression in non-small cell lung carcinoma: the association with treatment efficacy of pemetrexed. *Lung Cancer* **74**, 132–138.

8 Gangjee A, Jain HD, Phan J, Guo X, Queener SF & Kisliuk RL (2010) 2,4-Diamino-5-methyl-6-substituted arylthio-furo[2,3-d]pyrimidines as novel classical and nonclassical antifolates as potential dual thymidylate synthase and dihydrofolate reductase inhibitors. *Bioorg Med Chem* **18**, 953–961.

9 Muller IB & Hyde JE (2013) Folate metabolism in human malaria parasites – 75 years on. *Mol Biochem Parasitol* **188**, 63–77.

10 Yuthavong Y, Tarnchompoo B, Vilaivan T, Chitnumsub P, Kamchonwongpaisan S, Charman SA, McLennan DN, White KL, Vivas L, Bongard E *et al.* (2012) Malarial dihydrofolate reductase as a paradigm for drug development against a resistance-compromised target. *Proc Natl Acad Sci USA* **109**, 16823–16828.
11 Cheng CW, Yu JC, Huang CS, Shieh JC, Fu YP, Wang HW, Wu PE & Shen CY (2008) Polymorphism of cytosolic serine hydroxymethyltransferase, estrogen and breast cancer risk among Chinese women in Taiwan. *Breast Cancer Res Treat* **111**, 145–155.
12 Skibola CF, Smith MT, Hubbard A, Shane B, Roberts AC, Law GR, Rollinson S, Roman E, Cartwright RA & Morgan GJ (2002) Polymorphisms in the thymidylate synthase and serine hydroxymethyltransferase genes and risk of adult acute lymphocytic leukemia. *Blood* **99**, 3786–3791.
13 Eliot AC & Kirsch JF (2004) Pyridoxal phosphate enzymes: mechanistic, structural, and evolutionary considerations. *Annu Rev Biochem* **73**, 383–415.
14 Schirch V & Szebenyi DM (2005) Serine hydroxymethyltransferase revisited. *Curr Opin Chem Biol* **9**, 482–487.
15 Florio R, di Salvo ML, Vivoli M & Contestabile R (2011) Serine hydroxymethyltransferase: a model enzyme for mechanistic, structural, and evolutionary studies. *Biochim Biophys Acta* **1814**, 1489–1496.
16 Jagath-Reddy J, Ganesan K, Savithri HS, Datta A & Rao NA (1995) cDNA cloning, overexpression in *Escherichia coli*, purification and characterization of sheep liver cytosolic serine hydroxymethyltransferase. *Eur J Biochem* **230**, 533–537.
17 Jala VR, Prakash V, Rao NA & Savithri HS (2002) Overexpression and characterization of dimeric and tetrameric forms of recombinant serine hydroxymethyltransferase from *Bacillus stearothermophilus*. *J Biosci* **27**, 233–242.
18 Di Salvo ML, Delle Fratte S, De Biase D, Bossa F & Schirch V (1998) Purification and characterization of recombinant rabbit cytosolic serine hydroxymethyltransferase. *Protein Expr Purif* **13**, 177–183.
19 Schirch V, Hopkins S, Villar E & Angelaccio S (1985) Serine hydroxymethyltransferase from *Escherichia coli*: purification and properties. *J Bacteriol* **163**, 1–7.
20 Rao JV, Prakash V, Rao NA & Savithri HS (2000) The role of Glu74 and Tyr82 in the reaction catalyzed by sheep liver cytosolic serine hydroxymethyltransferase. *Eur J Biochem* **267**, 5967–5976.
21 Scarsdale JN, Kazanina G, Radaev S, Schirch V & Wright HT (1999) Crystal structure of rabbit cytosolic serine hydroxymethyltransferase at 2.8 Å resolution: mechanistic implications. *Biochemistry* **38**, 8347–8358.
22 Scarsdale JN, Radaev S, Kazanina G, Schirch V & Wright HT (2000) Crystal structure at 2.4 Å resolution of *E. coli* serine hydroxymethyltransferase in complex with glycine substrate and 5-formyl tetrahydrofolate. *J Mol Biol* **296**, 155–168.
23 Bhavani S, Trivedi V, Jala VR, Subramanya HS, Kaul P, Prakash V, Appaji Rao N & Savithri HS (2005) Role of Lys-226 in the catalytic mechanism of *Bacillus stearothermophilus* serine hydroxymethyltransferase – crystal structure and kinetic studies. *Biochemistry* **44**, 6929–6937.
24 Renwick SB, Skelly JV, Chave KJ, Sanders PG, Snell K & Baumann U (1998) Purification, crystallization and preliminary X-ray analysis of human recombinant cytosolic serine hydroxymethyltransferase. *Acta Crystallogr D Biol Crystallogr* **54**, 1030–1031.
25 Renwick SB, Snell K & Baumann U (1998) The crystal structure of human cytosolic serine hydroxymethyltransferase: a target for cancer chemotherapy. *Structure* **6**, 1105–1116.
26 Schirch L (1982) Serine hydroxymethyltransferase. *Adv Enzymol Relat Areas Mol Biol* **53**, 83–112.
27 Girgis S, Nasrallah IM, Suh JR, Oppenheim E, Zanetti KA, Mastri MG & Stover PJ (1998) Molecular cloning, characterization and alternative splicing of the human cytoplasmic serine hydroxymethyltransferase gene. *Gene* **210**, 315–324.
28 Kruschwitz H, Ren S, Di Salvo M & Schirch V (1995) Expression, purification, and characterization of human cytosolic serine hydroxymethyltransferase. *Protein Expr Purif* **6**, 411–416.
29 Byrne PC, Shipley JM, Chave KJ, Sanders PG & Snell K (1996) Characterisation of a human serine hydroxymethyltransferase pseudogene and its localisation to 1p32.3-33. *Hum Genet* **97**, 340–344.
30 Eichler HG, Hubbard R & Snell K (1981) The role of serine hydroxymethyltransferase in cell proliferation: DNA synthesis from serine following mitogenic stimulation of lymphocytes. *Biosci Rep* **1**, 101–106.
31 Thorndike J, Pelliniemi TT & Beck WS (1979) Serine hydroxymethyltransferase activity and serine incorporation in leukocytes. *Cancer Res* **39**, 3435–3440.
32 Rao NA, Talwar R & Savithri HS (2000) Molecular organization, catalytic mechanism and function of serine hydroxymethyltransferase – a potential target for cancer chemotherapy. *Int J Biochem Cell Biol* **32**, 405–416.
33 Capelluto DG, Hellman U, Cazzulo JJ & Cannata JJ (1999) Purification and partial characterization of three isoforms of serine hydroxymethyltransferase from *Crithidia fasciculata*. *Mol Biochem Parasitol* **98**, 187–201.
34 Vatsyayan R & Roy U (2007) Molecular cloning and biochemical characterization of *Leishmania donovani* serine hydroxymethyltransferase. *Protein Expr Purif* **52**, 433–440.

35 Di Salvo ML, Scarsdale JN, Kazanina G, Contestabile R, Schirch V & Wright HT (2013) Structure-based mechanism for early PLP-mediated steps of rabbit cytosolic serine hydroxymethyltransferase reaction. *Biomed Res Int* **2013**, 458571.
36 Acharya JK & Rao NA (1992) A novel intermediate in the interaction of thiosemicarbazide with sheep liver serine hydroxymethyltransferase. *J Biol Chem* **267**, 19066–19071.
37 Sopitthummakhun K, Thongpanchang C, Vilaivan T, Yuthavong Y, Chaiyen P & Leartsakulpanich U (2012) *Plasmodium* serine hydroxymethyltransferase as a potential anti-malarial target: inhibition studies using improved methods for enzyme production and assay. *Malar J* **11**, 194.
38 Fersht A (1999) Structure and Mechanism in Protein Science: A Guide to Enzyme Catalysis and Protein Folding. W.H. Freeman, New York, NY.
39 Hiromi K (1979) Kinetics of Fast Enzyme Reactions: Theory and Practice. Kodansha Ltd., Tokyo.
40 Prongjit M, Sucharitakul J, Wongnate T, Haltrich D & Chaiyen P (2009) Kinetic mechanism of pyranose 2-oxidase from *Trametes multicolor*. *Biochemistry* **48**, 4170–4180.
41 Sucharitakul J, Wongnate T, Montersino S, van Berkel WJ & Chaiyen P (2012) Reduction kinetics of 3-hydroxybenzoate 6-hydroxylase from *Rhodococcus jostii* RHA1. *Biochemistry* **51**, 4309–4321.
42 Studier W (2005) Protein production by auto-induction in high-density shaking culture. *Protein Expr Purif* **41**, 207–234.
43 Dawson RMC, Elliott DC, Elliott WH & Jones KM (1986) Data for Biochemical Research, 3rd edn. Oxford University Press, New York, NY.

Supporting information

Additional supporting information may be found in the online version of this article at the publisher's web site:

Fig. S1. The upper inset of Fig. 2(A). Absorption spectra of hcSHMT before and after addition of D-serine.

Fig. S2. The lower inset of Fig. 2(A). Absorbance changes of hcSHMT at 435 nm versus D-serine concentration.

Fig. S3. The upper inset of Fig. 2(B). Absorption spectra of hcSHMT before and after addition of L-serine.

Fig. S4. The lower inset of Fig. 2(B). Absorbance changes of hcSHMT at 412 nm versus L-serine concentration.

Fig. S5. The inset of Fig. 2(C). Absorption changes of PvSHMT after addition of D-serine.

Fig. S6. The upper inset of Fig. 2(D). Absorption spectra of PvSHMT before and after addition of L-serine.

Fig. S7. The lower inset of Fig. 2(D). Absorbance changes of PvSHMT at 438 nm versus L-serine concentration.

Fig. S8. The inset of Fig. 3. Activities of hcSHMT versus various concentrations of L-serine.

Fig. S9. The inset of Fig. 6. A plot of $\ln(k'_{cat})$ versus the reciprocal of the absolute temperature in the range 276–316 K of hcSHMT and PfSHMT.

Acta Crystallographica Section D
Biological Crystallography
ISSN 1399-0047

Structures of *Plasmodium vivax* serine hydroxymethyltransferase: implications for ligand-binding specificity and functional control

Penchit Chitnumsub,[a]* Aritsara Jaruwat,[a] Pinpunya Riangrungroj,[a] Wanwipa Ittarat,[a] Krittikar Noytanom,[a] Worrapoj Oonanant,[a] Jarunee Vanichthanankul,[a] Phimonphan Chuankhayan,[b] Somchart Maenpuen,[c] Chun-Jung Chen,[b] Pimchai Chaiyen,[d] Yongyuth Yuthavong[a] and Ubolsree Leartsakulpanich[a]*

[a]National Center for Genetic Engineering and Biotechnology (BIOTEC), National Science and Technology Development Agency (NSTDA), 113 Thailand Science Park, Phahonyothin Road, Klong Nueng, Klong Luang, Pathum Thani 12120, Thailand, [b]Life Science Group, Scientific Research Division, National Synchrotron Radiation Research Center, Hsinchu 30076, Taiwan, [c]Department of Biochemistry, Faculty of Science, Burapha University, Chonburi 20131, Thailand, and [d]Department of Biochemistry and Center for Excellence in Protein Structure and Function, Faculty of Science, Mahidol University, Bangkok 10400, Thailand

Correspondence e-mail: penchit@biotec.or.th, ubolsree@biotec.or.th

Received 12 June 2014
Accepted 20 October 2014

PDB references: SHMT with L-serine Schiff base, 4pfn; with PLP Schiff base, 4pff; complex with D-serine and folinic acid, 4oyt

Plasmodium parasites, the causative agent of malaria, rely heavily on *de novo* folate biosynthesis, and the enzymes in this pathway have therefore been explored extensively for antimalarial development. Serine hydroxymethyltransferase (SHMT) from *Plasmodium* spp., an enzyme involved in folate recycling and dTMP synthesis, has been shown to catalyze the conversion of L- and D-serine to glycine (Gly) in a THF-dependent reaction, the mechanism of which is not yet fully understood. Here, the crystal structures of *P. vivax* SHMT (*Pv*SHMT) in a binary complex with L-serine and in a ternary complex with D-serine (D-Ser) and (6*R*)-5-formyltetrahydrofolate (5FTHF) provide clues to the mechanism underlying the control of enzyme activity. 5FTHF in the ternary-complex structure was found in the 6*R* form, thus differing from the previously reported structures of SHMT–Gly–(6*S*)-5FTHF from other organisms. This suggested that the presence of D-Ser in the active site can alter the folate-binding specificity. Investigation of binding in the presence of D-Ser and the (6*R*)- or (6*S*)-5FTHF enantiomers indicated that both forms of 5FTHF can bind to the enzyme but that only (6*S*)-5FTHF gives rise to a quinonoid intermediate. Likewise, a large surface area with a highly positively charged electrostatic potential surrounding the *Pv*SHMT folate pocket suggested a preference for a polyglutamated folate substrate similar to the mammalian SHMTs. Furthermore, as in *P. falciparum* SHMT, a redox switch created from a cysteine pair (Cys125–Cys364) was observed. Overall, these results assert the importance of features such as stereoselectivity and redox status for control of the activity and specificity of *Pv*SHMT.

1. Introduction

Vivax malaria is prevalent in many tropical and subtropical regions. In contrast to *Plasmodium falciparum* (*Pf*), which causes virulent malaria and has been studied extensively, *P. vivax* (*Pv*) has received less attention and is considered to be a neglected pathogen since it usually causes benign symptoms. However, *Pv* infection leads to serious complications such as severe anaemia, malnutrition, spleen enlargement and coma (Quispe *et al.*, 2014; Tan *et al.*, 2008; Kochar *et al.*, 2005; Beg *et al.*, 2002). Similar to falciparum malaria, drug resistance in vivax malaria is widespread (Tjitra *et al.*, 2008). Therefore, the disease threat owing to *Pv* infection should not be underestimated.

Plasmodium serine hydroxymethyltransferase (SHMT) has recently been shown to be vital for parasite growth and development, making it a potential target for antimalarial drug development (Pornthanakasem *et al.*, 2012). SHMT is a pyridoxal-5′-phosphate (PLP)-dependent enzyme that cata-

lyzes the interconversion of L-serine (L-Ser) and tetrahydrofolate (THF) to glycine (Gly) and methylene tetrahydrofolate (MTHF). The enzyme provides activated one-carbon units for the synthesis of dTMP, choline and amino acids (Müller & Hyde, 2013). Heterologously expressed *Pv*SHMT was found to exhibit both THF-dependent and THF-independent catalytic activities, and could use D-serine in the THF-dependent reaction. However, unlike the binding of L-Ser, an enzyme–quinonoid intermediate was only observed upon binding with D-Ser (Sopitthummakhun *et al.*, 2009).

At present, structural coordinates for SHMT are available from nine organisms. Most of them are internal aldimines with a catalytic lysine residue linked to PLP or external aldimines with PLP linked to L-Ser or Gly. Among the *Bacillus stearothermophilus* SHMT (*bs*SHMT) structures, one is a PLP–L-*allo*-threonine (PLP-L-alloThr) Schiff base, while the others are PLP–Gly Schiff bases despite the presence of PLP and L-*allo*-Thr during crystallization (Pai *et al.*, 2009). Three structures of PLP–Gly and 5-formyltetrahydrofolate (5FTHF) complexes of *bs*SHMT, *E. coli* SHMT (*ec*SHMT) and mammalian mouse cytosolic SHMT (*m*SHMT) are also available (Trivedi *et al.*, 2002; Scarsdale *et al.*, 2000; Szebenyi *et al.*, 2000). In the tetrameric structure of rabbit cytosolic SHMT (*r*SHMT), triglutamated 5FTHF (triGlu-5FTHF) with a PLP internal aldimine was found in two active sites, while a PLP–Gly complex was found in the other two active sites (Fu *et al.*, 2003), and interestingly it also indicates favourable binding of the poly-γ-glutamate side chain of THF to mammalian SHMTs. Recently, the structure of *Pf*SHMT with a PLP internal aldimine revealed a cysteine pair at the THF pocket entrance acting as a redox switch that regulates the THF-dependent activity of SHMT, a unique feature of *Plasmodium* SHMT (Chitnumsub *et al.*, 2014). The distinct biochemical properties of *Plasmodium* SHMT and human SHMT (*h*SHMT; Pinthong *et al.*, 2014) can be used to design therapeutic species-specific inhibitors.

Although the structures of various complexes are essential for new antimalarial drug design and development, only one *Plasmodium* SHMT structure, that of *Pf*, has been successfully determined to date. In the present study, we have determined the structures of the binary complex *Pv*SHMT–L-Ser and the ternary complex of *Pv*SHMT with D-Ser and 5FTHF at 2.5 and 2.4 Å resolution, respectively. Differences in the accommodation of L-Ser and D-Ser in the *Pv*SHMT active site may account for the broad substrate specificity of SHMT and the lower catalytic efficiency for D-Ser in the THF-dependent catalytic function. In addition, the binding of D-Ser promoted the binding of (6*R*)-5FTHF instead of (6*S*)-5FTHF. Finally, a redox switch similar to that in *Pf*SHMT which can be induced by an oxidant drug such as methylene blue was found based on reversible disulfide formation between two cysteine residues.

2. Materials and methods

2.1. Expression and purification of *Pv*SHMT

E. coli BL21 (DE3) cells harbouring the pET-17b-*Pv*SHMT plasmid were cultured in Luria–Bertani medium containing 100 µg ml^{-1} ampicillin at 37°C. Expression of the *Pv*SHMT protein was induced by 0.4 m*M* IPTG when the culture OD_{600} reached 1 and was followed by incubation at 20°C for 22 h. The cells were harvested by centrifugation at 4420*g* for 10 min and were stored at −20°C. The frozen cell paste from a 6 l culture was resuspended in lysis buffer [25 m*M* HEPES pH 8.3, 0.5 m*M* EDTA, 1 m*M* dithiothreitol (DTT), 20%(*v*/*v*) glycerol] and passed though a French press at 10.3 MPa on ice three times. Soluble protein was fractionated by centrifugation at 39 000*g* for 1 h, and 20 µ*M* PLP was added to the crude extract followed by incubation with gentle stirring on ice for 30 min to prevent cofactor loss and to ensure formation of the holoenzyme. *Pv*SHMT was then fractionated by 0–30 and 30–80%(*w*/*v*) ammonium sulfate precipitation. After centrifugation at 39 000*g* for 30 min at 4°C, the 30–80%(*w*/*v*) ammonium sulfate precipitated protein fraction was resuspended and then dialyzed twice against 2 l lysis buffer at 4°C using a 10 kDa molecular weight cutoff dialysis bag. The dialyzed protein was centrifuged at 39 000*g* for 30 min at 4°C and applied onto a DEAE-Sepharose column (2.5 × 75 cm). The column was washed with two column volumes of lysis buffer plus 5 m*M* NaCl. *Pv*SHMT was eluted stepwise using two column volumes each of lysis buffer plus 10, 15 and 20 m*M* NaCl. The *Pv*SHMT fractions were yellow with an absorption peak at 422 nm. Fractions showing a single band of molecular weight 49 kDa on 12% SDS–PAGE were pooled and concentrated using Millipore centrifugal concentrators with 30 kDa molecular-weight cutoff. Purified *Pv*SHMT with freshly added 10 µ*M* PLP was exchanged into 25 m*M* HEPES pH 7.0, 0.5 m*M* EDTA, 10 m*M* DTT, 20%(*v*/*v*) glycerol. The protein concentration was assessed using the technique of Bradford (1976) using BSA as a standard. The purified *Pv*SHMT was stored at −80°C.

2.2. Interaction of *Pv*SHMT with D-Ser in the presence of (6*R*)- and (6*S*)-5FTHF and enzyme inhibition by (6*R*)- and (6*S*)-5FTHF

In order to observe enzyme spectrum changes in the presence of D-Ser and pure enantiomers of 5FTHF [(6*S*) or (6*R*); Merck Epova AG, Schaffhausen, Switzerland], *Pv*SHMT (30 µ*M*; A_{422} = 0.2) was incubated with folate (7.9 µ*M*) and the spectrum was recorded using a diode-array spectrophotometer. D-Ser (50 µ*M*) was then added and the spectral change was monitored for 20 min. The study was performed in 50 m*M* HEPES pH 8.0, 0.5 m*M* EDTA, 1 m*M* DTT at 25°C.

*Pv*SHMT activity was determined using a *Pv*SHMT–methylene tetrahydrofolate dehydrogenase (MTHFD) coupling assay as described previously (Sopitthummakhun *et al.*, 2012). Inhibition by either (6*S*)- or (6*R*)-5FTHF was assessed by measuring the initial velocity of the reaction in the presence of each enantiomer of 5FTHF [0.05–1.88 m*M* for (6*S*)-5FTHF and 1.55 m*M* for (6*R*)-5FTHF]. The inhibition constant (K_i) was calculated for (6*S*)-5FTHF based on the equation $V = (V_{max}K_i)/(K_i + [I])$ and the percentage inhibition was used to represent the inhibition efficacy of (6*R*)-5FTHF.

Table 1
Data-collection and refinement statistics of *Pv*SHMT complexes.

	PLP	PLP–L-Ser	PLP–D-Ser–(6*R*)-5FTHF
Wavelength (Å)	1	1	1
Space group	*C*2	*C*2	*C*2
Molecules in asymmetric unit	3	3	3
Resolution (Å)	29.17–2.30 (2.38–2.30)	29.49–2.50 (2.59–2.50)	28.84–2.40 (2.49–2.40)
Unit-cell parameters (Å, °)	*a* = 101.05, *b* = 58.33, *c* = 237.14, *β* = 90.014	*a* = 100.40, *b* = 57.94, *c* = 235.92, *β* = 90.014	*a* = 100.62, *b* = 58.12, *c* = 236.61, *β* = 90.002
No. of measured reflections	130608	129610	120462
No. of unique reflections	58848	44633	51056
Multiplicity	2.4 (2.0)	3.0 (2.7)	2.5 (1.8)
Completeness (%)	94.6 (85.0)	94.1 (82.5)	94.6 (84.9)
$\langle I/\sigma(I)\rangle$	27.2 (12.2)	38.73 (10.30)	20.4 (4.6)
$R_{\rm merge}$† (%)	3.2 (6.0)	2.8 (10.6)	4.7 (17.2)
Wilson *B* factor (Å^2)	34.9	44.3	47.7
Weight matrix in *REFMAC*5	0.05	0.04	0.06
FOM	0.826	0.804	0.804
R factor/$R_{\rm free}$ (%)	22.11/24.00	20.70/26.32	19.96/25.23
R.m.s. bond deviation (Å)	0.0072	0.0069	0.0083
R.m.s. angle deviation (°)	1.2138	1.1374	1.3820
Ramachandran plot, residues in (%)			
Most favoured regions	91.2	90.7	90.6
Additional allowed regions	8.0	8.3	8.8
Generously allowed regions	0.8	0.8	0.6
Disallowed regions	0.0	0.2	0.0
PDB code	4pff	4pfn	4oyt

† $R_{\rm merge} = \sum_{hkl}\sum_i |I_i(hkl) - \langle I(hkl)\rangle| / \sum_{hkl}\sum_i I_i(hkl)$, where $I_i(hkl)$ is the intensity of the *i*th measurement of an equivalent reflection with indices *hkl* and $\langle I(hkl)\rangle$ is the mean intensity of $I_i(hkl)$ for all *i* measurements.

2.3. Identification of a redox switch

To determine whether *Pv*SHMT activity is affected by the redox environment, *Pv*SHMT (100 µ*M*) prepared in the absence of DTT was incubated with 10 m*M* DTT, and an aliquot of the enzyme (0.5 µ*M*) was taken for initial velocity measurements at different time points. To test activity under oxidizing conditions, a similar experiment was performed by incubating the protein prepared in the presence of DTT with 50 m*M* hydrogen peroxide (H_2O_2). The percentage enzyme activity in the presence of DTT or H_2O_2 was plotted against incubation time.

Redox switching was also monitored by incubating the enzyme (100 µ*M*) in the presence of DTT (10 m*M*) followed by H_2O_2 (50 m*M*) or methylene blue (MB; 1 m*M*) and then DTT (10 m*M*). Activity was measured at different time points.

2.4. Crystallization of *Pv*SHMT

*Pv*SHMT was crystallized using the microbatch method in a 60-well plate (1 mm diameter at the bottom of each well) covered with 6 ml baby oil (a mixture of mineral oil, olive oil and vitamin E; PZ Cussons, Thailand; Chitnumsub *et al.*, 2004). Protein–ligand complexes were prepared by mixing 0.38 m*M* *Pv*SHMT with 0.86 m*M* PLP, 62 m*M* *β*-mercaptoethanol (BME), 87 m*M* Gly, L-Ser or D-Ser and 43 m*M* 5FTHF (Sigma–Aldrich, USA). The protein mixture was equilibrated on ice for 30 min for complex formation. Crystallization was set up on a microplate by first pipetting 1 µl crystallization solution into a well, which was then layered with 6 ml oil followed by addition of 1 µl of the protein complex through the oil layer. Protein crystals of *Pv*SHMT grew to optimum size in 1–4 d at 293 K in 20–21%(*w*/*v*) PEG 4000, 70–90 m*M* NaCl, 100 m*M* Tris–HCl pH 8.5, 15%(*v*/*v*) trifluoroethanol (TFE).

2.5. Structure determination

A single crystal was flash-vitrified in liquid nitrogen using 20%(*v*/*v*) glycerol in the crystallization condition as a cryoprotectant. X-ray diffraction data were collected at 100 K at a wavelength of 1 Å using an ADSC Quantum 315r CCD detector on beamline 13B1 at NSRRC, Taiwan. Data were processed using the *HKL*-2000 package (Otwinowski & Minor, 1997). X-ray diffraction data and refinement statistics are listed in Table 1. The structure of *Pv*SHMT was determined by molecular replacement using *Phaser* in the *CCP*4 suite (Winn *et al.*, 2011) with the chain *A* protomer from the *Pf*SHMT coordinates (PDB entry 4o6z; 83% identical to *Pv*SHMT) as the phasing model (Chitnumsub *et al.*, 2014). Model building and structure refinement were carried out using *Coot* (Emsley & Cowtan, 2004; Emsley *et al.*, 2010) and *REFMAC*5 (Murshudov *et al.*, 2011), respectively. The structure was validated by *PROCHECK* (Laskowski *et al.*, 1993) and using the wwPDB validation server. Superposition of structures was carried out using *LSQMAN* (Kleywegt, 1996) and figures were prepared using the *PyMOL* molecular-graphics program (http://www.pymol.org).

2.6. PDB codes

Atomic coordinates and structure factors have been deposited with the following PDB codes: 4pff for the PLP internal aldimine, 4pfn for the PLP–L-Ser external aldimine and 4oyt for the PLP–D-Ser aldimine with (6*R*)-5FTHF.

3. Results and discussion

3.1. Crystallization

The *Pv*SHMT complexes crystallized in two different space groups: $P3_2$ and *C*2. Space group $P3_2$ with unit-cell parameters *a* = 58.30, *b* = 58.30, *c* = 473.31 Å, *α* = *β* = 90, *γ* = 120° was obtained for the complex with an amino-acid substrate or mimic without folate, while space group *C*2 with unit-cell parameters *a* = 100, *b* = 58, c = 237 Å, *α* = *γ* = 90, *β* = 90.01° was obtained in the presence of a folate derivative. Although the diffraction quality of the crystals in the two space groups was comparable, a lower resolution was obtained for the $P3_2$ crystal data owing to incompleteness of the high-resolution shell caused by overlapping spots along the longest axis, and

these data were not used for further analysis. Two crystals of particular interest were obtained in space group *C*2. The first was a crystal of the binary complex of *Pv*SHMT with L-Ser, which diffracted to 2.5 Å resolution and was obtained in the presence of methotrexate (MTX), although there was no density for MTX in the final map. The second was a ternary complex of *Pv*SHMT with D-Ser and 5FTHF, which included positive density for D-Ser and (6*R*)-5FTHF (2.4 Å resolution).

3.2. Crystal structure of *Pv*SHMT

The overall structure of *Pv*SHMT was found to be very similar to that of *Pf*SHMT (Chitnumsub *et al.*, 2014), existing as a twofold symmetric homodimer with two catalytic sites. The folate binding pocket of *Pv*SHMT is distinct from that of bacterial SHMTs but is similar to that of mammalian SHMTs, although the kinetic properties of *Pv*SHMT and mammalian SHMT reflect the subtle differences in the binding pockets and overall quaternary structures (Pinthong *et al.*, 2014). The crystal structure of *Pv*SHMT with D-Ser and 5FTHF shows that the folate pocket of *Pv*SHMT is 1 Å wider than those of mammalian and bacterial SHMTs, possibly affecting the interactions and affinity between the active-site residues of *Pv*SHMT and folate analogues (see §3.4).

On the other hand, the PLP and amino-acid pockets of SHMTs from all organisms appear to be alike. The two active sites for the PLP cofactor in the *Pv*SHMT homodimer are very close, with distances between PLP α-phosphate moieties of the two active sites of 18.2 Å and distances between C4A (an aldehyde C atom) of 27 Å (Fig. 1*a*). The interface of the two protomers separating the active site comprises both hydrophobic and electrostatic interactions owing to residues Leu99, Arg243, His274 and Lys277 (Fig. 1*a*). Electrostatic interactions include hydrogen bonds from the His274 side chain to the Lys277 side chain and the Arg243 backbone of the second protomer and from the Ser51 carbonyl backbone to the Arg243 side chain. Starting from Lys237 in the middle of the active site, the PLP amino-acid pocket is surrounded by five conserved loops including residues 99–102, 181–185 and 234–237 from the first protomer and 51–64 and 272–274 from the second protomer. Residues Tyr′54, Glu′56 and Tyr′64 in the 51–64 or 'YEY' (SNK**Y**S**E**GYPKKRY**Y**) loop are important for substrate binding and catalysis (Szebenyi *et al.*, 2004; Rajaram *et al.*, 2007), with Glu′56 and Tyr′64 being particularly flexible (see §§3.3 and 3.4).

In structures with and without amino-acid substrates, the hydrogen-bond network at the PLP phosphate moiety is significantly different at Arg243, which adopts different side-

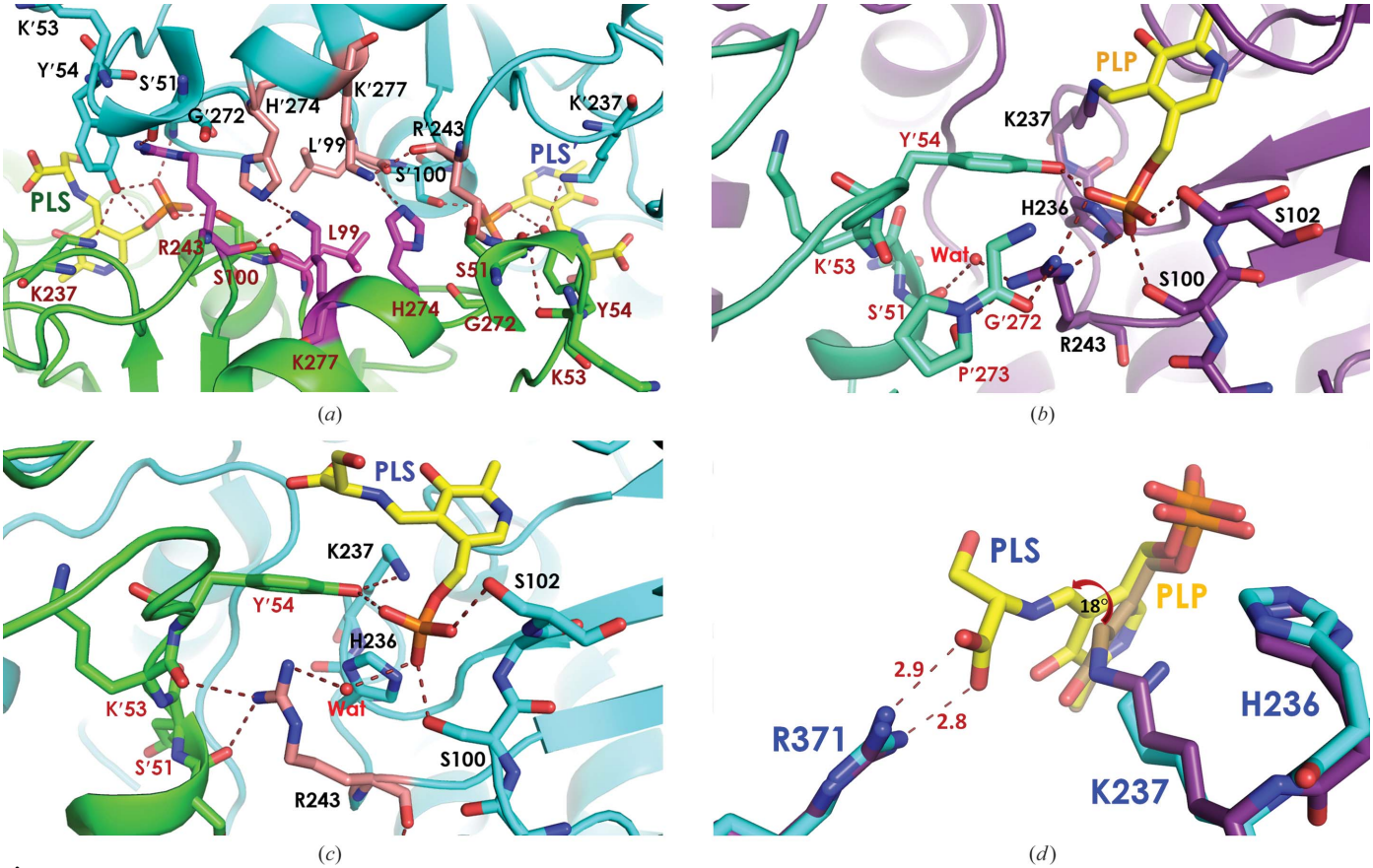

Figure 1
Crystal structure of *Pv*SHMT. (*a*) The dimer interface of two PLP and amino-acid substrate pockets with interactions contributed by Leu99, Arg243, His274 and Lys277 from protomers *A* (coloured cyan and pink) and *B* (coloured green and magenta). (*b*, *c*) Conformation of Arg243 (*b*) in the PLP–Lys237 Schiff-base complex and (*c*) in the PLP–L-Ser Schiff-base complex (PLS). (*d*) Superposition of the 4pff (violet) and 4pfn (cyan) dimers shows the rotation of the PLP ring by 18° from the PLP–Lys237 Schiff base (orange) to the PLP–L-Ser Schiff base (yellow).

chain conformations (Figs. 1*b* and 1*c*). In the internal aldimine complex, the Arg243 side chain hydrogen bonds directly to the PLP phosphate group and to the main-chain carbonyl of Gly′272 and Pro′273 (Fig. 1*b*). In contrast, in the external aldimine form of PLP bound to L-Ser the Arg243 side chain does not interact with PLP directly, but rather *via* a water bridge to the PLP phosphate moiety and direct hydrogen bonding to the main-chain carbonyl of Ser′51 on the 3_{10}-helix and Lys′53 of the YEY loop (Fig. 1*c*). This interaction with Ser′51 and Lys′53 probably provides additional anchoring interactions for holding the YEY loop in place during THF-dependent reactions. Overall, the difference in Arg243 conformation between the two PLP complexes is suggestive of functional significance of Arg243 in *Pv*SHMT catalysis. Finally, the internal and external aldimine forms also exhibit conformational differences in the PLP pyridoxal ring (Fig. 1*d*), which is rotated by 18° at C4A with a focal point at the pyridine N atom in the PLP Schiff base.

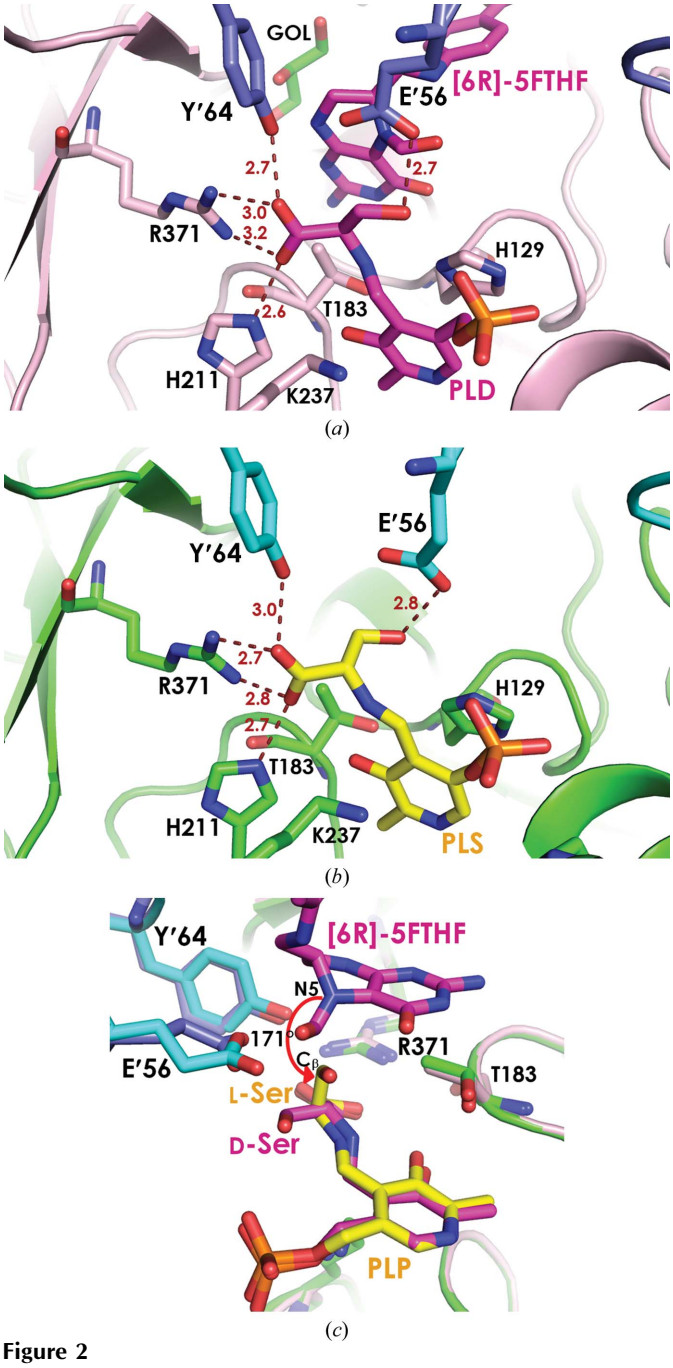

Figure 2
Amino-acid binding pocket of *Pv*SHMT. (*a*) D-Ser in the ternary complex *Pv*SHMT–D-Ser–5FTHF with the PLP–D-Ser (PLD) Schiff base and (6*R*)-5FTHF coloured in magenta in protomer *A* (pink) and protomer *B* (blue) with a glycerol (GOL) molecule in green. (*b*) L-Ser in the binary complex *Pv*SHMT–L-Ser with a PLP–L-Ser (PLS) Schiff base. (*c*) Superposition of the two complexes showing the configurations of D-Ser and L-Ser.

3.3. Binding of D-Ser and L-Ser

The structures of the *Pv*SHMT–L-Ser and *Pv*SHMT–D-Ser–5FTHF complexes were used to assess the amino-acid binding pocket. Like the L-Ser substrate, D-Ser was found in the crystal structure as an external aldimine with PLP, indicating that D-Ser is similarly capable of replacing the PLP–Lys237 Schiff base. This result agrees with the biochemical characterization of SHMT, which showed that the enzyme is catalytically active towards both serine isomers (Sopitthummakhun *et al.*, 2009).

Key interactions with both D-Ser and L-Ser consist of two components: hydrogen bonds from the conserved residues in the PLP pocket (Ser100, Ser102, Thr183, Asp208, His129, His236, Tyr′54 and Gly′272) and the amino-acid pocket (Ser34, His211, Arg371, Glu′56 and Tyr′64). Although the stabilizing interactions are from identical residues, three major differences between D-Ser and L-Ser binding can be observed. Firstly, the salt-bridge interactions between the Arg371 side chain and the carboxyl group of D-Ser are distorted, at distances of 3.0 and 3.2 Å, while two ideal salt bridges at distances of 2.7 and 2.8 Å are observed to L-Ser (Fig. 2). Also, D-Ser is mainly restrained by the side-chain carboxyl group of Glu′56 from a neighbouring protomer, with the D-Ser β-hydroxymethyl side chain binding in the space between the PLP phosphate moiety, Tyr′64 and Glu′56, and being sterically controlled by the carboxyl moiety of Glu′56 (Fig. 2*a*). In contrast, the L-Ser binding pocket is extended towards the folate pocket and is surrounded by His129, Glu′56 and Tyr′64 (Fig. 2*b*). Furthermore, superposition of the two complexes reveals different orientations of the D-Ser and L-Ser side chains (Fig. 2*c*). The D-Ser side chain is oriented away from N5 of THF and is found in the extended plane of the PLP ring, while the L-Ser side chain is perpendicular to N5. Altogether, these differences may contribute the differences in K_m between D-Ser and L-Ser (47 ± 6 and 0.18 ± 0.03 m*M*, respectively; Sopitthummakhun *et al.*, 2009) and the overall catalytic efficiency (0.006 and 28 s^{-1} mM^{-1}, respectively). Nevertheless, these observations indicate that the overall amino-acid binding site of *Pv*SHMT is sufficiently plastic to accommodate both the D- and L-isomers of the substrate.

3.4. Binding of (6*R*)-5FTHF in the presence of D-Ser

Folate binding can also be examined in the context of the *Pv*SHMT–D-Ser–5FTHF complex. Only (6*R*)-5FTHF was observed in the folate-binding pocket despite the use of a

racemic mixture of 5FTHF for crystallization, suggesting that only the (6*R*)-5FTHF enantiomer binds to *Pv*SHMT–D-Ser or that only the (6*R*)-5FTHF complex crystallized. The former is less likely, as (6*S*)-5FTHF has been observed with a Gly external aldimine in SHMT structures from other organisms (Scarsdale *et al.*, 2000; Trivedi *et al.*, 2002; Fu *et al.*, 2003) and (6*S*)-THF is an active substrate with both L-Ser and D-Ser for *Pf*SHMT and *Pv*SHMT. (6*R*)-5FTHF binding is stabilized by van der Waals interactions from Tyr′63, Phe′266, Pro′267, Phe134, Leu130, Leu124 and Val141. In the three protomers in each asymmetric unit, the distances between the D-Ser β-hydroxyl group and the 5FTHF 5-formyl group are 2.6, 2.8 and 3.6 Å, indicating hydrogen-bonding and van der Waals interactions. Structural comparisons of the THF pocket show that the *Pv*SHMT pocket is 1 Å wider from His129 to Asn356, where the pterin ring of THF is located, compared with mammalian and bacterial SHMTs at the equivalent pair of residues (His126^{r,ec} to Asn347^{r,ec}).

Interestingly, this wider pocket may have allowed the accommodation of a glycerol molecule in one active pocket of each native enzyme, occupying the space between (6*R*)-5FTHF and residues 354–357 and providing additional interaction between the protein and 5FTHF (Fig. 3*a*). The first hydroxyl group of the glycerol forms a hydrogen bond to the main-chain carbonyl of Lys355 (2.9 Å), and the second hydroxyl group forms a hydrogen bond to the side chains of Asn356 (2.9 Å) and Thr357 (3.2 Å). A water molecule links the second hydroxyl group (2.6 Å) and the 2-NH_2 moiety (3.1 Å) of the (6*R*)-5FTHF pterin ring. The third hydroxyl group of the glycerol was 3.4 Å from the sulfhydryl group of Cys364, which is one of a pair of cysteines that are involved in forming the redox switch that was found to regulate *Pf*SHMT activity (Chitnumsub *et al.*, 2014). These observations indicate interactions that can be useful for inhibitor design. In contrast, the binding of (6*S*)-5FTHF in *r*SHMT, *ec*SHMT and *bs*SHMT is stabilized *via* direct hydrogen bonding to Asn347^{r,ec} and Asn341^{bs}, which are equivalent to Asn356^{Pv}.

The position of the bound (6*R*)-5FTHF is also subtly different from that of (6*S*)-5FTHF in other SHMTs (Fig. 3*b*). Amino-acid sequence alignment suggests that THF binding to *Pv*SHMT may be influenced by steric hindrance from the nonconserved Thr183^{Pv} (equivalent to Ser203^{h} and Ser175^{r,ec}), lying underneath the pteridine ring of 5FTHF or THF. The distance of the β-methyl group of Thr183^{Pv} to C4a or C8a of the 5FTHF pterin ring in *Pv*SHMT–D-Ser–5FTHF is 3.9–4.1 Å, while that of the C$^{\beta}$ atom of Ser175^{r} to the same atoms of 5FTHF is 4.1–4.4 Å in *r*SHMT, suggesting a shift in THF positioning. *Pv*SHMT binding of (6*R*)-5FTHF and the D-Ser external aldimine alters the conformation of at least three residues, namely Glu′56, Tyr′63 and Tyr′64 (Fig. 3*b*).

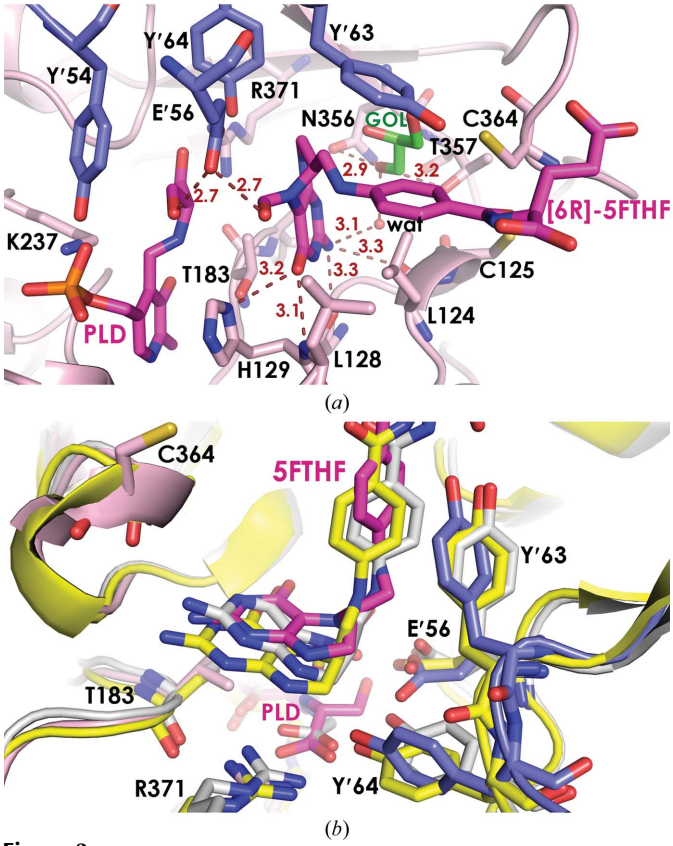

Figure 3
Binding of (6*R*)-5FTHF in the ternary *Pv*SHMT–D-Ser–(6*R*)-5FTHF complex. (*a*) Interactions between *Pv*SHMT and (6*R*)-5FTHF, with dashed lines indicating hydrogen-bond distances in Å from residues in protomers *A* (pink) and *B* (blue) to the substrates PLP–D-Ser Schiff base (PLD) and (6*R*)-5FTHF in magenta and a glycerol (GOL) molecule in green. A water molecule (wat; red sphere) forms a bridge between 5FTHF and the protein. (*b*) Superposition of *Pv*SHMT–D-Ser–(6*R*)-5FTHF (in blue and pink), *ec*SHMT–Gly–(6*S*)-5FTHF (PDB entry 1dfo, white) and *r*SHMT–PLP–(6*S*)-triGlu-5FTHF (PDB entry 1ls3, yellow). Residue labelling is based on the *Pv*SHMT sequence.

3.5. Probing the interactions of 5FTHF in the presence of serine isomers

To verify external aldimine formation with D-Ser in the presence of (6*R*)-5FTHF in solution, spectroscopic studies of *Pv*SHMT with D-Ser and either (6*S*)- or (6*R*)-5FTHF were performed. The formation of an external aldimine (420 nm) was observed for the binding of D-Ser to *Pv*SHMT in the presence of (6*R*)-5FTHF (Fig. 4*a*), while an additional peak at 500 nm indicative of an enzyme–quinonoid intermediate was detected for (6*S*)-5FTHF (Fig. 4*b*). These suggested that the stereoisomer of 5FTHF has an effect on the binding of D-Ser to *Pv*SHMT, resulting in different intermediates.

The interaction of *Pv*SHMT with each enantiomer of 5FTHF was further explored based on an inhibition study using an SHMT–MTHFD coupling assay *via* L-Ser–THF. Inhibition *via* D-Ser–THF was not studied owing to the low catalytic efficiency of the D-Ser substrate. Interestingly, while (6*S*)-5FTHF inhibited *Pv*SHMT with a K_i of 0.21 m*M*, (6*R*)-5FTHF inhibited *Pv*SHMT only slightly, with the activity decreasing by 30% at 1.55 m*M*. The results suggest that the binding affinity of (6*S*)-5FTHF to *Pv*SHMT in the presence of L-Ser is higher than that of (6*R*)-5FTHF.

3.6. Proposed *Pv*SHMT catalytic mechanism for the THF-dependent reaction

The mechanism of the THF-dependent SHMT reaction is still unclear. The reaction either proceeds through retro-aldol

cleavage to form free formaldehyde before the formation of MTHF, or the N5 atom of THF directly participates in nucleophilic replacement to form Gly (Schirch & Szebenyi, 2005; Schirch, 1998; Trivedi *et al.*, 2002). The likelihood of nucleophilic replacement was examined by superposition of *bs*SHMT co-complexed with (6*S*)-5FTHF and PLP–Gly (PDB entry 1kl2), PLP–Gly (PDB entry 1kl1) or PLP–L-Ser adducts (PDB entry 1kkp), revealing a sufficiently close distance of 2.8 Å between N5 of 5FTHF and C^{β} of the L-Ser external aldimine but an angle of 150° from the pteridine ring to the C^{β} methylene group of the L-Ser external aldimine. Nucleophilic displacement would require the serine C^{β} methylene group to be perpendicular to the pteridine ring of THF or to align close to 180° with the *p* orbital of N5. Unfortunately, PLP–L-Ser adducts of *m*SHMT and *r*SHMT are not available for additional analysis (Szebenyi *et al.*, 2000; Fu *et al.*, 2003). The *Pv*SHMT structures were therefore used to probe the position of THF and to gain insights into the SHMT mechanism.

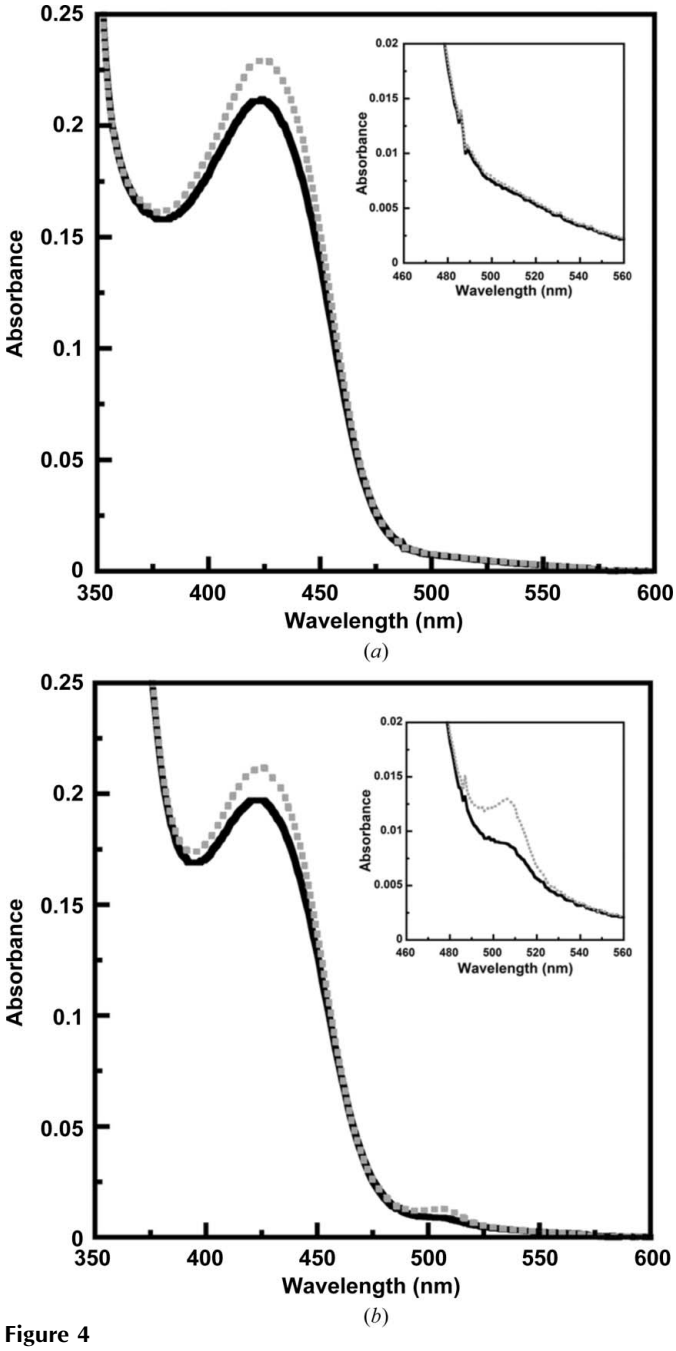

Figure 4
Spectral change of *Pv*SHMT upon binding of D-Ser in the presence of (*a*) (6*R*)-5FTHF and (*b*) (6*S*)-5FTHF. The solid line is the spectrum of *Pv*SHMT in the presence of 5FTHF, while the dashed line is the spectrum after the addition of D-Ser.

Structures of *Pv*SHMT–L-Ser and *Pv*SHMT–D-Ser–(6*R*)-5FTHF were superimposed to pinpoint the position of THF in the pocket (Fig. 2*c*). The N5 atom of 5FTHF was found to be perpendicular to the serine C^{β} methylene group and within 3 Å, which is shorter than the van der Waals distance, rendering nucleophilic attack feasible. Moreover, the C^{α}—C^{β}—N5 angle is 171°, which is nearly a 180° alignment with the *p* orbital of N5. Therefore, these structures support the proposal that *Pv*SHMT undergoes nucleophilic displacement in catalyzing the reaction between L-Ser and THF in the crystallization conditions at pH 8.

3.7. Implication for the preferred accommodation of poly-γ-glutamate–THF

Two solvent-exposed loops on the periphery of the folate-binding pocket were examined to assess whether *Pv*SHMT has a preference for polyglutamated or monoglutamated THF. In the *Pv*SHMT–D-Ser–5FTHF structure, the two stretches (residues Asp136–Lys140 of loop-C125^{Pv} and Asp361–Ser366 of loop-C364^{Pv}) have the highest temperature factors, with an average *B* value of 70 Å^2 compared with 44 Å^2 for the overall structure, suggesting that even in the presence of bound (6*R*)-5FTHF there is flexibility similar to that in structures solved without bound folate (Chitnumsub *et al.*, 2014). The positively charged Lys138 and Lys139 side-chain amines of loop-C125^{Pv} are 6.0–6.5 Å from the L-glutamate group of monoglutamated (6*R*)-5FTHF and unexpectedly remain in the same conformation in the presence or absence of bound folate, similar to their equivalent in *r*SHMT complexed with triGlu-5FTHF and PLP. This *r*SHMT ternary-complex structure (PDB entry 1ls3; Fu *et al.*, 2003) shows a distance of 3.1 Å between the α-carboxyl of the third glutamate moiety and the Lys134 side-chain amine situated on the apex of its loop-C125 equivalent, compared with 7.5 Å for the α-carboxyl of the first Glu moiety of triGlu-5FTHF. Whether or not the unchanged conformation of the loop observed for *Pv*SHMT is owing to the preferred accommodation of polyglutamated THF substrates is unclear. However, unlike mammalian and *Plasmodium* SHMTs, bacterial SHMTs contain only a short loop of small hydrophobic side chains (*ec*SHMT-P132V133) in the corresponding position and only accommodate monoglutamated THF.

Loop-C364^{Pv}, on the other hand, is adjacent to the *p*-aminobenzoic acid (*p*ABA) moiety of 5FTHF. Its equivalents in *ec*SHMT and *bs*SHMT adopt a closed conformation in the presence of bound 5FTHF, in which Pro356^{ec} makes van der Waals contact with the *p*ABA moiety and Phe357^{ec} makes a π-edge interaction with Tyr′64^{ec} (equivalent to Tyr′63^{Pv}).

This conformational change in bacterial SHMTs contributes to the THF binding affinity. However, such a closed conformation was not observed in *Plasmodium* and mammalian SHMTs (Fu *et al.*, 2003).

Another difference lies in the SHMT architecture and the electrostatic potential. The surface of mammalian and *Plasmodium* SHMTs is positively charged near the folate glutamate moiety, while that of bacterial SHMTs is negatively charged (Fig. 5). Additionally, positively charged residues, namely Lys138 and Lys139 on loop-C125^{Pv} and Lys′60 and Lys′61 on the YEY loop of the second protomer, are located on the surface of the THF-binding pocket (Fig. 5*a*). It is likely that these residues contribute to the binding affinity of poly-γ-glutamate–THF.

Altogether, the positively charged surface and the characteristics of loop-C125^{Pv} and loop-C364^{Pv} suggest that *Plasmodium* SHMT may preferentially accommodate the poly-γ-glutamate side chain of THF rather than the mono-γ-glutamate side chain. This is in good agreement with previous findings that a polyglutamated THF pool is present in *Plasmodium* by the conversion of *p*ABA to THF with 3–5 glutamate residues (Wang *et al.*, 2004; Müller & Hyde, 2013).

3.8. Oxidative inhibition in *Pv*SHMT

A previous study revealed that the THF-dependent activity of *Pf*SHMT is regulated by the redox status of a cysteine pair (Chitnumsub *et al.*, 2014). Sequence conservation (Cys125 and Cys364) and the presence of the sulfhydryl form in the *Pv*SHMT–D-Ser–5FTHF and *Pv*SHMT–L-Ser complexes and the disulfide in the *Pv*SHMT–PLP structure prompted an examination of the dependence of *Pv*SHMT activity on its

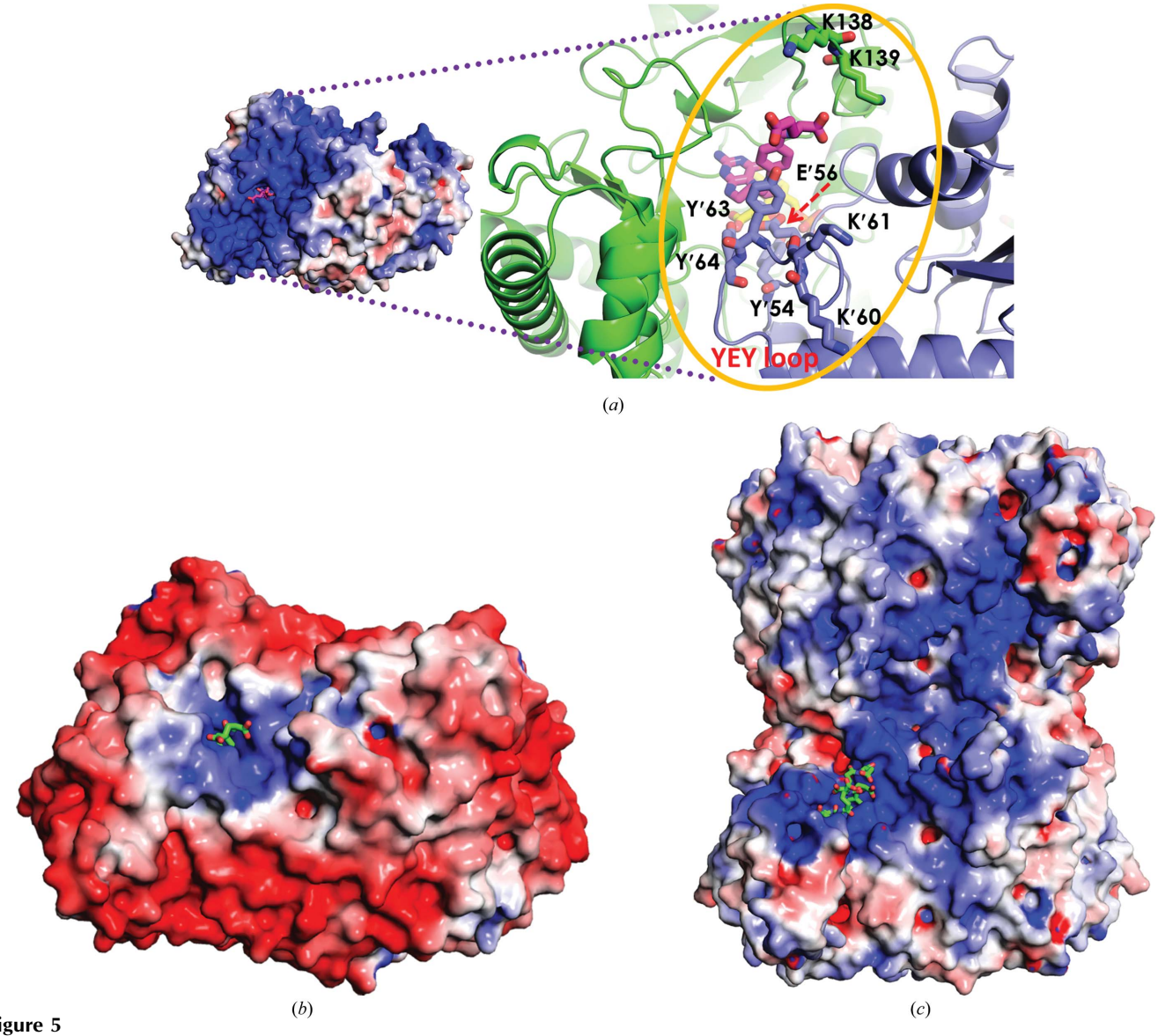

Figure 5
Surface electrostatic potential. (*a*) Dimeric *Pv*SHMT–D-Ser–(6*R*)-5FTHF, with the inset showing key residues involved in folate binding: Tyr′54, Glu′56, Lys′60, Lys′61, Tyr′63 and Tyr′64 in the YEY loop and Lys138 and Lys139 in loop-C125. (*b*) Dimeric *ec*SHMT (PDB entry 1dfo). (*c*) Tetrameric *r*SHMT (PDB entry 1ls3). Each structure contains 5FTHF, but that of *r*SHMT contains triGlu-5FTHF.

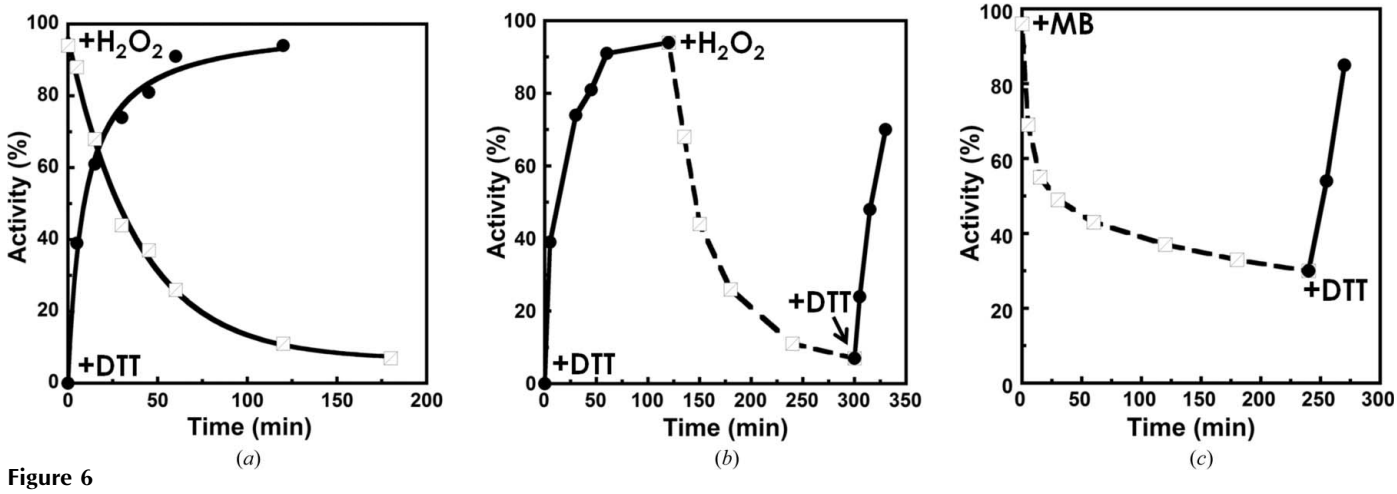

Figure 6
THF-dependent activity of *Pv*SHMT in relation to the redox environment. (*a*) Time course of *Pv*SHMT activity in the presence of DTT (black circles) and H_2O_2 (empty squares). (*b*, *c*) Alteration of *Pv*SHMT activity in response to redox switching using the oxidant–reductant pairs DTT–H_2O_2 and DTT–methylene blue (DTT, solid line with black circles; H_2O_2 and methylene blue, dashed line with empty squares), respectively.

redox state. In this study, H_2O_2 and DTT were used as oxidizing and reducing agents, respectively. The presence of DTT (10 m*M*) led to ∼40% enzyme activity within 5 min of incubation at 0°C and to 90% activity within 1 h (Fig. 6*a*). The addition of 50 m*M* H_2O_2 to *Pv*SHMT in 10 m*M* DTT resulted in a decreased *Pv*SHMT activity over time to less than 10% after a 3 h incubation (Fig. 6*a*).

Switching of enzyme activity based on the redox environment was also observed for *Pv*SHMT. The activity was altered sequentially when it was incubated with DTT, H_2O_2 and then DTT (Fig. 6*b*). Based on the results obtained, the sensitivity of the enzyme to the antimalarial drug methylene blue, a redox dye, was then examined. The effect was similar to that of H_2O_2 but at a slower rate, and was reversed if DTT was subsequently added (Fig. 6*c*). These observations indicated that *Pv*SHMT activity can be controlled through a redox switch like that of *Pf*SHMT. The oxidation/reduction reactions were slow, suggesting that there are other steps occurring as a result of the change in the cysteine redox status. Further investigation is warranted to explore this switch as a drug-development target by focusing on small molecules that alter the redox state of *Plasmodium* SHMT to the stable and inactive oxidized state. This molecule could also serve as an adjuvant to augment the antimalarial activity of other drugs.

4. Conclusions

Although SHMT has long been proposed to be a drug target for the development of anticancer agents and antibacterials, progress has been slower than with other enzymes of the folate-biosynthesis pathway. SHMT from various organisms is known to catalyze diverse reactions including THF-dependent and THF-independent reactions and can use different amino-acid substrates such as serine, glycine and β-phenylserine. Furthermore, *Plasmodium* and human SHMTs have recently been shown to catalyze both D- and L-isomers of serine in a THF-dependent manner (Pinthong *et al.*, 2014). Nonetheless, the underlying mechanism that controls enzyme activity is not obvious, as different lines of evidence support different mechanisms.

The crystal structures of complexes of *Pv*SHMT with L-Ser and D-Ser–(6*R*)-5FTHF revealed that the arrangement of the residues in the amino-acid binding pocket is restricted by the configuration of the bound amino-acid substrate, leading to different catalytic efficiencies towards each substrate isomer. Although both (6*R*)- and (6*S*)-5FTHF can bind *Pv*SHMT in the presence of L-Ser and D-Ser, different binding affinities and intermediates were observed depending on the stereoisomeric substrate pair between the amino acids and folates, suggesting that the occurrence of a specific stereoisomer pair has a role in controlling the enzyme activity. The plasticity and chemical space in the *Pv*SHMT active site are also factors in allowing the binding of different amino acids, as demonstrated previously (Sopitthummakhun *et al.*, 2009). These findings have several implications. For example, it is possible that SHMT follows different mechanisms for catalysis depending on the substrate present. Therefore, understanding the chemistry of PLP-dependent reactions and the structure of specific SHMTs is necessary. The knowledge gained may lead to other applications of this enzyme such as stereospecific biocatalysis (Gutierrez *et al.*, 2008; Kreuzman *et al.*, 1997). From a drug-discovery point of view, inhibitor design with stereoisomers should be performed cautiously as non-equivalent efficacy can be foreseen.

Based on the structure–function analysis of *Pv*SHMT, several types of antimalarials targeting SHMT can be designed. The first category comprises conventional inhibitors occupying the amino acid- or folate-binding site. For this type of inhibitor, the stereoisomer form should be taken into account in order to gain maximum efficacy, as demonstrated by biochemical and structural studies of D-Ser *versus* L-Ser and (6*S*)-5FTHF *versus* (6*R*)-5FTHF. Another consideration is the polarity of the compound. Compounds that mimic the poly-glutamate moiety of the folate substrate would preferably inhibit the enzyme, as a large surface area of *Plasmodium* SHMT is highly positively charged. Owing to the different

electrostatic surface potentials between bacterial and *Plasmodium* SHMTs, inhibitors can be specifically designed for malarial and bacterial SHMTs. Last but not least, inhibitors that irreversibly oxidize the disulfide bond of the cysteine redox switch in *Plasmodium* SHMT could constitute another family of promising antimalarial drugs.

This study was supported financially by the Cluster Program and Management Office, National Science and Technology Development Agency, Thailand (grants CPMO-P-00-20029, CPMO-DD/P-10-11274 and CPMO-P-13-00835), Synchrotron Light Research Institute (Public Organization) (grant 2-2549/LS01 to UL and grant 2551/08 to P. Chitnumsub), Thailand Research Fund grant No. RTA5680001 and the Faculty of Science, Mahidol University (to P. Chaiyen) and Thailand Research Fund grant No. MRG5580066 and the Faculty of Science, Burapha University (to SM). We thank Merck Epova AG (Schaffhausen, Switzerland) and Professor Martino di Salvo (Università di Roma) for providing all of the high-quality folate derivatives used and the plasmid for expressing MTHFD, respectively. We gratefully acknowledge the National Synchrotron Radiation Research Center (Taiwan) for the use of beamline 13B1 and the Synchrotron Light Research Institute (Public Organization) for the use of the home X-ray diffractometer. We specially thank Dr Samaporn Teeravechyan for final language editing.

References

Beg, M. A., Khan, R., Baig, S. M., Gulzar, Z., Hussain, R. & Smego, R. A. Jr (2002). *Am. J. Trop. Med. Hyg.* **67**, 230–232.
Bradford, M. M. (1976). *Anal. Biochem.* **72**, 248–254.
Chitnumsub, P., Ittarat, W., Jaruwat, A., Noytanom, K., Amornwatcharapong, W., Pornthanakasem, W., Chaiyen, P., Yuthavong, Y. & Leartsakulpanich, U. (2014). *Acta Cryst.* D**70**, 1517–1527.
Chitnumsub, P., Yavaniyama, J., Vanichtanankul, J., Kamchonwongpaisan, S., Walkinshaw, M. D. & Yuthavong, Y. (2004). *Acta Cryst.* D**60**, 780–783.
Emsley, P. & Cowtan, K. (2004). *Acta Cryst.* D**60**, 2126–2132.
Emsley, P., Lohkamp, B., Scott, W. G. & Cowtan, K. (2010). *Acta Cryst.* D**66**, 486–501.
Fu, T.-F., Scarsdale, J. N., Kazanina, G., Schirch, V. & Wright, H. T. (2003). *J. Biol. Chem.* **278**, 2645–2653.
Gutierrez, M. L., Garrabou, X., Agosta, E., Servi, S., Parella, T., Joglar, J. & Clapés, P. (2008). *Chem. Eur. J.* **14**, 4647–4656.
Kleywegt, G. J. (1996). *Acta Cryst.* D**52**, 842–857.
Kochar, D. K., Saxena, V., Singh, N., Kochar, S. K., Kumar, S. V. & Das, A. (2005). *Emerg. Infect. Dis.* **11**, 132–134.
Kreuzman, A. J., Zock, J. M., Dotzlaf, J. E., Vicenzi, J. T., Queener, S. W. & Yeh, W. K. (1997). *J. Ind. Microbiol. Biotechnol.* **19**, 369–377.
Laskowski, R. A., MacArthur, M. W., Moss, D. S. & Thornton, J. M. (1993). *J. Appl. Cryst.* **26**, 283–291.
Müller, I. B. & Hyde, J. E. (2013). *Mol. Biochem. Parasitol.* **188**, 63–77.
Murshudov, G. N., Skubák, P., Lebedev, A. A., Pannu, N. S., Steiner, R. A., Nicholls, R. A., Winn, M. D., Long, F. & Vagin, A. A. (2011). *Acta Cryst.* D**67**, 355–367.
Otwinowski, Z. & Minor, W. (1997). *Methods Enzymol.* **276**, 307–326.
Pai, V. R., Rajaram, V., Bisht, S., Bhavani, B. S., Rao, N. A., Murthy, M. R. & Savithri, H. S. (2009). *Biochem. J.* **418**, 635–642.
Pinthong, C., Maenpuen, S., Amornwatcharapong, W., Yuthavong, Y., Leartsakulpanich, U. & Chaiyen, P. (2014). *FEBS J.* **281**, 2570–2583.
Pornthanakasem, W., Kongkasuriyachai, D., Uthaipibull, C., Yuthavong, Y. & Leartsakulpanich, U. (2012). *Malar. J.* **11**, 387–395.
Quispe, A. M., Pozo, E., Guerrero, E., Durand, S., Baldeviano, G. C., Edgel, K. A., Graf, P. C. & Lescano, A. G. (2014). *Am. J. Trop. Med. Hyg.* **91**, 11–17.
Rajaram, V., Bhavani, B. S., Kaul, P., Prakash, V., Appaji Rao, N., Savithri, H. S. & Murthy, M. R. (2007). *FEBS J.* **274**, 4148–4160.
Scarsdale, J. N., Radaev, S., Kazanina, G., Schirch, V. & Wright, H. T. (2000). *J. Mol. Biol.* **296**, 155–168.
Schirch, V. (1998). *Comprehensive Biological Catalysis*, edited by M. Sinnott, Vol. 1, pp. 211–252. San Diego: Academic Press.
Schirch, V. & Szebenyi, D. M. (2005). *Curr. Opin. Chem. Biol.* **9**, 482–487.
Sopitthummakhun, K., Maenpuen, S., Yuthavong, Y., Leartsakulpanich, U. & Chaiyen, P. (2009). *FEBS J.* **276**, 4023–4036.
Sopitthummakhun, K., Thongpanchang, C., Vilaivan, T., Yuthavong, Y., Chaiyen, P. & Leartsakulpanich, U. (2012). *Malar. J.* **11**, 194–205.
Szebenyi, D. M., Liu, X., Kriksunov, I. A., Stover, P. J. & Thiel, D. J. (2000). *Biochemistry*, **39**, 13313–13323.
Szebenyi, D. M., Musayev, F. N., di Salvo, M. L., Safo, M. K. & Schirch, V. (2004). *Biochemistry*, **43**, 6865–6876.
Tan, L. K. K., Yacoub, S., Scott, S., Bhagani, S. & Jacobs, M. (2008). *Lancet Infect. Dis.* **8**, 449–454.
Tjitra, E., Anstey, N. M., Sugiarto, P., Warikar, N., Kenangalem, E., Karyana, M., Lampah, D. A., Price, R. N. & Rogerson, S. (2008). *PLoS Med.* **5**, e128.
Trivedi, V., Gupta, A., Jala, V. R., Saravanan, P., Rao, G. S., Rao, N. A., Savithri, H. S. & Subramanya, H. S. (2002). *J. Biol. Chem.* **277**, 17161–17169.
Wang, P., Nirmalan, N., Wang, Q., Sims, P. F. & Hyde, J. E. (2004). *Mol. Biochem. Parasitol.* **135**, 77–87.
Winn, M. D. *et al.* (2011). *Acta Cryst.* D**67**, 235–242.